2011

Effect of building geometry on wind loads on low-rise buildings in a laboratory-simulated tornado with a high swirl ratio

Jeremy Michael Case
Iowa State University

Effect of building geometry on wind loads on low-rise buildings in a laboratory-simulated tornado with a high swirl ratio

by

Jeremy Michael Case

A thesis submitted to the graduate faculty

in partial fulfillment of the requirements for the degree of

MASTER OF SCIENCE

Major: Civil Engineering (Structural Engineering)

Program of Study Committee:
Partha Sarkar, Co-major Professor
Sri Sritharan, Co-major Professor
Vinay Dayal
Bruce Bassler

Iowa State University

Ames, Iowa

2011

Dedication

To my wife Imelda.

Table of Contents

List of Figures

List of Tables

Acknowledgments

Several people have played important and irreplaceable roles in the completion of this thesis. I would like to thank my major professors, Dr. Partha Sarkar and Dr. Sri Sritharan, for their invaluable input and guidance throughout the research and thesis writing process. I feel privileged to have had the opportunity to work with and learn from them.

Thanks is also due to my committee members, Dr. Vinay Dayal and Bruce Bassler for their ideas and encouragement. The help given to me by Bill Rickard during design and construction of the building models studied in this research is greatly appreciated. Further thanks is due to all of the other students and staff in the Iowa State University Wind Simulation and Testing Laboratory (WiST) who were most helpful in answering questions and offering advice.

I would also like to thank my wife, Imelda, for her patience, encouragement and support for me throughout this project.

Abstract

Despite the destructive effects of tornadoes, few attempts have been made to quantify tornado-induced loading. Low-rise building models were used to study the effects of variations in building geometry on tornado-induced wind loads in a laboratory-simulated tornado of high swirl ratio. The building orientation with respect to the path of the tornado and the translation speed of the simulated tornado were also varied to study their effects. The required strengths of the roof-to-wall and roof sheathing-to-rafter connections were calculated based on the measured loads and compared with their capacities to assess the possibility of failure. The geometry and orientation of the buildings were found to influence the wind loads and occurrence of failure in the roof connections.

Chapter 1 Introduction

1.1 Motivation

Single tornado events have caused insurance losses exceeding $1 billion (Pan et al., 2002) and as many as 695 deaths (Brooks and Doswell, 2001). Despite the large cost and devastation caused by tornadoes, the body of knowledge concerning tornadoes has grown relatively slowly. This is due to the short-lived nature of tornadoes, the difficulty of predicting where and when they will occur, and the difficulty in collecting real-time wind speed and pressure data in actual tornadoes. For the most part, this has limited the study of tornado vortices to laboratory simulators and to numerical models. Attempts have been made to quantify tornado characteristics based on studies of the tornado-like vortices simulated in laboratories and with CFD programs, but few attempts have been made to quantify the loading induced by the swirling tornado winds on low-rise buildings in the form of force and pressure coefficients.

The flow structure of tornadoes is dependent on the relationship between the tangential flow and radial flow in the vortex. This relationship, known as the swirl ratio, is defined as the ratio of angular momentum of the swirling flow to the radial inflow into the vortex at a given radial distance from its center. Historically, the swirl ratio (S) has been the parameter most often used to categorize the flow structure of simulated tornadoes. Haan et al. (2010) conducted a series of tests on a low-rise building model in several simulated tornadoes with swirl ratios ranging from 0.08 to 1.14. These tests demonstrated that the wind loading on low-rise buildings in a tornado is also a function of the swirl ratio. The reported estimated swirl ratios of several full-scale tornadoes have been reported to be 2.0 or greater (Wurman, 2002; Lee and Wurman, 2005), which is larger than the swirl ratios reported by any of the recent studies that have measured the wind loads on low-rise buildings in simulated tornadoes. Therefore, in order to be able to quantify the loads on low-rise buildings due to realistic tornadoes, investigation of the pressures and forces on low-rise building models in simulated tornadoes with high swirl ratios is needed.

The insufficient number of studies done to investigate the pressures and loading on structures in tornadoes has prevented, ipso facto, any attempt to quantify design loads or required strengths of structural members and connections. The small number of recent studies that investigated tornado induced pressures on structures has also precluded the comparison of those pressures as a function of structure type, or, in the case of low-rise buildings, building geometry. Therefore, before the

required strengths of the different members and connections can be established for low-rise buildings a study should be conducted comparing the pressures and loads on low-rise buildings as a function of building geometry and building orientation with respect to the path of the tornado.

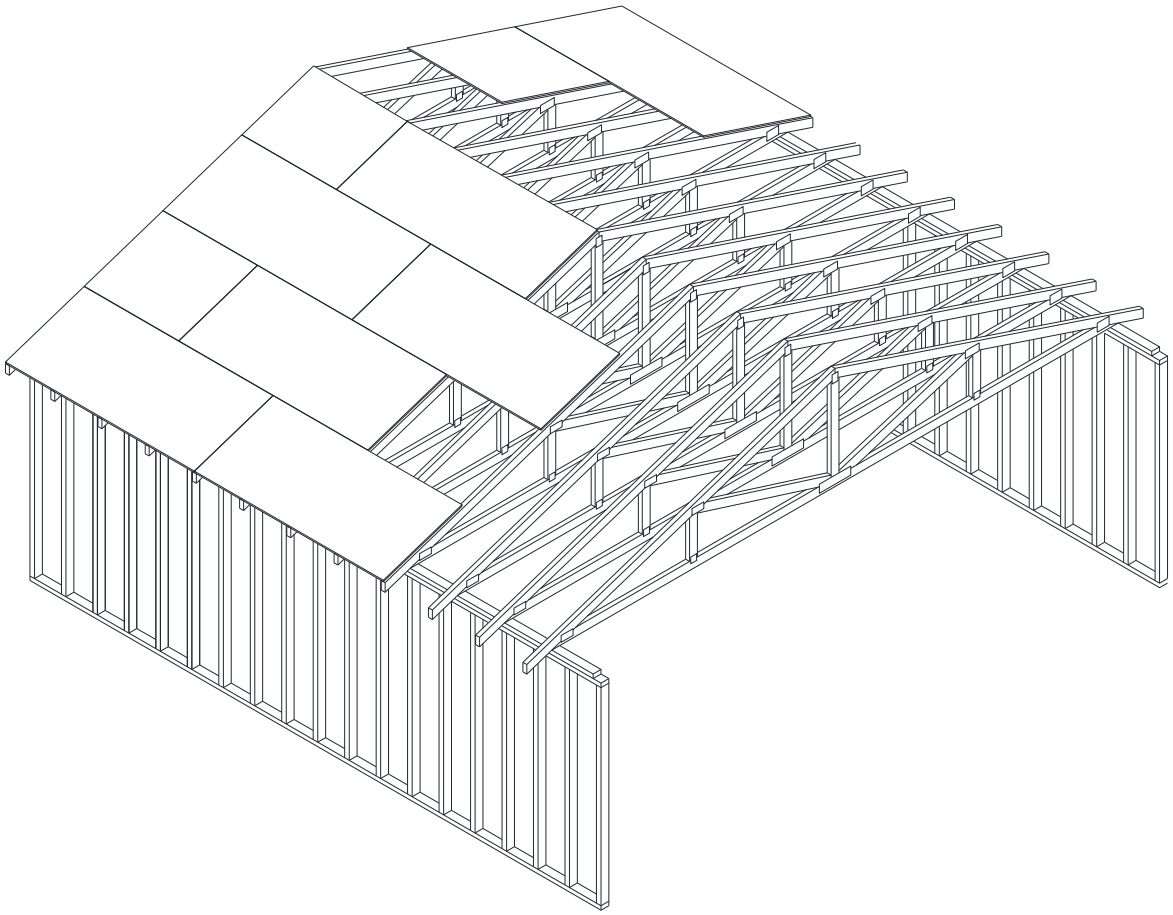

FIGURE 1-1 RESIDENTIAL ROOF STRUCTURAL SYSTEM. SOME OF THE ROOF SHEATHING AND STUD WALL OMITTED FOR CLARITY

Since pressure and loading data on any type of structure in simulated tornadoes is scarce, any effort to obtain tornado-induced pressure and force data for structures most often damaged in tornadoes should be the focus of any research done in this area. This scope of the research should include not only obtaining pressure and force coefficients, but also a calculation of required forces in the most vulnerable structural elements in these structures based on the force and pressure coefficients obtained.

A majority of the damage caused by tornadoes is to non-engineered, low-rise buildings. Most of these buildings are residential and are of timber, light-framed construction. The walls of these structures consist of diaphragms made of stud walls covered in either structural or non-structural sheathing. These diaphragms are held together by the roof structural system. When the roof remains intact and connected to the walls, the entire structure has been found to perform well under extreme wind events such as hurricanes (Reed et al., 1997). This is conceivable because the wall diaphragms are, in a sense, "tied" together by the roof structural system; if the roof fails, then little is left to hold the walls together. Therefore, research into tornado-induced loading on structures should be focused on the tornado-induced loads on low-rise, residential building roofs.

The roof structural system of modern residential construction consists of a series of either roof trusses or rafters and ceiling joists. Each truss/rafter and joist is connected to the wall either by nails driven at an angle from the bottom chord of the truss or ceiling joist into the top plate of the wall (i.e., toe-nailed) or by using pieces of sheet metal commonly called hurricane ties that are attached to the roof framing member and the top plate by nails. This connection between the roof and the wall is often referred to as the roof-to-wall connection (RTWC). The trusses are given lateral stability by being joined together by pieces of wood sheathing which form the surface of the roof and receive the loading induced by wind.

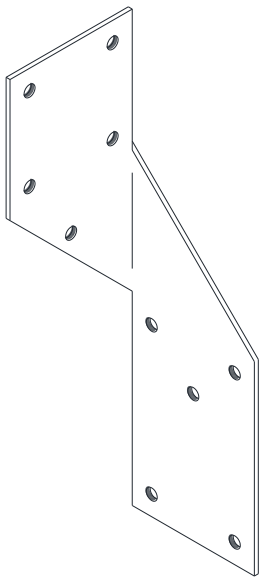

FIGURE 1-2 A COMMON TYPE OF HURRICANE TIE AVAILABLE IN IOWA

This structural system, as described above, works quite well for gravity loads, but the majority of pressures and loads induced by extreme winds such as tornadoes create uplift forces in the roof connections such as the sheathing-to-truss connection and the RTWC. This becomes a major concern because the roof sheathing panels are attached to the trusses/rafters by nails and the common RTWC in tornado prone regions of the United States is the toe-nailed connection and both of these connections are weak in resisting uplift. The weakness of nails in uplift makes the roof sheathing panels vulnerable to being blown off. If a significant number of roof sheathing panels are blown off, the roof framing members lose their lateral stability and the roof-to-wall connections become even more prone to failure. Once the roof fails, there is little else holding the walls of the residential building together, and total collapse could possibly ensue. Therefore, two of the critical connections are the sheathing-to-truss/rafter connection and the roof-to-wall connection. Any initial effort at tornado-resistant design of residential buildings should seek to understand the capacities of these connections under tornado induced loads and attempt to quantify the required strengths for these connections.

Several recent studies have investigated both laboratory and in-situ strengths of both roof sheathing connections and roof-to-wall connections (RTWC). The results of these studies have found relatively good agreement in determining the variables that influence the failure modes and mean uplift capacities of these connections. When the capacities of the these connections are combined with the pressure data obtained in the tornado simulator, the difference between the required strength and the capacities of these connections for various roof pitches, configurations, eave heights and building orientations could be determined. Using the pressure time histories, the point in time at which initial failure would occur for a connection of a given strength could be estimated. By considering the amount of time left in the time history before the tornado has completely passed the structure, how much further damage would occur could also be estimated. Which critical connection is most likely to fail first (i.e., sheathing or RTWC) could also be calculated based upon the respective capacities reported in the literature. This would be useful in further understanding the failure and collapse mechanisms of light-framed, low-rise buildings when under tornado-induced loading.

The scarcity of pressure and loading data on low-rise buildings in tornadoes with high swirl ratios, the need to determine the loading and pressures on low-rise buildings as a function of building and

roof geometry, the importance of the roof structural system in maintaining the integrity of residential structures, the vulnerability of the sheathing-to-truss connections and RTWCs in the roof structural systems of residential structures, and the lack of any attempt to quantify or define the required strengths of these connections for tornado-induced loading form the motivation for this study.

It is the hypothesis of this study that several variables influence the forces and pressures acting on the roof of low-rise buildings during a tornado with a high (greater than 2.0) swirl ratio. Some of these variables include roof pitch, eave height, aspect ratios, roof overhang, building orientation to tornado path, and tornado translation speed. It is also hypothesized that these variables not only influence the loads and pressures but also affect whether or not the roof connections will fail, at what point in the tornado time history the failure will occur and which connection will fail first.

1.2 Objectives

The objectives of this study, in light of the above hypotheses are as follows:

1. To determine the effect low-rise building geometry such as of roof pitch, eave height, building orientation, roof overhang and soffit, and attached garage, along with building orientation, on the external wind loads acting on buildings in a high-swirl ratio tornado through testing of low-rise building models in a laboratory simulated tornado;
2. To determine the effect of low-rise building geometry and orientation have on the failure of roof sheathing and roof-to-wall connections in a design tornado;
3. To compare the loads obtained from the experimentally simulated tornado which the roof connections are subjected to with the capacities of these connections as reported in the published literature;
4. To make recommendations for roof connections based on the results of objectives numbers 2 and 3.

1.3 Organization of Thesis

Chapter 2 presents a review of what is known concerning the structure of tornadoes from full-scale observations and laboratory simulations for vortices with high-swirl ratios, the results of model-scale testing of buildings in laboratory simulated tornadoes, and the effect of tornadoes on the roofs of low-rise buildings as reported in damage surveys. The findings of other studies concerning the

capacities of sheathing panels in uplift and roof-to-wall connections are also surveyed and reported on. An explanation of the experimental set up, the characteristics of the tornado simulated for this study, and the geometry of the model buildings tested can be found in Chapter 3. Chapter 4 consists of two parts. The first part examines the force coefficient time histories for all of the models. Time histories are presented for the force coefficients in the vertical and the parallel and transverse to the tornado translation directions. The vector sum of the horizontal force coefficients is also presented as the total aerodynamic drage force acting on the building structure. The second part of Chapter 4 investigates the loading on the sheathing-to-truss and roof-to-wall connections for two of the building models using the pressure time histories obtained in the laboratory scaled up to full-scale values. The times at which failure first occurs for each type of connection are reported and noted on the vertical force time histories. Contour plots of the peak pressures are also presented for the two models. Chapter 5 summarizes what was done in this study, makes conclusions based on the experimental results and the analysis of those results, and provides recommendations as to possible means for making low-rise, timber structures better able to withstand tornadoes of low to moderate intensity.

Chapter 2 Literature Review

2.1 Tornado Structure

The swirling nature of tornadoes separates them from the usual straight-line boundary layer winds simulated in wind tunnels. This difference implies the need for tornado specific parameters to be able to describe the character and structure of individual vortices, both for being able to categorize specific tornadoes and in order to measure how accurately laboratory simulated tornadoes compare with naturally occurring, full-scale ones. The latter reason is especially important for the field of wind engineering, which attempts to quantify the loading on various types of structures due to wind events. Several parameters describing vortex structure have been proposed and discussed including swirl ratio, the radial Reynolds number, the vortex Reynolds number and, the aspect ratio (Jischke and Light, 1983; Haan et al., 2008). The swirl ratio has historically been the most commonly used parameter due to the inherent difficulty in measuring the turbulent viscosity in a tornado (Haan et al., 2008) and the dependence of the radius of the core on the swirl ratio (Davies-Jones, 1973). The swirl ratio (S) has been defined as the circulation ($\Gamma = 2\pi V_\theta r$) at the radius of the updraft (r_u) multiplied by the radius of the updraft (r_u) divided by the volume flow rate (Q) by Jischke and Light (1983) and as the circulation (Γ) at an arbitrary radial distance (r_0) from the axis of the vortex divided by twice the volume flow rate per unit length (Q') times the aspect ratio (a) by Church et al. (1979). The equation defining the swirl ratio as given by Jischke and Light (1983) is shown as Eqn. 2-1 and the equation given by Church et al. (1979) is shown as Eqn. 2-2. The radial Reynolds number (Re_r) is defined as the ratio of the volume flow rate per unit length to the kinematic viscosity of air and is given in Eqn. 2-3. The aspect ratio (a) is defined as the ratio of the inflow height to the radius of some domain, often taken as the radius of the core, which is considered important in describing the flow.

$$S = \frac{r_u \Gamma}{Q} = \frac{\pi r_u^2 V_\theta}{Q} \qquad (2\text{-}1)$$

$$S = \frac{\Gamma}{2Q'a} = \frac{r_0 \Gamma}{2Q'h} = \frac{\pi r_0^2 V_{\theta max}}{2Q} \qquad (2\text{-}2)$$

$$Re_r = \frac{Q'}{2\pi\upsilon} \qquad (2\text{-}3)$$

The two equations for the swirl ratio are similar except for the definition of the radius at which the circulation is measured. Field measurements and measurements in Ward-type (Ward, 1972)

tornado simulators usually base their swirl ratios on the radius of the updraft (r_u), whereas the swirl ratio as measured in the Iowa State University Tornado Simulator is usually determined by measuring circulation at the radius of the core (r_c), which for tornadoes that are fully formed such as those simulated in the laboratory is equal to the radius of the maximum wind. Therefore, the value of the swirl ratio for a given tornado is dependent on which radial distance is used.

Church et al. (1979) conducted experiments using a Ward type tornado simulator that demonstrated the variation of vortex structure with swirl ratio. They found that the structure of the core of the tornado for vortices with low swirl ratios is a single cell configuration and as the swirl ratio increases the vortex begins to break down into a multiple cell structure. Church et al. (1979) also found that the transitions from a laminar core to a two cell core and then to a multiple cell structure occur at specific swirl ratios. Based upon their observations, they concluded that the main parameter determining the vortex core structure was the swirl ratio (Church et al., 1979).

The data collected for several recent tornadoes using Doppler on Wheels (DOW) indicate multiple vortex structure (Karstens et al., 2010; Lee and Wurman, 2005; Wurman, 2002). Based upon the conclusions of Church et al. (1979), a high swirl ratio should be expected for these tornadoes. In fact the swirl ratio for the Mulhall, South Dakota, tornado of May 3, 1999 was estimated to be between 2 and 6 at various stages in the life of the tornado (Lee and Wurman, 2005).

The observed multiple vortex structure and high swirl ratio estimates of full-scale tornadoes have also been found to match well with numerically simulated vortices. Hangan and Kim (2008) conducted CFD analysis for a numerically simulated tornado with a fixed swirl ratio of S = 0.28 and benchmarked the results against a laboratory simulated tornado (Hangan and Kim, 2008). The numerical analysis was then continued for increasing swirl ratios up to S = 2.0. The tangential velocity profiles of the numerically simulated tornadoes were then compared with data from the Spencer, South Dakota, tornado of May 30, 1998 that was rated F4 on the Fujita scale. Hangan and Kim (2008) found that matching between the radial profiles of tangential velocity of the numerical simulations and the full-scale data improved as the swirl ratio increased and found that the best fit was for the swirl ratio of S = 2.0 (Hangan and Kim, 2008).

2.2 Iowa State University's Tornado Simulator

A large tornado simulator was designed and constructed at Iowa State University (ISU) with some unique features that allow for more realistic tornado simulation and for measuring pressures on models with length scales between 1: 100 and 1:500 (Sarkar et al., 2005). In contrast with earlier simulators, designed mainly for studying the flow structure of tornado like vortices (Davies-Jones, 1976), that were both incapable of movement with respect to a ground plane (i.e., translating) and for the most part were constructed in such a way as to prevent placing building models in them without disrupting the flow, the tornado simulator at Iowa State University (ISU) is capable of translating at various speeds and was designed with the capability of placing building models in the path of the tornado . The types of simulators used before the ISU tornado simulator were also limited to simulating vortices with swirl ratios less than or equal to one (Davies-Jones, 1976).

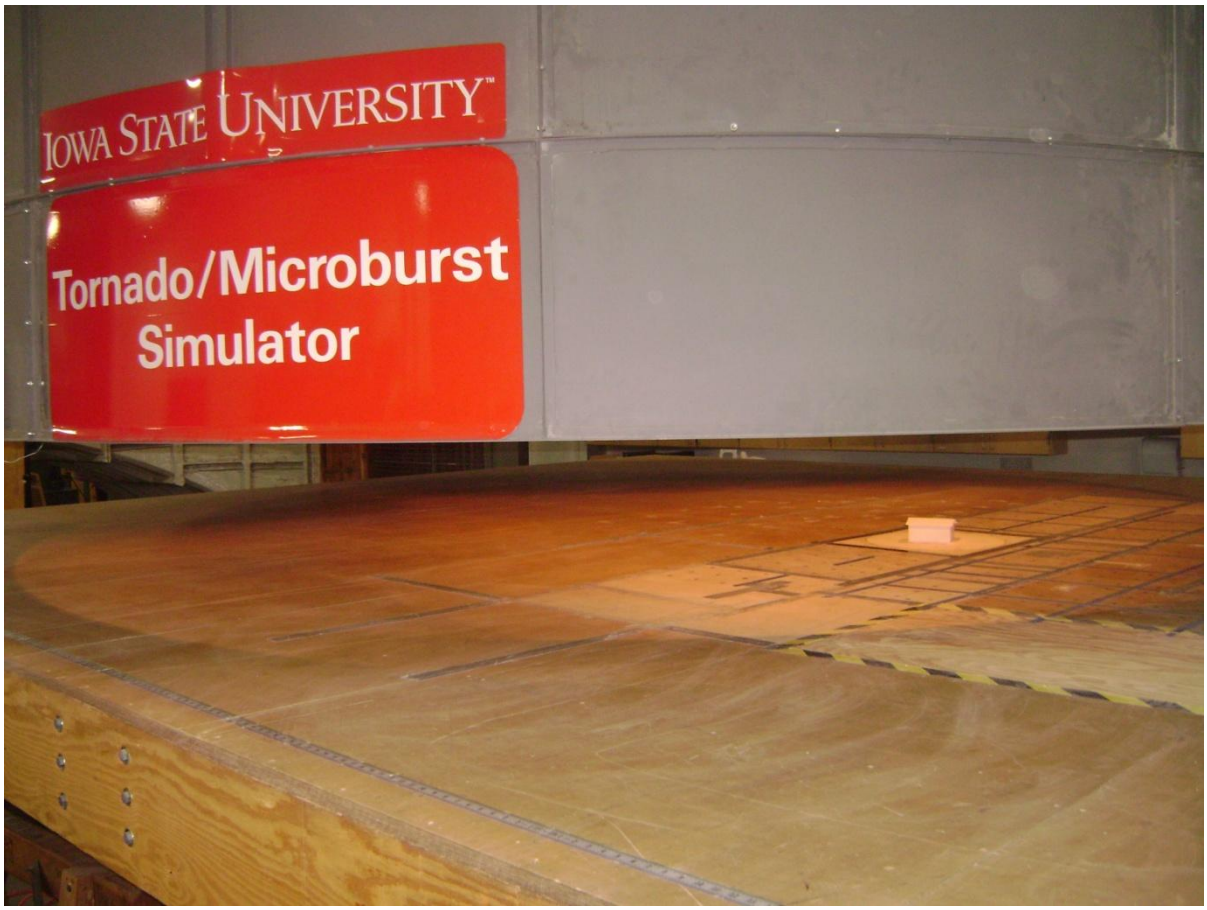

FIGURE 2-1 ISU TORNADO SIMULATOR WITH LOW-RISE BUILDING MODEL

The structure of the vortex flow field created by the ISU simulator was found to reasonably match the full-scale data collected with Doppler on wheels from the Spencer, South Dakota tornado and with numerical simulations (Sarkar et al., 2005). The capabilities of the ISU tornado simulator were further compared with the Mulhall, South Dakota tornado, which had a much larger diameter of the core than did the Spencer tornado (Haan et al., 2008). A series of tests were also conducted with the simulator to measure the effect of changing settings such as the vane angle, ground plane height and fan speed on the various characteristics of the simulated vortices such as swirl ratio, aspect ratio, radius of maximum wind, maximum tangential velocity, and total flow rate (Haan et al., 2008). In these tests, the maximum measured swirl ratio was 1.14 (measured at the radius of the core) with a 55° vane angle. This value for swirl ratio is approximately equivalent to a swirl ratio of 1.9 when measured at the radius of the updraft. This is the largest swirl ratio in a laboratory simulated tornado to date showing that tornadoes can be simulated at swirl ratios greater than one and is comparable to the best fit swirl ratio of 2.0 (measured at the radius of the updraft) found by Hangan and Kim (2008), but less than the estimated swirl ratios (between 2 and 6) for the Mulhall tornado by Lee and Wurman (2005).

In wind engineering applications, in addition to correctly simulating the flow field, it is also important that the simulated tornado be able to produce pressures and forces that when scaled up to full-scale can be correlated with the damage that happens during tornado events. Thampi et al. (2011) conducted a study using the ISU tornado simulator with the intention of reproducing the damage to a particular residential structure that suffered complete loss of its roof during the Parkersburg, Iowa, tornado of May 25, 2008 (Thampi et al., 2011). Using nail withdrawal capacities and other mechanical properties of the connections obtained from laboratory tests, a finite element model was created of the house before it was damaged. A 1:75 geometric scale model of the house was tested in the ISU tornado simulator which reproduced a scaled vortex comparable to the Parkersburg tornado to get the external and internal pressures on the house. For each time step the pressures obtained in the laboratory were input into the finite element model. If the structural elements or connections of the finite element model of the house exceeded stability, strength or deflection failure criteria, then the stiffness of the failed components was set to zero in the next finite element analysis in order to simulate failure of the member. Those members of the model that had failed were then physically removed from the laboratory model and updated pressures for the succeeding time steps were obtained for the “damaged” model. This iterative process was

repeated until the tornado had reached the point where it no longer affected the pressures on the structure. The resulting finite element model closely resembled the actual damage to the residential structure due to the Parkersburg tornado (Thampi et al., 2011) demonstrating the validity of using the pressures obtained in the ISU Tornado Simulator to establish probable pressures a low-rise building would experience in a full-scale tornado.

The ISU Tornado Simulator has been found to simulate vortex-like tornadoes that have characteristics that match well with the available full-scale data and has been shown to be able to generate surface pressures on a low-rise building model that when used in a finite element analysis produce structural failure of the same type and magnitude as what occurred to the prototype building in an actual tornado. The ISU tornado simulator has also produced the tornado-like vortex with the highest swirl ratio to date. Based on these considerations, the ISU Tornado Simulator was considered by the researcher to be the most appropriate facility to investigate the loading on low-rise buildings due to a high swirl ratio tornado.

2.3 Model-Scale Testing of Buildings

The research studies done by testing building models in laboratory simulated tornadoes have found that not only are tornado loadsmuch greater than those caused by straight-line, boundary layer winds, but the distribution of the pressures on the surface of the building is also different. Jischke and Light (1983) found that the imposed updraft of a tornado results in larger force coefficients than straight-line winds. The increase in force coefficients was attributed by Jiscke and Light (1983) to the different pressure distribution on the model due to the rotational aspect of the wind in a tornado. Their results also showed that the loads induced by tornadoes are also dependent on the structure's location with respect to the center of the tornado and the structure's orientation to the tangential wind.

Haan et al. (2010) found that there are several factors that influence the loading induced by tornado winds on low-rise buildings including swirl ratio (vortex size), translation speed, and building orientation. The negative and positive peak loading caused by the tornadoes with smaller swirl ratios occurred when the tornado was at equal distances from the center of the building, but those with larger diameters (higher swirl ratios) did not. This was attributed to either the center of the tornado not lying exactly on the center of the axis of translation or the multi-cell structure of the tornado itself (Haan et al., 2010). It was also found that the simulated tornadoes with smaller

diameters (i.e., smaller swirl ratios) produced much higher uplift forces than the tornadoes with larger swirl ratios. Haan et al. (2010) showed a general trend for the peak longitudinal (along the direction of translation of the tornado) force coefficient for increasing vane angle (i.e., increasing swirl ratio). As the vane angle increases the negative peak of the longitudinal force coefficient for building orientations 15°, 30°, and 45° approaches zero. This trend was also shown by Haan et al. (2010) for the peak transverse force coefficient for the same building angles, while for the peak vertical force coefficient the values remain relatively constant for vane angles of 35°, 45°, and 55° (i.e., swirl ratios of 0.24, 0.82 and 1.14)).

Haan et al. (2010) also found that the translation speed of a tornado plays an important role in the nature and magnitude of the aerodynamic forces acting on low-rise buildings in tornadoes. The magnitudes of the forces were found to be larger for slower translation speeds. It was also found that for faster translation speeds, the entire time history shifted with respect to the x axis that measured the distance of the center of the vortex to the center of the building model and was normalized with the diameter of the core of the vortex (x/D) (Haan et al., 2010).

Haan et al. (2010) found that building orientation affected the value of the peak horizontal force coefficients, but did not affect the peak vertical force coefficient. This was attributed to the notion that the uplift force is dominated by the pressure deficit created in the center of the vortex core. This was confirmed by the fact that the peak uplift force occurred when the tornado was directly over the building, and the peak horizontal forces occurred when the tornado was at a distance equal to the radius of the maximum tangential wind (Haan et al., 2010). Haan et al. (2010) also showed that the vertical forces acting on the roof of the low-rise building where significantly higher than the horizontal forces acting on the walls.

2.4 Feasibility of Tornado Resistant Design

McDonald and Selvam (1990) determined from their damage survey after the West Memphis, Arkansas, tornado of December 14, 1987 that if engineering knowledge were applied to the design of a structure (i.e., adequate capacity in its connections and sufficient anchorage to its foundation) it would be able to withstand tornado induced forces without suffering major damage (McDonald and Selvam, 1990). Following the Carolinas tornado outbreak of March 28, 1984, Sparks (1986) compared the damage to low-rise, non-engineered structures that were built according to the strict North Carolina building code (North Carolina Building Code Council, 1984) with those that were built

according to the minimum requirements of the building codes modeled after the Standard Building Code. From his observations Sparks (1986) concluded that with relatively minor changes buildings could be built to resist tornado induced loads reasonably well. Marshall (2002) returned to the location of the May 3, 1999, Oklahoma City tornado 3 months after he completed his damage survey and found that the houses being built to replace those that had been destroyed were not of better quality than the ones that had been destroyed and were being built to the minimum of the local building code requirements. These building code requirements allow for toe nailed RTWCs, which have been shown to be less than adequate for the design wind speeds in the building codes (Sparks et al., 1988; Cheng, 2004), much less for tornado induced loading. It is clear from these studies that in order to achieve tornado resistant design, the building code provisions must be changed. Building code provisions related to tornado resistant design should, of course, be based on the results of engineering and scientific research which quantifies the pressures and loads acting on low-rise buildings during a tornado. At present, the most feasible method of obtaining these pressures and loads is by testing low-rise building models in laboratory simulated tornadoes that have characteristics, such as swirl ratio, that match well with the available full-scale data.

One of the main objections to updating the building code provisions to make low-rise, non-engineered structures more tornado resistant is that it is not economically feasible due to the low probability of a tornado hitting a particular structure in the course of its lifetime (Simiu and Scanlan 1996). One method commonly used to improve the performance of low rise buildings in hurricanes are hurricane ties. Hurricane ties increase the capacity of the roof-to-wall connection in uplift which is a critical loading situation for RTWCs in all extreme wind events including tornadoes. Canfield et al. (1991) tested the capacities of several types of rafter/hurricane ties and calculated an estimated cost of installing 100 of each type of tie. The cost, including labor, of installing 100 of the tie with the highest capacity was estimated at US$95 in 1990. The mean capacity of this particular tie was found to be more than 15 times the mean capacity of the commonly used 8d toe-nailed connection. This demonstrates the fact that the strength of residential construction in resisting tornadoes could be increased significantly for a cost that is insignificant compared to the construction of a new house. A cost benefit analysis was done by Sutter et al. (2009) and found that for the states most prone to tornado occurrences if damage due to tornadoes could be reduced by 30% an increase in construction cost of $500 would be economically justifiable. Considering the fact that damage to buildings in tornadoes not only results in damage to buildings but also in loss of life, damage of the

contents of the house, emotional distress and the shattering of lives through injuries and homelessness, the ethics of leaving the provisions of the building codes in their present state based on economic objections alone, especially when the costs have been shown to be insignificant, should be brought into question.

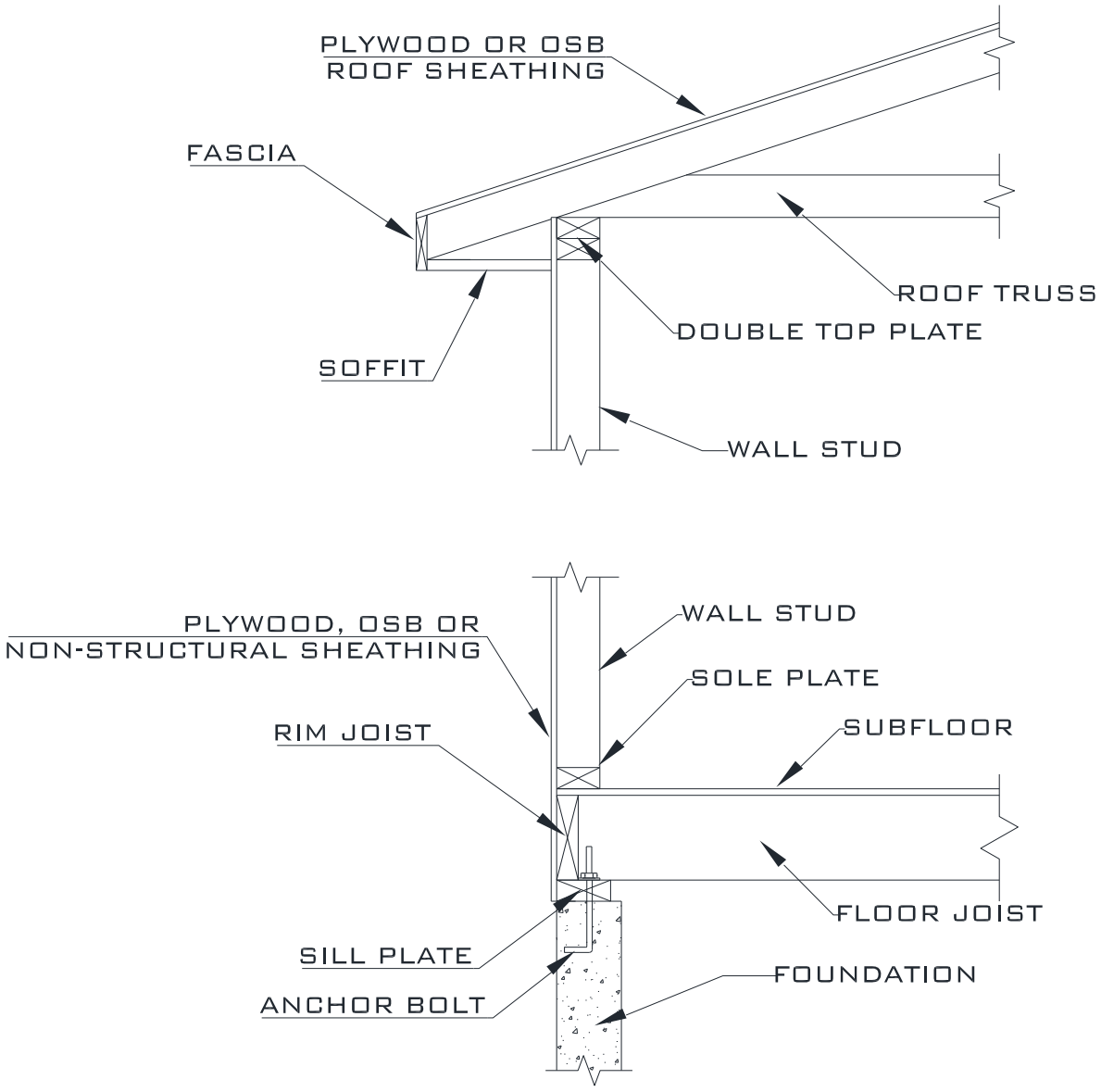

FIGURE 2-2 DIAGRAM OF FRAMING SYSTEM IN LIGHT-FRAMED LOW-RISE BUILDINGS

2.5 Load Path for Uplift Pressures in Low-Rise Residential Construction

The load path for uplift pressures acting on the roof sheathing is generally the same as for gravity loads but places the connections and members in tension rather than compression. Roof sheathing panels commonly consist of either plywood or oriented strand board (OSB). The pressures that act on the roof sheathing panels are transferred to the roof trusses or rafters through nails or staples. The nails are usually spaced either 150 mm (6 inches) on the edges of the panels and 300 mm (12 inches) in the middle of the panel or are spaced 150 mm on both the edges and the middle of the panel. The former nailing schedule is often referred to as 6/12 and the latter schedule is referred to as 6/6. The load on the truss/rafter is then transferred to the top plate through the roof-to-wall connection (RTWC) which usually consists of 2 or 3 nails placed through the bottom chord of the truss or through the rafter into the top plate at an angle of around 30° to 45°. The installation of these nails at an angle is referred to as a "toe-nailed" connection. Some of these RTWCs have metal straps often referred to as "hurricane ties", which have ends that are nailed to the truss/rafter and to the top plate or wall stud. For a one story house, the load is then transferred from the wall stud to the sole plate. Most modern residential construction (i.e., platform framing) requires properly installed structural wood sheathing to continue the load path to the foundation. If the structural wood sheathing has been correctly nailed from the top of the stud wall to the sill plate (see Figure 2-1) it not only transfers the load from the stud wall to the rim joist and then to the sill plate but aids the stud wall in resisting the tension force from the uplift and aids in resisting the shear caused by the horizontal forces (Marshall, 2002). A recent trend has been to replace structural wood wall sheathing with non-structural foam sheathing and placing a 25 mm x 100 mm (1 in x 4 in) board at a 45° to 60° angle let in to the stud wall at the corners. This system has been found to perform extremely poorly in tornadoes (Readling, 2003).

The connections in this framing system work well for gravity loads, but are often the source of failure in extreme wind events (Shanmugam et al., 2009; Marshall, 2002; Canfield et al., 1991; van de Lindt et al., 2007). The roof sheathing-to-truss connection and the roof-to-wall connection (RTWC) have been repeated sources of failure in tornadoes and other high wind events (Shanmugam et al., 2009). The importance of these connections in maintaining the integrity of the roof structural system and, therefore, the structure of the entire building structure is discussed below.

FIGURE 2-3 DAMAGE FROM THE MAPLETON, IOWA TORNADO OF APRIL 10, 2011 SHOWING AN ENTIRE ROOF LIFTED OFF OF ITS SUPPORTING WALLS

2.6 Vulnerability of Roofs in Tornadoes

Only pressures acting on the roof of low-rise buildings have a vertical component that when integrated become the vertical forces. In light of the findings of Haan et al. (2010) that the vertical forces are much larger than the horizontal forces, it is not surprising that many damage surveys done after tornado events have found that residential roof damage is one of the most common types of damage to occur in tornadoes. The occurrence of roof damage is further aggravated by the fact that, for residential construction in the regions of the United States where tornadoes most often occur, the connections in the load path from the surface of the roof to the wall and then to the foundation are almost always nailed. Nailed connections increase the vulnerability of roofs to uplift failure because nails are inherently weak in tension. The loss of the roof increases the vulnerability of the rest of the house, because the exterior walls are composed of diaphragms that are tied together and braced at their tops by the roof structure (Marshall, 2002). Therefore, the roof is vital to the survivability of the house.

Sparks et al. (1988) demonstrated that the roof of low-rise buildings is critical to the integrity of the structure and that for straight-line winds failure of roof connections is dependent not only on wind speeds but also on roof geometry. Sparks et al. (1988) found that the roof structural system usually found in modern residential construction composed of plywood or oriented strand board (OSB) sheathing and wood roof trusses is generally very strong and under extreme wind loading can separate from the house as a whole or in large sections (Sparks et al., 1988). These researchers also noted that failures of entire residential structures can occur quickly after the loss of the roof. Based on their findings, the connection between the roof trusses and the stud walls was considered to be the critical connection for the survival of the entire house (Sparks et al., 1988). In addition to finding that the roof-to-wall connection (RTWC) was the most critical, they found that for several different roof geometries the toe nailed RTWC would fail at wind speeds as low as 54 mph (3 second gust) which is much less than the design wind speed of 90 mph (3 second gust) in boundary layer winds. This structural inadequacy is turned into tragedy when toe nailed RTWCs are used in "Tornado Alley", as is often the case (Marshall, 2002; Pan et al., 2002).

The roof structural system composed of several trusses or rafters and ceiling joists gains most of its out of plane (i.e., normal to the plane of the truss) stiffness from being connected to roof sheathing panels (Cramer et al., 2000). This lateral stability also causes a load sharing effect between the trusses, where heavily loaded trusses transfer some of their load to some of the more lightly loaded or stiffer trusses (Cramer et al., 2000). This effect is found to occur especially when the loading is normal to the plane of the roof sheathing, as is the case for wind induced pressures. If the sheathing panels connecting the trusses in the roof were to fail in uplift, this load sharing effect would be lost, further increasing the vulnerability of the roof structure and, therefore, the entire house.

2.7 Roof Sheathing Panel Capacity

Several studies have been done in attempts to quantify the uplift capacities of roof sheathing panels. These studies have looked at the capacities of various types of fasteners, fastener spacing, types of loading, tolerances, rate-of-loading and duration of loading effects, and failure modes. Knowledge of how these variables influence the capacity of roof sheathing panels should inform recommendations on making low-rise building roofs tornado-resistant. The findings of these studies can be found in Table 2-1 and Table 2-2.

One study was conducted at The University of Florida in order to quantify the effect of several different variables on the capacity of a sheathing panel (Hill, 2009). The variables Hill (2009) compared included the effect of dynamic versus static loading, the effect of age and weathering, and various fastener types and spacing between fasteners. This author found that dynamic loading reduced the capacity of a panel in uplift by around 20% when compared to static loading. He also tested 38 panels that were harvested from existing homes that were scheduled for demolition. The harvested panels ranged in age from 29 to 33 years and were found to have the same mean capacity as panels newly constructed in the laboratory.

Hill (2009) also found that using longer nails (8d) resulted in an increase in panel uplift capacity as compared to using shorter nails (6d), that using ring shank nails resulted in a higher capacity than when smooth shank nails were used, and that using a heavier nailing schedule also resulted in a higher uplift capacity. The failure mode that occurred most often changed from nail withdrawal to pull through as the spacing between the nails decreased and when ring shank nails were used. The failure mode described as nail withdrawal is defined as the nail being completely removed from the framing member while still being attached to the sheathing. The failure mode described as pull through is where the nail only partially comes out of the framing member or does not come out at all, but the head of the nail breaks through the sheathing.

Cunningham (1993) conducted a series of tests on panels with different nailing schedules including some with “missing nails”, different conditions such as wet and dry, different types of sheathing, and different fasteners. This author reported, based on his findings, that nail withdrawal capacity depends on the specific gravity of the framing lumber, depth of penetration of the nail, the diameter of the nail, and nail shank characteristics (i.e., smooth, ring, annularly threaded, twisted, etc.). Cunningham also demonstrated that for the 6/12 nailing schedule (i.e., nails spaced 6 inches along the edge and 12 inches in the middle or “field”), the first nail to fail was always one of the field nails. The reason given for this was that the tributary areas of the field nails (which are spaced twice as far apart as the edge nails in a 6/12 nailing schedule) are 4 times as large as those of the edge nails (Cunningham, 1993).

TABLE 2-1 CAPACITIES OF SHEATHING PANELS WITH 6/12 NAILING SCHEDULES

Reference	Sheathing thickness	Sheathing Type	Wood member species	Nail size	Shank type	Nailing schedule	Spacing of rafters	# of samples	Mean uplift capacity	SD	COV
	(in.)					(in/in)	(in)		(psf)	(psf)	
Hill (2009)*	1/2	OSB	SYP	6d	smooth	6/12	24	5	52	12	0.23
Cunningham (1993)	15/32	5-ply	DF	6d	smooth	6/12	24	1	55	N/A	N/A
Hill (2009)	1/2	OSB	SYP	6d	smooth	6/12	24	5	62	10	0.16
Cunningham (1993)	7/16	OSB	DF	6d	smooth	6/12	24	1	65	N/A	N/A
Hill (2009)	1/2	OSB	SYP	6d	smooth	6/12	24	15	74	16	0.22
Hill (2009)**	1/2	OSB	SYP	6d	smooth	6/12	24	9	80	37	0.46
Rosowsky and Schiff (1996)	15/32	CDX plywood	SPF	8d	smooth	6/12	24	10	60	12	0.2
Dao and van de Lindt (2008)	15/32	OSB	SPF	8d	smooth	6/12		10	66	16	0.24
Sutt (2000)	7/16	OSB	SYP	8d	smooth	6/12	24	7	67	10	0.15
Sutt (2000)	1/2	plywood	SYP	8d	smooth	6/12	24	7	79	7.1	0.09
Cunningham (1993)	5/8	4-ply	DF	8d	smooth	6/12	24	1	106	N/A	N/A
Hill (2009)	1/2	OSB	SYP	8d	smooth	6/12	24	15	129	15	0.11
Cunningham (1993)	15/32	5-ply	DF	8d	smooth	6/12	24	1	130	N/A	N/A
Hill (2009)	1/2	OSB	SYP	8d	ring	6/12	24	10	161	28	0.18
Hill (2009)	1/2	OSB	SYP	8d	ring	6/12	24	15	174	23	0.13

SPF = Spruce Pine Fir
DF = Douglas Fir
SYP = Southern Yellow Pine
SD = standard deviation
COV = coefficient of variation
*Dynamic loading
**Harvested from existing structures

6d nails - shank length = 51 mm (2 in.) shank diameter = 3.3 mm (0.131 in.)
8d nails - shank length = 63.5 mm (2.5 in.) shank diameter = 3.3 mm (0.131 in.)

TABLE 2-2 CAPACITIES OF SHEATHING PANELS WITH 6/6 NAILING SCHEDULES

Reference	Sheathing (in.)	Sheathing	Wood	Nail	Shank	Nailing (in/in)	Spacing (in)	# of	Mean (psf)	SD (psf)	COV
Hill (2009)*	1/2	OSB	SYP	6d	smooth	6/6	24	5	90	31	0.34
Hill (2009)	1/2	OSB	SYP	6d	smooth	6/6	24	5	108	29	0.27
Cunningham (1993)	15/32	5-ply	DF	6d	smooth	6/6	24	1	120	N/A	N/A
Rosowsky and Schiff (1996)	15/32	CDX plywood	SPF	8d	smooth	6/6	24	10	107	17	0.16
Murphy et al. (1996)	15/32	OSB	SYP	8d	smooth	6/6	24	30	131	18	0.14
Hill (2009)	1/2	OSB	SYP	8d	smooth	6/6	24	15	205	21	0.1
Cunningham (1993)	5/8	4-ply	DF	8d	smooth	6/6	24	1	218	N/A	N/A
NAHB (2003)	7/16	OSB	SPF	8d	smooth	6/6	24	3	228	16	0.07
Hill (2009)	1/2	OSB	SYP	8d	ring	6/6	24	13	252	18	0.07
Cunningham (1993)	5/8	4-ply	DF	8d	ring	6/6	24	1	397	N/A	N/A

SPF = Spruce Pine Fir
DF = Douglas Fir
SYP = Southern Yellow Pine
SD = standard deviation
COV = coefficient of variation
*Dynamic loading

6d nails - shank length = 51 mm (2 in.) shank diameter = 3.3 mm (0.131 in.)
8d nails - shank length = 63.5 mm (2.5 in.) shank diameter = 3.3 mm (0.131 in.)

Murphy et al. (1996) used a finite element analysis to find the effective tributary area of a single fastener in a panel and found that this effective tributary area did not vary significantly from the usual geometric tributary areas. An attempt was made by Murphy et al. (1996) to correlate the strength of single fasteners in withdrawal to the uplift capacity of an entire panel by comparing the results of 30 panel tests and 40 single fastener withdrawal tests. The mean capacity of the panel was found to be lower than that of a single fastener but the 5% exclusion value was greater due to the decrease in variability of the panel capacities. This decrease in variability was attributed to load sharing or system effects in the panel. During the panel tests, failure of a single fastener was followed by failure of the other fasteners along the same framing member and failure of the entire panel quickly followed. It was concluded based upon this observation that the capacity of a panel in uplift is first fastener critical; the ultimate capacity of a sheathing panel in uplift is determined by the capacity of the first fastener to fail. This observation and conclusion was also reported by NAHB (2003). The attempt to predict panel capacity was continued by Rosowsky and Schiff (1996) by using a probabilistic model based on the capacity of individual fasteners. Rosowsky and Schiff (1996) found that their probabilistic model worked well for mean values of capacity, but was overly conservative for predicting the lower percentile capacities.

The attempts at correlating nail withdrawal to panel uplift capacity are based on the assumption that only axial forces act on the fastener. This is true in single fastener withdrawal tests, but Hill (2009) made an observation that implies that it is not the case for nail withdrawal when connected to a roof sheathing panel. Hill (2009) found that as spacing between the fasteners in a panel increases the individual fastener withdrawal strength decreases. This is explained by Dao and van de Lindt (2008) as being caused by eccentric pressure on a panel creating a moment arm that acts on the nail. Dao and van de Lindt (2008) modeled the nails in roof sheathing panels as non-linear springs with 6 degrees of freedom as opposed to only one degree of freedom in the axial direction by combining the results from individual fastener withdrawal and bending moment tests. The results they obtained from finite element analysis show that the common single degree-of-freedom nail element results in an overestimated capacity of the roof sheathing panel. Since wind pressures vary across the surface of a single panel result in eccentricities, the results by Dao and van de Lindt (2008) could indicate that laboratory panel uplift tests using uniform pressure over estimate the capacity of the sheathing panel in uplift.

The capacity of roof sheathing panels is usually measured in the laboratory under controlled conditions where care is taken to ensure that the panels are constructed properly. This is quite different than how low-rise wood buildings are actually constructed. The result of this is that the spacing of fasteners, the distance between the fasteners and the edge of the panel, and the amount of over drive of the fastener when pneumatic nail guns are used can all vary considerably. This consideration formed the motivation for a study done by the National Association of Homebuilders which sought to provide recommendations for nailing tolerances in the building code guidelines (NAHB, 2003). The study found that a tolerance of 25 mm (1 inch) could be allowed in the spacing between nails without an effect on the capacity of the panel. It was also observed that fastener overdrive as a percentage of the thickness of the panel had a nearly linear relationship with decrease in capacity. The installation guidelines of the American Plywood Association call for nails to be driven 3/8 of an inch from the edge of roof sheathing. The study done by the NAHB found that the edge nailing at 1/4 inch and 3/4 inch from the edge did not significantly reduce the capacity of the panel but when the nails where driven at 1/8 inch from the edge, the capacity was not only reduced by more than 50% but that the edge nails failed first for the 6/12 nailing schedule whereas for all other studies the field nails always failed first for the same 6/12 nailing schedule.

The effects of combined shear and uplift on the capacities of sheathing panels was investigated by (Sutt Jr., 2000) by performing tests on panels in pure uplift, pure shear and combined shear and uplift. The combined shear and uplift tests were conducted by first applying a shear load to the panel and then applying an uplift pressure until the panel failed. Both plywood and oriented strand board (OSB) panels under combined shear and uplift showed an increase in capacity when compared to simple uplift loading (Sutt Jr., 2000).

Other important aspects to consider in determining the capacity of sheathing panels in uplift are those of load duration and rate-of-loading. These aspects are especially important for tornado loading which is not only highly turbulent, but is by nature transient. A study was done to investigate the effect of rate-of-load and load duration effects on nailed connections by testing nails in withdrawal at the rates of 0.1 inch/minute, 0.5 inch/minute, 1 inch/minute, 5 inches/minute, 10 inches/minute and “near instantaneous” (Rosowsky and Reinhold, 1999). The results of the study indicated that neither rate-of-loading nor duration-of-loading significantly affect the withdrawal capacity of nails (Rosowsky and Reinhold, 1999).

Shanmugam et al. (2009) conducted a series of tests on both in-situ roof-to-wall connections and in-situ roof sheathing to rafter connections both having been constructed approximately 50 to60 years ago. The roof sheathing was composed of 19 mm x 140 mm (nominal 1" x 6") planks nailed to rafters spaced at 410 mm (16 inches) on center. The plank sheathing was found to have an uplift capacity of almost twice that of reported capacities of OSB/plywood sheathing. As these authors pointed out, this is quite understandable as the plank sheathing requires almost twice as many nails as the OSB/plywood sheathing (Shanmugam et al., 2009).

2.8 Roof-to-Wall Connection Capacity

The testing of 50 to 60 year old in-situ RTWC by Shanmugam et al. (2009) was done using a spreader beam to apply uniform deflection to 4 connections simultaneously. The connection consisted of a notched rafter nailed to a ceiling joist which was then toe-nailed to the top plate of the wall. The testing was done cyclically by increasing the load to achieve loads corresponding to 1.6, 3.2 and 4.8 mm deflections, then reducing the force to zero after each target deflection was achieved. After reaching the 4.8 mm deflection, the force was increased until the connection failed. The force applied to the connections was reduced to zero after achieving each target deflection. The dominant failure mode (81%) for the toe-nailed connections was nail withdrawal from the top plate (Shanmugam et al., 2009). Shanmugam et al. (2009) considered the ceiling joist to top plate connection to be weaker than the rafter to joist connection, because uplift forces on the roof loaded the nails in the rafter-to-joist connection in shear while the nails in the joist-to-top plate were loaded axially in tension.

Testing was done on full-scale models of roof truss to wall connections under the auspices of the National Institute of Standards and Technology (NIST) to ascertain their capacities under uplift and lateral loading (Riley and Sadek, 2003). The full-scale model consisted of 4 pre-manufactured roof trusses purchased locally with attached stud wall and roof sheathing. One model was tested using toe-nailed connections at the roof-to-wall interface and another test was done on a model using a hurricane clip. A load tree was used to induce uniform load across all 8 connections (4 on each side). The failure mode of the toe-nailed connections was nail withdrawal from the wall top plate. The hurricane clip initially caused the separation of the top plate from the stud wall, showing the need to have sufficient capacity in this region if the hurricane clip does not additionally attach to the studs, but was then repaired and retested until failure occurred when the upper member of the top

TABLE 2-3 CAPACITIES OF TOE-NAILED RTWCS

Reference	Species	Grade	Fastener	No. of Fasteners	No. of Samples	Mean Max load		SD		COV
						lbs	kN	lbs	kN	
Canfield et al. (1991)	SPF	1, 2	8d common	3	21	208	0.93	34	0.15	0.163
Reed et al. (1997) individual connections	SYP/SPF	2	8d common	3	16	430	1.92	99	0.44	0.23
Reed et al. (1997) system tests	SYP/SPF	2	8d common	3	2	670	2.99	--	--	--
Morrison & Knopp (2010)			12d twisted shank	2 (same side)	16	427	1.9	103	0.46	0.24
Morrison & Knopp (2010)			12d twisted shank	2 (1 on each side)	16	495	2.2	108	0.48	0.22
Morrison & Knopp (2010)			12d twisted shank	3	63	630	2.8	135	0.6	0.21
Morrison & Knopp (2010)			12d twisted shank	3	25	630	2.8	--	--	--
Cheng (2004)	SPF	2	16d box	2	10	255	1.13	22	0.1	0.09
Cheng (2004)	DF	2	16d box	2	25	627	2.79	103	0.46	0.16
Shanmugam et al. (2009)	SYP	N/A	16d common	2	81	341	1.51	123	0.54	0.36
Riley and Sadek (2003)	SPF	2	16d common	3	1	630	2.8	N/A	N/A	N/A
Shanmugam et al. (2009)	SYP	N/A	16d common	3	19	442	1.97	168	0.75	0.38
Conner et al. (1987)	DF	N/A	16d box	3	3	670	2.98	62.5	0.28	0.09
Canfield et al. (1991)	SPF	1, 2	16d box	3	30	415	1.85	108	0.48	0.26
Canfield et al. (1991)	SPF	1, 2	16d box (rafter split prior to testing)		10	333	1.48	75	0.33	0.225
Canfield et al. (1991)	SPF	1, 2	16d pole barn		20	648	2.88	127	0.56	0.196

8d nails - shank length = 63.5 mm (2.5 in.) shank diameter = 3.3 mm (0.131 in.) smooth shank

16d box (common) nails - shank length = 89 mm (3.5 in.) shank diameter = 3.51 mm (0.138 in.) smooth shank

16d pole barn nails - shank length = 89 mm (3.5 in.) shank diameter = 4.19 mm (0.165 in.) annularly threaded shank

SD = standard deviation COV = coefficient of variation

TABLE 2-4 CAPACITIES OF SMALL HURRICANE TIE

Reference	Wood member species	Wood grade	Sheet metal gauge	Fasteners			No. of Samples	Mean load capacity		SD		COV
				To rafters/ truss	To top plate	Construction toe nails		lbs	kN	lbs	kN	
Riley and Sadek	SPF	2		4 8d common	4 8d common	yes	1	1012	4.5	N/A	N/A	N/A
Canfield et al. (1991)	SPF	1, 2	18	5 1-1/4" long 0.43" diameter annular ring shank	5 1-1/4" long 0.43" diameter annular ring shank	no	16	1216	5.4	188	0.8	0.15
Reed et al. (1997)	SYP/SPF	2	18	5 8d short	5 8d short	yes	16	1900	8.5	209	0.9	0.11

SD = standard deviation COV = coefficient of variation

plate separated from the bottom member. For this failure mode the hurricane clip remained connected to the upper member of the top plate (Riley and Sadek, 2003).

Testing was done by Reed et al. (1997) to investigate the improvement in capacity of several different retrofit methods to the RTWC over the capacity of a toe-nailed connection using three 8d common nails. The three categories of connections that were tested were toe-nailed connections, toe-nailed connections with various types of hurricane ties and the use of epoxy in connecting the rafter to the wall top plate. The failure mode for the toe-nailed connection was nail withdrawal from the top plate. The failure mode for the hurricane ties depended on the type of hurricane tie and how it was installed (on the inside or outside of the wall, etc.) and the dominant failure mode for the epoxy connections was wood fiber failure. All types of connections outperformed the toe-nailed connections that only used three 8d nails.

System tests were also done on seven RTWCs simultaneously for several of the connection types to compare the capacities obtained from individual connection tests and the capacities of the connections when tested in a more realistic configuration (Reed et al., 1997). Each connection type was tested twice, once using a spreader beam to induce uniform displacement and once using a load tree to uniformly load all seven connections. These system tests showed a significant increase in capacity of the connections when tested using a spreader beam when compared to when tested using a load tree. The authors explained that wind loading does not induce either uniform loading nor does it induce uniform displacement, because of this and because of the discrepancy mentioned above, they suggested the need to determine the “correct” loading mechanism. They also found that there was a significant increase in the capacity of the toe-nailed connection, but not for the hurricane tie connections. This was attributed to the fact that load sharing behavior is more predominant because of the high variability in capacity of the toe-nailed connections (Reed et al., 1997).

Morrison and Kopp (2011) conducted several tests on toe-nailed roof-to-wall connections using both ramp loading at several different rates and fluctuating loading based on the pressure time histories obtained from wind tunnel testing. They found that the overall mean maximum load capacity was the same for both the ramp loading cases and for the fluctuating load tests. This implies a lack of dependence of the connection capacity on the loading rate and agrees with the findings of Rosowsky and Reinhold (1999). The difference between the ramp loading and the fluctuating load

was that for the fluctuating load cases the failure occurred incrementally where the nail withdrawal occurred at several different peaks during the time history. The dominant failure mode (76% overall) was nail withdrawal from the top plate, but the capacities of the connections that experienced splitting failure of the rafter were higher than for the connections that failed in nail withdrawal. A possible conclusion from this is that splitting is most likely to occur when the nails are closer to the edge of the rafter, which implies that the nails were driven at a small angle indicating that the nails would have been loaded more in shear than in tension.

Cheng (2004) completed a study on the capacities of toe-nailed connections to investigate the influence of different variables such as nail size, wood species, and framing member size on the capacity of the connection and to see if these capacities would meet the requirements of different building codes. Connections using Douglas Fir (DF) timber framing members were found to have a higher capacity than the same type of connections that used Spruce-Pine-Fir (SPF) timber framing members. This was attributed to the significantly higher specific gravity of the Douglas Fir species of wood. The dominant failure mode of all of the toe-nailed connections was nail withdrawal from the top plate. Cheng also found that the allowable capacities (the average maximum load divided by a safety factor of 2.5) of all of the toe-nailed connections using nails were smaller than the required uplift loads of the model building codes ASCE 7-98, IBC 2000, and SSTD 10-99 for a 90 mph wind.

Conner et al. (1987) conducted tests on several different roof-to-wall connections and compared their capacities to the capacity of the conventional three 16d toe-nailed connection. They then calculated the wind speeds necessary to induce failure in these connections and compared them to the velocity frequency distributions of several different types of extreme wind events and found that with only small changes in the connection strengths would improve the connection performance to be able to resist the loading induced by almost all of the extreme wind events, including tornadoes (Conner et al., 1987).

Canfield et al. (1991) investigated the capacities of several types of roof-to-wall connections including toe-nailed connections with different types of nails, lag screw connections, and twelve different types of hurricane ties. The tests were done on individual connections. The capacities of the all of the hurricane ties were greater than all of the toe-nailed connections except for the toe-nailed connections using annularly threaded 16d nails which performed better than two types of hurricane clips. The lag screws also performed quite well with capacities larger than most of the

hurricane ties. The failure mode of the toe-nailed connections was predominately nail withdrawal from the top plate. The failure mode of the hurricane ties was dependent on how many and what types of nails were used to connect them to the wood framing members and the thickness of the metal tie. Canfield et al. (1991) also calculated the cost to install 100 of each of the types of hurricane ties and lag screws and found that the cost was insignificant compared to both the cost of construction of the house and the improved load capacity (Canfield et al., 1991).

Chapter 3 Experimental Set-up and Procedure

3.1 Introduction

The data obtained in any scaled experiment is only valuable if the experiment has been scaled correctly so as to adequately represent actual phenomenon. Although limited by the availability of data obtained in the field from actual tornadoes, enough is known about some characteristics of tornadoes that model-scale simulation of tornadoes can be carried out with a reasonable amount of confidence. These characteristics include maximum horizontal wind speed, radius of the core of the tornado and its path, swirl ratio, and translation speed. These characteristics have been shown by Haan et al. (2010) to influence the loading on low-rise buildings. Therefore, care was taken in this study to adjust the settings on the Iowa State University Tornado Simulator in order to simulate a tornado-like vortex that could be scaled up to represent a full-scale tornado. Attention was also paid to how the data was taken in order to ensure correct, usable data and that the dimensions of the models represented reasonable dimensions of full-scale low-rise buildings.

3.2 Tornado Simulator

The Iowa State University laboratory tornado simulator used in this study is composed of two concentric, circular ducts suspended over a ground plane which is capable of being raised or lowered with respect to the tornado simulator. The diameter, width and height of the outer duct are 5.49 m, 0.3 m and 3.35 m, respectively. The fan that supplies the updraft in the simulated tornado is housed in the inner duct and has a diameter of 1.83 m, has a maximum flow rate of 40.0 m^3/s, and is powered by 38 kW (50 Hp) motor. The updraft created by the fan is forced through angled vanes at the top of the simulator that initiate rotation in the flow which is then directed downward through the outer duct. As the rotating flow approaches the ground plane it is then drawn up through the fan creating a tornado-like vortex. The entire simulator hangs from an overhead crane allowing translation of the simulated tornado across the ground plane. The article by Haan et al. (2008) contains a detailed and full description of the design, construction and the tests done to validate the design of the simulator.

Several of the settings on the simulator can be varied to create tornadoes with different characteristics. These settings include fan speed, vane angle, floor height, crane translation speed, and ground plane roughness. The characteristics of the simulated tornado that are affected by the change in the settings include the tangential, radial and vertical velocities, radius of the maximum

tangential velocity, swirl ratio, inflow height, translation velocity, and ground roughness. The effect of a particular tornado characteristic on the wind loading on a given structure can be studied by varying one or more of the settings while keeping the rest of the settings constant. In this study all of the settings were kept constant except the translation speed. This resulted in one tornado that translated at two different velocities, allowing the effect of the translation velocity to be studied and to observe whether or not some of the trends due to varying translation speeds noted in previous studies were reproduced.

The tornado characteristics simulated in this study were chosen based on several considerations: physical limitations of the simulator, the importance of modeling a vortex that is as similar to an actual tornado as possible (this consideration is limited by the limited full-scale data available), scaling considerations, continuity with previous research, and the characteristics of tornadoes with high swirl ratios.

. Based on forensic evidence, most tornadoes (around 90%) are rated F2 or less (Bluestein and Golden, 1993) and, therefore, have estimated maximum horizontal wind speeds of around 72 m/s with an averaging time equivalent to a 3 second gust or less. In the Enhanced Fujita, or EF, scale this corresponds to an upper bound EF3 tornado, which is estimated to have a maximum velocity of 73.76 m/s (Texas Tech University, 2004). In ASCE 7-05 (ASCE, 2006) straight-line design wind speeds of many areas of the Gulf of Mexico and the Atlantic coasts of the United States are over 60 m/s and reach up to 67 m/s. The inclusion of straight-line design wind speeds of 67 m/s in ASCE-7 implies that it is possible to design low-rise structures to withstand wind speeds of those magnitudes. There is little evidence to show that if low-rise structures along the coasts of the United States can be designed to withstand 67 m/s wind speeds in a hurricane or other straight-line wind events then low-rise structures in “Tornado Alley” cannot be designed to withstand 72 m/s wind speeds in a tornado. Therefore, the design of low-rise structures to withstand tornadoes with maximum horizontal wind speeds of around 72 m/s (EF3) appears feasible.

Based on the statistics showing that 90% of all tornadoes are rated EF3 or less and that it seems feasible to design a low-rise building to resist EF3 tornado wind speeds, it was decided to collect wind load data corresponding to a simulated EF3-like tornado. Therefore, the tornado simulator vane settings were chosen with the intention of simulating a tornado-like vortex that would resemble a tornado of EF3 intensity.

In order to simulate a model-scale EF3 tornado the fan speed on the simulator was set at 20% of its maximum speed and the vane angle was set at 75°. These settings produced a maximum tangential velocity ($V_{\Theta max}$) in the simulated tornado that was measured to be 11.6 m/s at a height (z) of 19.05 mm and a maximum horizontal velocity (V_H) of 11.7 m/s at the same height. Using a full-scale tornado with a maximum horizontal velocity of 73.76 m/s as the full-scale tornado to be modeled gives a vortex velocity scale of λ_V = 11.7/73.76 or λ_V = 1/6.3 for a full-scale averaging time equivalent to the model-scale averaging time. Figure 3-1 presents profiles of the tangential velocity (normalized with respect to $V_{\Theta max}$ and the radius of the core, r_c) at 25.4 mm (1 inch) intervals; showing that as height increases the maximum tangential velocity at the respective heights decreases while the radius at which the maximum tangential velocity can be found increases. A contour plot of the tangential velocity can be found in Figure 3-2. As the distance from the center of the vortex increases the tangential velocity contours start to look more like boundary layer velocity profiles.

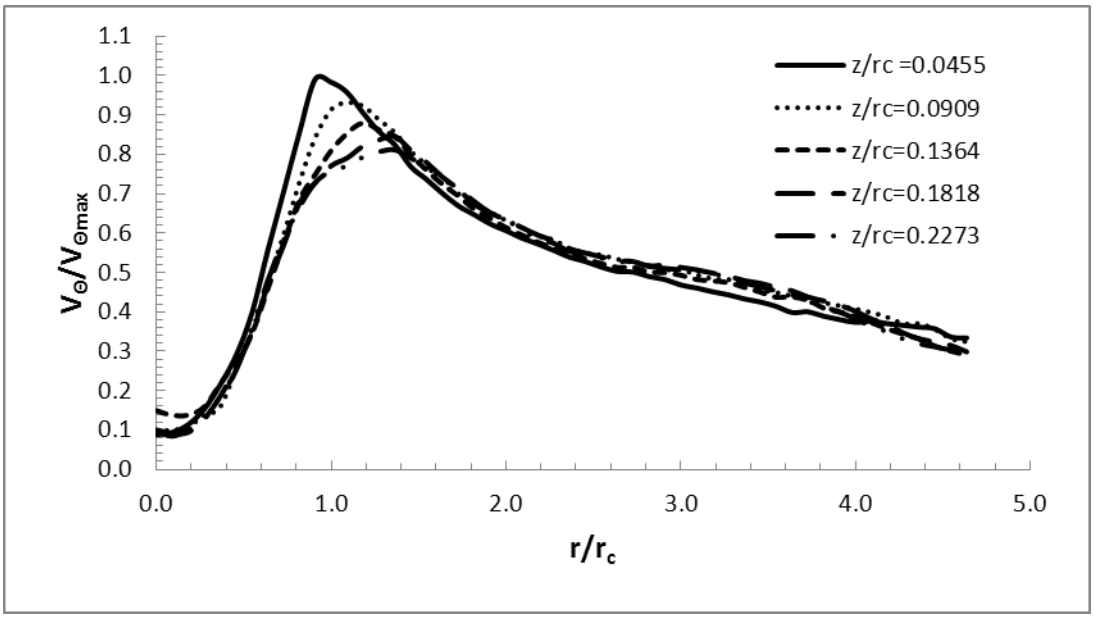

FIGURE 3-1 NORMALIZED TANGENTIAL VELOCITY PROFILES AT 25.4 MM INTERVALS

Brooks (2004) conducted a study using reported tornado damage path lengths and widths to model Weibull distributions of Fujita scale levels. The distributions produced by the study showed the probability of a tornado path width given the occurrence of a tornado at a specific Fujita scale

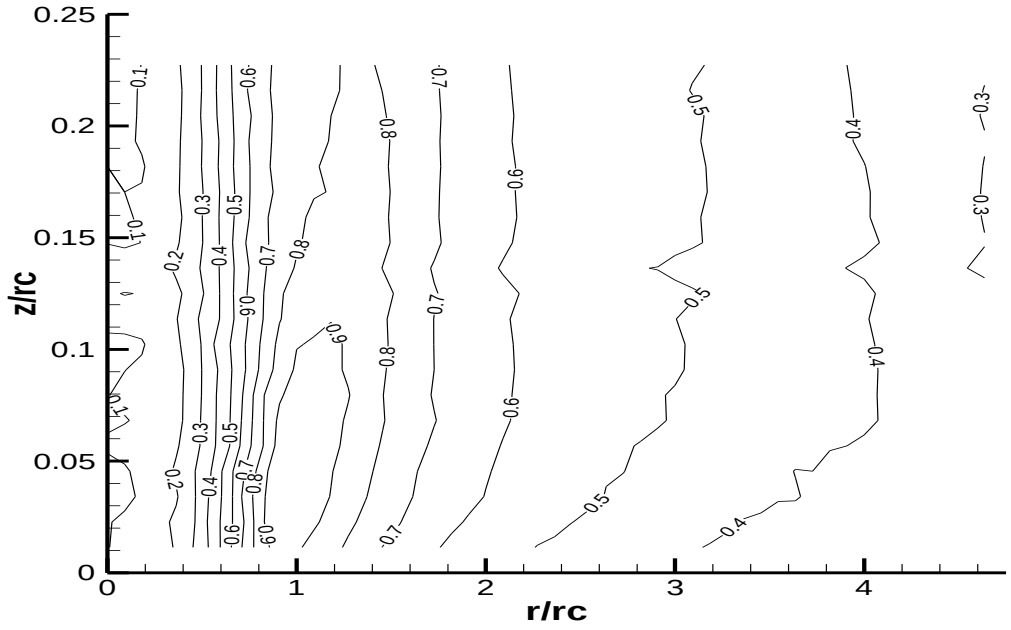

FIGURE 3-2 CONTOUR PLOT OF TANGENTIAL VELOCITY MAGNITUDES NORMALIZED WITH RESPECT TO $V_{\Theta MAX}$

intensity. His study showed that a tornado's mean path width increased with its Fujita scale rating. According to Brooks for a F1 or a F2 tornado (corresponding approximately to an EF2 or EF3 tornado) the path would most likely be between 100 and 500 meters.

One of the most commonly used parameters for laboratory and numerically simulated tornadoes is the swirl ratio (Haan et al., 2008; Hangan and Kim, 2008). Several studies have shown that the swirl ratio (S) is the parameter that governs other characteristics of a tornado (Church et al., 1979) (Hangan and Kim, 2008) including the radius of the vortex core (Davies-Jones, 1973). Both Davies-Jones (1973) and Church et al. (1979) showed that the vortex structure is related to the swirl ratio: as the swirl ratio increases the vortex breaks down into multiple vortices.

The data from full-scale tornadoes indicate swirl ratio values of 2.0 or greater. When comparing the full-scale data from the Spencer, South Dakota tornado with 3D numerical simulations, Hangan and Kim (2008) found that the best fit was for a swirl ratio of S=2 (Hangan and Kim 2008). Using data obtained with a Doppler on wheels (DOW), the swirl ratios of the Mulhall tornado were calculated by Lee and Wurman (2005) to be between 2 and 6 for the F4 (EF5) level tornado. Based on the latest data obtained by DOW and the best fit of that data with numerical results, it was decided that

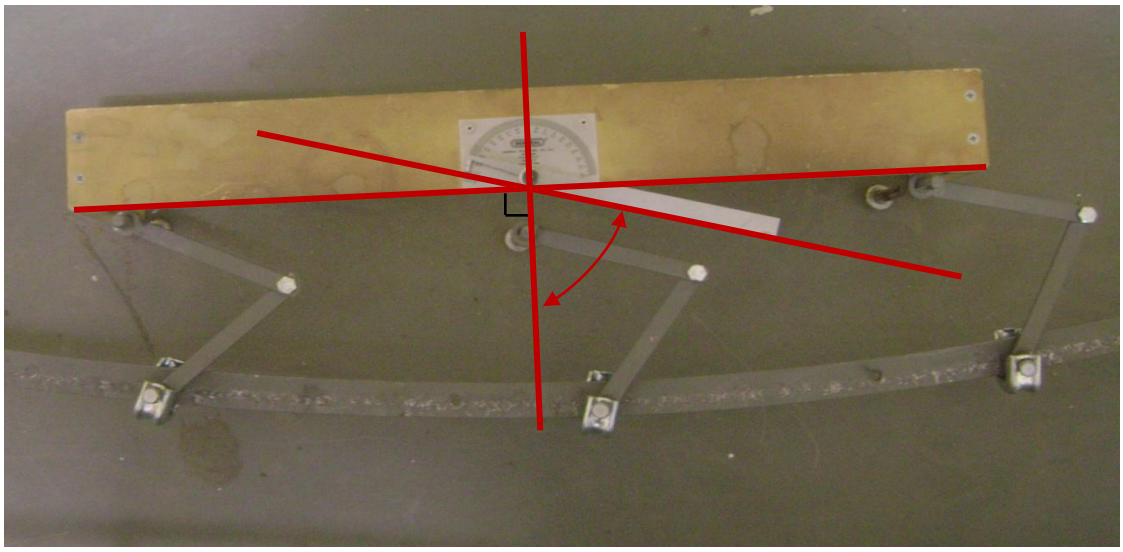

FIGURE 3-3 VANE ANGLE 75 SETTING SHOWING VANE ANGLE MEASURED FROM NORMAL TO THE TANGENT AT THE VANE LOCATION

an attempt should be made to increase the swirl ratio of the tornado used in this study to a value of 2 or greater.

The largest swirl ratio value reported in the literature is 1.14 (Haan et al., 2008). This swirl ratio was obtained in the ISU tornado simulator by using a vane angle of 55° on the tornado simulator (Haan et al., 2008). The easiest way to increase the swirl ratio on the Iowa State University's tornado simulator is to increase the vane angle (Haan et al., 2008). In order to obtain a swirl ratio higher than 1.14, the vane angle was set at 75°. Figure 3-3 shows the how the vane angle was set. This vane angle resulted in a radius of the core of 0.56 m and a swirl ratio of 2.6 as calculated using Eqn. 3-1. Using a length scale of λ_L = 1:100 the scaled up diameter of the vortex core was found to be 112 m. This matches well with the probable path width of an EF3 tornado according to the findings of Brooks (2004).

$$S = \frac{r_1 \Gamma}{2Q^{'} h} = \frac{\pi r_1^2 V_{\theta max}}{Q} \qquad (3\text{-}1)$$

Another setting on the ISU tornado simulator that can be adjusted to simulate the tornadoes with different characteristics is the floor height (i.e., the distance between the ground plane and the bottom of the circular ducts of the simulator). According to Haan et al. (2008) adjusting the floor height changes the inflow height which changes the radius of the maximum tangential velocity and changes the character of the radial velocity profile. According to Haan et al. (2008) the 0.46 m floor

height produced a radial velocity profile that matched the Spencer, South Dakota tornado quite well. A floor height of 0.46 m was chosen because it produced a radial velocity profile that matched well with full-scale data and to allow comparisons with previous studies that have used the same floor height (Haan et al., 2008; Sengupta et al., 2008; Haan et al., 2010; Thampi et al. 2011; Yang et al., 2010).

Pressure measurements on the building models were taken for translation speeds of 0.15 m/s and 0.46 m/s. If the same length scale (λ_L) is used to model both the vortex and the low-rise building model then, based on the concept of similarity, it is assumed that the amount of time for the full-scale tornado to pass over the full-scale building would be the same as the amount of time it would take the simulated tornado to pass over the model-scale building (i.e., the vortex translation time scale, λ_T, is equal to 1.0). The translation velocity scale is, therefore, the same as the length scale. This assumption was initially proposed by Haan et al. (2008). For a scale of 1:100, the two translation speeds become 15 m/s (33.6 mph) and 46 m/s (102.9 mph), respectively. Various translation speeds of full-scale tornadoes have been reported: 16.5 m/s (Thampi et al., 2011), 13 m/s (Lee and Wurman, 2005) and 23 m/s (Haan et al., 2008). The slower translation speed compares well with the reported speeds. The faster translation velocity was chosen to compare the loading effects of a rapidly moving tornado with those of the slower one and to verify the trends observed by other researchers (Haan et al., 2008).

The ground plane was made of smooth, varnished plywood, without being augmented by surface roughness blocks in order to represent smooth open terrain. Since much of "Tornado Alley" is rural farmland, open terrain was considered to be a valid and useful exposure to use in the study.

3.3 Models

Nine models were constructed using rapid prototyping and contained anywhere from 106 to 124 pressure taps depending on the model. Model dimensions were selected so that the models would have realistic, scaled low-rise building dimensions and so that the effect of roof height, aspect ratio, roof pitch, overhang and an attached garage on the external pressures and forces due to the simulated tornado could be observed. The selection of the dimensions was based on commonly available, simple house plans. A table similar to Figure 6-6 in ASCE-7 2005 (ASCE, 2006) (see Table 3-1 below) where roof pressure coefficients are tabulated as functions of mean roof height divided by

the length of the building, wind direction and roof pitch, was also used to aid in selecting the model dimensions.

Table 3-1 SELECTION OF MODELS 1-6 AS ADAPTED FROM TABLE 6-6 OF ASCE 7-05 (ASCE, 2006)

h/L	5°	10° ≤ Θ < 15°	15° ≤ Θ < 20°	20° ≤ Θ < 25°	25° ≤ Θ < 30°	30° ≤ Θ < 35°	35° ≤ Θ < 45°	45° ≤ Θ < 60°	60°≤Θ< 80°
≤ 0.25									
0.5							**6**		
			1						
	3		4				**5**		
			2						
≥ 1.0									

Table 3-2 FULL-SCALE DIMENSIONS OF MODELS 1-6

	Θ	B	L	he	ht	h	L/B	h/L
model	degrees	ft	ft	ft	ft	ft		
1	16	32	48	19.59	24.18	21.88	1.5	0.46
2	16	32	48	35.99	40.58	38.29	1.5	0.80
3	4.6	32	32	17.32	18.64	17.32	1	0.54
4	16	32	32	15.65	20.24	17.95	1	0.56
5	35.5	32	32	12.17	23.65	17.91	1	0.56
6	35	73	73	12.17	37.43	24.80	1	0.34

ht = total height he = eave height h = mean roof height as defined in ASCE 7-05
L = longer plan dimension B = shorter plan dimension Θ = roof pitch

Table 3-3 DIMENSIONS FOR MODELS 1-6

	Θ	B	L	he	ht	h	L/B	h/L
		mm	mm	mm	mm	mm		
model 1	15.95°	98	146	59.7	73.7	66.7	1.5	0.46
model 2	15.95°	98	146	109.7	123.7	116.7	1.5	0.80
model 3	4.6°	98	98	52.8	56.8	52.8	1.0	0.54
model 4	15.95°	98	98	47.7	61.7	54.7	1.0	0.56
model 5	35.5°	98	98	37.1	72.1	54.6	1.0	0.56
model 6	35°	221	221	37.1	114.1	75.6	1.0	0.34

ht = total height he = eave height h = mean roof height as defined in ASCE 7-05
L = longer plan dimension B = shorter plan dimension Θ = roof pitch

The full-scale and model-scale dimensions of models 1-6 can be found in Table 3-1 and Table 3-2, respectively. Model 7 was based on model 1 with an overhang and an enclosed soffit. Model 8 was simply model 5 with an attached 2 car garage. Model 9 was model 1 with an attached 2 car garage. Both garage additions were 89 mm long, 98 mm wide and had an eave height of 33 mm, a ridge height of 47 mm and a roof pitch of 15.95°. A scaled drawing of the 9 models can be found in Figure 3-4.

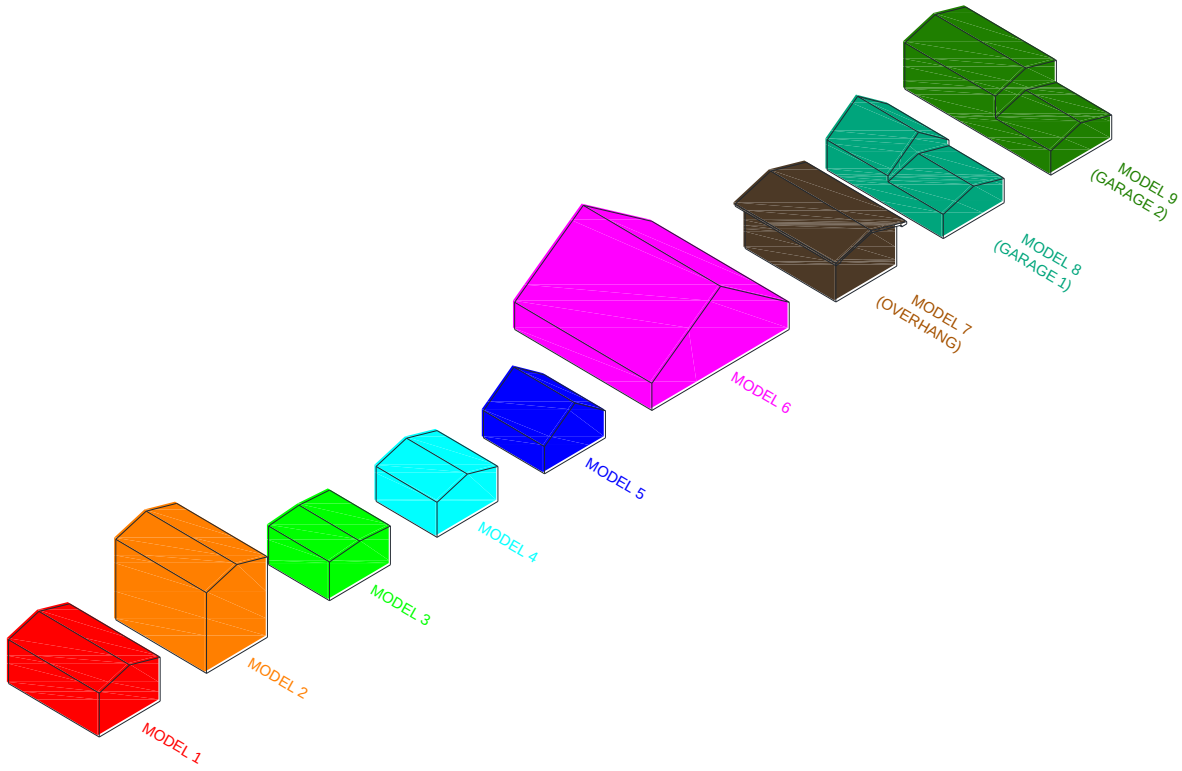

Figure 3-4 SCALED DRAWING OF MODELS 1-9

For models 1 through 6 and the overhang model the pressure taps along the walls and roof were placed in an evenly spaced grid with 3 rows and 5 columns of pressure taps on each plane of the respective models. The first and fifth columns were placed 6 mm from the edge, the middle column was located half the plan dimension from the edge and the other two columns were placed half the distance between the edge columns and the middle columns of taps. A 3x3 array of pressure taps was also placed on the leading-windward and the trailing-leeward corners of the roof. The 3x3

corner array taps were spaced 10 mm on center for models 1, 2, 6 and the model with the overhang. The smaller size of models 3, 4 and 5 required spacing other than 10 mm x 10 mm in order to prevent overlapping of pressure taps in the smaller corner array with the pressure taps in the larger 3 x 5 array. The garage model pressure taps were placed in arrays so that the effect of the garage on the roof and gable pressures could be measured. The overhang model had an additional 5 pressure taps on the soffit on each side of the house. Figures of the pressure tap locations and numbers can be found in Appendix A.

Rapid prototyping was considered to be more appropriate for constructing the models used in this study when compared with Plexiglas. Rapid prototyping not only allowed the models to be constructed with fewer difficulties, but also allowed the dimensions of the model and the locations of the pressure taps to be both more precise and more accurate. Rapid prototyping also made placing pressure taps in the soffit of the overhang model possible.

3.4 Instrumentation

Pressure measurements were taken using two high speed 64-channel Scanivalve ZOC33/64Px pressure scanners. Pressure readings were taken for 20 seconds at a frequency of 390 Hz for the 0.15 m/s translation speed and for 11 seconds at a frequency of 390 Hz for the 0.46 m/s translation speed. These times (20 seconds and 11 seconds) were sufficiently long enough to capture the complete pressure time histories of the tornado influencing the external pressures on the low-rise building models. The translation of the crane and the taking of pressure readings were synchronized using an external trigger.

The tubing system used to convey the pressures from the surface of the models to the pressure scanners consisted of 381 mm long, 1 mm inner diameter tubing glued to the pressure taps and short 1 mm inner diameter tubing connected to the pressure scanners. The 381 mm long tubing and the short tubing were connected using small metal restrictor tubing to aid in switching between models.

Pressure measurements of the stationary tornado were also taken on the ground plane using the high speed 64-channel Scanivalve ZOC33/64Px pressure scanner. Pressures were taken for 26 seconds at a frequency of 390 Hz. The pressure taps on the ground plane consisted of 29 pressure taps spaced 50.8 mm apart in a line perpendicular to the direction of the tornado translation. The pressures on the ground plane were taken with the tornado simulator centered above the row of pressure taps. The simulator was moved in intervals of 25.4 mm for each subsequent sampling. The process was repeated by re-centering the simulator above the row of pressure taps and then moving it in the opposite direction of the first set of data sampling in intervals of 25.4 mm. The normalized pressure distribution on the ground plane in the center of the simulator for a stationary (i.e. non-translating) tornado can be found in Figure 3-4

Wind velocity measurements were taken for 26 seconds at a sampling frequency of 78.1 Hz with a 4-hole Cobra probe. Measurements were taken at points spaced at 50.8 mm horizontally and 6.35mm vertically. The measurements were taken starting at a height of 6.35 mm until a height of 127 mm (corresponding to a full-scale height of 12.7 m) and for a horizontal length of 2.64 meters at each height.

The cobra probe set-up can be seen in Figure 3-5. The hole in the cobra probe measuring the U component of the wind velocity was aligned perpendicular to the crane translation direction and placed on the centerline of the simulator. This configuration was assumed to measure the

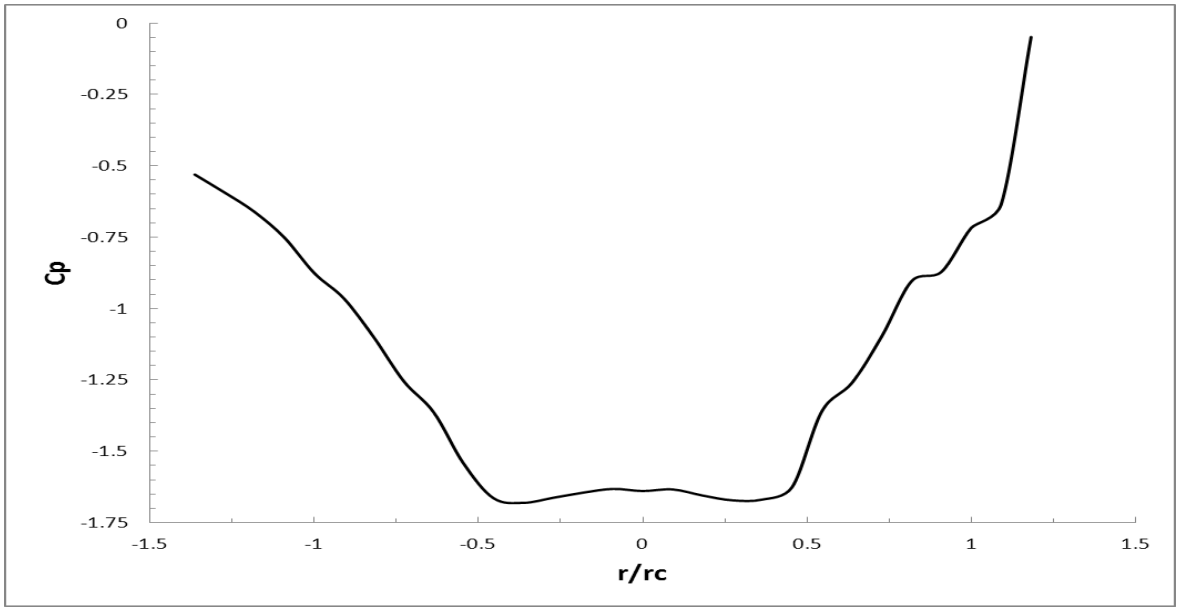

FIGURE 3-5 GROUND PLANE PRESSURE COEFFICIENT DISTRIBUTION NORMALIZED USING V_{HMAX}

FIGURE 3-6 COBRA PROBE SET UP FOR WIND VELOCITY MEASUREMENTS

tangential velocity as the U component of the wind as recorded by the Cobra probe. The Cobra probe was moved vertically using a vertical traverse and the tornado simulator was moved horizontally to achieve the readings at each desired location in the simulated tornado. The readings were taken while the tornado simulator was stationary (i.e. not translating).

Velocity measurements were taken only until a height of 127 mm for several reasons. The foremost reason is that all of the models tested had heights of less than 127 mm; therefore, the maximum wind velocity experienced by each of the models could be determined without taking velocity measurements above 127 mm. The second reason, which is related to the first, is that this study is more focused on the effect of the tornado on low-rise buildings rather than on the structure of the tornado itself. Another reason is that the maximum horizontal velocity is the most relevant velocity for correlating the external pressures with building damage and the maximum wind in a tornado is generally very close to the ground (Hangan and Kim, 2008). Haan et al. (2008) found that the tangential velocities reached a constant, maximum value at a height typically less than $0.25r_c$. The

simulated tornado used in this study was found to have a radius of the core (r_c) of 0.56 meters giving a value of $0.25r_c$ = 139.7 mm. The velocity measurements taken in this study confirm the findings of Haan et al. (2008) as the maximum tangential velocity was found to be at a height of less than 127 mm. If comparison between straight line and tornado wind speeds were of interest, 127 mm scales up to 12.7 meters which is higher than the 10 meter height often used as a reference height in straight line wind studies.

The static pressure used in both the pressure and the velocity measurements was taken as the laboratory ambient pressure under the ground plane.

3.5 Experimental Procedure

For each test case the pressures were recorded 10 times. The peak pressures were calculated as the average of the peak pressures from each of the 10 runs. The orientation of the building with respect to the direction of translation of the tornado was varied from 0° to 90° with a step size of 15°. The building orientation angle (BOA) of 0° was for the test case when the roof ridge of the model was parallel to the direction of translation of the tornado. The garage models (models 8 and 9) were tested from 0° to 90° (orientation A) and from 180° to 270° (orientation B). The house part of the garage models experienced the tornado first for orientation A and the garage experienced the tornado first for orientation B, as shown in Figure 3-8. For all of the test cases the tornado translation axis passed through the center of the building model. The test matrix can be seen in Table 3-4.

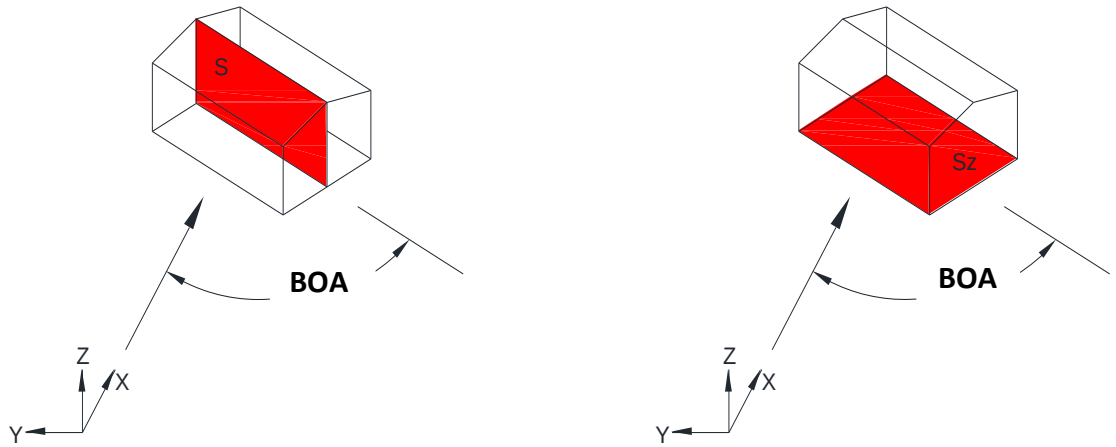

Figure 3-7 BUILDING ORIENTATION ANGLE (BOA) WITH RESPECT TO TORNADO PATH AND AREAS USED TO NORMALIZE FORCE COEFFICIENTS

Table 3-4 TEST MATRIX SHOWING TEST CASES 1-154

	VT= 0.15 m/s							VT= 0.46 m/s						
Model	0°	15°	30°	45°	60°	75°	90°	0°	15°	30°	45°	60°	75°	90°
Model 1	1	2	3	4	5	6	7	8	9	10	11	12	13	14
Model 2	15	16	17	18	19	20	21	22	23	24	25	26	27	28
Model 3	29	30	31	32	33	34	35	36	37	38	39	40	41	42
Model 4	43	44	45	46	47	48	49	50	51	52	53	54	55	56
Model 5	57	58	59	60	61	62	63	64	65	66	67	68	69	70
Model 6	71	72	73	74	75	76	77	78	79	80	81	82	83	84
Overhang	85	86	87	88	89	90	91	92	93	94	95	96	97	98
Garage 1														
orientation A	99	100	101	102	103	104	105	106	107	108	109	110	111	112
orientation B	113	114	115	116	117	118	119	120	121	122	123	124	125	126
Garage 2														
orientation A	127	128	129	130	131	132	133	134	135	136	137	138	139	140
orientation B	141	142	143	144	145	146	147	148	149	150	151	152	153	154

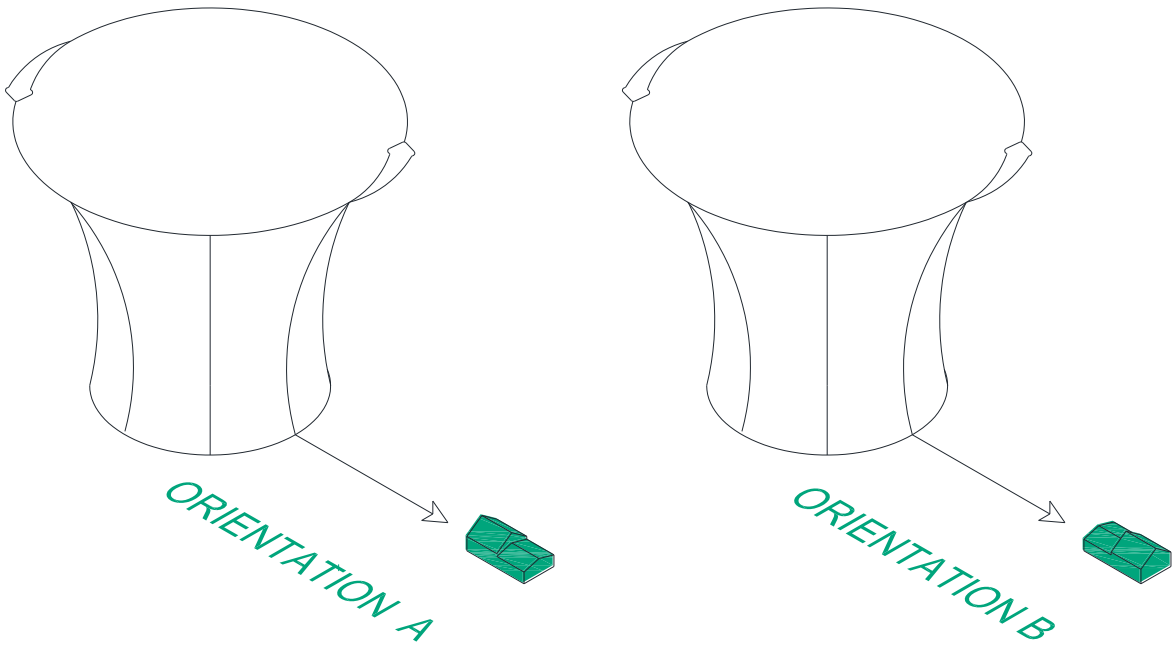

Figure 3-8 ORIENTATIONS A AND B OF MODELS 8 AND 9

Chapter 4 Results and Analysis

This chapter presents the results from testing the nine low-rise building models in a high swirl ratio tornado like vortex simulated at the Wind Simulation and Testing Laboratory at Iowa State University. The first part of this chapter presents the results of the laboratory tests by comparing the effect of the roof and building geometry on the aerodynamic force coefficients obtained in the tornado simulation. The second part of the chapter discusses what effects forces from a full-scale tornado similar to the one simulated would have on the roofs of the full-scale equivalents of model 1 and model 5.

4.1 Effect of Roof Geometry on Aerodynamic Force Coefficients

Nine low-rise building models were tested in a laboratory simulated, high swirl ratio tornado with building orientation angles (BOA) with respect to the tornado path varying from 0° to 90°. Two of those models were also tested for BOA's varying from 180° to 270° (i.e. the two garage models orientation B).

4.1.1 Conventions Used in Presentation of the Data

The aerodynamic force coefficients (C_{Fx}, C_{Fy}, and C_{Fz}) were computed along the x (horizontal direction parallel to the tornado's translation direction), y (horizontal direction perpendicular to the tornado's translation direction), and z (vertical) directions. An xy force coefficient (C_{Fxy}) which was computed as the square root of the sum of the squares of the x and y force coefficients was also considered important as a quantity expressing the total drag force on the low-rise building model. The x and y force coefficients were normalized with an area of the model equal to the height of the ridge of the roof times the length of the roof ridge. The z coefficient was normalized with an area equal to the floor plan of the model.

$$C_{F_x} = \frac{F_x}{\frac{1}{2}\rho V_H^2 S} \quad (4\text{-}1)$$

$$C_{F_y} = \frac{F_y}{\frac{1}{2}\rho V_H^2 S} \quad (4\text{-}2)$$

$$C_{F_z} = \frac{F_z}{\frac{1}{2}\rho V_H^2 S_z} \quad (4\text{-}3)$$

$$C_{F_{xy}} = \sqrt{C_{F_x}^2 + C_{F_y}^2} \quad (4\text{-}4)$$

The forces used to calculate the force coefficients were obtained by summing the respective components of the average pressure from each of the 10 trials at each time step for each pressure tap multiplied by its respective tributary area.

Time histories of each force coefficient were plotted with respect to both simulation time and to the distance of the center of the simulator to the center of the model normalized with the diameter of the simulated tornado. The color of each plot corresponds to the color of the model in Figure 3-6. The time histories of the two garage models (i.e. model 8 and model 9) for the "B" orientation (i.e. the model turned 180° from the "A" orientation) are plotted in purple and black respectively. The models were plotted in 3 separate subplots for clarity. The subplots for a given translation speed and building orientation angle (BOA) are plotted at the same scale and share the same x axes but have respective y axes.

The peaks of each force coefficient were then tabulated for each BOA with respect to the tornado path. The tables are formatted with a color scale where the maximum for each model is red, circled and has bold font, the lowest peak for each model is green and the 50th percentile is yellow.

4.1.2 C_{Fx}

The x direction force coefficient time histories of each model for the 0°-90° building orientations and 0.15 m/s translation speed are given in Figures 4-1 through 4-7 and the time histories for the 0.46 translation speed are shown in Figures 4-8 through 4-14. The tabulated peak values are given in Table 4-1 for the 0.15 m/s translation speed and Table 4-2 for the 0.46 m/s translation speed. The peaks listed in the tables are absolute values.

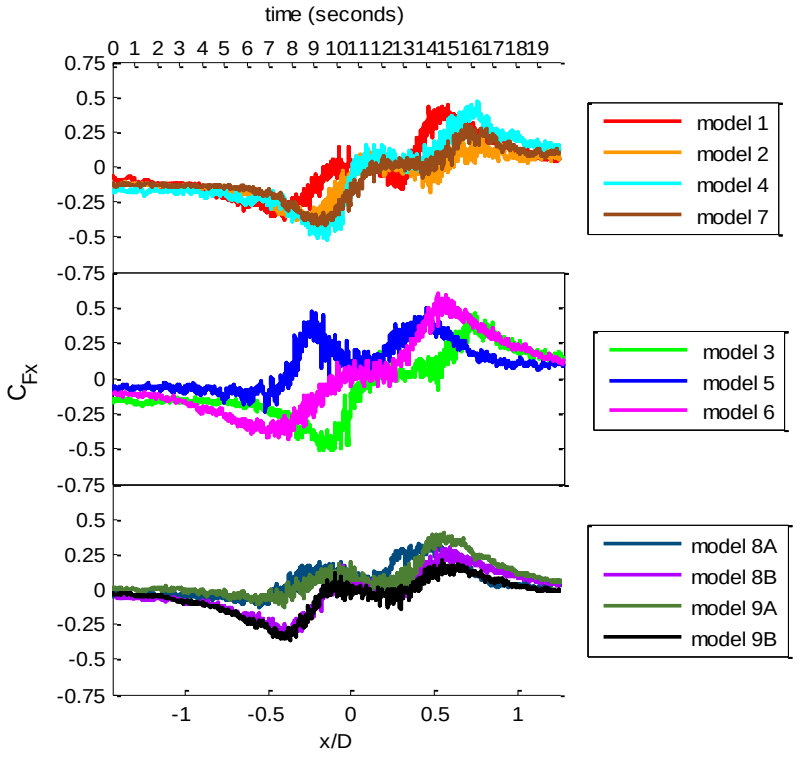

FIGURE 4- 1 CFX TIME HISTORIES VT=0.15 M/S BUILDING ORIENTATION = 0 DEGREES

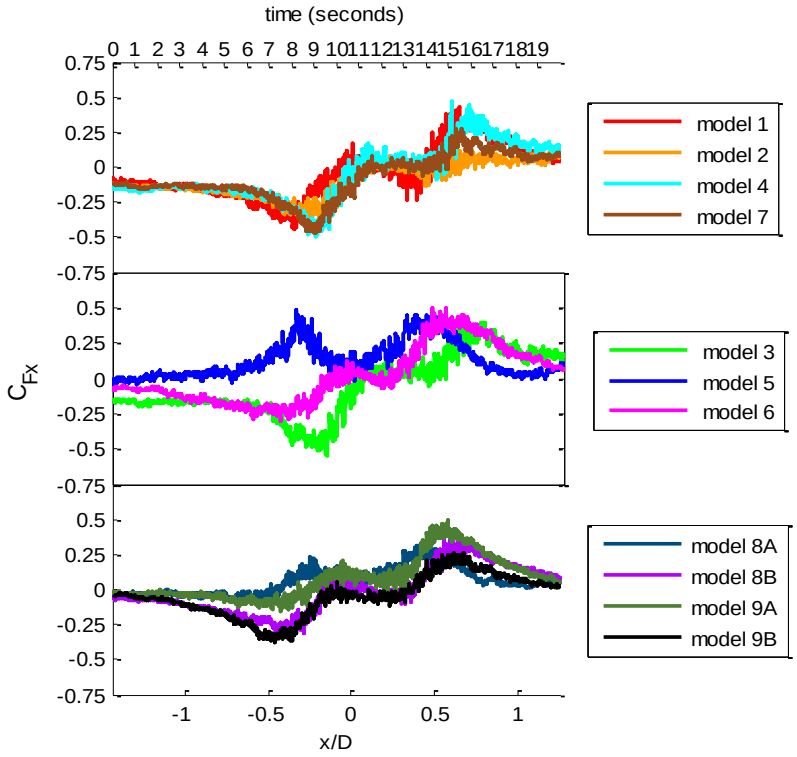

FIGURE 4- 2 CFX TIME HISTORIES VT=0.15 M/S BUILDING ORIENTATION = 15 DEGREES

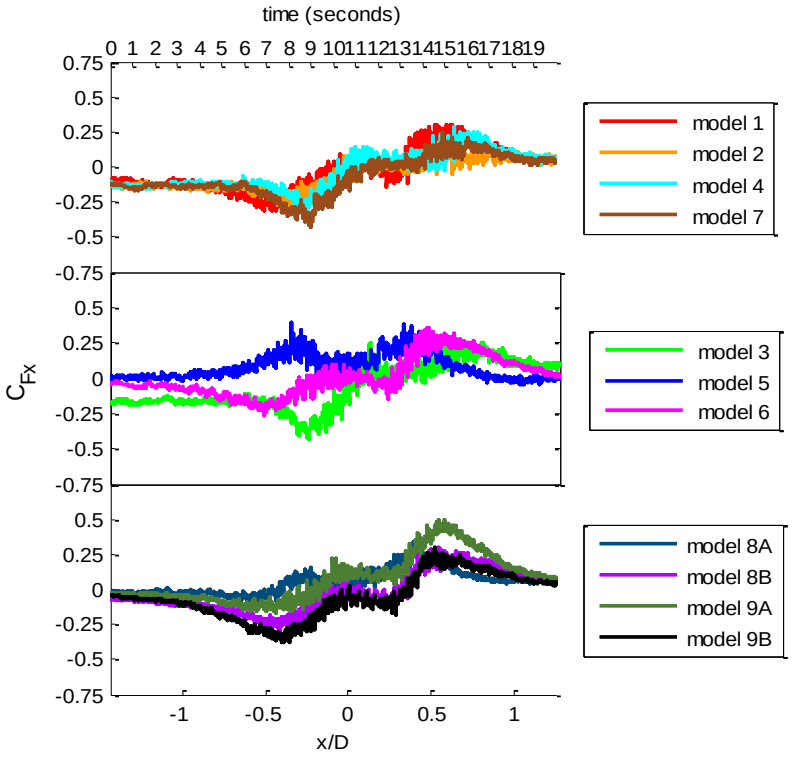

FIGURE 4- 3 CFX TIME HISTORIES VT = 0.15 M/S BUILDING ORIENTATION = 30 DEGREES

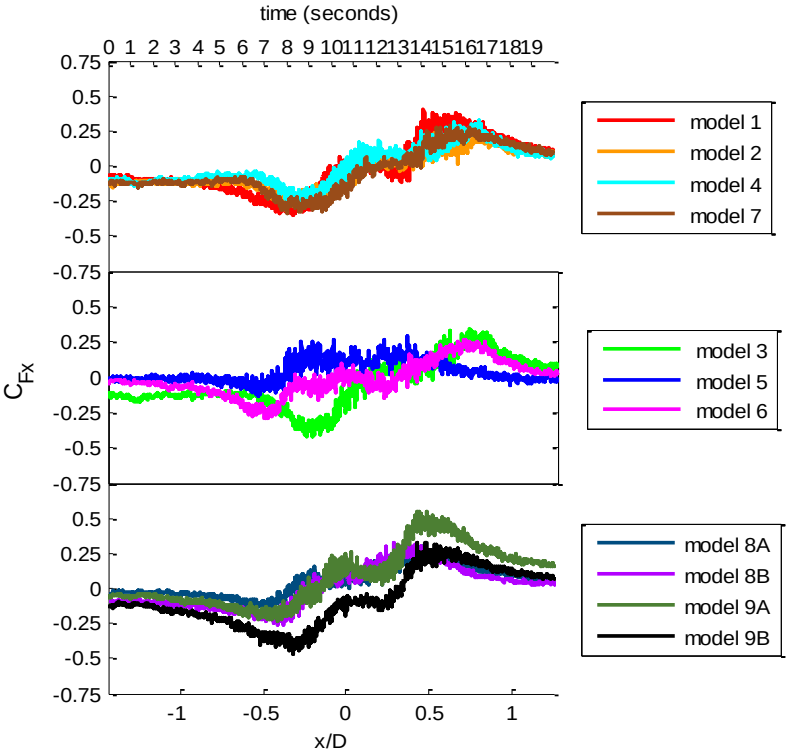

FIGURE 4- 4 CFX TIME HISTORIES VT = 0.15 M/S BUILDING ORIENTATION = 45 DEGREES

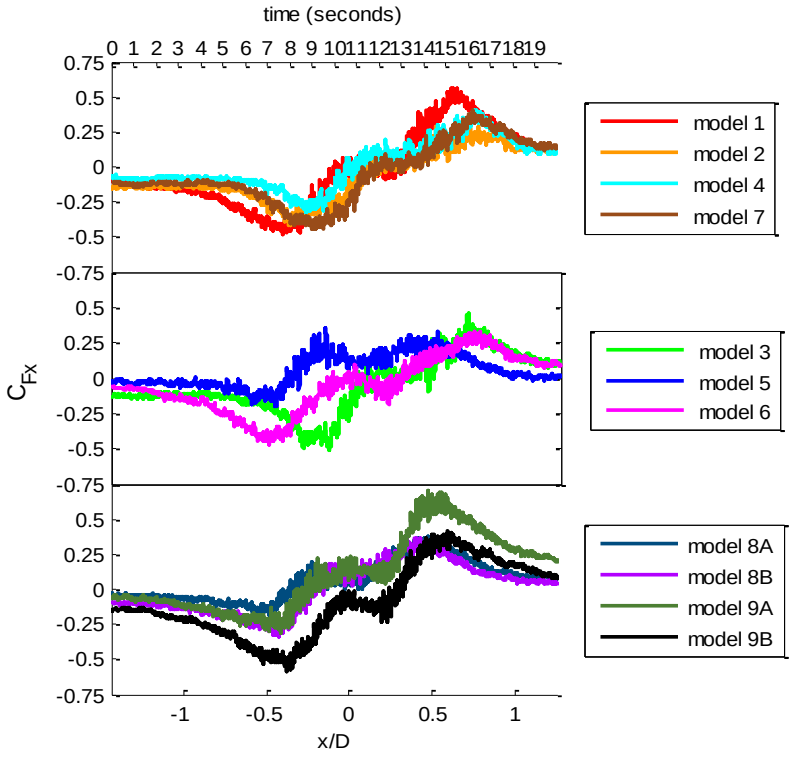

FIGURE 4- 5 CFX TIME HISTORIES VT = 0.15 M/S BUILDING ORIENTATION = 60 DEGREES

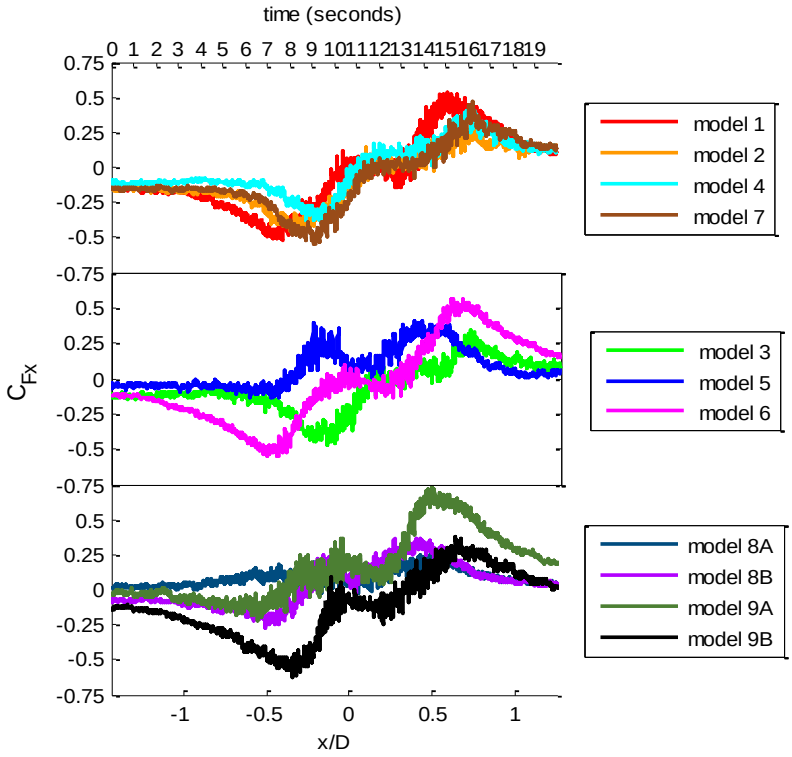

FIGURE 4- 6 CFX TIME HISTORIES VT = 0.15 M/S BUILDING ORIENTATION = 75 DEGREES

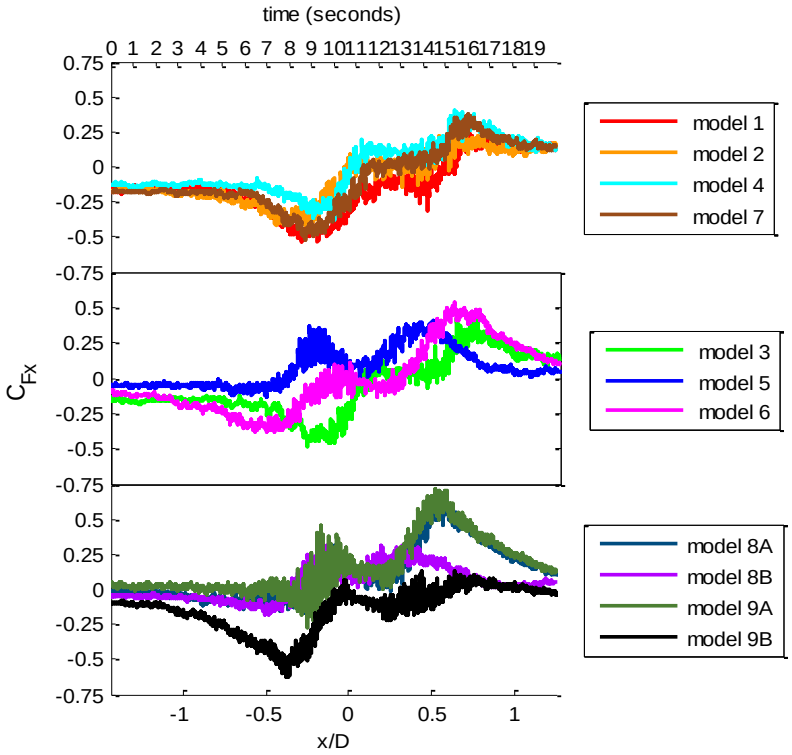

FIGURE 4- 7 CFX TIME HISTORIES VT = 0.15 M/S BUILDING ORIENTATION = 90 DEGREES

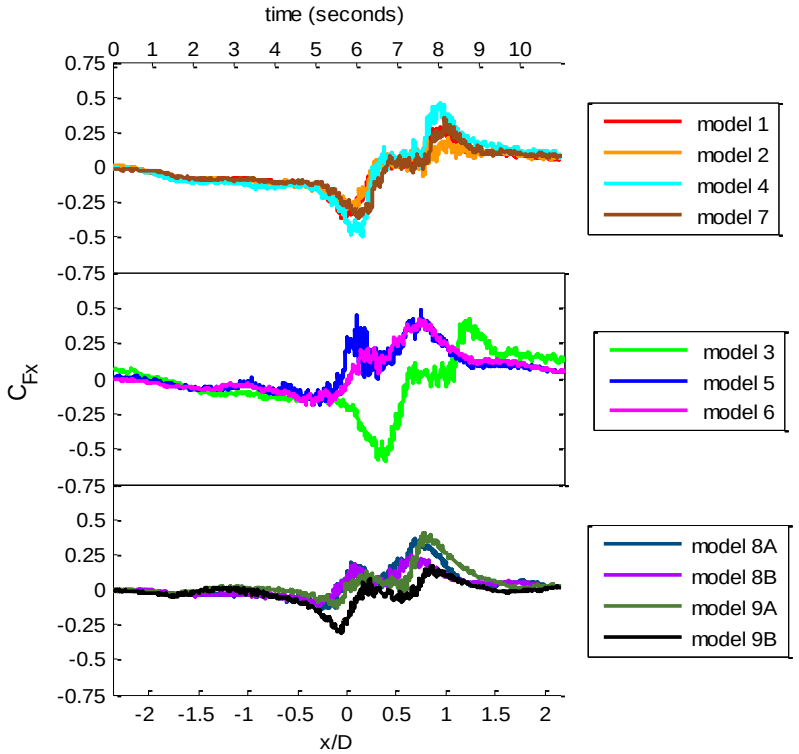

FIGURE 4- 8 CFX TIME HISTORIES VT = 0.46 M/S BUILDING ORIENTATION = 0 DEGREES

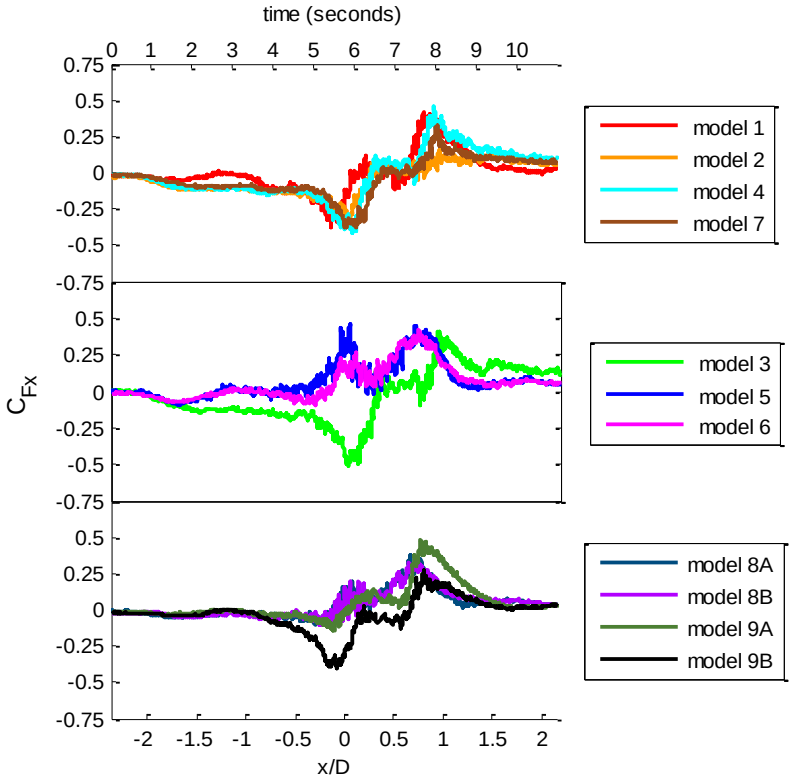

FIGURE 4- 9 CFX TIME HISTORIES VT = 0.46 M/S BUILDING ORIENTATION = 15 DEGREES

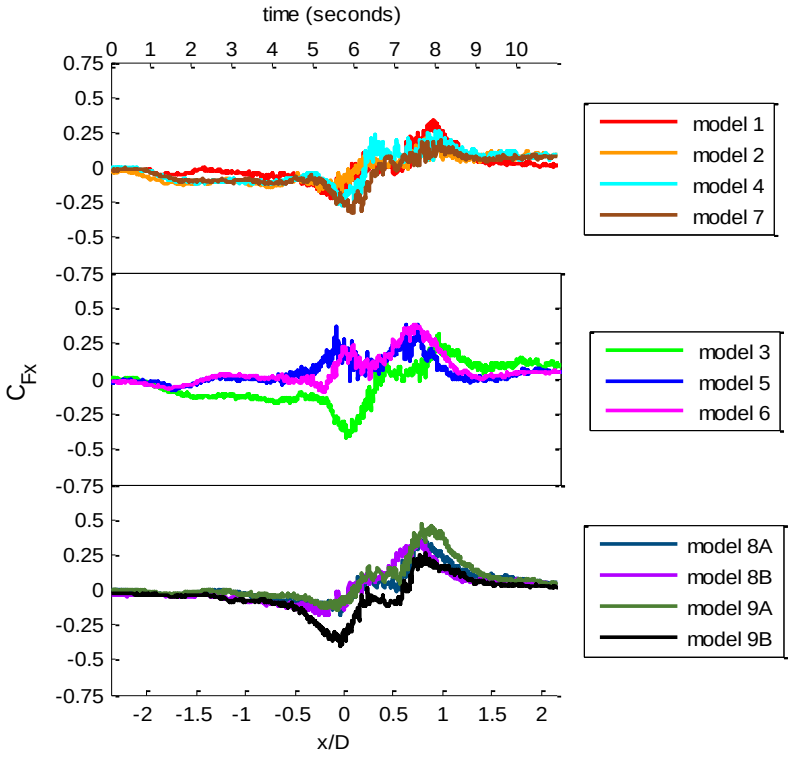

FIGURE 4- 10 CFX TIME HISTORIES VT = 0.46 M/S BUILDING ORIENTATION = 30 DEGREES

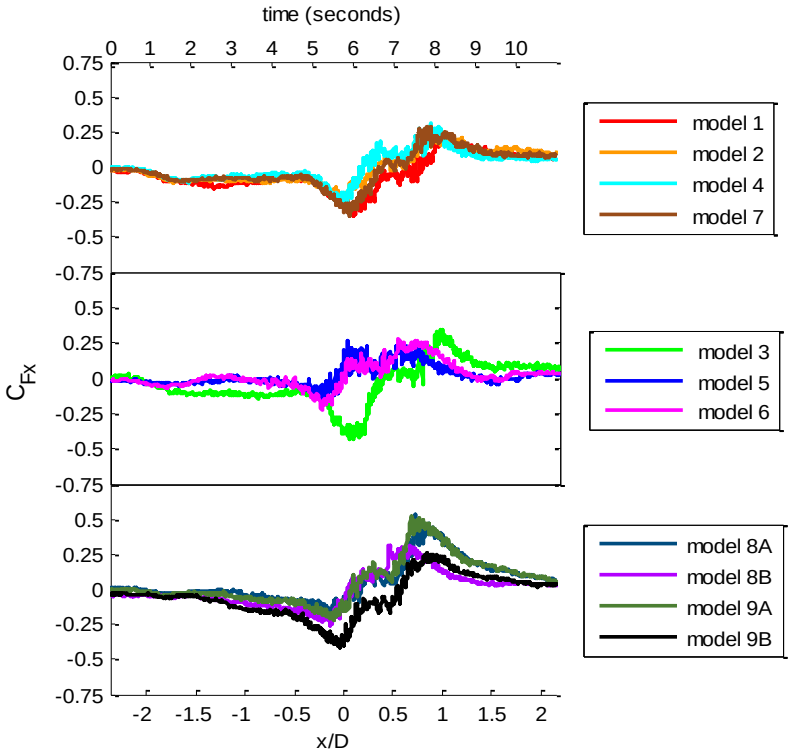

FIGURE 4- 11 CFX TIME HISTORIES VT = 0.46 M/S BUILDING ORIENTATION = 45 DEGREES

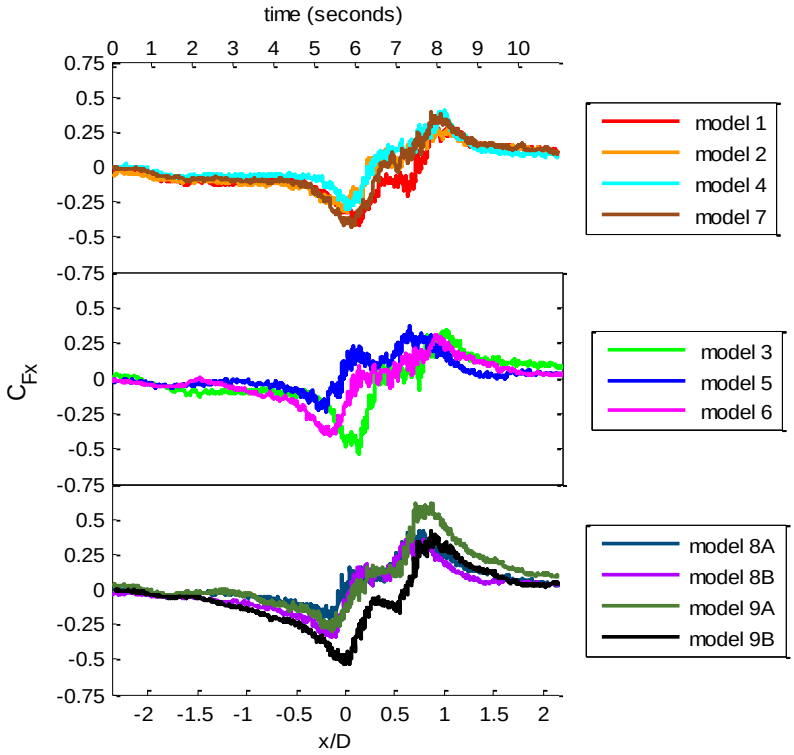

FIGURE 4- 12 CFX TIME HISTORY VT = 0.46 M/S BUILDING ORIENTATION = 60 DEGREES

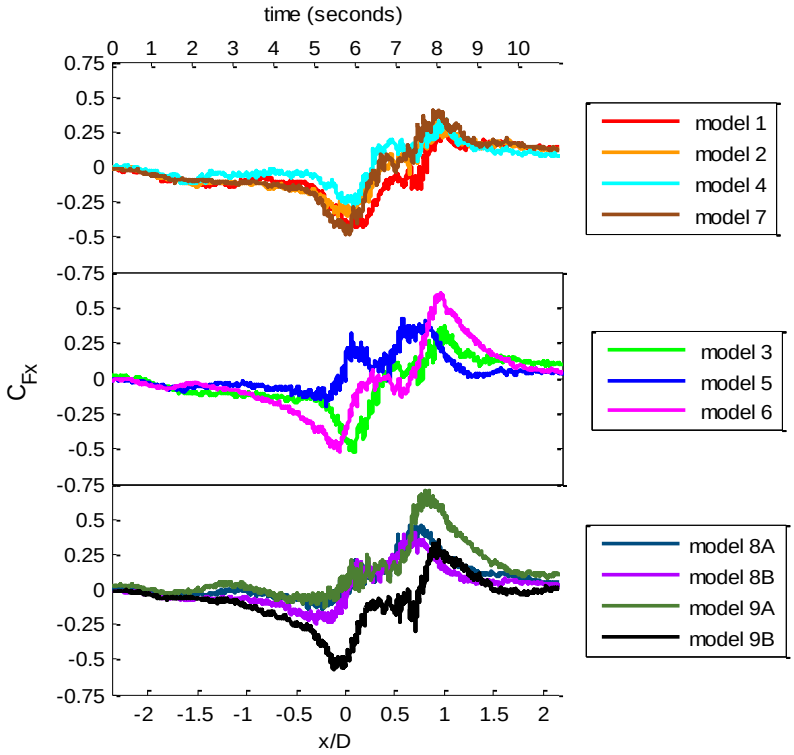

FIGURE 4- 13 CFX TIME HISTORIES VT = 0.46 M/S BUILDING ORIENTATION = 75 DEGREES

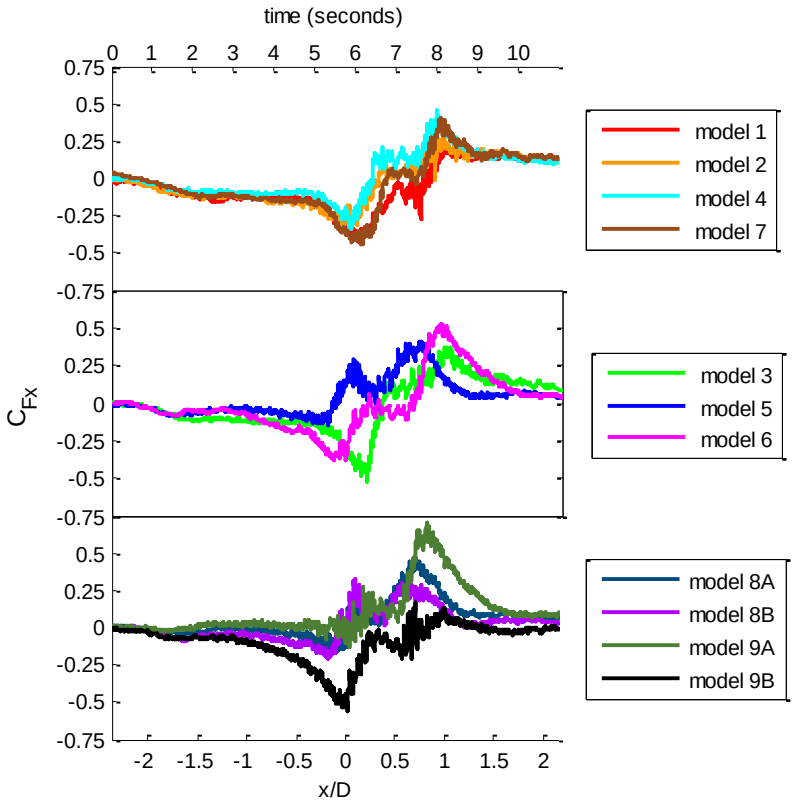

FIGURE 4- 14 CFX TIME HISTORIES VT = 0.46 M/S BUILDING ORIENTATION = 90 DEGREES

The C_{FX} time histories are composed of several distinct parts. The time history begins at a value close to zero and continues almost constant until the tornado is close enough to begin affecting the pressure on the surface of the model. The second part causes a force in the negative x direction (opposite of the direction of translation) as the tornado reaches the model and the model begins to experience negative surface pressures caused by the atmospheric pressure drop due to the swirling winds. For some models this negative part of the time history is very small or even non-existent. This is especially the case for model 5 for building orientations 15° and 30°. As the tornado passes over the building model the force coefficient in the direction of translation returns to zero and then becomes increasingly positive until it reaches a peak and then returns to zero as the tornado continues past it. For the 0.15 m/s translation speed cases, the CFx changes from zero and then back to zero between the x/D values of -1 and 1 indicating that the loading of the building in the x direction begins when the tornado is about a distance equal to one core diameter from the center of the building. The time histories for the VT = 0.46 m/s cases show that the tornado loading mainly occurs between the normalized distances of x/D = -0.5 until about x/D = 1.5. This is caused by the lagging behind of the lower portion of the tornado due to the faster translation speed.

Haan et al (2010) conducted a study on a model of similar in geometry and the same roof angle as model 5 for various simulator vane settings. It was found that the peak minimum C_{Fx} decreased in magnitude and approached zero as the vane angle was increased. For the Vane 5 (55°) setting and building orientations of 15° through 45° the minimum C_{Fx} was determined to be almost zero and was attributed to the multi-cell structure of the vortex (Haan et al., 2010). This trend is continued for the Vane 7 (75°) settings used in this study to the point that the minimum peak is no longer negative but rather positive for model 5.

The two pronounced positive C_{Fx} peaks for model 5 and building orientations 15° and 30° can be observed also for the tests with a translation speed of 0.46 m/s. It is also interesting to note that model 6, which has the same roof pitch and eave height but much larger plan dimensions, follows the trend of the other models when the translation speed is 0.15 m/s but follows the trend of model 5 when the translation speed is 0.46 m/s. It can also be seen from the time histories that for some building orientations even model 5 follows the expected trend. This phenomenon, therefore, is not necessarily caused solely by building height, plan area, roof pitch, translation speed, or other

tornado characteristics but rather by certain combinations of these variables. The exploration of this phenomenon is outside the scope of this study and is therefore left to future research.

TABLE 4- 19 PEAK CFX VT = 0.15 M/S

MODEL / orientation	1	2	3	4	5	6	Overhang	G1A	G1B	G2A	G2B
0°	0.44	0.40	0.52	**0.52**	**0.50**	**0.60**	0.42	0.33	0.33	0.41	0.36
15°	0.44	0.38	**0.55**	0.50	0.49	0.50	0.47	0.32	**0.38**	0.50	0.37
30°	0.32	0.29	0.43	0.32	0.40	0.36	0.43	0.33	0.31	0.49	0.38
45°	0.40	0.31	0.42	0.32	0.29	0.29	0.34	0.31	0.33	0.55	0.47
60°	**0.57**	0.41	0.51	0.41	0.36	0.47	0.45	0.38	0.37	0.70	0.58
75°	0.54	**0.46**	0.48	0.41	0.41	0.56	**0.55**	0.27	0.37	**0.73**	**0.62**
90°	0.54	0.43	0.49	0.40	0.41	0.54	0.52	**0.69**	0.32	0.71	0.62

G = garage A and B = orientation

TABLE 4- 20 PEAK CFX VT = 0.46 M/S

MODEL / orientation	1	2	3	4	5	6	Overhang	G1A	G1B	G2A	G2B
0°	0.36	0.30	**0.58**	**0.49**	**0.49**	0.42	0.36	0.36	0.25	0.41	0.32
15°	0.42	0.35	0.51	0.46	0.45	0.42	0.38	0.38	0.36	0.48	0.40
30°	0.34	0.20	0.42	0.27	0.39	0.38	0.33	0.35	0.37	0.47	0.40
45°	0.35	0.26	0.44	0.31	0.26	0.28	0.35	**0.53**	0.32	0.52	0.42
60°	0.42	0.32	0.54	0.41	0.37	0.41	0.43	0.42	0.36	0.61	0.54
75°	0.43	**0.36**	0.52	0.34	0.42	**0.60**	**0.48**	0.46	**0.41**	0.71	**0.57**
90°	**0.43**	0.34	0.52	0.45	0.41	0.53	0.45	0.47	0.32	**0.71**	0.56

G = garage A and B = orientation

From a comparison of Table 4-1 and Table 4-2 it was observed that the maximum CFx between the two models for each building orientation was not always due to the slower moving tornado. For the garage 1 orientation A model (G1A) the maximum CFx occurred during the test with the tornado simulator moving at 0.46 m/s for all building orientations except 90°. The source of the maximum C_{Fx}'s for model 3 was also the faster moving tornado for all building orientations except for 15° and 30°.

The C_{Fx} 's for model 1, the overhang model and the garage 2 orientation A (G2A) model are all similar for orientations 0° and 15°, but as the building orientation angle increases so does its peak C_{Fx}. It is interesting to note that the garage 2 orientation B (G2B) model follows this trend, but the peak C_{Fx}'s for both orientation A and B of the garage 1 model remain relatively constant for each building orientation angle.

Models 1, 2 and overhang (i.e. model 7) have a length to width ratio of1.5; models 3, 4, 5, and 6 have a length to width ratio of 1.0. The garage 1 model (model 8) has a length to width ratio of 1.9 and the garage 2 model (model 9) length to width ratio is 2.4. From Table 4-1 and Table 4-2 the effect of this ratio is clear. For the models with length to width ratios greater than 1.0 have peak C_{FX}'s at the larger building orientation angles when the longer side of the model is almost perpendicular to the direction of translation of the tornado. Whereas for the models with length-to-width ratios of 1.0, except model 6, the peak C_{FX}'s occur at building angles close to 0°. Model 6 has relatively large plan dimensions but the same eave height as model 5 and a steep roof pitch (35°) which results in a large total height-to-eave height ratio. The large total height-to-eave height ratio means that a larger area of the building is normal to the x direction for a BOA of 90° than for a BOA of 0° resulting in large C_{FX}'s at both 0° 90°.

For all of the models, orientations and translation speeds the peak force coefficients for the direction along the path of the tornado (C_{Fx})are smaller than 1.0 and in most cases smaller than 0.5. This indicates that the loading on low-rise buildings due to tornadoes is not dominated by the forces in the direction that the tornado is traveling.

The peak CFx values for each building orientation are plotted for models 3, 4 and 5 in Figure 4-15 for V_T = 0.15 m/s and in Figure 4-16 for V_T = 0.46 m/s. Models 3, 4 and 5 all have the same plan dimensions and mean roof height to length ratio but increasing roof pitch. The trend for the positive peak C_{Fx} coefficient is constant across all three roof pitches for both translation speeds. The value of the negative peak C_{Fx} coefficient decreases as the roof pitch increases.

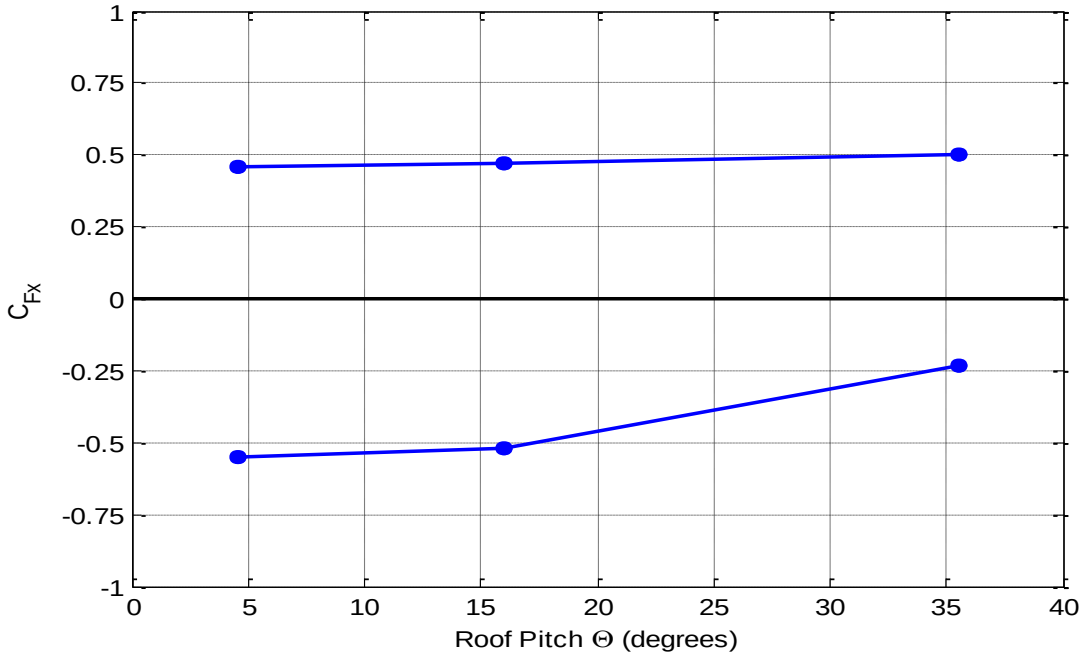

FIGURE 4- 15 PEAK CFX AS A FUNCTION OF ROOF PITCH VT = 0.15 M/S

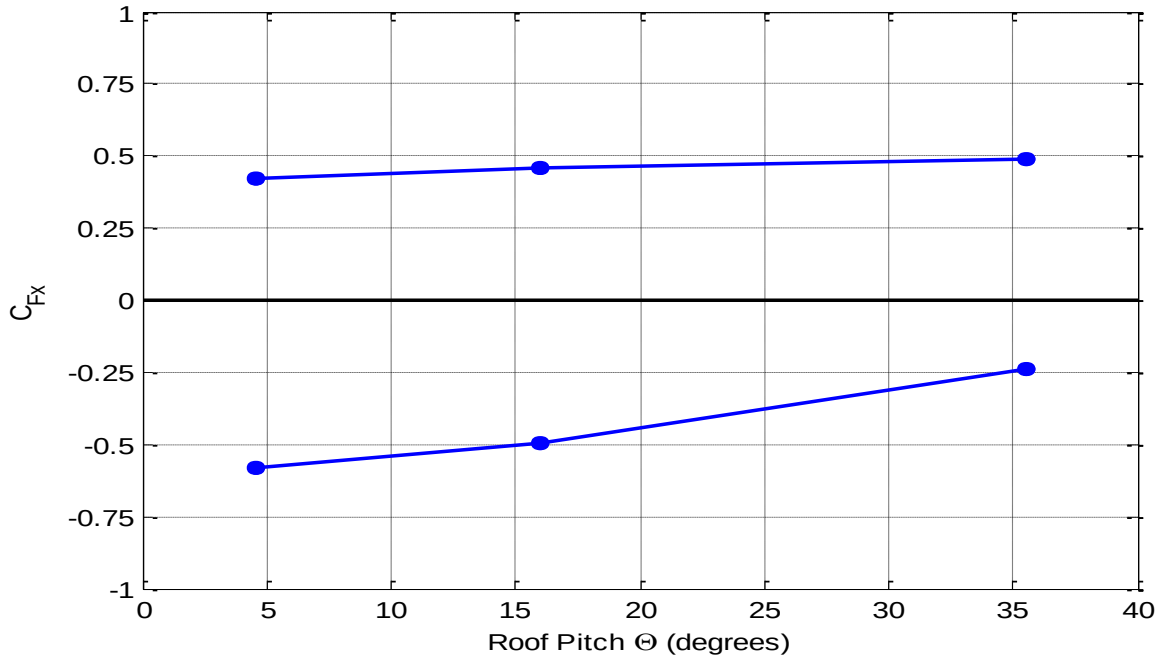

FIGURE 4- 16 PEAK CFX AS A FUNCTION OF ROOF PITCH VT = 0.46 M/S

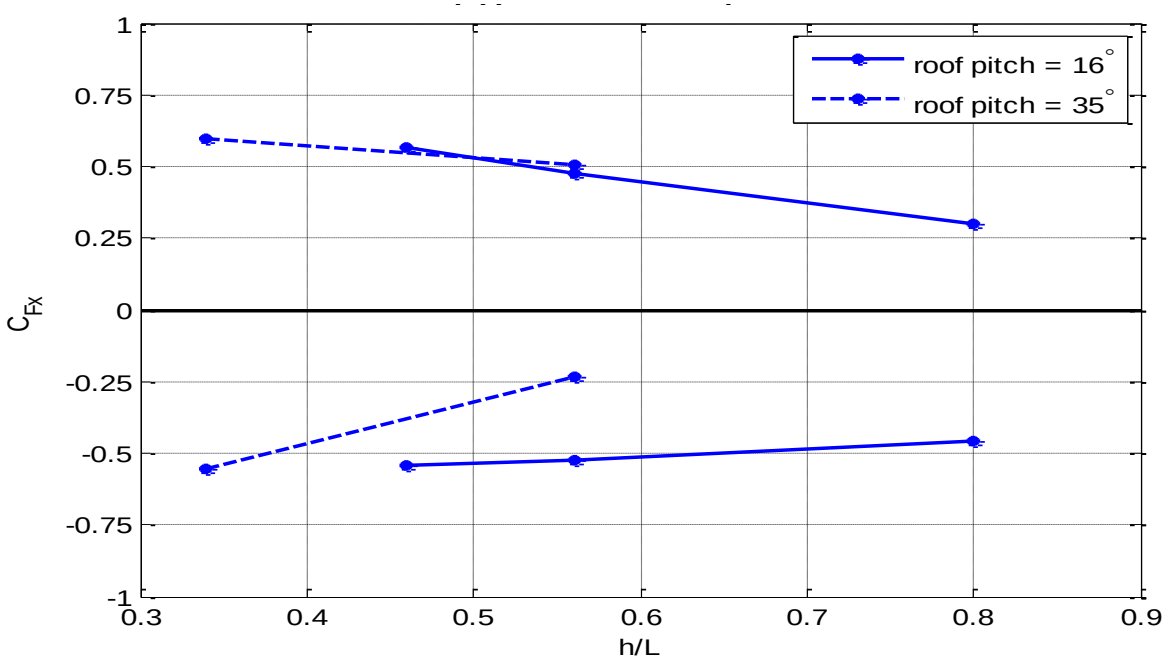

FIGURE 4- 17 PEAK CFX AS A FUNCTION OF h/L VT = 0.15 M/S

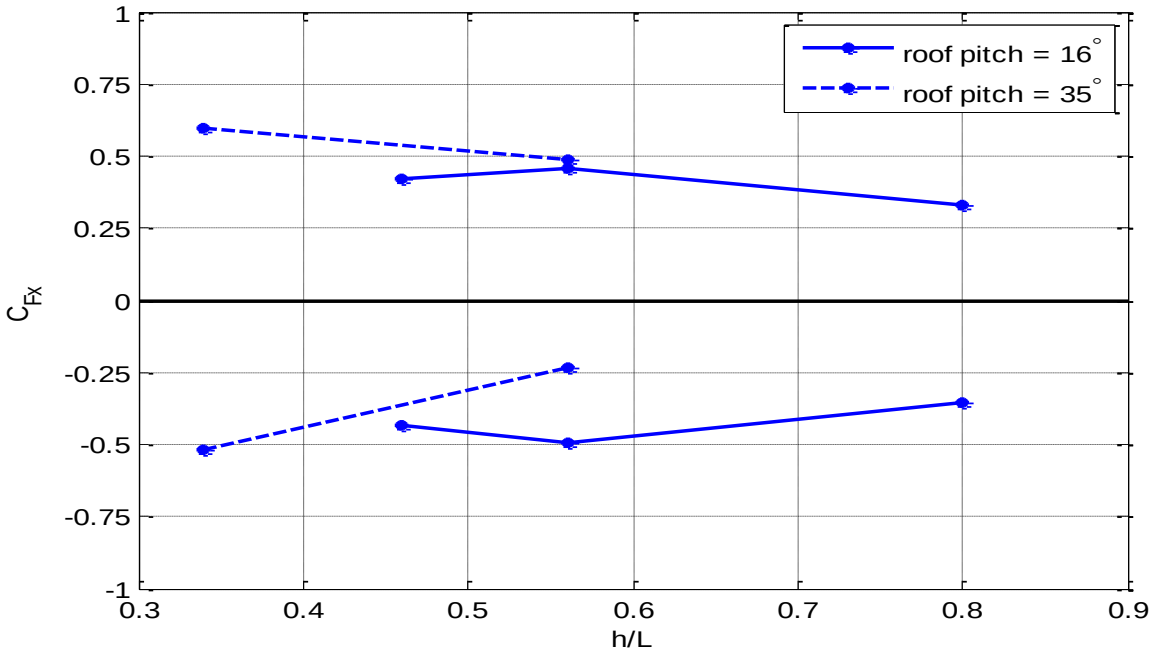

FIGURE 4- 18 PEAK CFX AS A FUNCTION OF h/L VT = 0.46 M/S

The peak C_{Fx}'s were plotted also as a function of the ratio of mean roof height to longest plan dimension in Figures 4-17 and 4-18. In these plots the solid lines represent the peak coefficients from models 1, 4 and 2 (increasing h/L) and the dashed lines are models 6 and 5 (increasing h/L).

The positive and negative peak C_{Fx}'s for both roof pitches decrease in magnitude with increasing h/L. As can be seen in Figures 4-19 and 4-20 the negative peaks for model 5 are very close to zero for BOA's of 15° and 30° as was also shown in the time histories. Figures 4-19 and 4-20 also show the peak C_{Fx} envelopes. The positive and negative envelopes are for the most part symmetric about C_{Fx} = 0 although the negative envelope is slightly less in magnitude than the positive envelope.

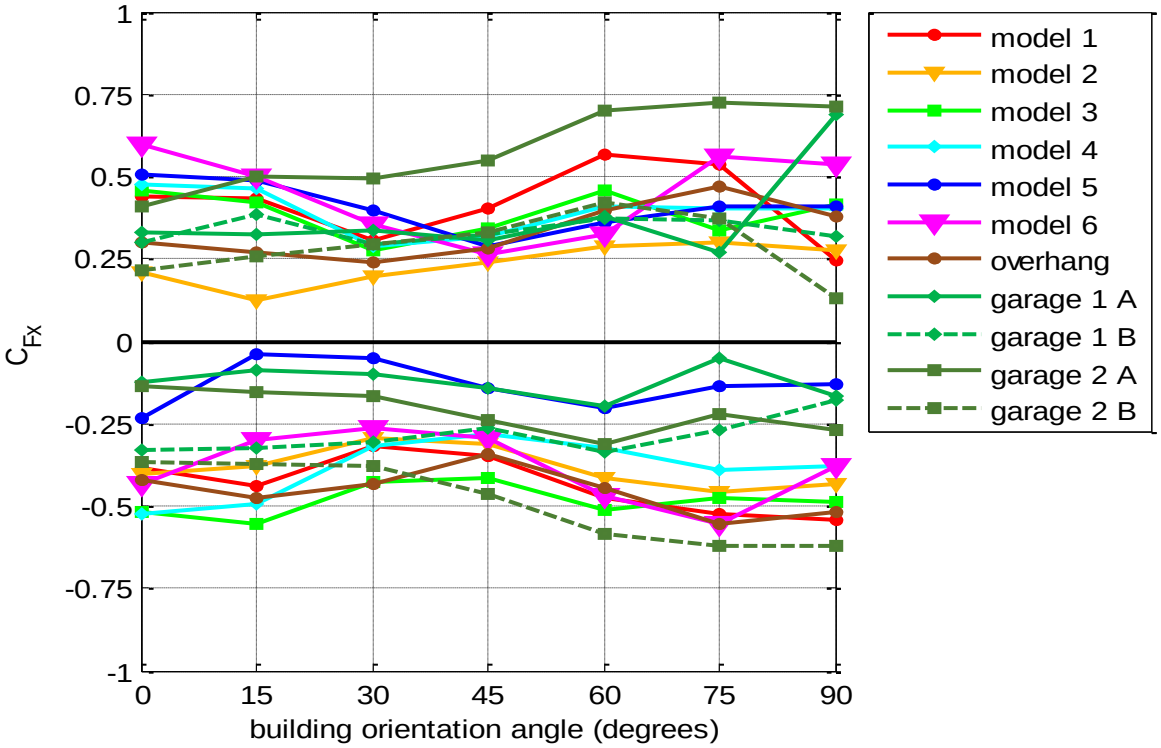

FIGURE 4- 19 PEAK CFX VT = 0.15 M/S

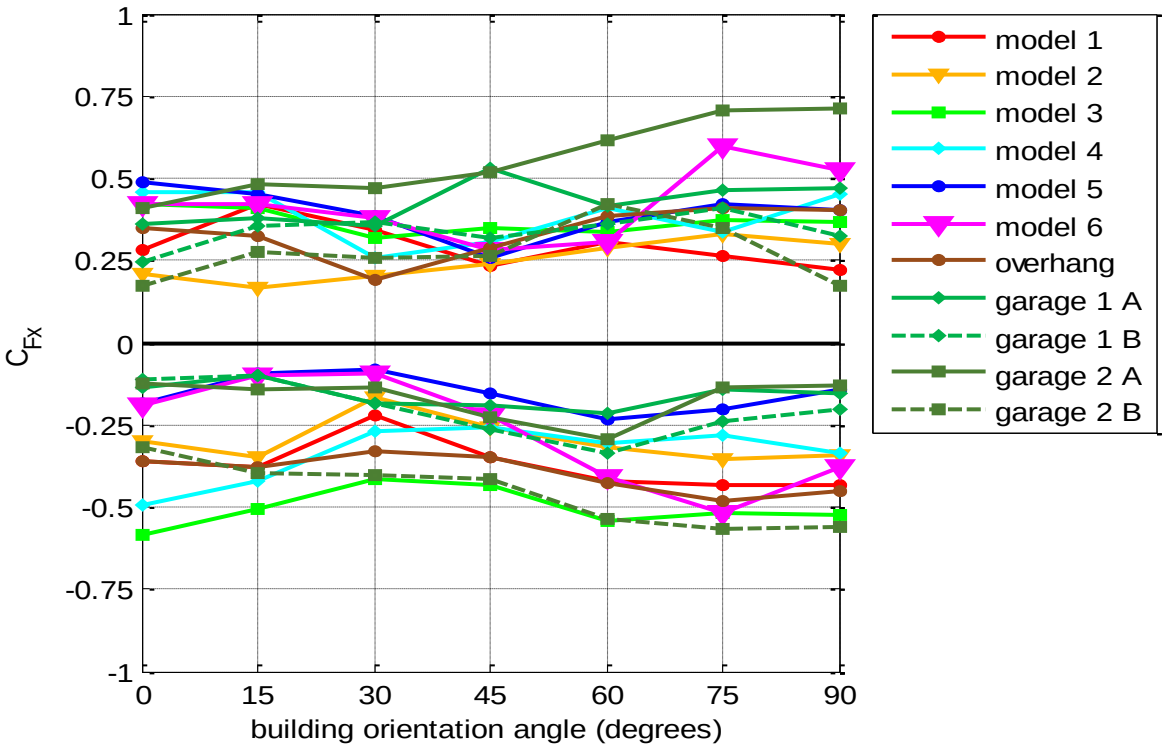

FIGURE 4- 20 PEAK CFX VT = 0.46 M/S

4.1.3 C_{Fy}

The y direction (perpendicular to the direction of translation) force coefficient time histories of each model for the 0°-90° building orientations and 0.15 m/s translation speed are given in Figures 4-21 through 4-27 and the time histories for the 0.46 translation speed are shown in Figures 4-28 through 4-34. The tabulated peak values are given in Table 4-3 for the 0.15 m/s translation speed and Table 4-4 for the 0.46 m/s translation speed. The peaks listed in the tables are absolute values.

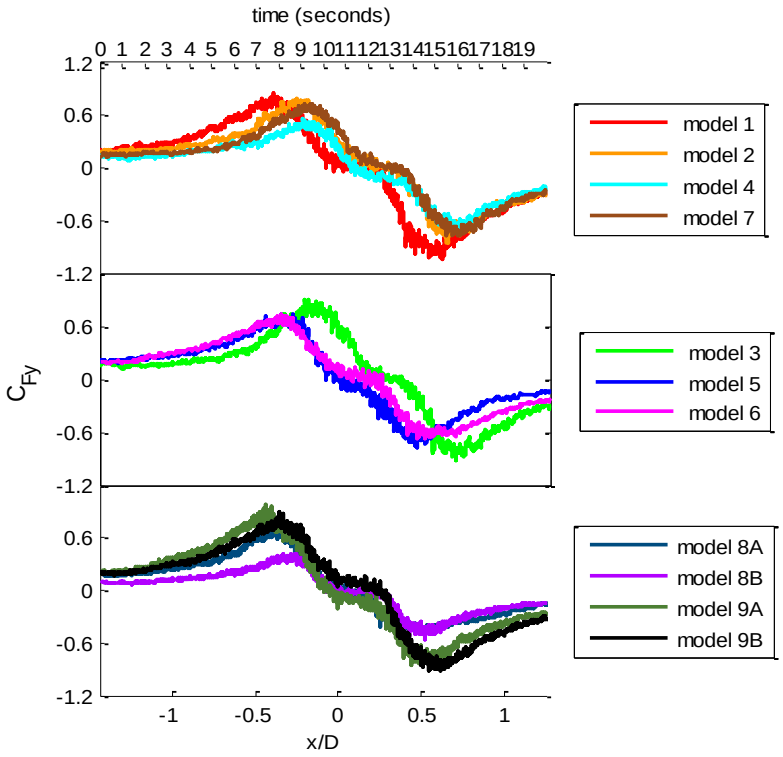

FIGURE 4- 21 CFY TIME HISTORIES VT = 0.15 M/S BUILDING ORIENTATION = 0 DEGREES

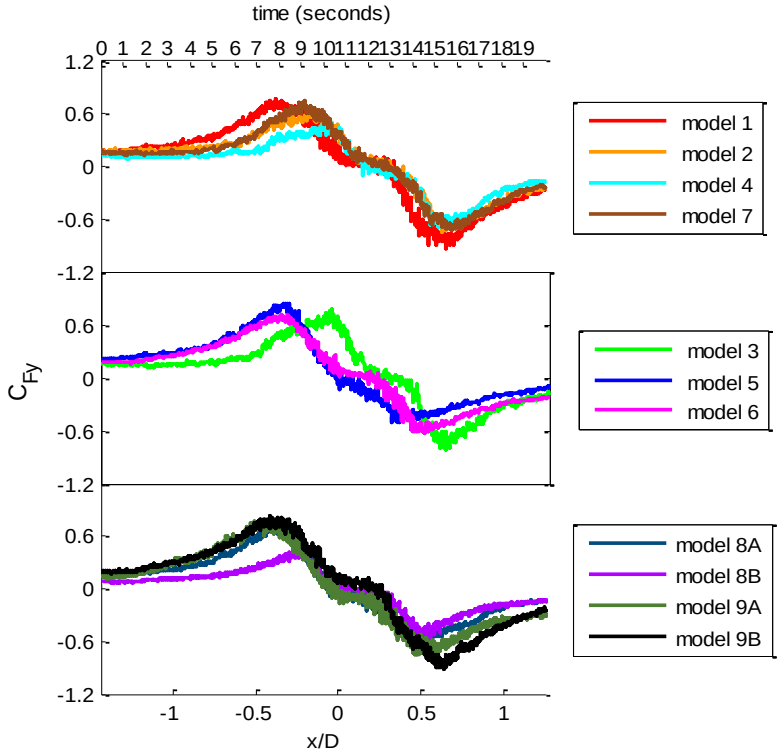

FIGURE 4- 22 CFY TIME HISTORIES VT = 0.15 M/S BUILDING ORIENTATION = 15 DEGREES

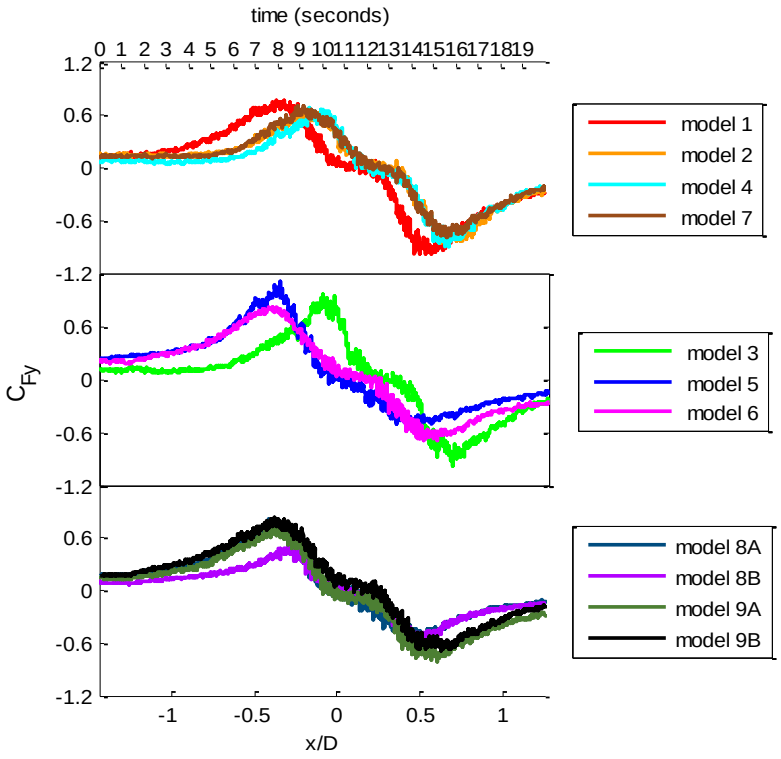

FIGURE 4- 23 CFY TIME HISTORIES VT = 0.15 M/S BUILDING ORIENTATION = 30 DEGREES

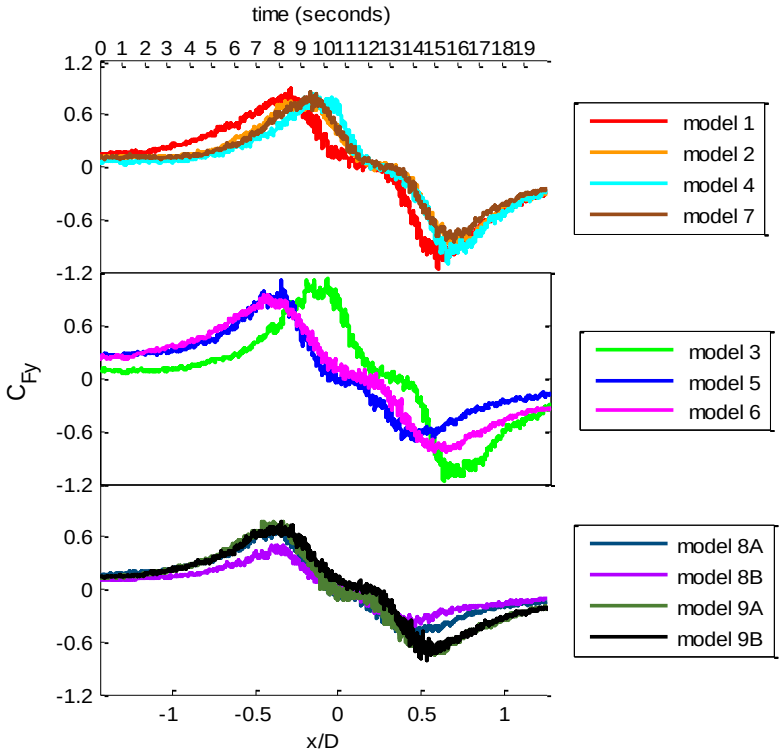

FIGURE 4- 24 CFY TIME HISTORIES VT = 0.15 M/S BUILDING ORIENTATION = 45 DEGREES

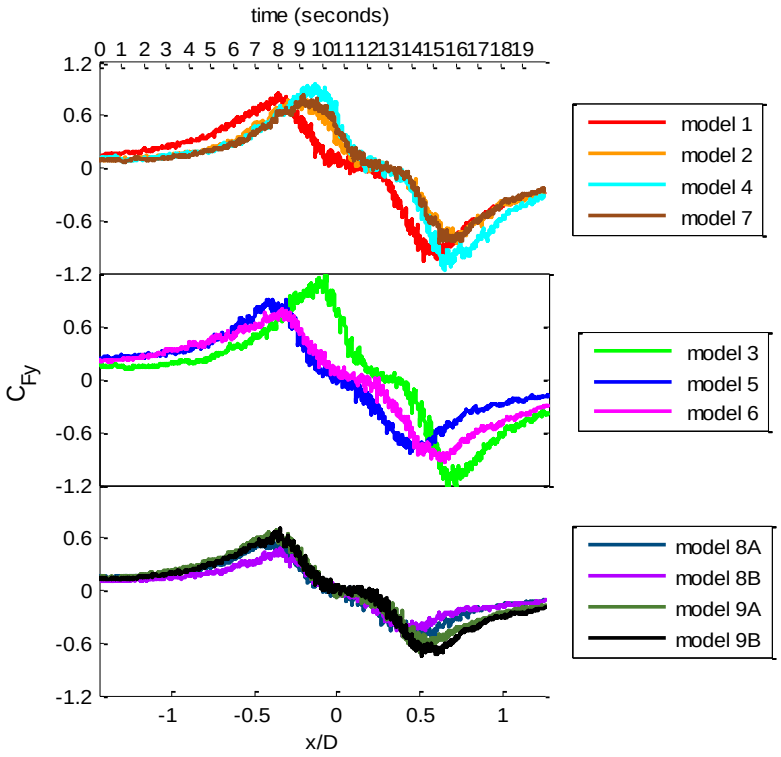

FIGURE 4- 25 CFY TIME HISTORIES VT = 0.15 M/S BUILDING ORIENTATION = 60 DEGREES

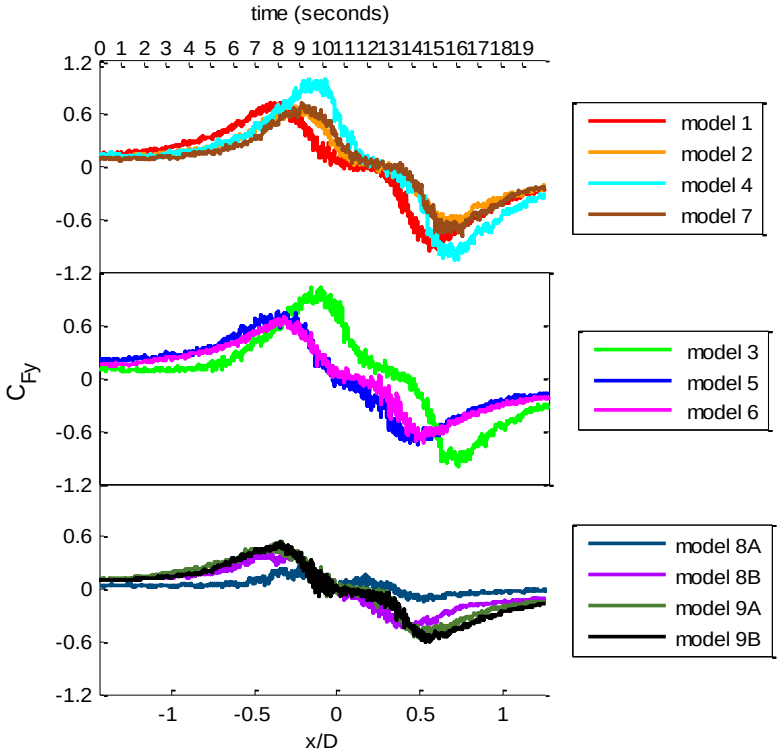

FIGURE 4- 26 CFY TIME HISTORIES VT = 0.15 M/S BUILDING ORIENTATION = 75 DEGREES

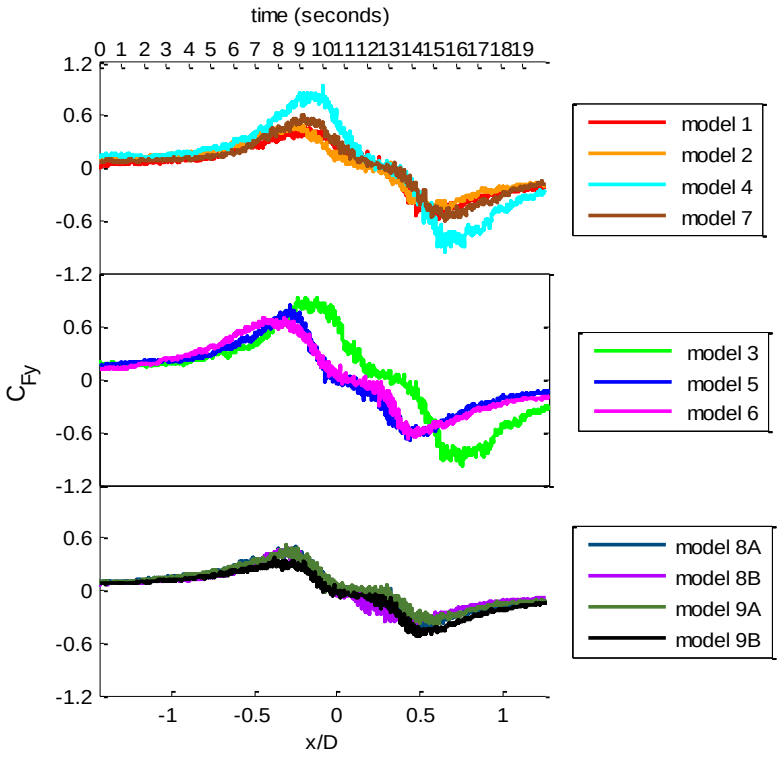

FIGURE 4- 27 CFY TIME HISTORIES VT = 0.15 M/S BUILDING ORIENTATION = 90 DEGREES

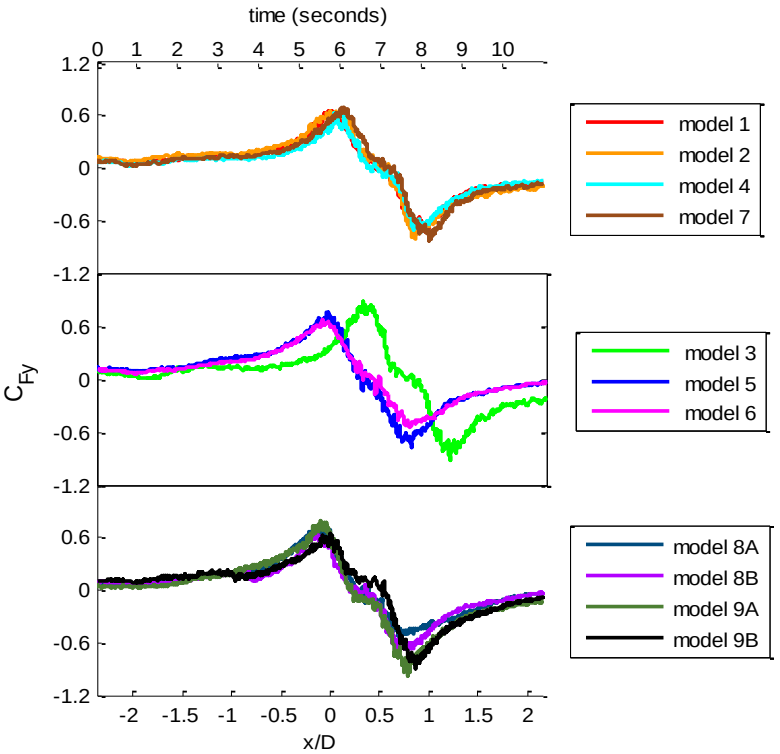

FIGURE 4- 28 CFY TIME HISTORIES VT = 0.46 M/S BUILDING ORIENTATION = 0 DEGREES

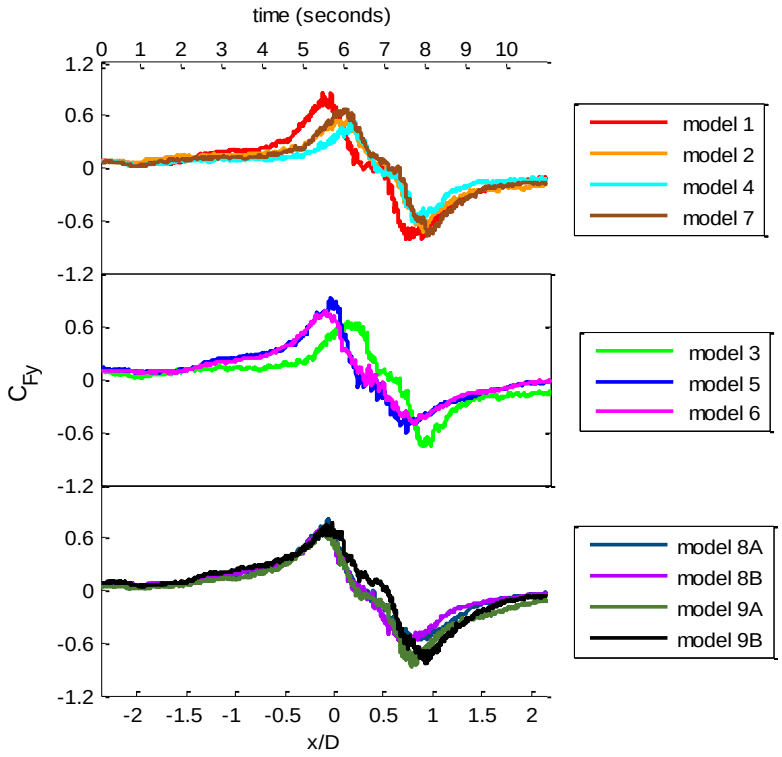

FIGURE 4- 29 CFY TIME HISTORIES VT = 0.46 M/S BUILDING ORIENTATION = 15 DEGREES

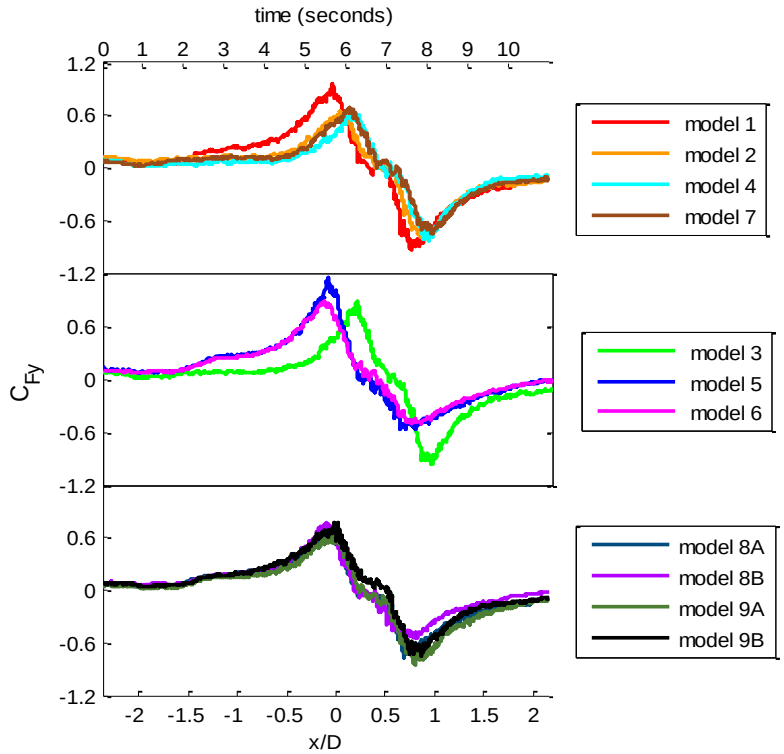

FIGURE 4- 30 CFY TIME HISTORIES VT = 0.46 M/S BUILDING ORIENTATION = 30 DEGREES

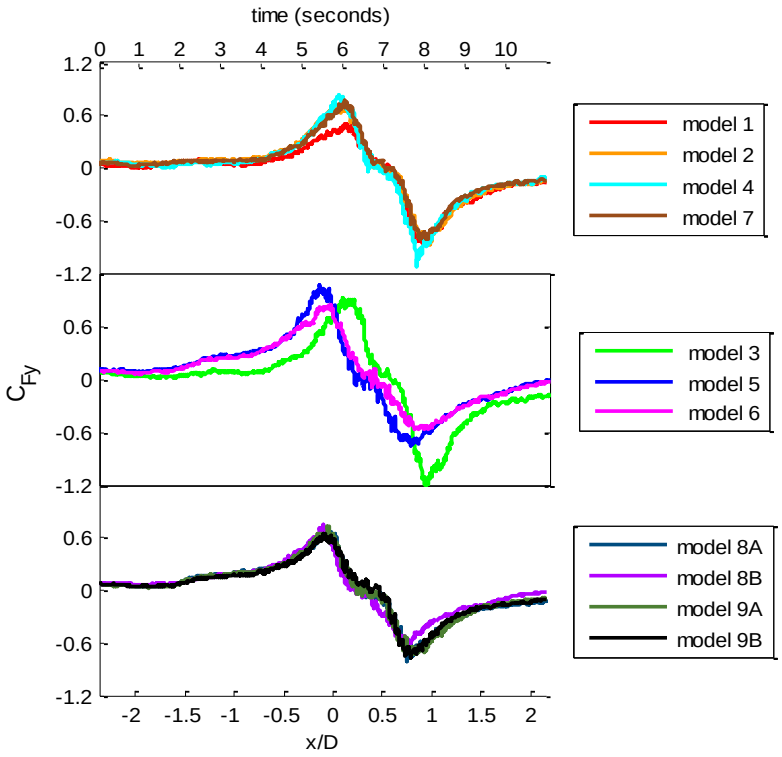

FIGURE 4- 31 CFY TIME HISTORIES VT = 0.46 M/S BUILDING ORIENTATION = 45 DEGREES

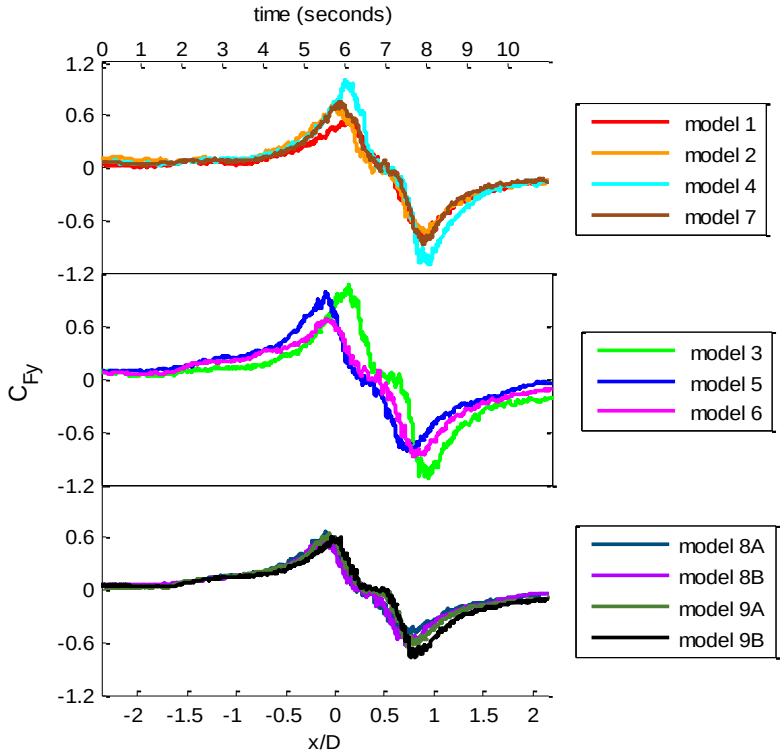

FIGURE 4- 32 CFY TIME HISTORIES VT = 0.46 M/S BUILDING ORIENTATION = 60 DEGREES

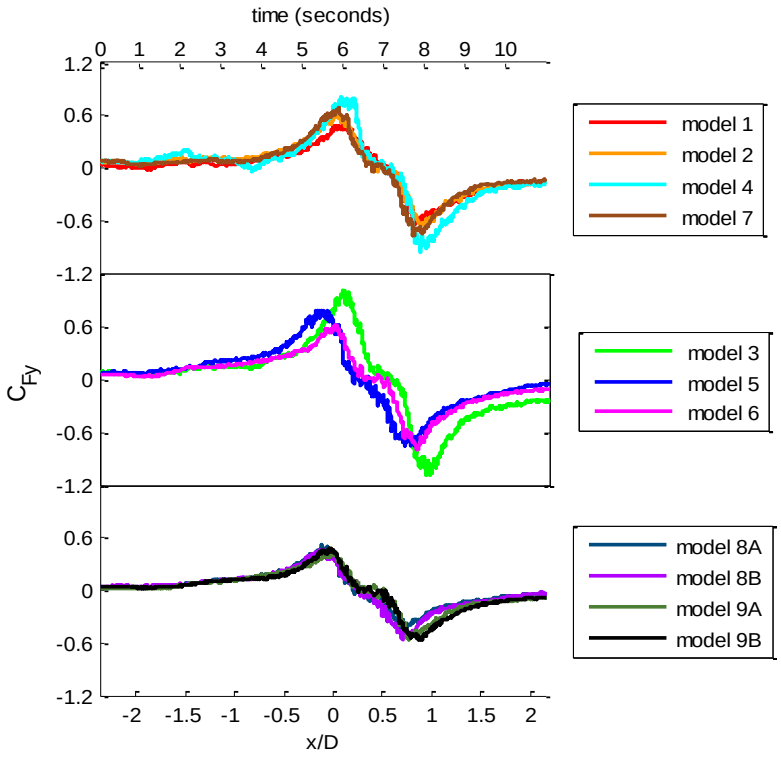

FIGURE 4- 33 CFY TIME HISTORIES VT = 0.46 M/S BUILDING ORIENTATION = 75 DEGREES

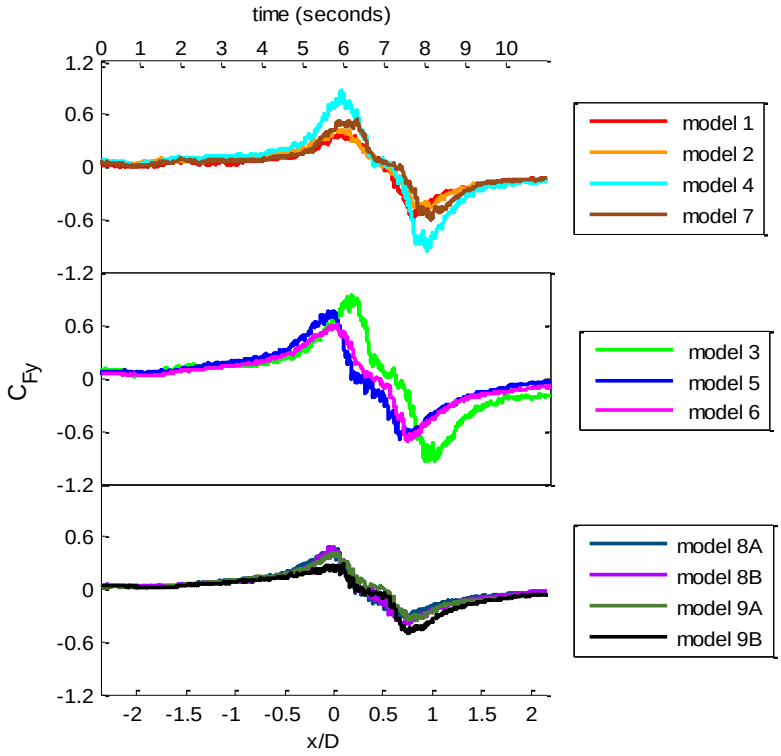

FIGURE 4- 34 CFY TIME HISTORIES VT = 0.46 M/S BUILDING ORIENTATION = 90 DEGREES

The C_{Fy} time histories also follow a distinct pattern. As the tornado approaches the building model the tangential velocity component of the wind in the tornado is parallel to and in the direction of the positive Y axis. The positive pressures on the windward side of the building caused by the strong tangential velocity overcome the negative pressures due to the vortex suction causing the force coefficient to reach a positive peak. As the tornado passes over the center of the building the tangential velocity component comes from the opposite direction causing the y direction force coefficient to peak in the opposite direction. The time histories reach their positive peak at a distance x/D = -0.5 and reach their negative peak at a distance x/D = 0.5 from the center of the building. This matches well with the mathematical vortex models where the maximum tangential velocity is at a distance equal to the radius of the core from the center of the vortex.

TABLE 4- 21 PEAK CFY VT = 0.15 M/S

MODEL / orientation	1	2	3	4	5	6	Overhang	G1A	G1B	G2A	G2B
0°	1.03	0.86	0.93	0.73	0.78	0.73	0.78	0.69	0.56	**0.98**	**0.92**
15°	0.94	0.76	0.82	0.69	0.84	0.72	0.75	0.75	0.58	0.79	0.92
30°	0.99	0.85	0.97	0.90	**1.11**	0.82	0.80	**0.82**	**0.64**	0.82	0.83
45°	**1.17**	**0.90**	1.17	1.11	1.10	**0.94**	**0.86**	0.73	0.51	0.77	0.81
60°	1.06	0.85	**1.23**	**1.17**	0.91	0.93	0.85	0.57	0.51	0.71	0.75
75°	0.96	0.69	1.03	1.07	0.75	0.73	0.78	0.29	0.47	0.57	0.61
90°	0.59	0.51	0.99	0.95	0.85	0.70	0.60	0.49	0.47	0.52	0.53

G = garage A and B = orientation

TABLE 4- 22 PEAK CFY VT = 0.46 M/S

MODEL / orientation	1	2	3	4	5	6	Overhang	G1A	G1B	G2A	G2B
0°	0.75	0.82	0.92	0.73	0.77	0.66	0.83	0.72	0.67	**0.99**	**0.89**
15°	0.86	0.72	0.76	0.62	0.93	0.78	0.78	**0.81**	0.73	0.87	0.84
30°	**0.96**	0.81	0.96	0.83	**1.14**	**0.88**	0.75	0.78	**0.78**	0.85	0.78
45°	0.88	**0.88**	**1.21**	**1.12**	1.07	0.83	0.81	0.81	0.74	0.74	0.77
60°	0.80	0.77	1.12	1.11	0.97	0.87	**0.87**	0.67	0.62	0.65	0.78
75°	0.65	0.66	1.09	0.96	0.78	0.81	0.77	0.52	0.56	0.56	0.56
90°	0.61	0.49	0.95	0.95	0.76	0.71	0.60	0.46	0.48	0.42	0.50

G = garage A and B = orientation

A comparison of Table 4-3 and Table 4-4 shows that for the majority of cases the slower moving tornado produces higher force coefficients and that the peak C_{Fy} decreases for increasing building orientation angle.

The only difference between model 5 and the garage 1 model is the addition of the garage, but when the peak C_{Fy}'s of model 5 and the garage 1 model are compared model 5 has a higher value for every building orientation and translation speed. The comparison between model 1 and garage 2 is similar; even though garage 2 is geometrically similar to garage 1 with only an additional attached "garage" the y direction peak force coefficients are for the most part smaller in magnitude. It can also be noted that for the garage 2 model orientation A has larger peak C_{Fy}'s for building orientations 0° – 30° and orientation B has larger peak C_{Fy}'s for building orientations 45° – 90°.

A comparison of Tables 4-1 and 4-2 with Tables 4-3 and 4-4 shows that the building orientation angles that are critical (shaded red) in the x direction have the smallest peaks (shaded green) in the y direction and vice versa. As was discussed above for C_{Fx} the largest peaks are for smallest and largest building orientation angles while for CFy the largest peaks are for the building orientation angles of 30°, 45°, and 60°. This trend is not followed by the garage models (i.e. models 8 and 9) which generally have peak C_{Fx}'s for BOA's of 75° and 90° and have peak C_{Fy}'s for BOA's of 0°, 15°, and 30°.

Similar trends can be seen for both translation speeds from Figure 4-35 and Figure 4-36. For both translation speeds the positive and negative peaks are symmetric about $C_{Fy} = 0$. It can also be observed that not only are the peaks symmetric for the respective models but also that the envelopes of the peak values are symmetric.

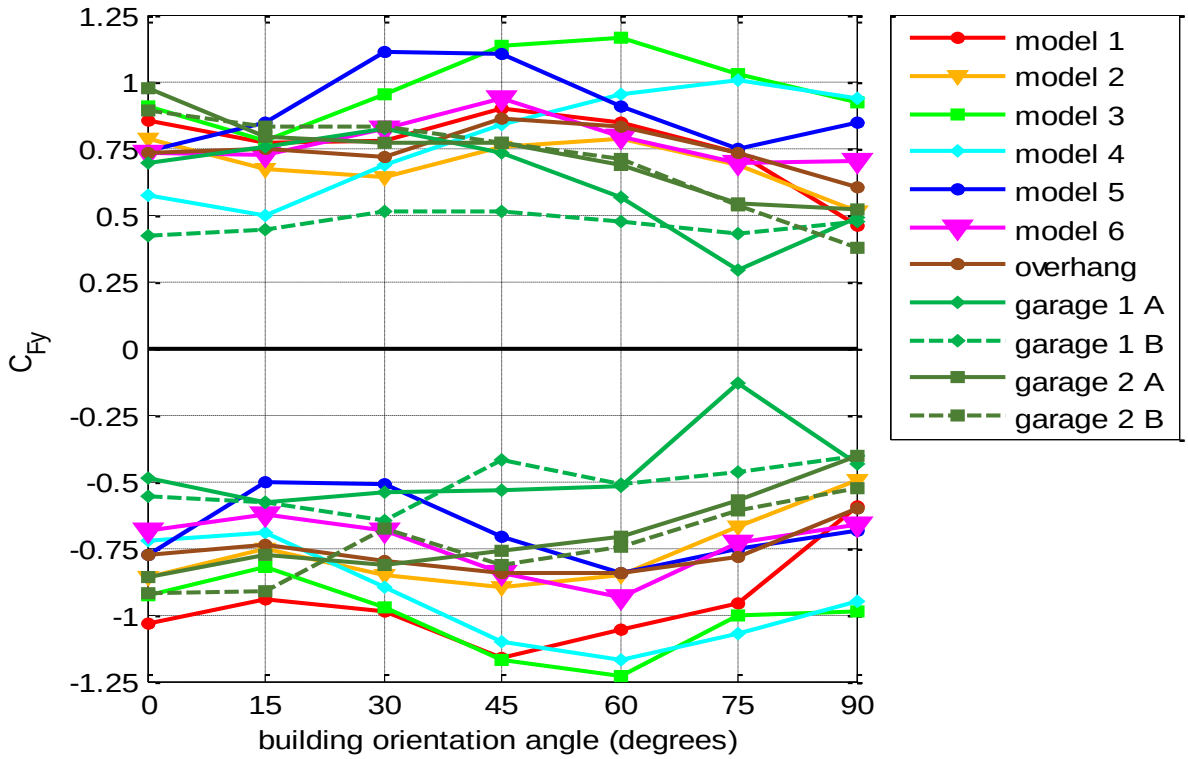

FIGURE 4- 35 PEAK CFY VT = 0.15 M/S

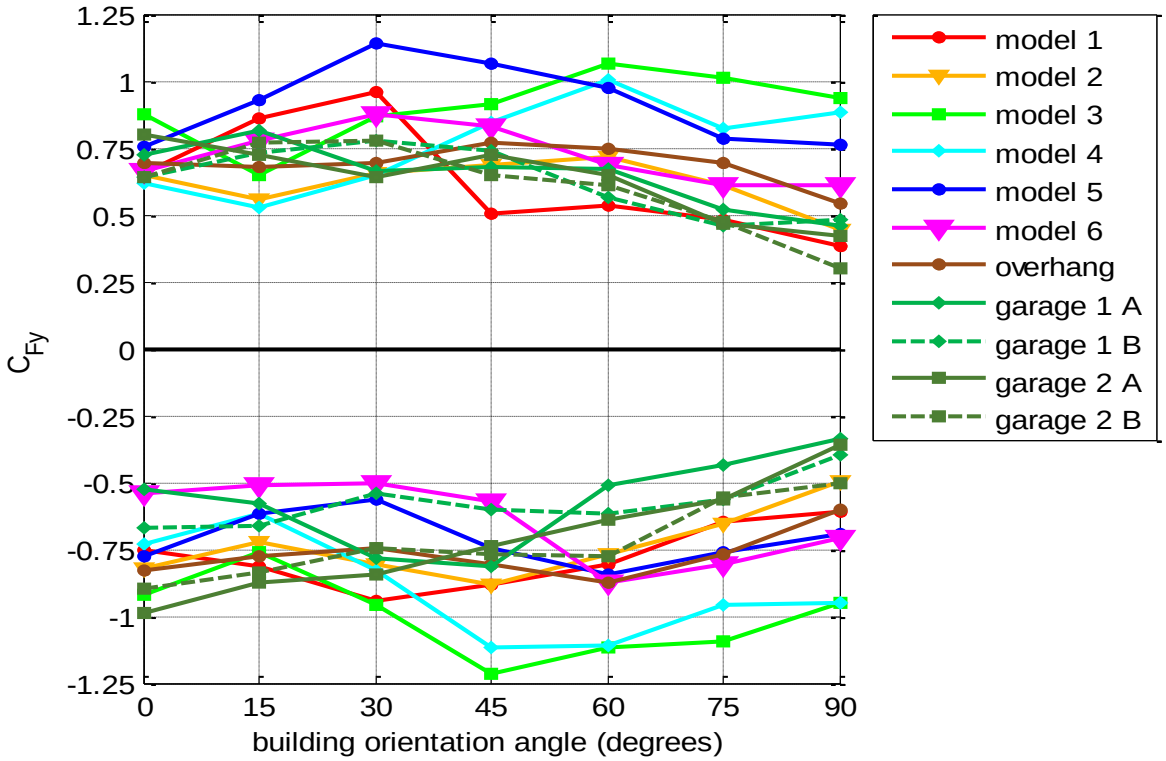

FIGURE 4- 36 PEAK CFY VT = 0.46 M/S

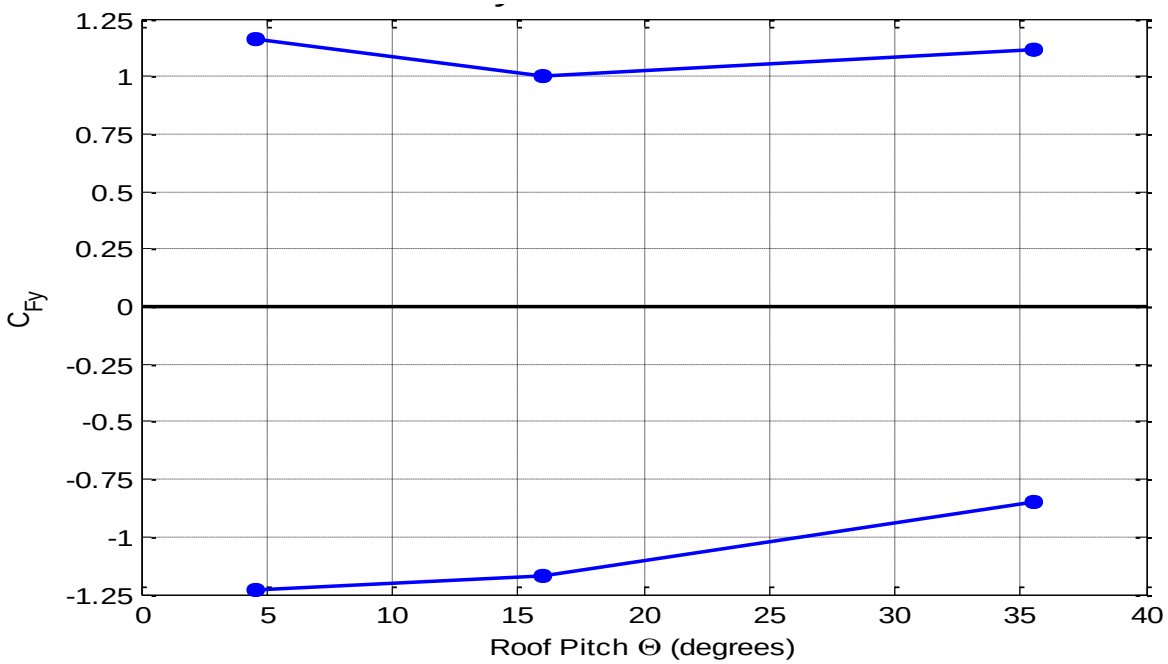

FIGURE 4- 37 PEAK CFY AS A FUNCTION OF ROOF PITCH VT = 0.15 M/S

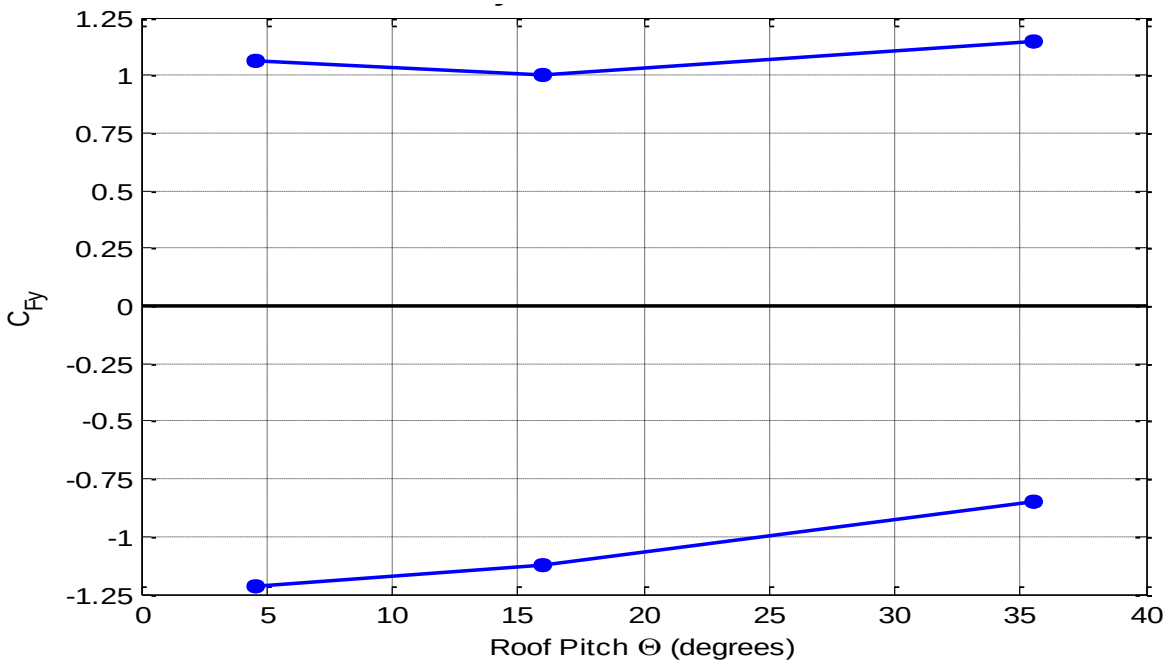

FIGURE 4- 38 PEAK CFY AS A FUNCTION OF ROOF PITCH VT = 0.46 M/S

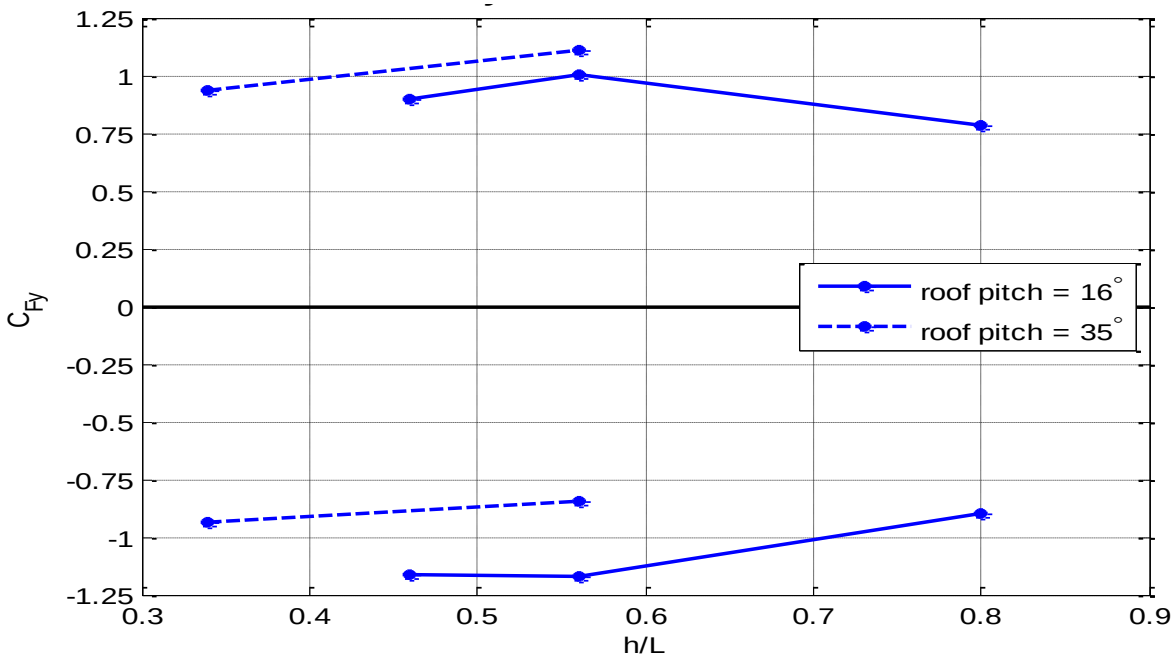

FIGURE 4- 39 PEAK CFY AS A FUNCTION OF h/L VT = 0.15 M/S

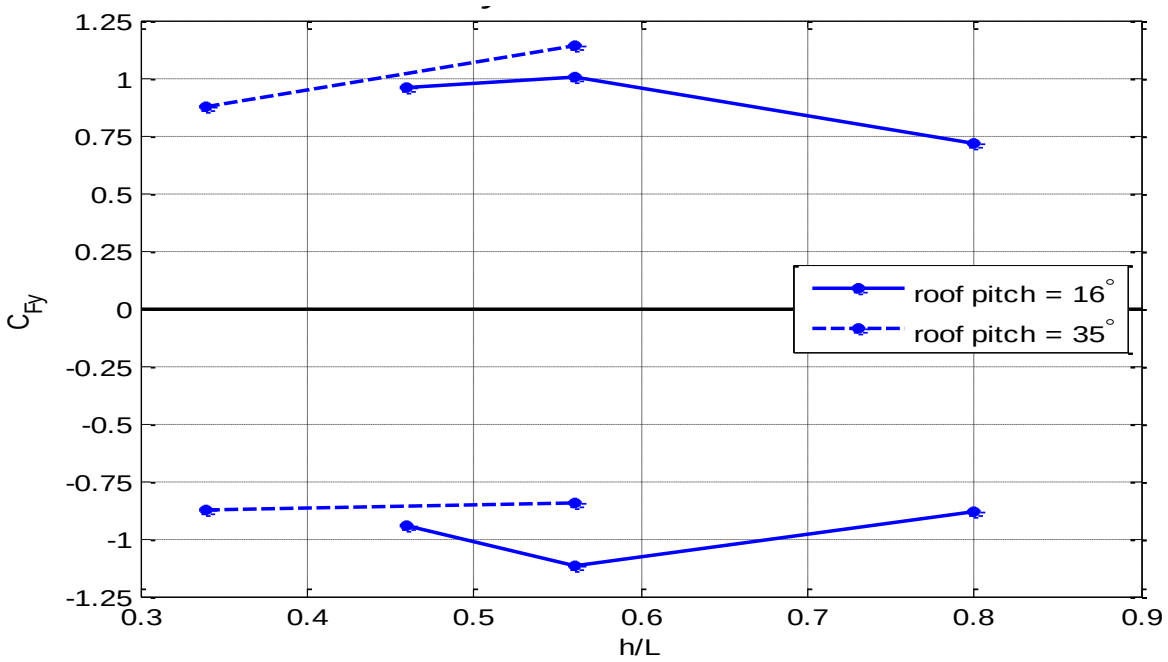

FIGURE 4- 40 PEAK CFY AS A FUNCTION OF h/L VT = 0.46 M/S

The peak C_{Fy} values for each building orientation are plotted for models 3, 4 and 5 in Figure 4-37 for V_T = 0.15 m/s and in Figure 4-38 for V_T = 0.46 m/s to show the change in C_{Fy} as a function of roof pitch. The positive peak C_{Fy} coefficient first decreases then increases as roof pitch increases. The magnitude of the negative peak C_{Fy} coefficient decreases as the roof pitch increases.

The peak C_{Fy}'s were plotted also as a function of the ratio of mean roof height to longest plan dimension in Figures 4-39 and 4-40. In these plots the solid lines represent the peak coefficients from models 1, 4 and 2 (increasing h/L) and the dashed lines are models 6 and 5 (increasing h/L). The magnitude of the negative peak decreases as h/L increases. The positive peak C_{Fy}'s for both roof pitches increases in magnitude until h/L = 0.55 then the peak for the 16° roof pitch decreases with increasing h/L.

It can also be observed from Figures 4-15 through 4-18 and Figures 4-38 through 4-40 that the trends of the respective peak force coefficients as a function of the respective building geometry variables are the same for both translation speeds; only the magnitudes are slightly different for the two translation speeds.

4.1.4 C_{Fxy}

The x y force coefficient time histories of each model for the 0°-90° building orientations and 0.15 m/s translation speed are given in Figures 4-41 through 4-47 and the time histories for the 0.46 translation speed are shown in Figures 4-48 through 4-54. The tabulated peak values are given in Table 4-5 for the 0.15 m/s translation speed and Table 4-6 for the 0.46 m/s translation speed.

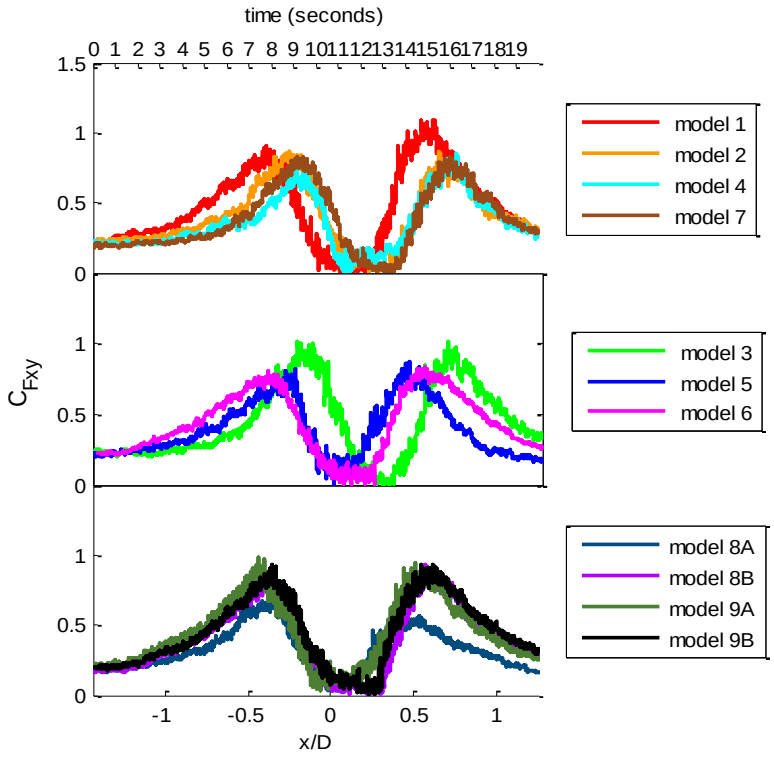

FIGURE 4- 41 CFXY TIME HISTORIES FOR VT = 0.15 M/S BUILDING ORIENTATION = 0 DEGREES

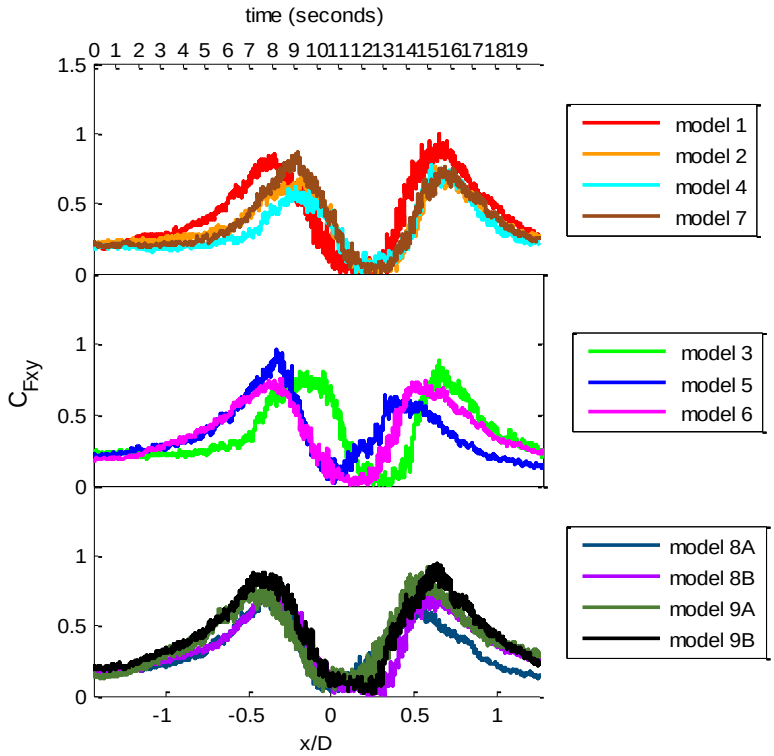

FIGURE 4- 42 CFXY TIME HISTORIES FOR VT = 0.15 M/S BUILDING ORIENTATION = 15 DEGREES

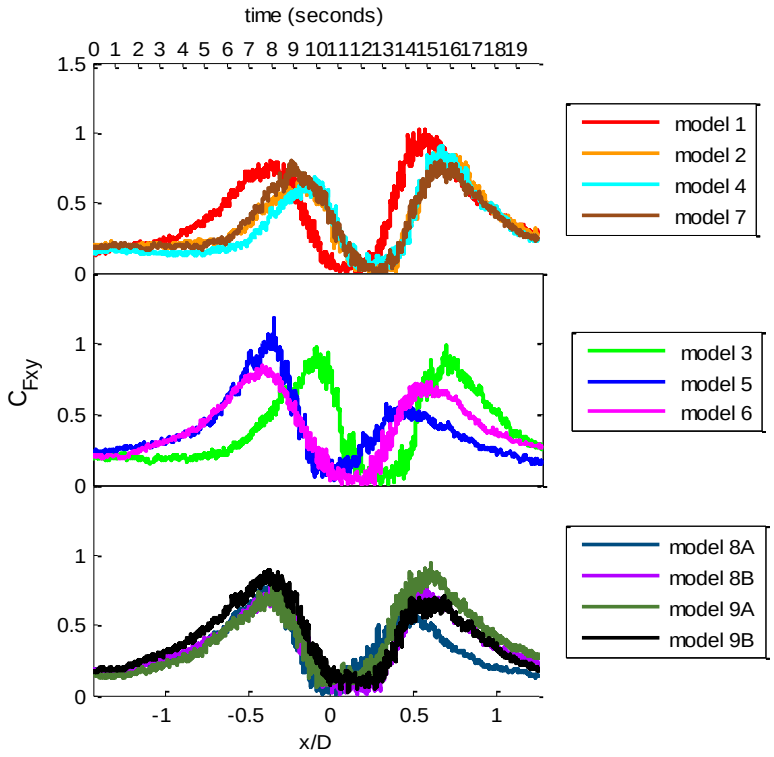

FIGURE 4- 43 CFXY TIME HISTORIES VT = 0.15 M/S BUILDING ORIENTATION = 30 DEGREES

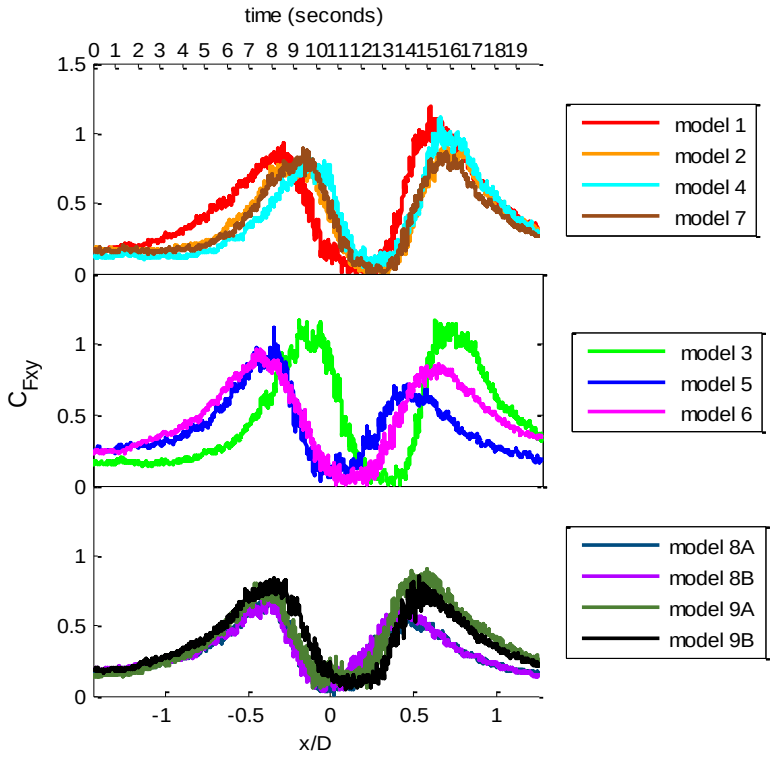

FIGURE 4- 44 CFXY TIME HISTORIES VT = 0.15 M/S BUILDING ORIENTATION = 45 DEGREES

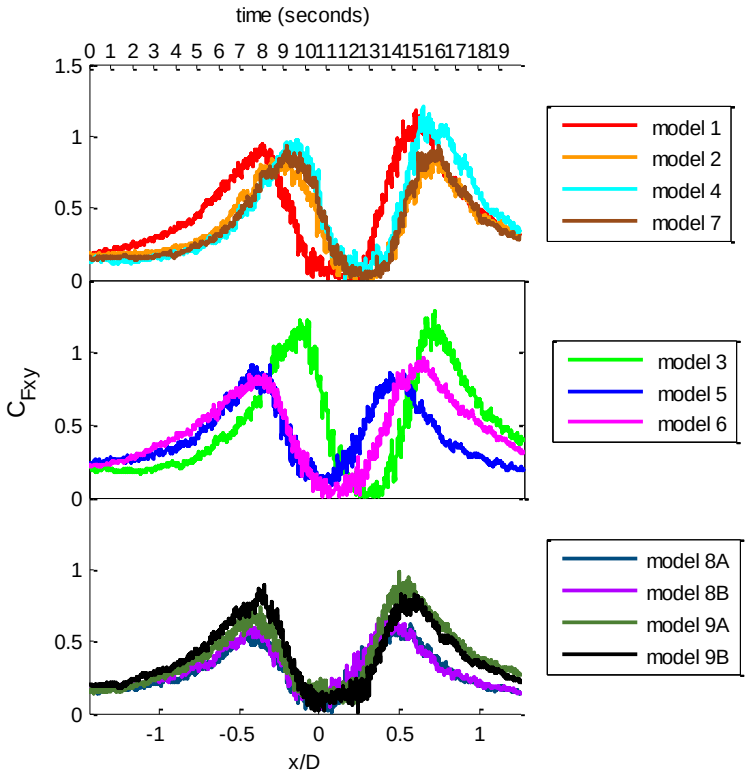

FIGURE 4- 45 CFXY TIME HISTORIES VT = 0.15 M/S BUILDING ORIENTATION = 60 DEGREES

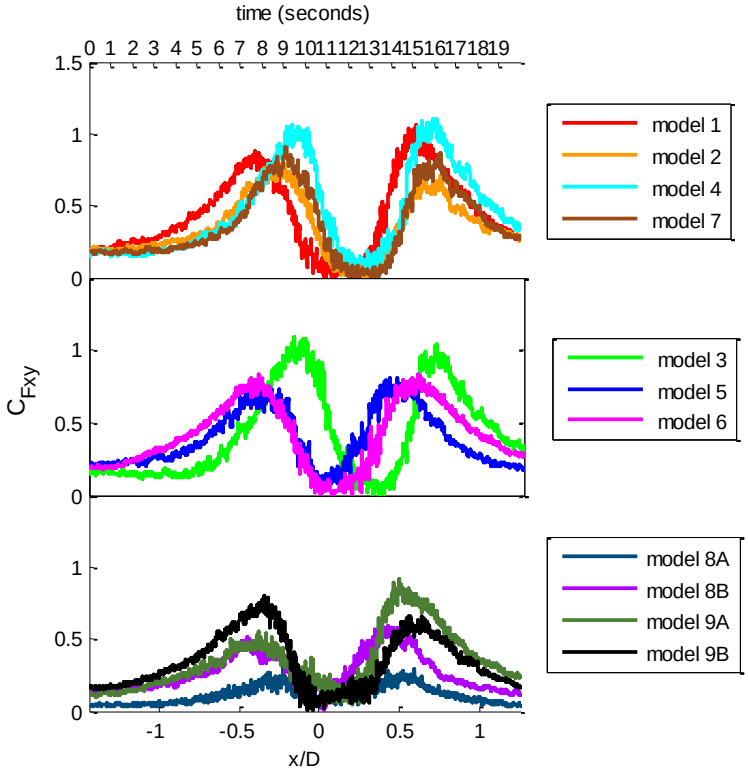

FIGURE 4- 46 CFXY TIME HISTORIES VT = 0.15 M/S BUILDING ORIENTATION = 75 DEGREES

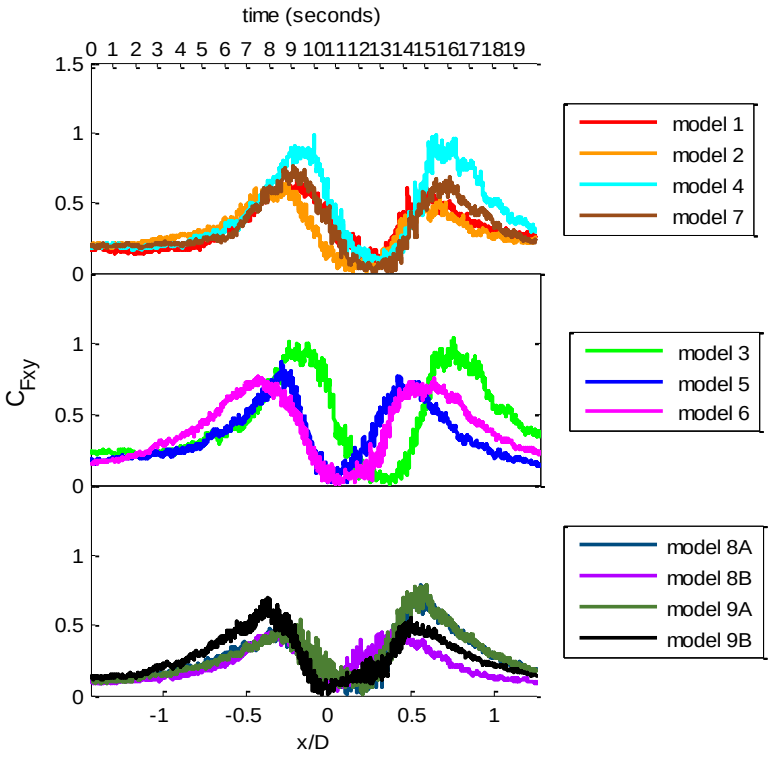

FIGURE 4- 47 CFXY TIME HISTORIES VT = 0.15 M/S BUILDING ORIENTATION = 90 DEGREES

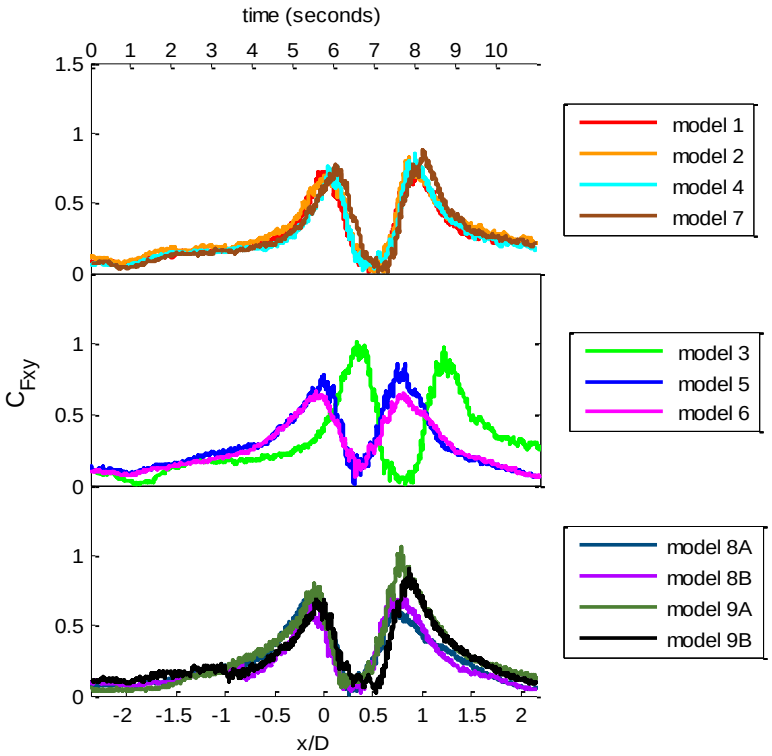

FIGURE 4- 48 CFXY TIME HISTORIES VT = 0.46 M/S BUILDING ORIENTATION = 0 DEGREES

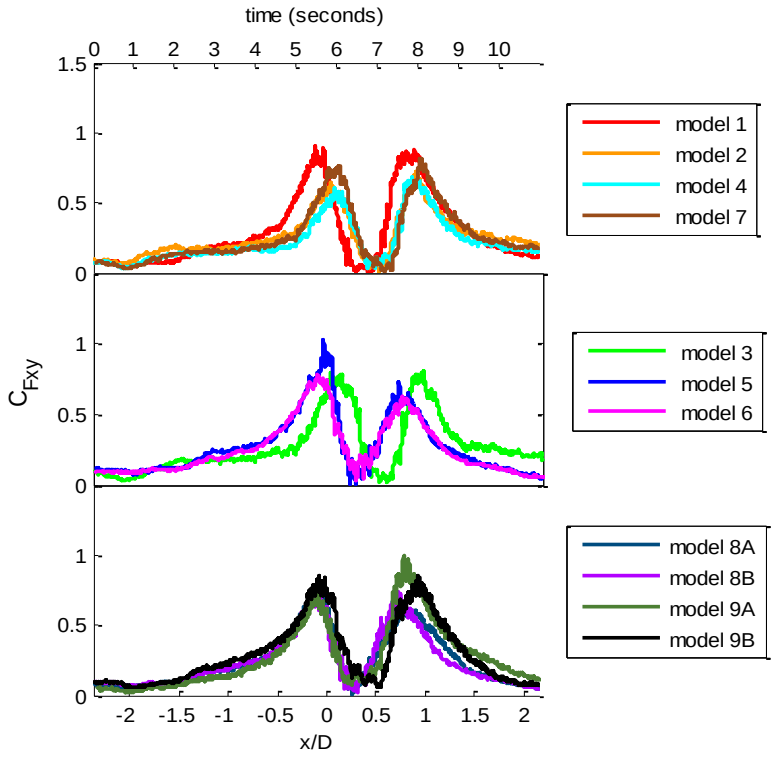

FIGURE 4- 49 CFXY TIME HISTORIES VT = 0.46 M/S BUILDING ORIENTATION = 15 DEGREES

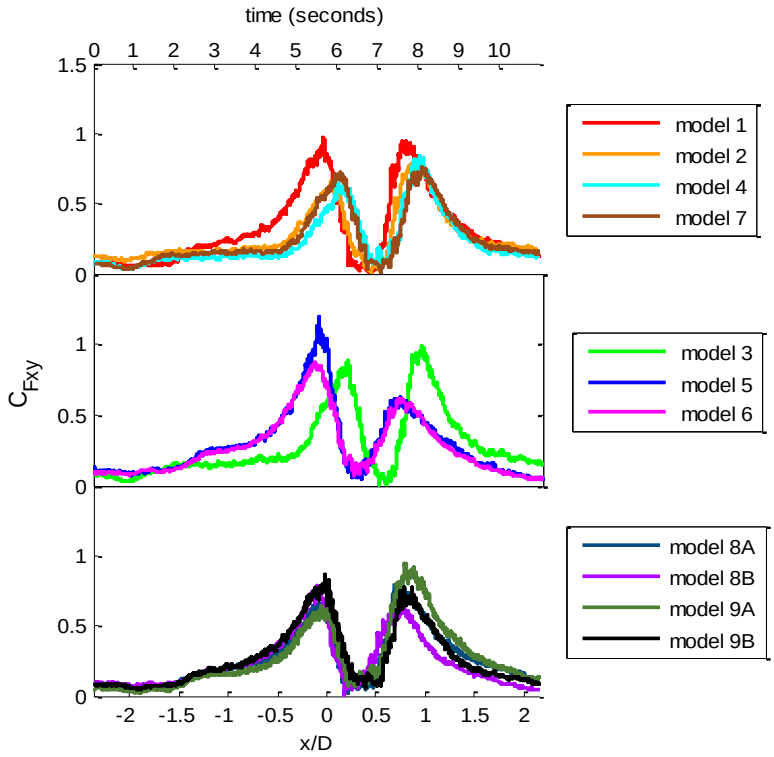

FIGURE 4- 50 CFXY TIME HISTORIESSS VT = 0.46 M/S BUILDING ORIENTATION = 30 DEGREES

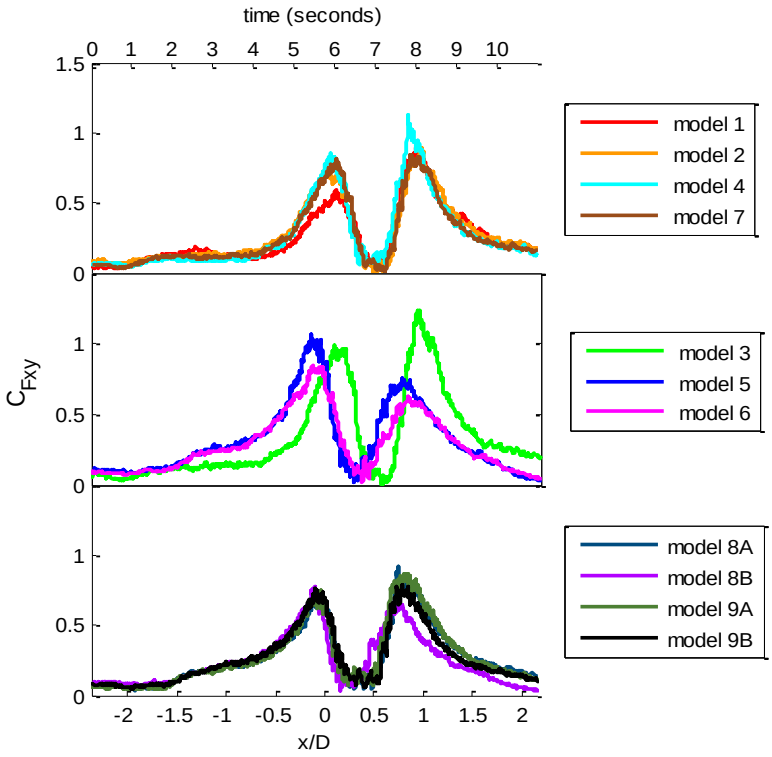

FIGURE 4- 51 CFXY TIME HISTORIES VT = 0.46 M/S BUILDING ORIENTATION = 45 DEGREES

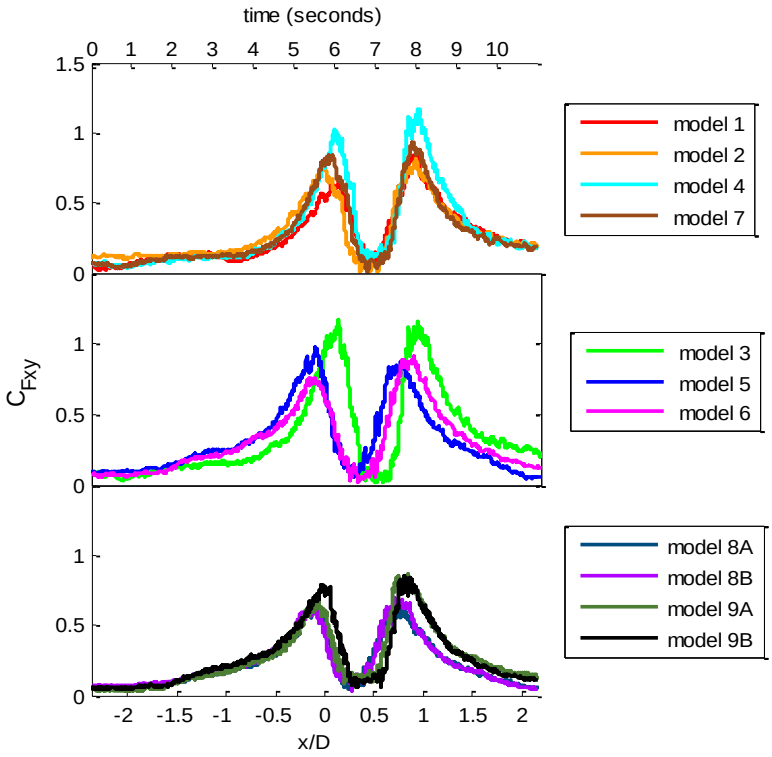

FIGURE 4- 52 CFXY TIME HISTORIES VT = 0.46 M/S BUILDING ORIENTATION = 60 DEGREES

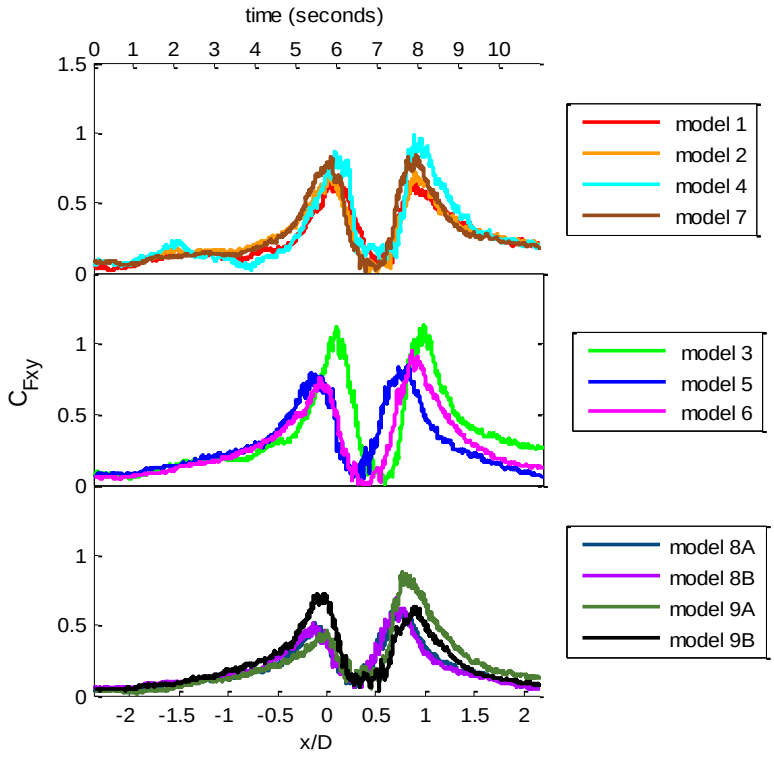

FIGURE 4- 53 CFXY TIME HISTORIES VT = 0.46 M/S BUILDING ORIENTATION = 75 DEGREES

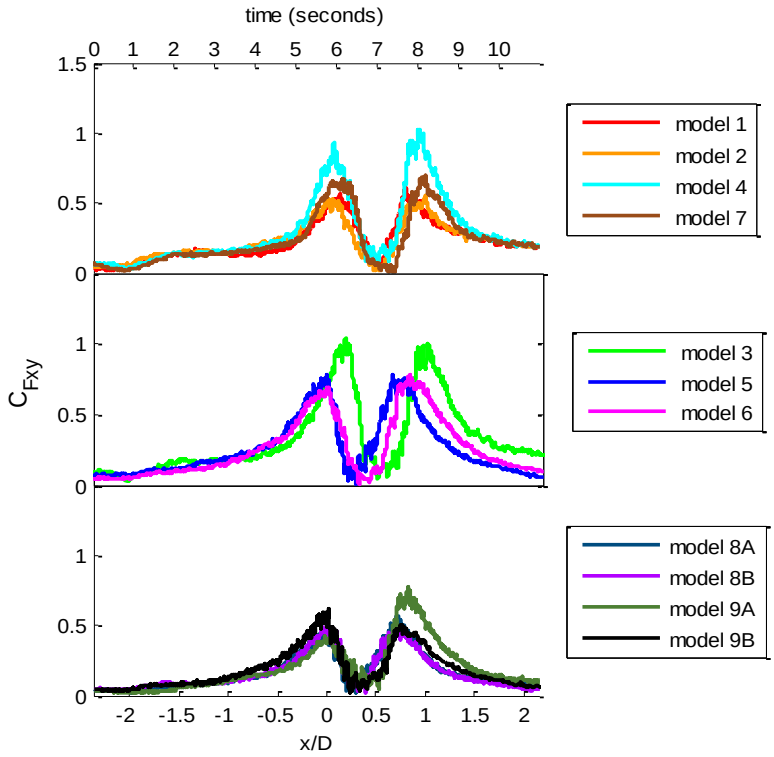

FIGURE 4- 54 CFXY TIME HISTORIES VT = 0.46 M/S BUILDING ORIENTATION = 90 DEGREES

The CF_{xy} time histories are the result of combing the C_{Fx} and C_{Fy} coefficients at each time step and are composed of two positive peaks with the time history approaching zero between the two peaks. The CF_{xy} coefficient is something akin to the total base shear as used in earthquake engineering. In the damage survey done for the Mapleton, Iowa tornado and as published in other damage survey reports it has been observed that many building structures are moved off of their foundations due to inadequate anchoring. The total drag force coefficient as presented here would serve to quantify the loading that needs to be resisted by the anchorage system for the structure.

The green arrows in Figure 4-55 shows the general direction the total drag acts if the C_{Fx} and C_{Fy} time histories follow the general trend. The exact direction and magnitude of CF_{xy} is, of course, dependent upon the magnitudes of the components C_{Fx} and C_{Fy} and if they follow the general trend (not the case for all building orientations of certain models as mentioned above).

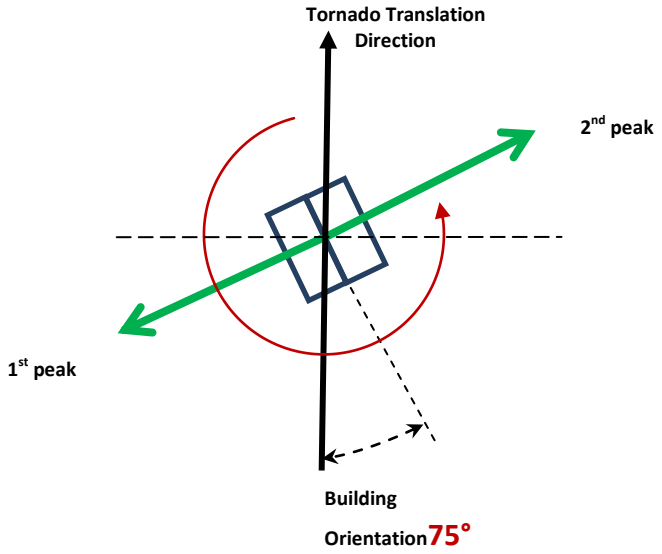

FIGURE 4- 55 GENERAL DIRECTION OF TOTAL DRAG FORCE

In an ideal vortex the tangential velocity at the vortex center would be zero, which would eliminate the drag force on the building when the vortex is at x/D = 0, leaving only a uniform negative external pressure on the surface of the building due to the pressure deficit. In this ideal vortex, both the C_{Fx} and C_{Fy} time histories would cross zero as the tornado passed over the center of the building which in turn would result in a C_{Fxy} value of zero at that particular time step. This is obviously not the case for the CFxy time histories in Figures 4-41 through 4-54. The reason for this is that the vortex used

in these tests, as well as real tornadoes, translate causing asymmetry of the vortex flow field and asymmetry of the time history about x/D = 0. The particular vortex used in these tests has a high swirl ratio resulting in a highly turbulent and dynamic vortex structure where the center "wanders" at each time step. This is also likely the reason why the time histories for models with the same plan dimensions are not super-imposed upon one another.

TABLE 4- 23 PEAK CFXY VT = 0.15 M/S

MODEL / orientation	1	2	3	4	5	6	Overhang	G1A	G1B	G2A	G2B
0°	1.10	0.87	1.02	0.85	0.88	0.83	0.83	0.70	**0.93**	0.98	0.94
15°	1.00	0.76	0.88	0.77	0.97	0.75	0.87	0.75	0.77	0.92	**0.94**
30°	1.02	0.85	0.99	0.91	**1.18**	0.84	0.80	**0.82**	0.80	0.94	0.90
45°	**1.19**	**0.91**	1.18	1.12	1.12	**0.97**	0.90	0.73	0.72	0.91	0.85
60°	1.18	0.89	**1.29**	**1.21**	0.92	0.96	**0.93**	0.61	0.68	**0.98**	0.89
75°	1.06	0.79	1.09	1.11	0.81	0.84	0.90	0.31	0.59	0.91	0.81
90°	0.69	0.66	1.05	0.99	0.88	0.77	0.76	0.79	0.50	0.79	0.70

G = garage A and B = orientation

Generally, the slower translation speed results in the larger C_{Fxy}. For almost all building orientations, model 1 has higher peak C_{Fxy} values compared to model 2. The sole difference between models 1 and 2 is that model 2 has an 84% higher eave. The drag coefficients, C_{Fx} and C_{Fy}, were normalized with an area that is a function of the height of the building and, therefore, it is possible that the drag force on model 2 is larger than that of model 1.

TABLE 4- 24 PEAK CFXY VT = 0.46 M/S

MODEL / orientation	1	2	3	4	5	6	Overhang	G1A	G1B	G2A	G2B
0°	0.78	0.83	1.01	0.85	0.86	0.67	0.88	0.72	0.70	**1.07**	**0.91**
15°	0.91	0.73	0.81	0.69	1.02	0.79	0.82	0.81	0.73	1.00	0.86
30°	**0.97**	0.81	0.99	0.85	**1.19**	0.88	0.76	0.80	**0.79**	0.95	0.87
45°	0.89	**0.90**	**1.24**	1.13	1.07	0.84	0.84	**0.91**	0.77	0.87	0.79
60°	0.85	0.82	1.17	**1.17**	0.98	0.91	**0.94**	0.69	0.70	0.86	0.85
75°	0.65	0.72	1.13	0.98	0.84	**0.95**	0.84	0.61	0.69	0.88	0.73
90°	0.61	0.55	1.04	1.02	0.78	0.78	0.69	0.56	0.49	0.78	0.62

G = garage A and B = orientation

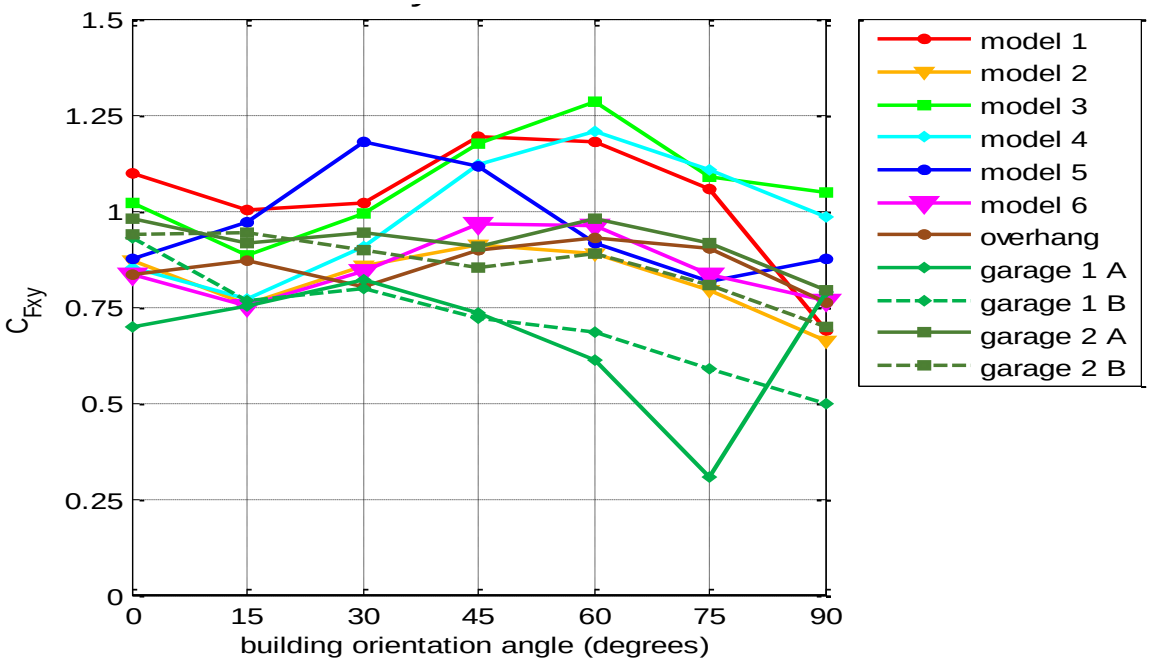

FIGURE 4- 56 PEAK CFXY VT = 0.15 M/S

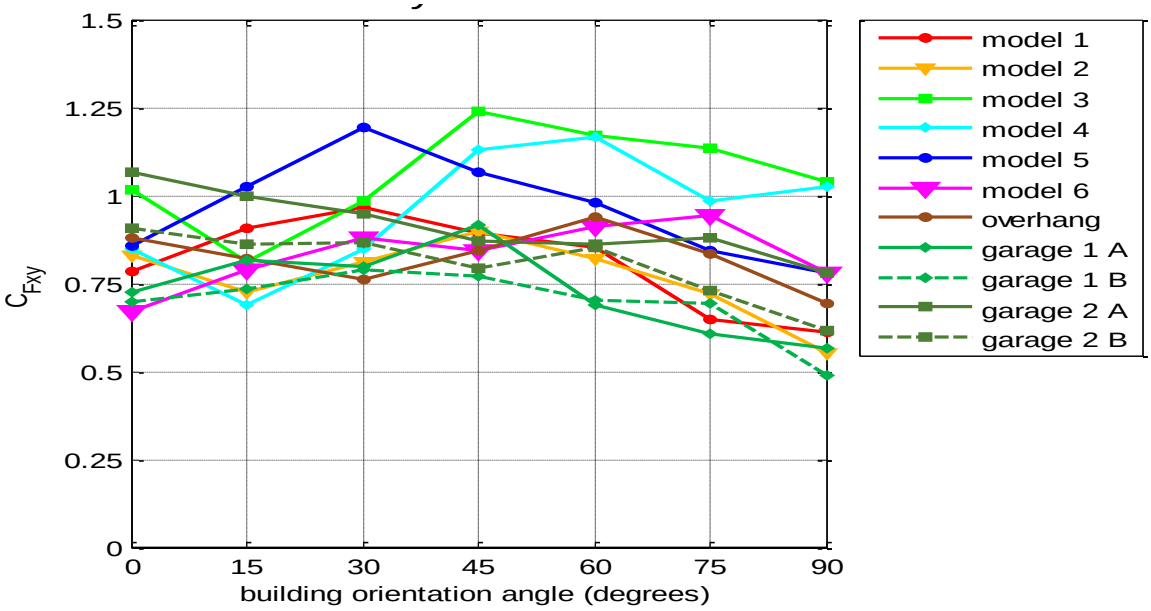

FIGURE 4- 57 PEAK CFXY VT = 0.46 M/S

4.1.5 C_{Fz}

The vertical (z) force coefficient time histories of each model for the 0°-90° building orientations and 0.15 m/s translation speed are given in Figures 4-58 through 4-64 and the time histories for the 0.46 translation speed are shown in Figures 4-65 through 4-71. The tabulated peak values are given in Table 4-7 for the 0.15 m/s translation speed and Table 4-8 for the 0.46 m/s translation speed.

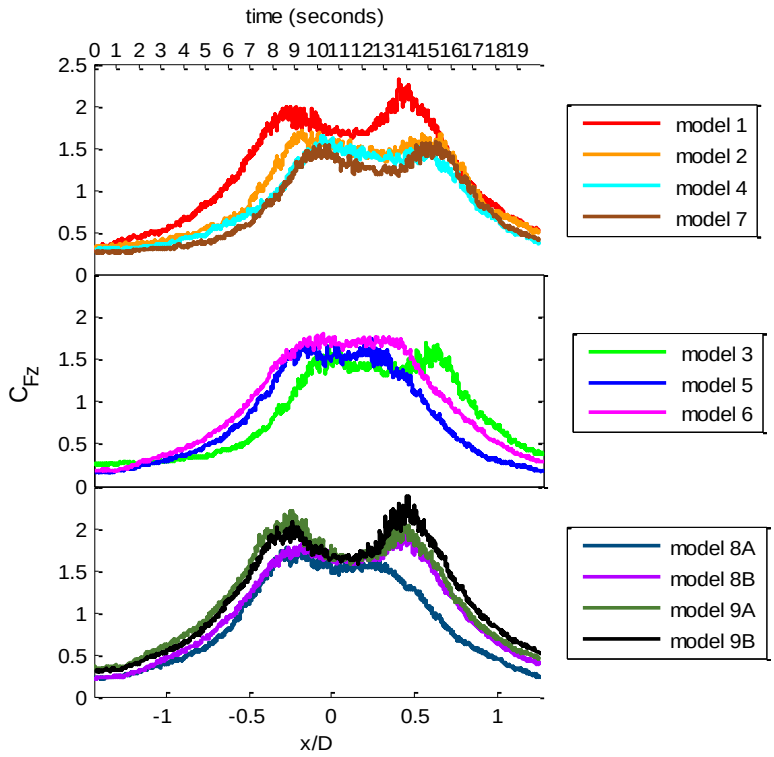

FIGURE 4- 58 CFZ TIME HISTORIES VT = 0.15 M/S BUILDING ORIENTATION = 0 DEGREES

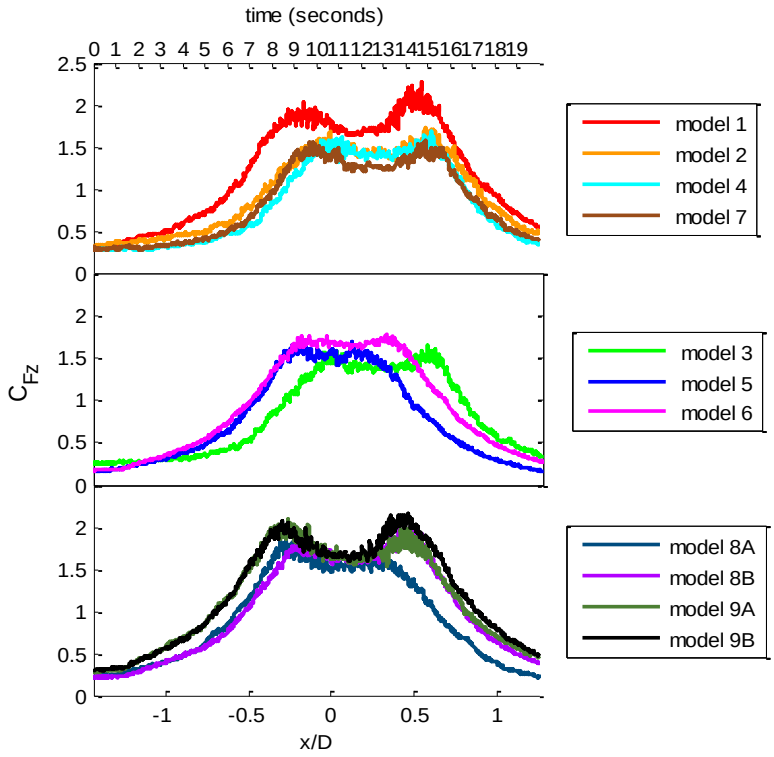

FIGURE 4- 59 CFZ TIME HISTORIES VT = 0.15 M/S BUILDING ORIENTATION = 15 DEGREES

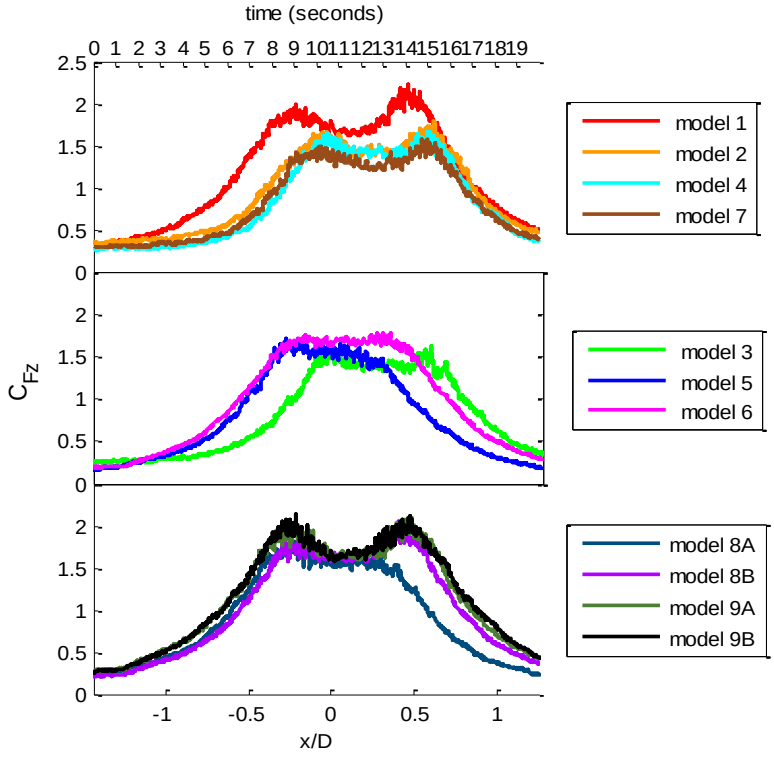

FIGURE 4- 60 CFZ TIME HISTORIES VT = 0.15 M/S BUILDING ORIENTATION = 30 DEGREES

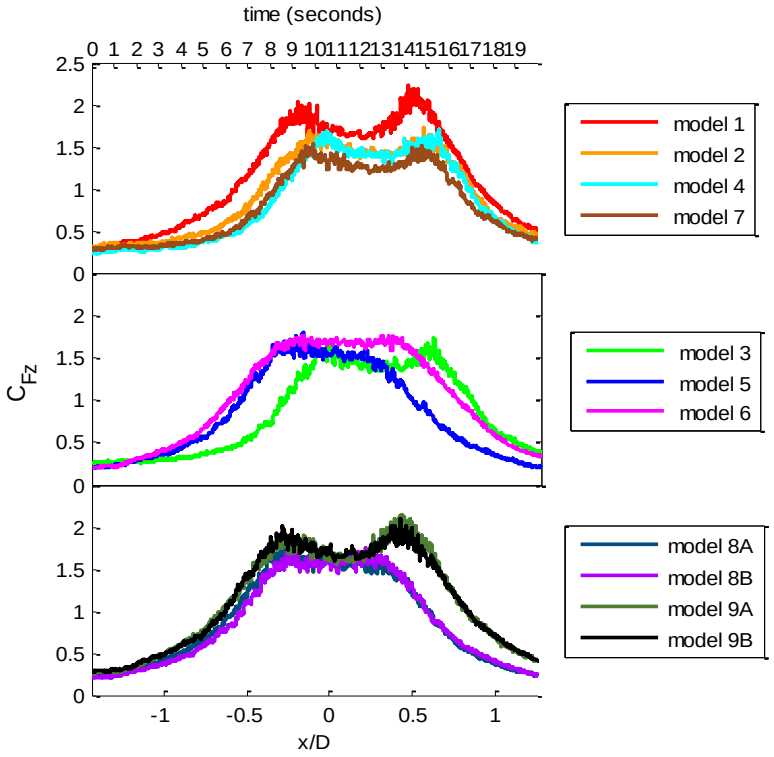

FIGURE 4- 61 CFZ TIME HISTORIES VT = 0.15 M/S BUILDING ORIENTATION = 45 DEGREES

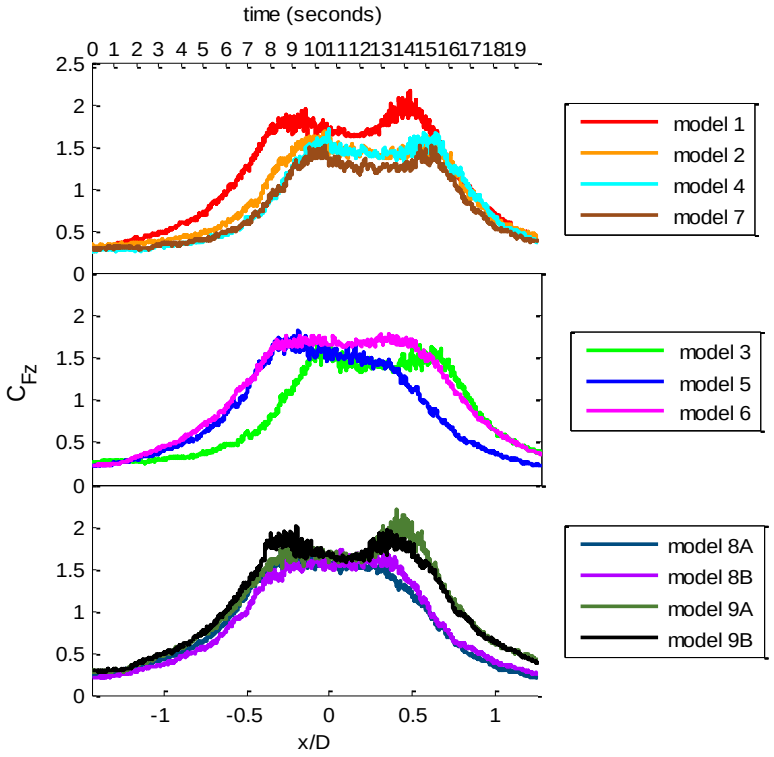

FIGURE 4- 62 CFZ TIME HISTORIES VT = 0.15 M/S BUILDING ORIENTATION = 60 DEGREES

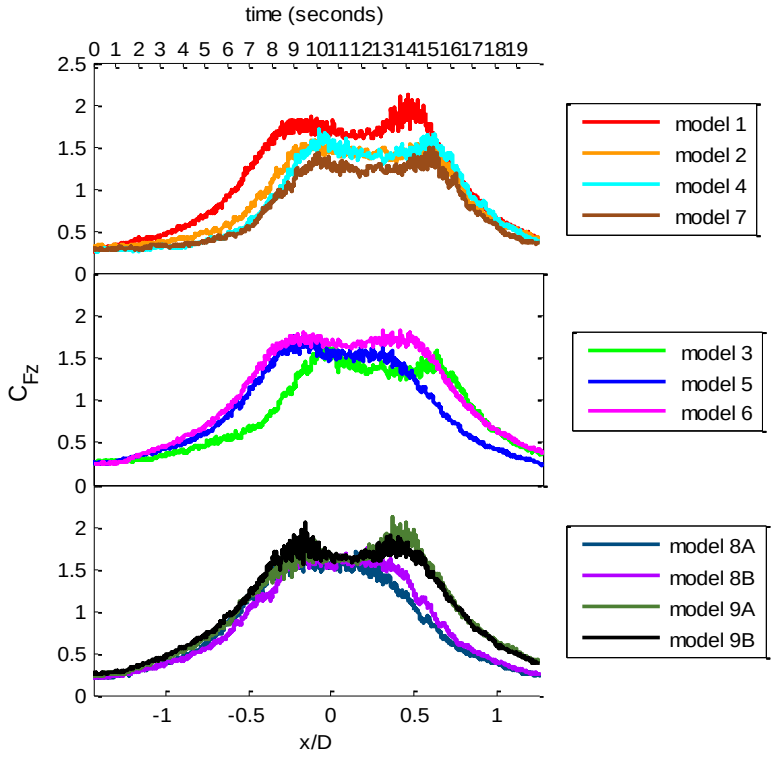

FIGURE 4- 63 CFZ TIME HISTORIES VT = 0.15 M/S BUILDING ORIENTATION = 75 DEGREES

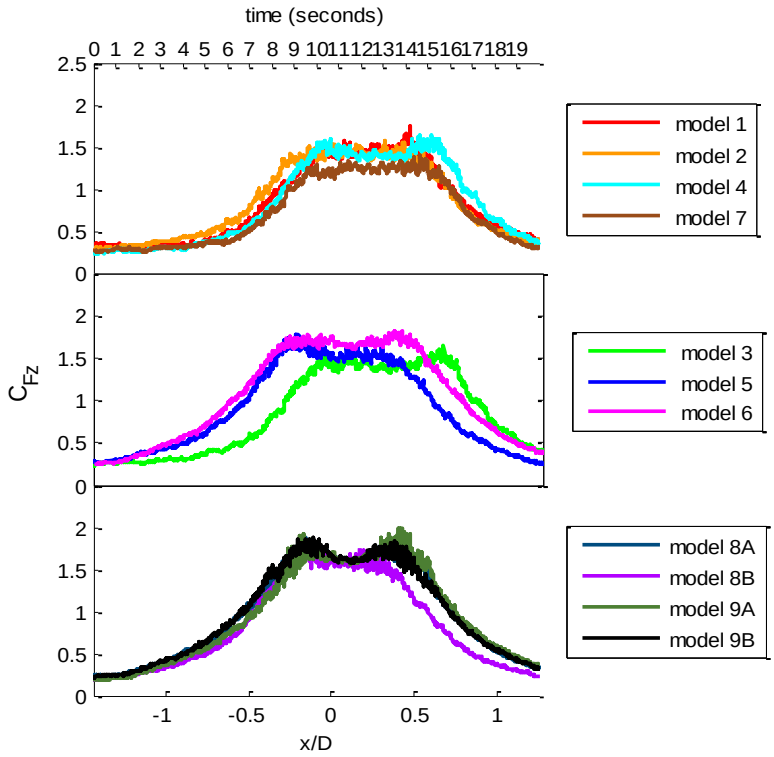

FIGURE 4- 64 CFZ TIME HISTORIES VT = 0.15 M/S BUILDING ORIENTATION = 90 DEGREES

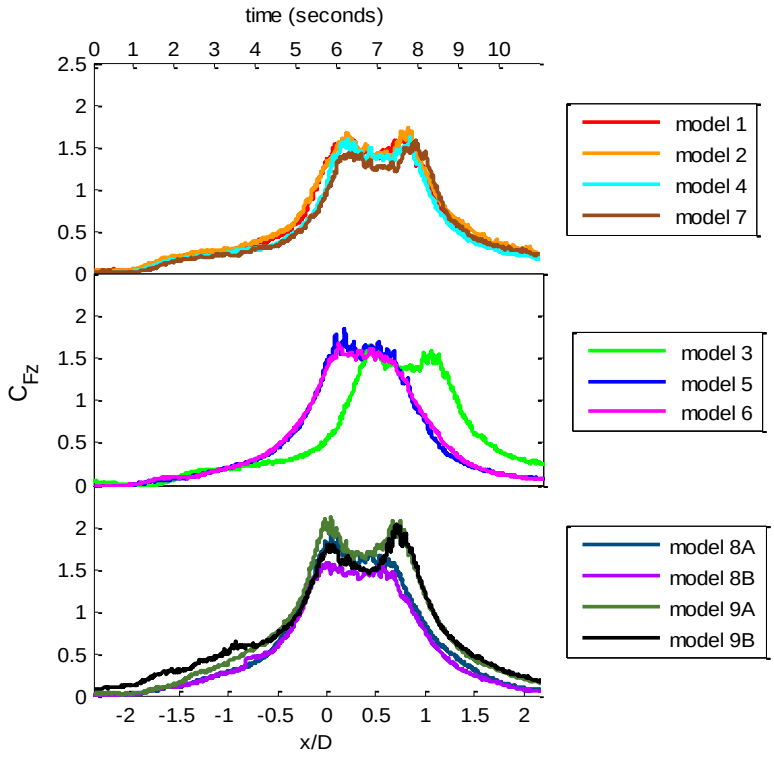

FIGURE 4- 65 CFZ TIME HISTORIES VT = 0.46 M/S BUILDING ORIENTATION = 0 DEGREES

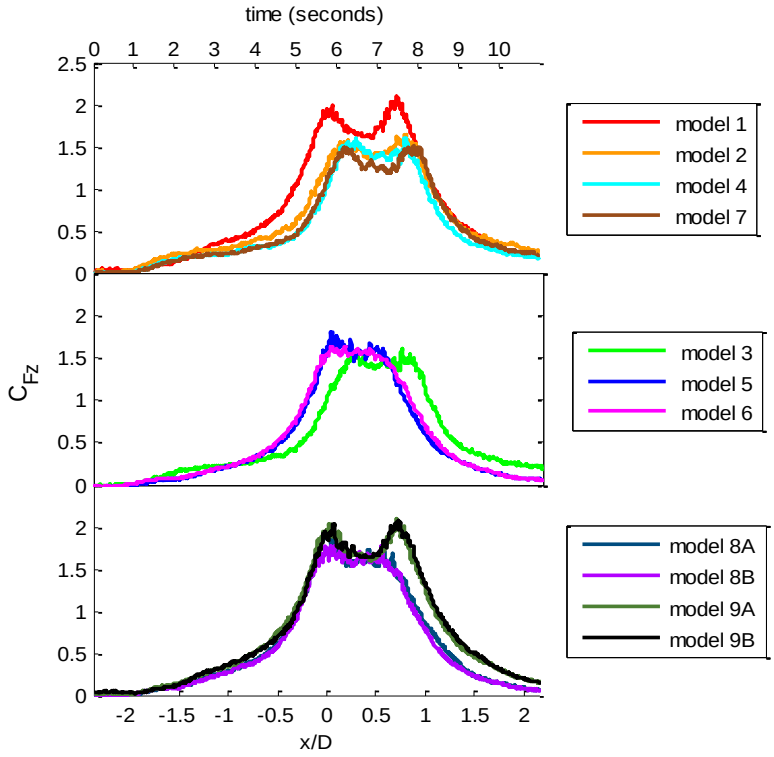

FIGURE 4- 66 CFZ TIME HISTORIES VT =0.46 M/S BUILDING ORIENTATION = 15 DEGREES

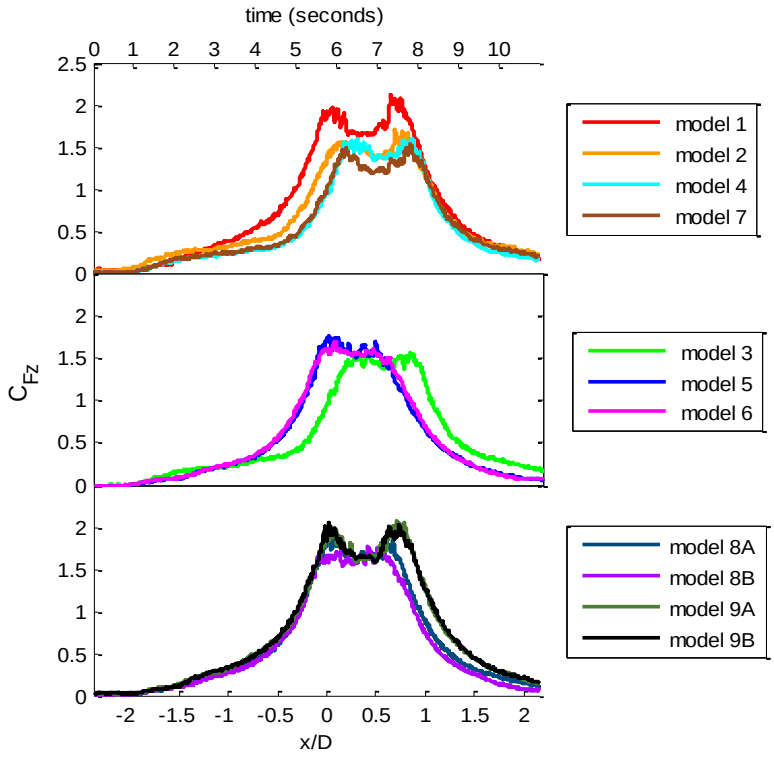

FIGURE 4- 67 CFZ TIME HISTORIES VT = 0.46 M/S BUILDING ORIENTATION = 30 DEGREES

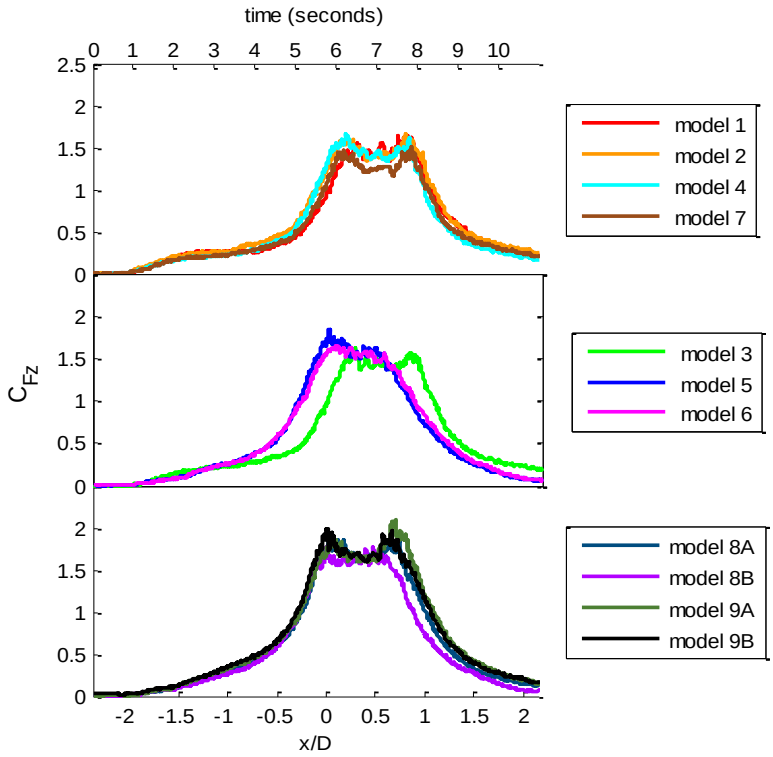

FIGURE 4- 68 CFZ TIME HISTORIES VT = 0.46 M/S BUILDING ORIENTATION = 45 DEGREES

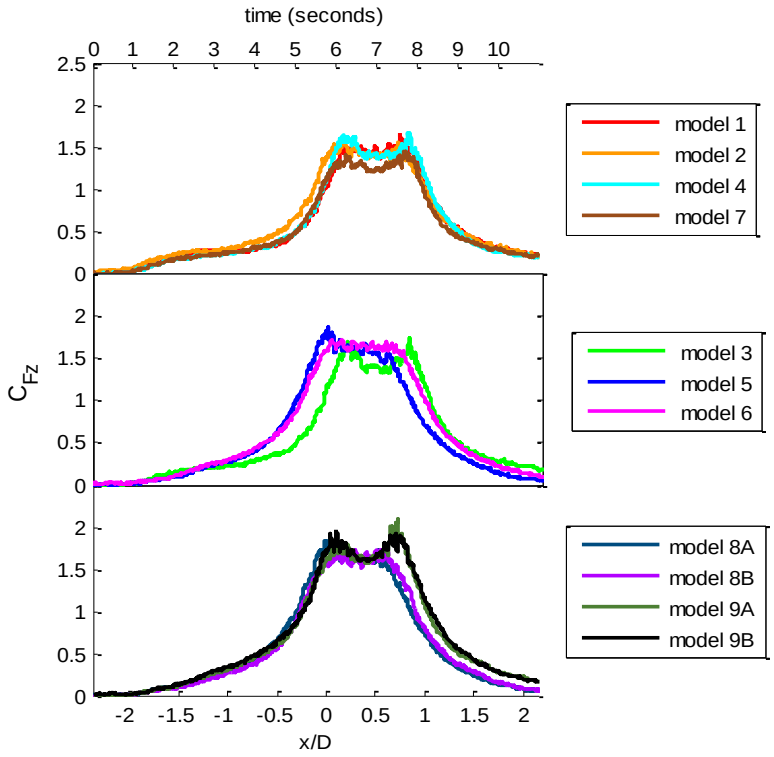

FIGURE 4- 69 CFZ TIME HISTORIES VT = 0.46 M/S BUILDING ORIENTATION = 60 DEGREES

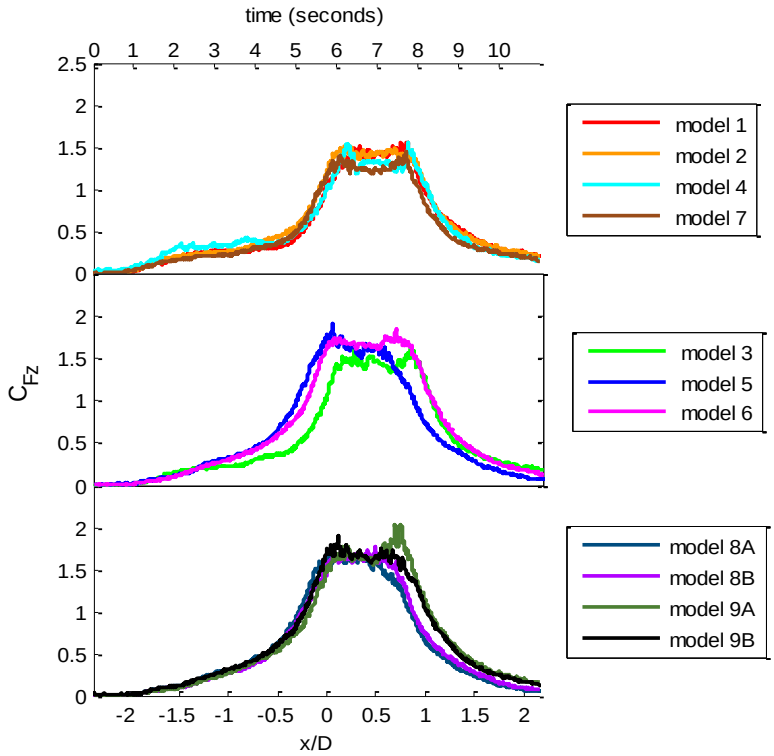

FIGURE 4- 70 CFZ TIME HISTORIES VT = 0.46 M/S BUILDING ORIENTATION = 75 DEGREES

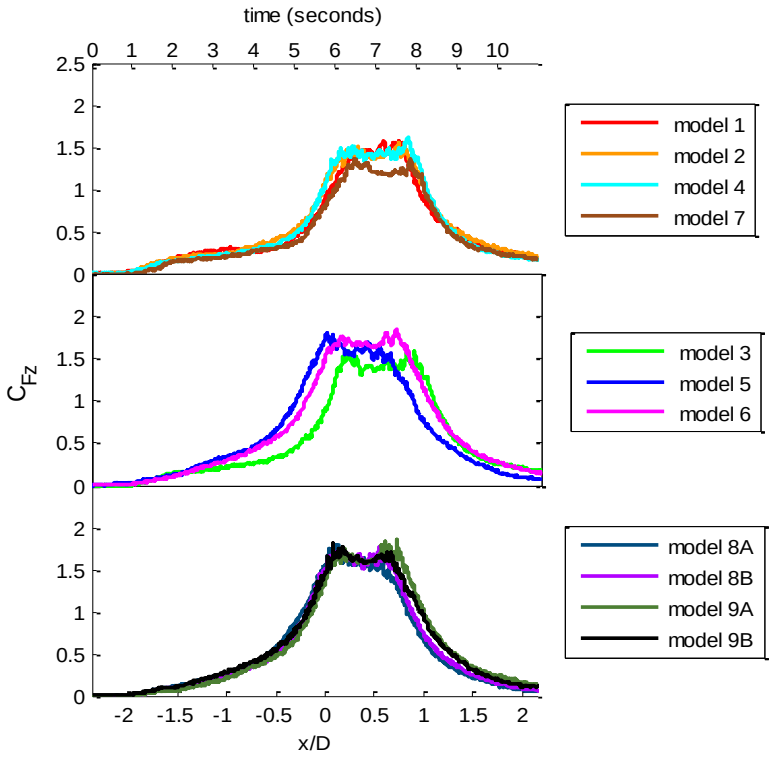

FIGURE 4- 71 CFZ TIME HISTORIES VT = 0.46 M/S BUILDING ORIENTATION = 90 DEGREES

There are two important observations that should be made concerning the C_{Fz} coefficients. The first is that the C_{Fz} time histories peak at a much higher value than C_{Fx}, C_{Fy} and C_{Fxy}. Where C_{Fx} never reached 1.0 for the models tested in the particular simulated tornado and the peaks of the C_{Fy} time histories rarely exceeded 1.0, all of the peaks of all of the models for all of the translation speeds and building orientations exceed one and several exceed 2.0. The second observation that should be made is that only the pressures on the roofs of the models contribute to the aerodynamic force in the vertical direction. In fact only the vertical components of the pressures which act normal to the surface of the roof contribute to the vertical force, which means that the value of the pressures acting normal to the roof are of an even greater magnitude than the vertical force coefficients.

Haan et al. (2010) showed that for a low swirl ratio, single cell vortex that the C_{Fz} time history reached a single, well-defined peak. The time histories above clearly show two distinct peaks. This is most likely due to the high swirl ratio vortex simulated for this study. The valley between the two peaks does not drop to zero because even though the tangential velocity component of the swirling wind approaches zero at the center of the vortex, the pressures on the surface of the building are still affected by the pressure drop at the center of the tornado.

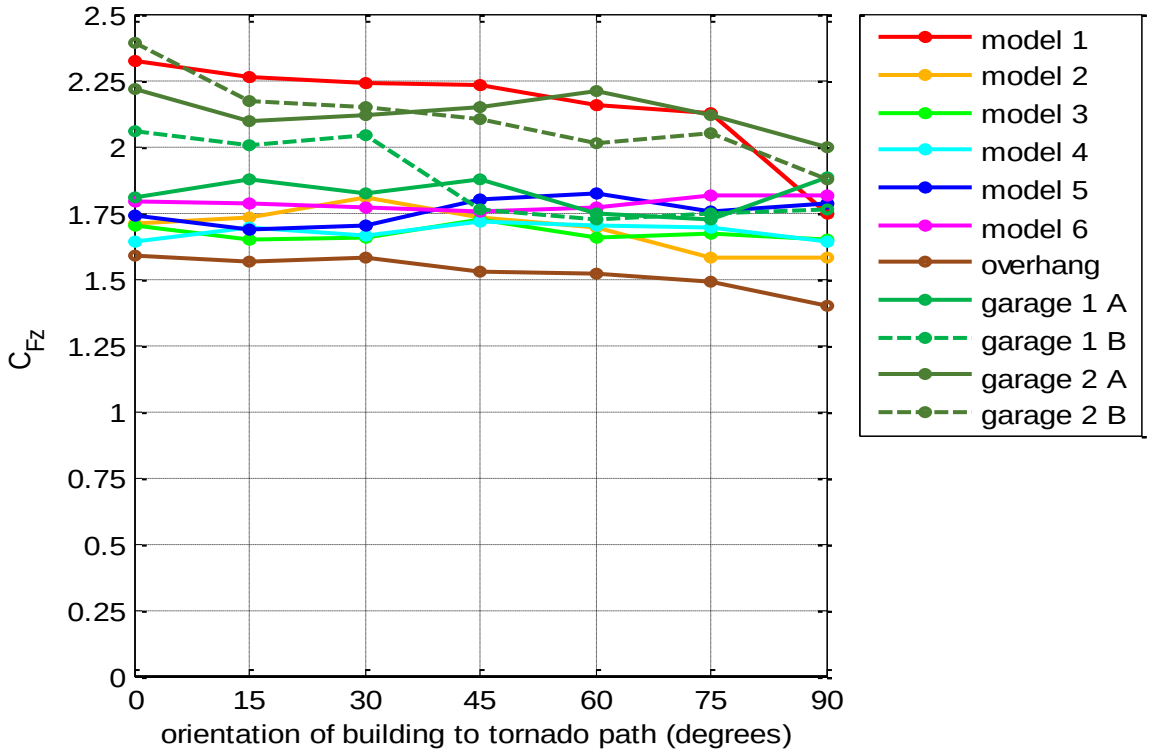

FIGURE 4- 72 PEAK CFZ VT = 0.15 M/S

The duration of the loading on the roofs of the models between the peaks for the 0.15 m/s translation velocity time histories is about 6 seconds and about 2 seconds for the 0.46 m/s translation speed. This shows a 1:1 ratio between translation speed and duration of loading.

TABLE 4- 25 PEAK CFZ VT = 0.15 M/S

MODEL / orientation	1	2	3	4	5	6	Overhang	G1A	G1B	G2A	G2B
0°	**2.32**	1.71	1.70	1.64	1.74	1.79	**1.58**	1.81	**2.06**	**2.21**	**2.39**
15°	2.26	1.73	1.65	1.69	1.69	1.78	1.57	1.88	2.00	2.10	2.17
30°	2.24	**1.80**	1.65	1.67	1.70	1.77	1.58	1.82	2.04	2.12	2.15
45°	2.23	1.73	**1.72**	**1.71**	1.80	1.76	1.52	1.88	1.76	2.14	2.10
60°	2.15	1.69	1.65	1.70	**1.82**	1.77	1.52	1.74	1.72	2.20	2.01
75°	2.13	1.58	1.67	1.70	1.76	1.82	1.49	1.72	1.75	2.12	2.05
90°	1.74	1.58	1.65	1.64	1.79	**1.82**	1.40	**1.88**	1.76	1.99	1.87

G = garage A and B = orientation

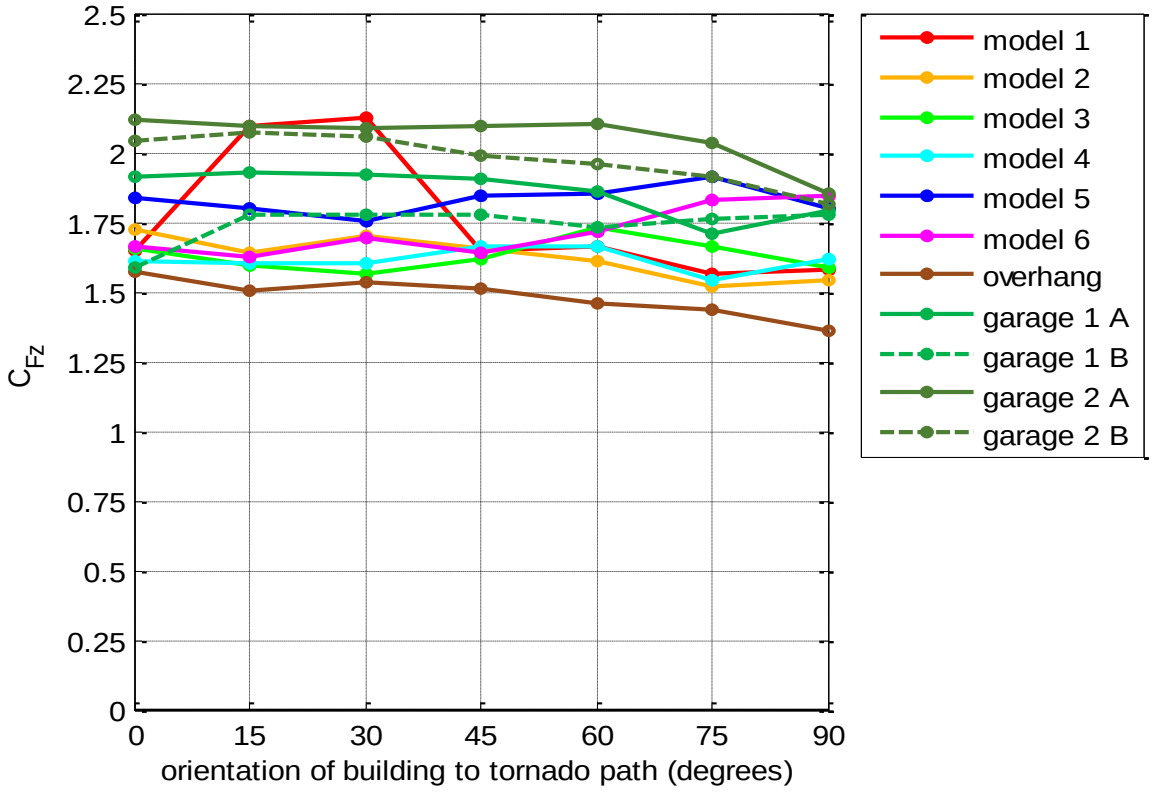

FIGURE 4- 73 PEAK CFZ VT = 0.46 M/S

TABLE 4- 26 PEAK CFZ VT = 0.46 M/S

MODEL / orientation	1	2	3	4	5	6	Overhang	G1A	G1B	G2A	G2B
0°	1.65	**1.72**	1.66	1.61	1.84	1.66	**1.57**	1.91	1.59	**2.12**	2.04
15°	2.09	1.64	1.60	1.60	1.80	1.63	1.50	**1.93**	**1.78**	2.10	**2.07**
30°	**2.12**	1.70	1.57	1.60	1.75	1.70	1.53	1.92	1.77	2.09	2.06
45°	1.65	1.65	1.62	**1.67**	1.84	1.64	1.51	1.91	1.77	2.10	1.99
60°	1.66	1.61	**1.73**	1.66	1.86	1.72	1.46	1.86	1.73	2.10	1.96
75°	1.56	1.52	1.66	1.54	**1.91**	1.83	1.44	1.71	1.76	2.04	1.91
90°	1.58	1.54	1.59	1.62	1.80	**1.84**	1.36	1.79	1.78	1.85	1.81

G = garage A and B = orientation

From Tables 4-7 and 4-8 it can be seen that for almost every case the peak C_{Fz} for model 1 is higher than for models 2 and 4 which have the same roof pitch but different eave heights. For the V_T = 0.46

m/s cases the peak C_{Fz} for model 1 are much closer to the values for models 2 and 4 than they are for the V_T = 0.15 m/s cases. It is also interesting to note that the peak C_{Fz} values for model 1 are similar to those for the garage 2 model which is geometrically similar to model 1 except for the addition of a "garage" to one end.

Model 1 also has much higher peaks than the overhang model which is geometrically the same except for an overhang on all four sides with an enclosed soffit on the sides parallel to the ridge of the roof. The reason for the considerable difference between the overhang model and model 1 is that the soffit of the overhang model experienced downward pressures reducing the total aerodynamic uplift force on the model. This observation may point to a possible mitigation measure to reduce the net pressure on the roof sheathing by reducing the difference between the internal pressure in the attic and the pressure drop in the vortex core through adequate soffit ventilation area.

Models 3, 4 and 5 all have the same plan dimensions and similar h/L ratios but different roof pitches (mode 3 = 4.6° model 4 = 15.95° model 5 = 35.5°). For the cases with V_T = 0.15 m/s they all have similar peak CFz values centered around 1.75 for all building orientations. For the cases with V_T = 0.46 m/s the peak values increase for model 5 but decrease slightly for models 3 and 4.

For most cases the garage 1 model has higher peak values when compared to model 5 which is geometrically similar to the garage 1 model without the addition of the garage. This cannot be directly attributed to the uplift on the garage portion of the model which has a roof pitch of 15.95° because model 4 has the same roof pitch as the garage addition and a similar eave height but has lower peak C_{Fz}'s than model 5. In most cases there is a bigger difference between the peak values for the A and B orientations of garage A than there is between model 5 and orientation A (house part of model experiences tornado first for the building orientation of 0°) of the garage 1 model.

Models 5 and 6 have the same roof pitch, the same eave height and are both square in plan but have different plan dimensions and ridge heights. For the VT = 0.15 m/s cases both models have similar peak values but for the cases with VT = 0.46 m/s the peaks for model 5 are slightly higher. This cannot be solely attributed to the different plan dimensions because models 3 and 4 have the same plan dimensions and area as model 5 but have peak values closer to model 6 even though they have different roof angles.

4.2 Evaluation of Roof-to-Wall Connections and Sheathing Uplift Failures

It is clear from the above analysis that the roof of a low-rise building experiences loads much greater than the other parts of the building. These loads are also observed to be uplift loads as the vertical direction force coefficients are all positive. Combining these two observations with the fact that nailed connections are weak in uplift and that most residential roof construction methods utilize nailed joints explains why roofs are the most vulnerable part of a house during extreme wind events including tornadoes.

The two main connections in residential roof construction that are most susceptible to uplift loads are the roof sheathing to rafter/truss connection and the roof-to-wall-connection (RTWC). In the region of the United States most prone to tornado strikes, both of these are traditionally nailed connections. Therefore, it was considered valuable to evaluate their performance when undergoing the tornado loading based on the tests simulated in the laboratory.

The sequence of progressive failure of low-rise residential structures in tornadoes is not well understood. Thampi et al. (2011) demonstrated that once the building envelope is breached, either through failure due to wind pressures or debris impact, internal pressures change the sequence of failure and failure mode of the structure. Thampi et al. (2011) also demonstrated that for the low-rise building tested that the failure of the roof occurred for a sealed building, but the failure of a door caused failure of the gable end. Therefore, for the purpose of tornado resistant design, it is useful to understand where the initial failure is most likely to occur. Due to the complexity of failure sequences of low-rise buildings in tornadoes and the value of understanding where initial failure would occur, the following analysis only attempts to determine which of the two roof connections mentioned above would fail first if the rest of the structure remained intact.

Several objectives were formulated for analyzing the performance of sheathing to rafter/truss connections and RTWC on full-scale roofs geometrically similar to the models in this study.

1. To evaluate the effect of building height and roof pitch on the performance of these connections
2. To determine at which point in the tornado loading time history initial failure occurs and which connection fails first

3. To compare the two connections' performance under tornado loading with the expected performance as described in the proposal for the Enhanced Fujita Scale
4. To compare the performance of different combinations of fasteners in order to make recommendations for tornado resistant design

The effect of roof pitch and h/L ratio on the type location of initial failure was considered to be a valuable contribution that fell within the scope of this study. Only the initial failure was considered to lie within the scope of this study, because the inherent complexity of the sequence of failure requires an in-depth investigation. It was, therefore, believed that the use of a simplified analysis procedure would produce acceptable results in predicting initial failure. Several assumptions were made in the analysis. The assumptions were as follows:

1. Internal pressures were not considered (i.e. the building remained sealed until the initial failure).
2. Failures were considered to be independent (i.e. failure times were calculated for each connection as if no other connections had failed).
3. Only initial (first) failures were considered.
4. Pressures were considered to be uniform over the entire pressure tap tributary area.
5. Loads on the tributary area of a roof truss did not affect the support reactions of other trusses (i.e. load sharing was not considered).
6. The testing methods used by other studies to determine the capacities of the connections were considered to adequately represent the loading induced by tornado winds.

4.2.1 Analysis Procedure

In order to evaluate the effect of both building height and roof pitch on the performance of the sheathing to rafter/truss connection and the RTWC, model 1 and model 5 were selected to be analyzed. The pressure time histories of the two models for the V_T = 0.15 m/s cases were first converted to pressure coefficient time histories using Eqn. 4-5, where P_i is the recorded pressure (i.e. the total pressure minus the static pressure) at time step i, V_H is the maximum horizontal component of the wind velocity at the radius of the core (r_c), and ρ is the density of air.

$$C_{P_i} = \frac{P_i}{\frac{1}{2}\rho V_H^2} \qquad (4\text{-}5)$$

The velocity measurements were taken for 26 seconds while the simulated vortex was stationary. Twenty-six seconds was, therefore, considered to be the model-scale averaging time. The full-scale tornado that was simulated was considered to have a maximum horizontal velocity of 73.76 m/s at the full-scale averaging time equivalent to the model-scale averaging time. The velocity scale was then calculated by dividing the maximum horizontal model-scale velocity (11.7 m/s) by 73.76 m/s. The full-scale averaging time was calculated to be 413 seconds using the velocity scale and a length scale of λ_L = 1:100.

The wind velocity considered to be the expected velocity at which both the sheathing to rafter connection and the RTWC would have reached their capacity based upon the proposal for the Enhanced Fujita scale (Texas Tech University, 2004) is 54.54 m/s (122 mph) 3-second gust. Using the Durst curve the 54.54 m/s 3 second averaging time was converted to a 413 second averaging time giving a horizontal wind speed of 38.5 m/s (86.1 mph).

The roof dimensions of the models were then scaled up to their full-scale equivalents using a length scale of λ_L = 1:100. Based on the full-scale dimensions of the roofs, roof trusses at 0.61 m (24 inches) on center were used in the analysis.

Rectangular tributary areas were used for the trusses and the pressure taps for the analysis. The truss tributary areas and the pressure tap tributary areas were then combined to form a grid of tributary areas as can be seen in Figure 4-74. Each area of the grid corresponds to a particular truss

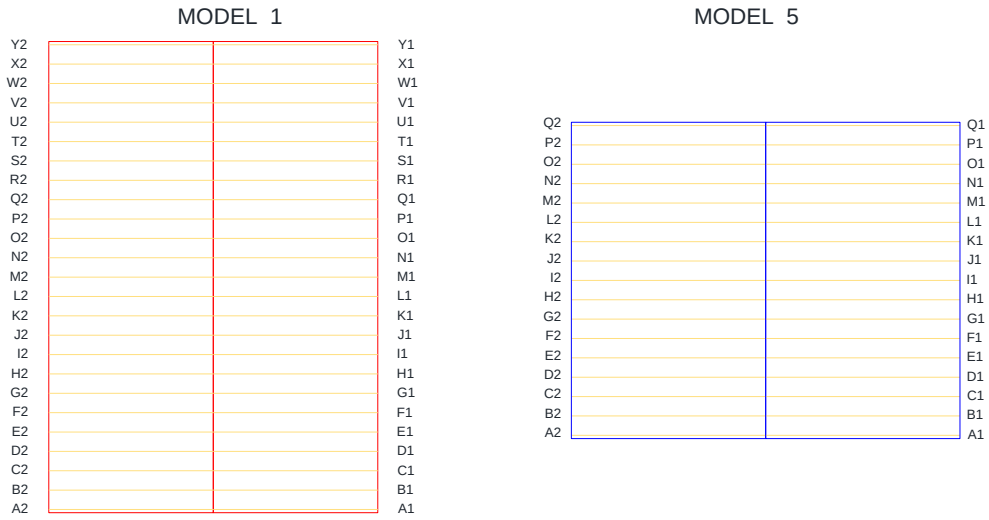

FIGURE 4- 74 ROOF TRUSS LAYOUT SHOWING THE NUMBERING OF THE REACTIONS

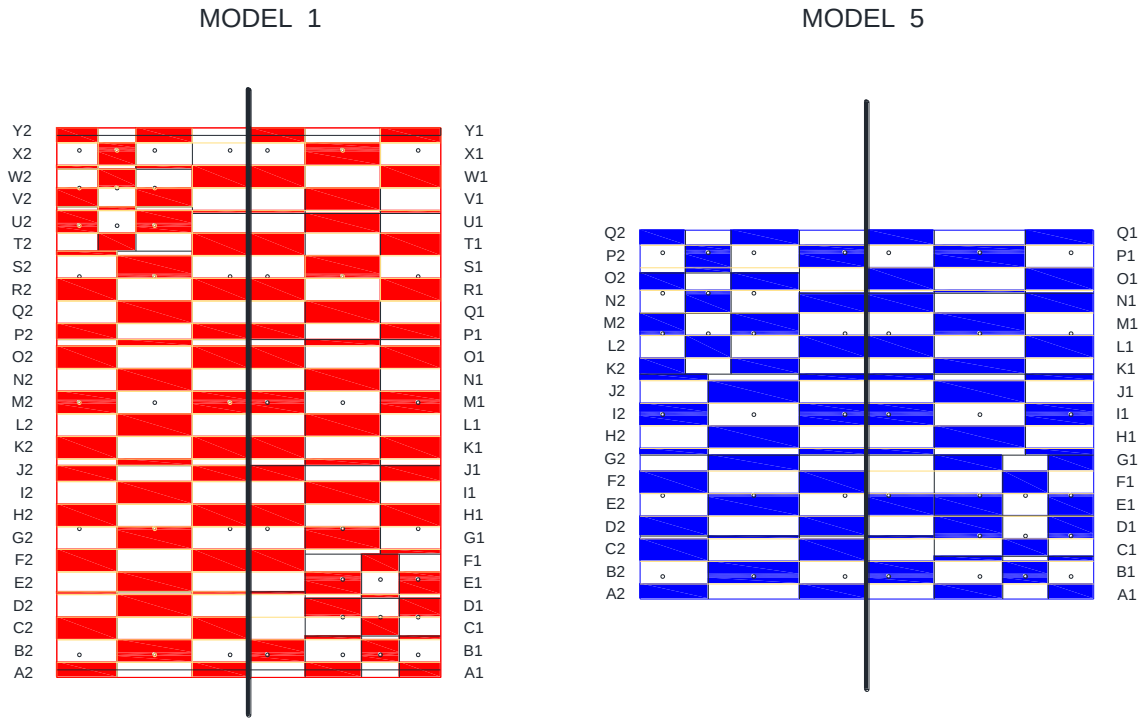

FIGURE 4- 75 ROOF TRIBUTARY AREA GRIDS SHOWING LOCATION OF PRESSURE TAPS (THICK BLACK LINES INDICATING LOCATION OF ROOF RIDGE)

and a particular pressure tap. Using the pressure coefficient time histories and Eqn. 4-5 the full-scale pressures were calculated for each area at each time step. The resultant forces were calculated for each grid area and their vertical components used to calculate the truss reactions using standard static structural analysis methods.

The dead load of the roof was calculated based on the following assumptions

1. All of the roofing material above the sheathing (i.e. shingles etc.) was assumed to have already blown away and therefore was not considered in the dead load
2. The roof is symmetrical about its center ridge line and therefore the dead load could be distributed equally to each reaction of each truss
3. The roof sheathing was considered to be ½" (12.7 mm) thick OSB with a specific gravity of 0.64
4. The roof trusses were Howe trusses composed of nominal 2" x 4" SPF lumber having a specific gravity of 0.47

Since the roof of the models is symmetric about its ridge the dead load was simply subtracted from the calculated reactions due to the tornado loading.

In order to achieve the second objective for this analysis the time step at which the loading exceeded the ultimate capacity of the connection was noted for both the sheathing to truss/rafter connection and the RTWC. The time steps at first failure for both types of connections for each run were then compared to see which type of failure would occur first and at which location.

The analysis was done for 8 combinations of capacities of each of the two types of connections. The capacities used were based upon the reported findings of other researchers as discussed in chapter 2 of this thesis. The sheathing capacities were derived from the published literature by taking the number of samples of each study multiplied by their respective mean maximum capacity then divided by the total number of the samples from all of the studies. The same method was used to derive the capacity for the toe nailed roof-to-wall connection. The hurricane tie capacity was based on the study by Canfield et al. (1991). The reason for this is that the hurricane tie tested by Canfield et al. (1991) is readily available locally in Iowa and the mean maximum capacity is the allowable load given by the manufacturer times a safety factor of 2, which is a reasonable safety factor for timber engineering. The capacities and the combinations thereof can be found in Tables 4-9 through 4-11.

TABLE 4- 27 SHEATHING CAPACITIES USED IN ANALYSIS

Capacity Number	Nail Type	Nailing Schedule	Capacity (psf)	Capacity (kN/m^2)
1	8d smooth shank	6”/12”	87	4.16
2	8d ring shank	6”/12”	168	8.04
3	8d smooth shank	6”/6”	152	7.3
4	8d ring shank	6”/6”	261	12.5

TABLE 4- 28 RTWC CAPACITIES USED IN ANALYSIS

Capacity Number	Connection Method	Fasteners	Capacity (lbs.)	Capacity (kN)
1	toe nailed	3 x 16d smooth shank nails	445	1.98
2	18 gauge hurricane tie	5 x 8d 1-1/2" nails in top plate 5 x 8d 1-1/2" nails in bottom chord of truss	1216	5.4

TABLE 4- 29 COMBINATIONS OF SHEATHING AND RTWC CAPACITIES USED IN ANALYSIS

Combination	RTWC Capacity Number	Sheathing Capacity Number
1	1	1
2	1	2
3	1	3
4	1	4
5	2	1
6	2	2
7	2	3
8	2	4

4.2.2 First Failure Analysis Results

The procedure described above was used to determine which type of roof failure would occur first and at which point in the time history the failure occurred. For both model 1 and model 5 both types of roof-to-wall connections were found to have failed first in every case, although the time separating failure was much less than one second in several cases. Failure for the sheathing panels only occurred for the capacity number one (i.e. 8d smooth shank 6"/12" spacing) and then only for a few panels and only for a few cases. The failure critical time step was the first time step at which the capacity of the connection was exceeded. This is an area for improvement in future analyses which could include the concept of damaging peaks as described by Morrison and Kopp (2011).

The failure times for the two types of roof-to-wall connections and the 8d smooth shank 6"/12" spacing for the sheathing connections for model 1 can be found in Table 4-12, Table 4-13 and Table 4-14 and graphically illustrated in Figure 4-76.

TABLE 4- 30 TIMES OF FIRST TOE NAIL CONNECTION FAILURE FOR MODEL 1 (SECONDS)

run	0°	15°	30°	45°	60°	75°	90°
1	4.5	4.5	4.7	4.5	5.1	4.6	6.9
2	4.1	5.1	5.1	4.9	5.3	4.4	6.3
3	4.5	4.5	4.7	5.2	5.3	5.4	6.9
4	4.5	5.2	4.7	5.2	4.9	4.5	7.0
5	4.3	4.8	4.7	5.3	5.2	5.2	6.7
6	4.2	4.9	5.0	5.5	4.9	4.5	7.3
7	3.4	5.3	4.8	5.3	5.1	4.7	6.2
8	4.2	4.9	4.8	5.2	4.7	4.4	6.0
9	4.0	5.2	3.8	5.2	4.6	4.4	5.8
10	4.2	5.1	5.0	5.5	4.9	4.5	6.7

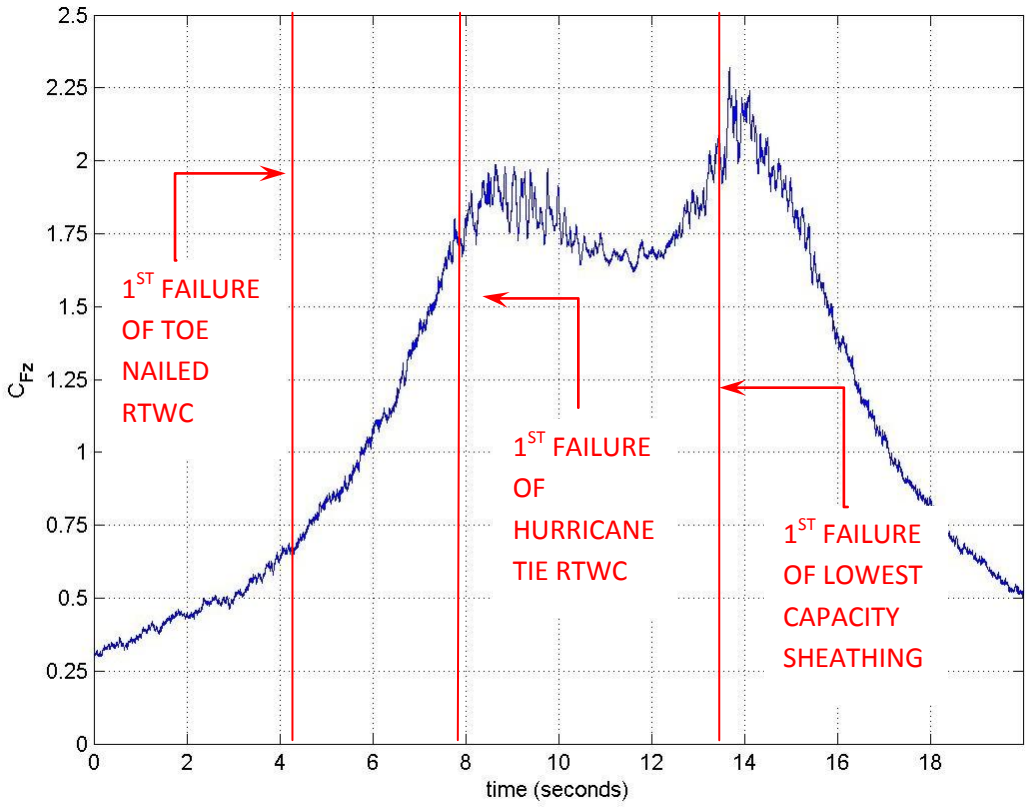

FIGURE 4- 76 CFZ TIME HISTORY MODEL 1 VT = 0.15 M/S BUILDING ORIENTATION = 0 DEG WITH FAILURE TIMES OF CONNECTIONS

TABLE 4- 31 TIMES OF FIRST HURRICANE TIE CONNECTION FAILURE FOR MODEL 1(SECONDS)

run	0°	15°	30°	45°	60°	75°	90°
1	8.3	7.6	8.0	8.3	7.3	7.4	9.9
2	7.7	7.5	7.0	8.5	7.6	7.4	10.5
3	8.3	7.7	7.6	8.2	7.8	8.1	9.6
4	8.0	7.5	8.0	8.1	7.9	7.7	10.3
5	7.7	8.1	7.6	8.4	7.5	7.2	9.9
6	8.1	7.9	7.9	8.4	7.7	8.0	10.4
7	7.7	8.6	7.8	8.0	7.8	8.3	12.2
8	7.7	8.8	7.4	8.4	7.3	7.7	13.2
9	7.4	8.4	7.9	8.0	7.2	7.2	10.0
10	8.1	8.2	7.8	8.7	7.7	7.3	9.9

TABLE 4- 32 TIMES OF FIRST ROOF SHEATHING FAILURE FOR MODEL 1 FOR CAPACITY NUMBER = 1 (SECONDS). A "--" SHOWS THAT NO FAILURE OCCURED FOR THAT PARTICULAR RUN

run	0°	15°	30°	45°	60°	75°	90°
1	14.0	13.6	13.8	8.8	13.2	7.5	--
2	14.0	--	14.1	9.3	8.6	8.7	14.1
3	14.0	13.3	13.8	13.9	8.0	13.7	--
4	13.7	14.0	8.6	8.6	9.1	8.8	--
5	13.3	14.2	13.7	13.9	9.1	14.0	--
6	13.3	14.2	8.7	14.3	7.7	9.2	--
7	13.7	14.3	8.1	9.2	9.2	9.3	--
8	13.2	14.2	8.2	9.0	8.4	8.4	14.0
9	12.9	9.5	9.0	14.0	8.1	8.4	--
10	13.8	14.5	13.4	8.9	13.7	9.0	--

The failure times for the two types of roof-to-wall connections and the 8d smooth shank 6”/12” spacing for the sheathing connections for model 5 can be found in Table 4-15, Table 4-16 and Table 4-17 and graphically illustrated in Figure 4-77.

TABLE 4- 33 TIMES OF FIRST TOE NAIL CONNECTION FAILURE FOR MODEL 5 (SECONDS)

run	0°	15°	30°	45°	60°	75°	90°
1	6.5	6.5	5.9	5.4	5.5	4.6	5.2
2	6.6	6.7	5.8	5.6	5.0	4.9	4.4
3	6.3	6.4	5.8	5.6	5.1	5.3	5.6
4	6.2	6.7	6.2	5.5	5.1	5.0	5.1
5	6.1	6.5	6.5	5.7	5.2	5.3	5.0
6	6.3	6.5	6.2	6.0	5.4	4.8	4.4
7	6.4	6.3	6.1	5.6	5.4	5.2	5.5
8	6.7	6.4	6.0	5.7	4.8	4.6	4.8
9	6.1	6.2	6.0	5.6	5.2	4.9	5.2
10	6.2	6.6	6.3	6.0	4.9	5.2	5.5

TABLE 4- 34 TIMES OF FIRST HURRICANE TIE CONNECTION FAILURE FOR MODEL 5 (SECONDS)

run	0°	15°	30°	45°	60°	75°	90°
1	9.3	8.8	8.5	8.0	7.4	7.5	7.9
2	12.5	8.6	8.2	7.9	7.6	8.1	8.1
3	12.7	9.4	8.7	8.0	7.1	8.3	8.4
4	10.1	8.7	8.1	8.2	7.4	7.9	8.2
5	9.4	9.0	8.3	7.8	7.5	7.6	8.4
6	8.7	9.1	8.4	8.2	7.6	8.3	7.7
7	10.8	11.6	8.3	7.8	7.9	7.7	8.2
8	8.2	8.5	8.5	7.9	7.4	8.6	8.1
9	9.3	8.8	8.0	8.2	7.4	7.2	8.2
10	9.7	8.3	8.2	8.2	7.7	8.6	8.2

TABLE 4- 35 TIMES OF FIRST ROOF SHEATHING FAILURE FOR MODEL 5 FOR CAPACITY NUMBER = 1 (SECONDS). A "--" SHOWS THAT NO FAILURE OCCURED FOR THAT PARTICULAR RUN

run	0°	15°	30°	45°	60°	75°	90°
1	--	--	9.2	9.0	8.4	--	--
2	--	--	--	8.9	8.5	--	--
3	--	--	--	--	9.0	--	--
4	--	--	--	--	8.2	--	--
5	--	--	--	--	8.4	--	--
6	--	--	--	8.9	8.8	--	--
7	--	--	9.0	9.0	--	--	--
8	--	--	--	8.7	--	--	--
9	--	--	--	--	--	--	--
10	--	--	--	8.9	8.0	13.5	--

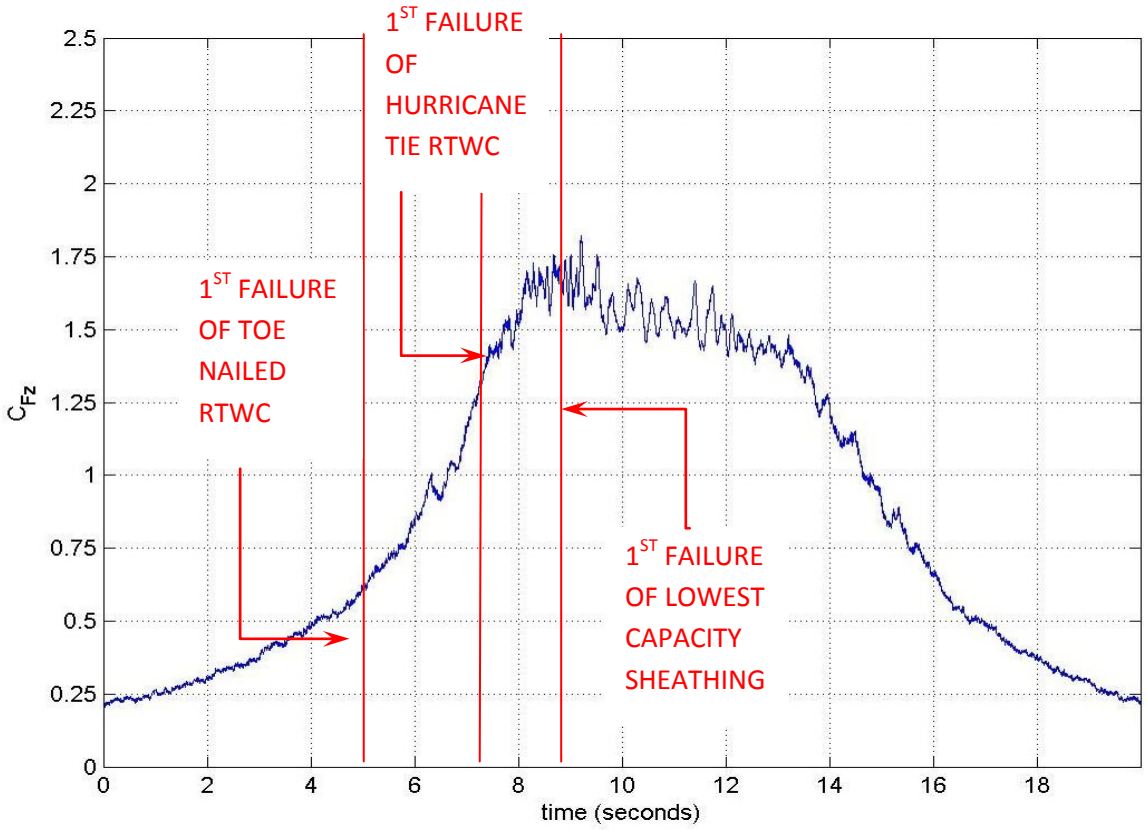

FIGURE 4- 77 CFZ TIME HISTORY MODEL 5 VT = 0.15 M/S BUILDING ORIENTATION = 60 DEG WITH FAILURE TIMES OF CONNECTIONS

The time of failure of RTWC's varies for the different building orientations and the two different models. Sheathing uplift failure is also dependent not only on the maximum tangential velocity and other tornado characteristics, but also on building orientation to the path of the tornado, eave height and roof pitch.

4.2.3 Peak Pressure Coefficients

In order to design for sheathing panel uplift the peak pressures and their distribution must be known. The common way of presenting these peak pressures is in the form of non-dimensionalized pressure coefficients. The peak pressure coefficient contours for model 1 and model 5 are given in Figure 4-79 through 4-92. For the figures with a building orientation of 0° the tornado translation direction is from the bottom of the figure to the top of the figure. For the other figures the tornado path is rotated by the building orientation angle in a clockwise direction (e.g. for the 90° building orientation figure the tornado path is from left to right).

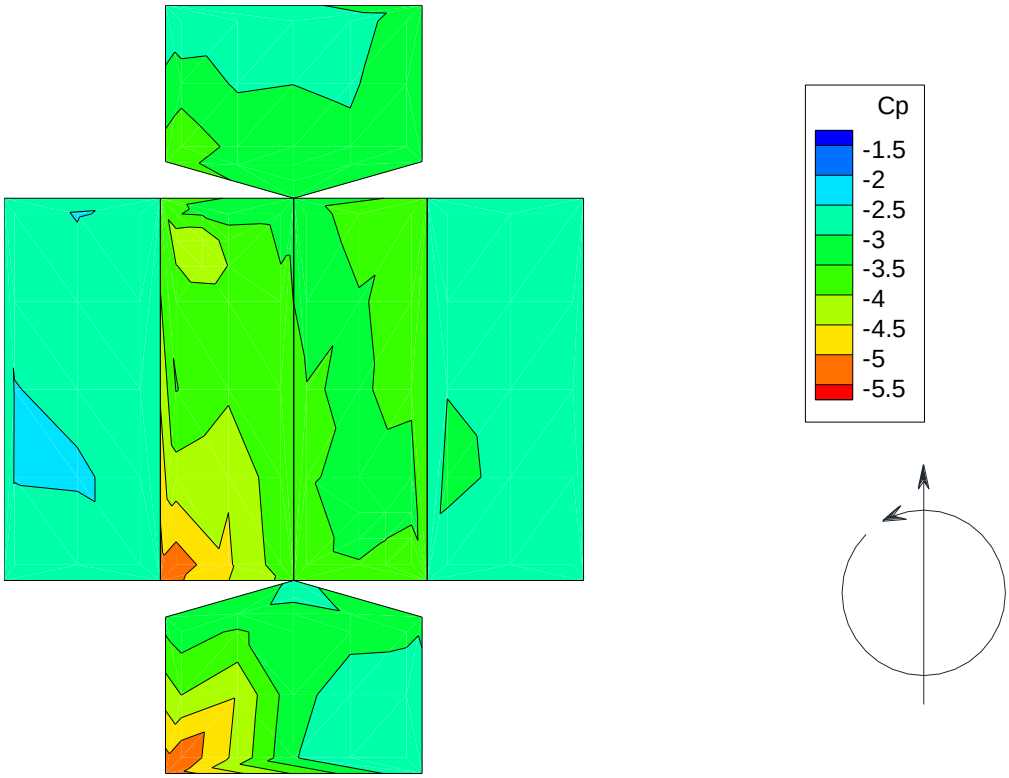

FIGURE 4- 78 PEAK PRESSURE CONTOURS MODEL 1 VT = 0.15 M/S BUILDING ORIENTATION = 0 DEG

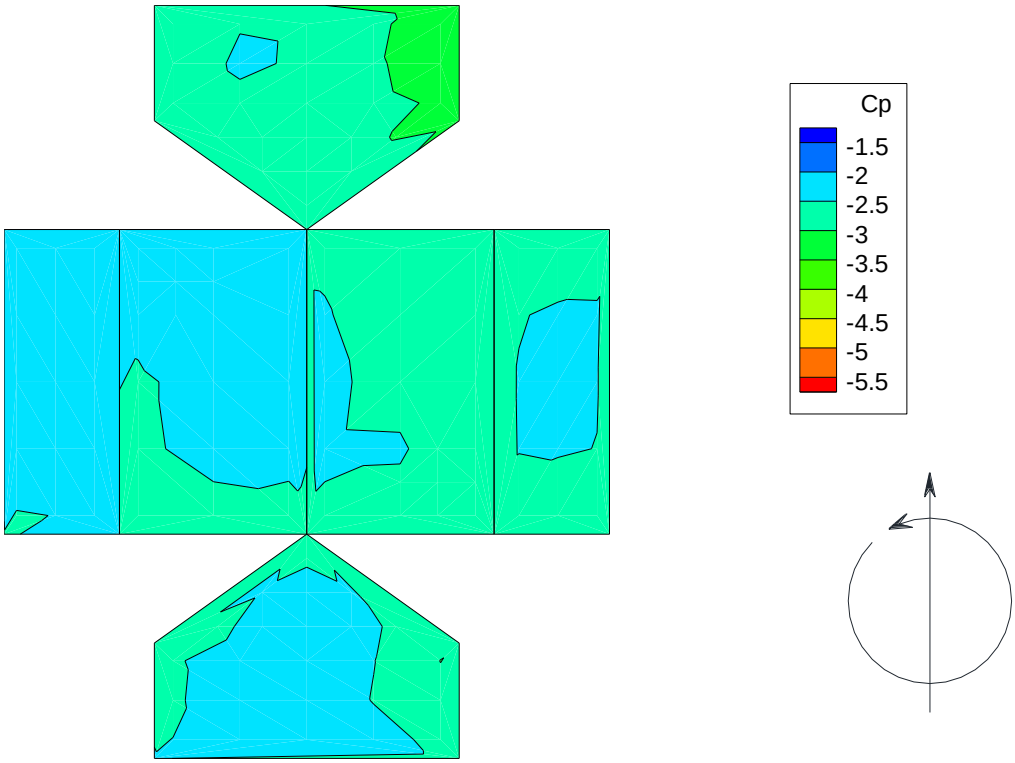

FIGURE 4- 79 PEAK PRESSURE CONTOURS MODEL 5 VT = 0.15 M/S BUILDING ORIENTATION = 0 DEG

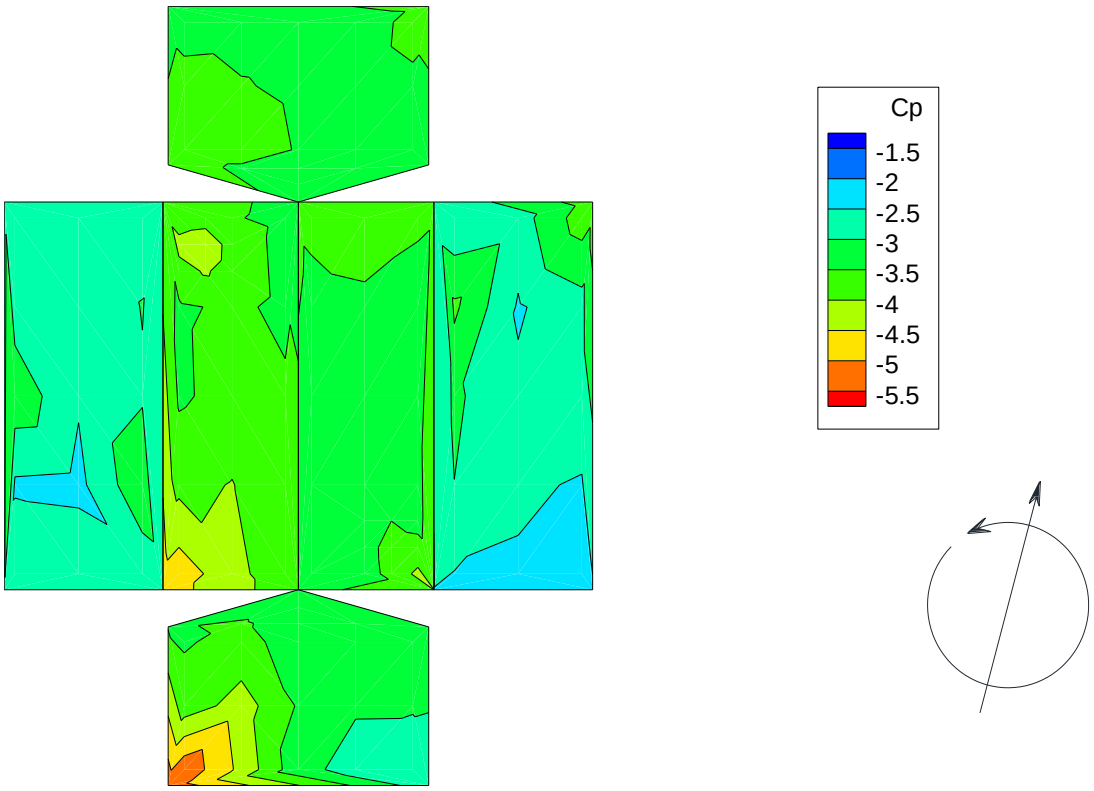

FIGURE 4- 81 PEAK PRESSURE CONTOURS MODEL 1 VT = 0.15 M/S BUILDING ORIENTATION = 15 DEG

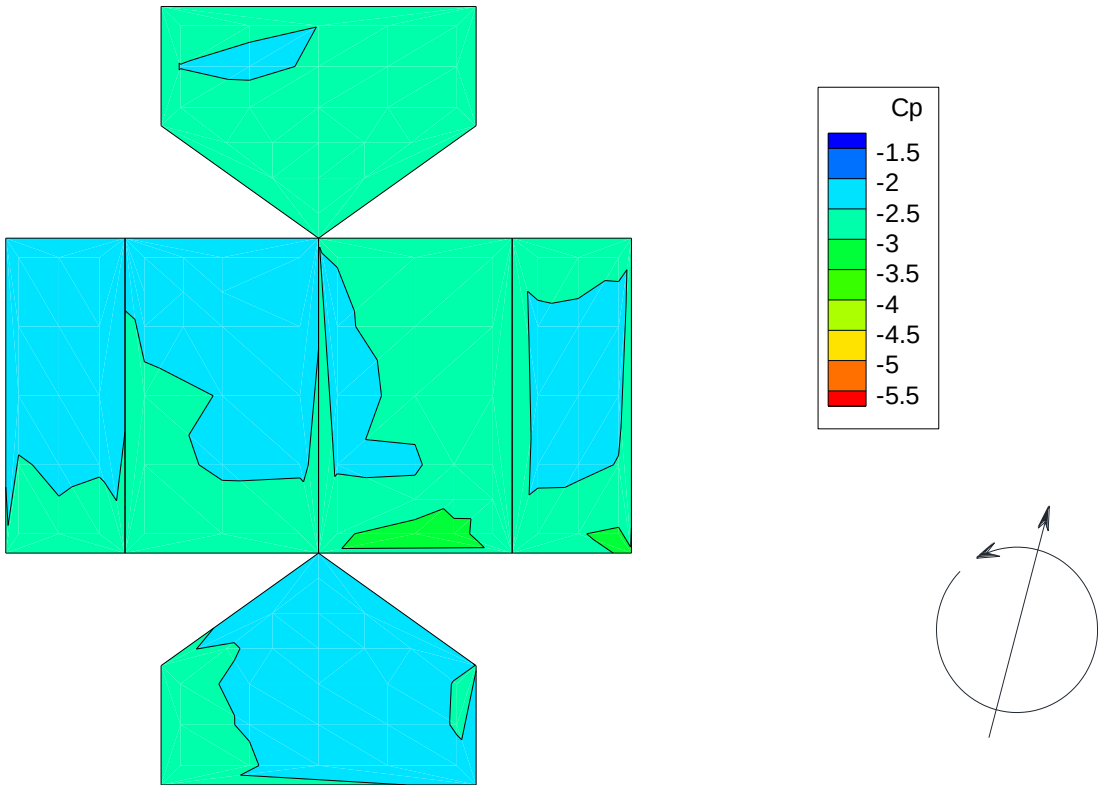

FIGURE 4- 80 PEAK PRESSURE CONTOURS MODEL 5 VT = 0.15 M/S BUILDING ORIENTATION = 15 DEG

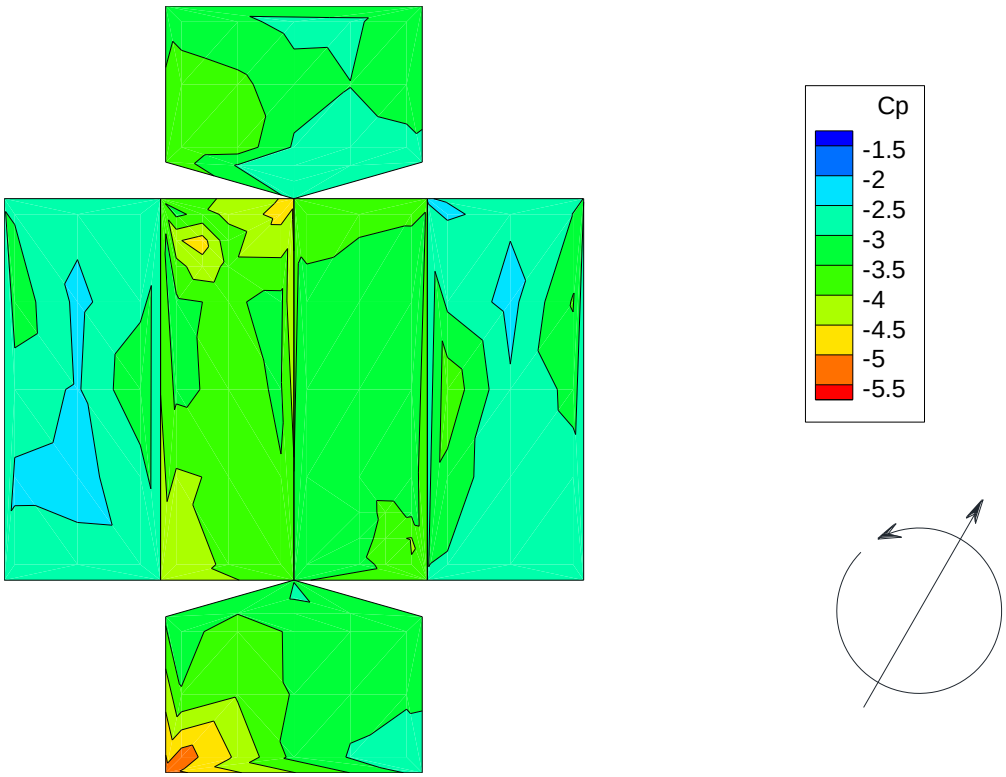

FIGURE 4- 83 PEAK PRESSURE CONTOURS MODEL 1 VT = 0.15 M/S BUILDING ORIENTATION = 30 DEG

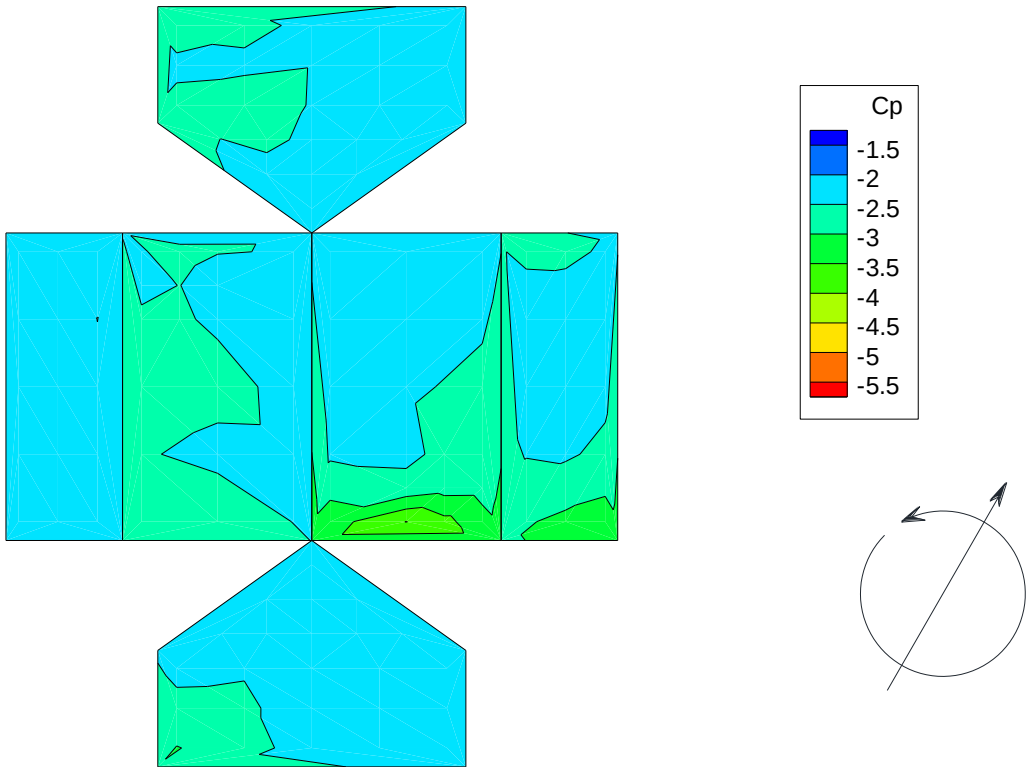

FIGURE 4- 82 PEAK PRESSURE CONTOURS MODEL 5 VT = 0.15 M/S BUILDING ORIENTATION = 30 DEG

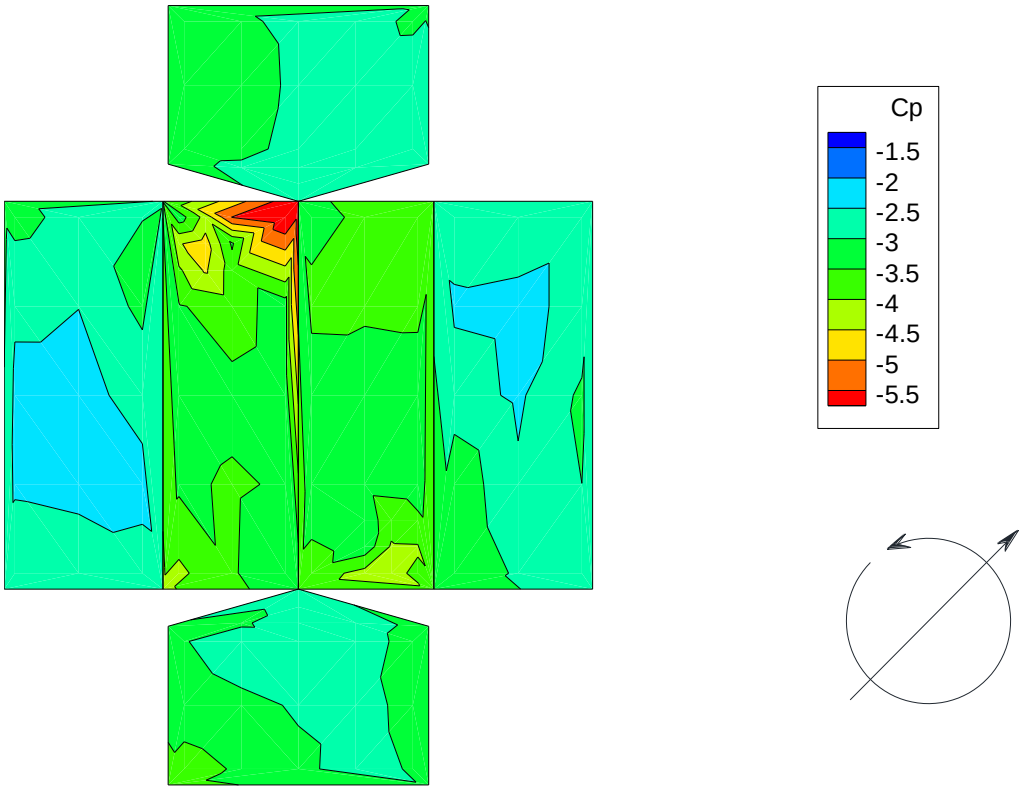

FIGURE 4- 84 PEAK PRESSURE CONTOURS MODEL 1 VT = 0.15 M/S BUILDING ORIENTATION = 45

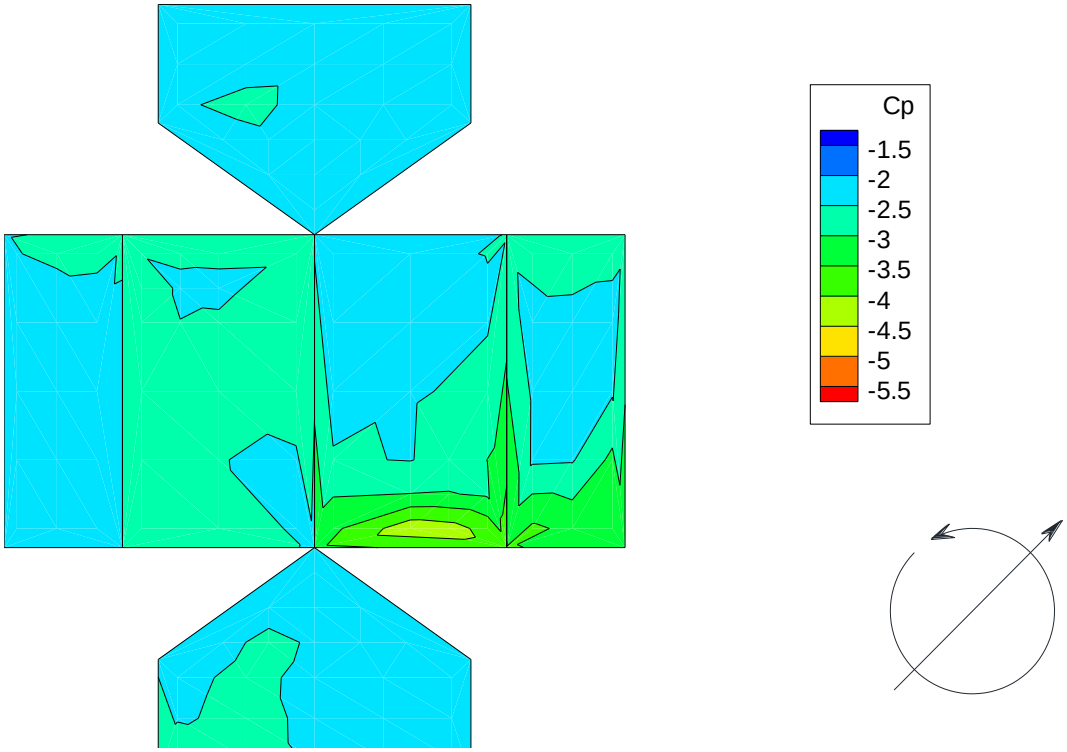

FIGURE 4- 85 PEAK PRESSURE CONTOURS MODEL 5 VT = 0.15 M/S BUILDING ORIENTATION = 45 DEG

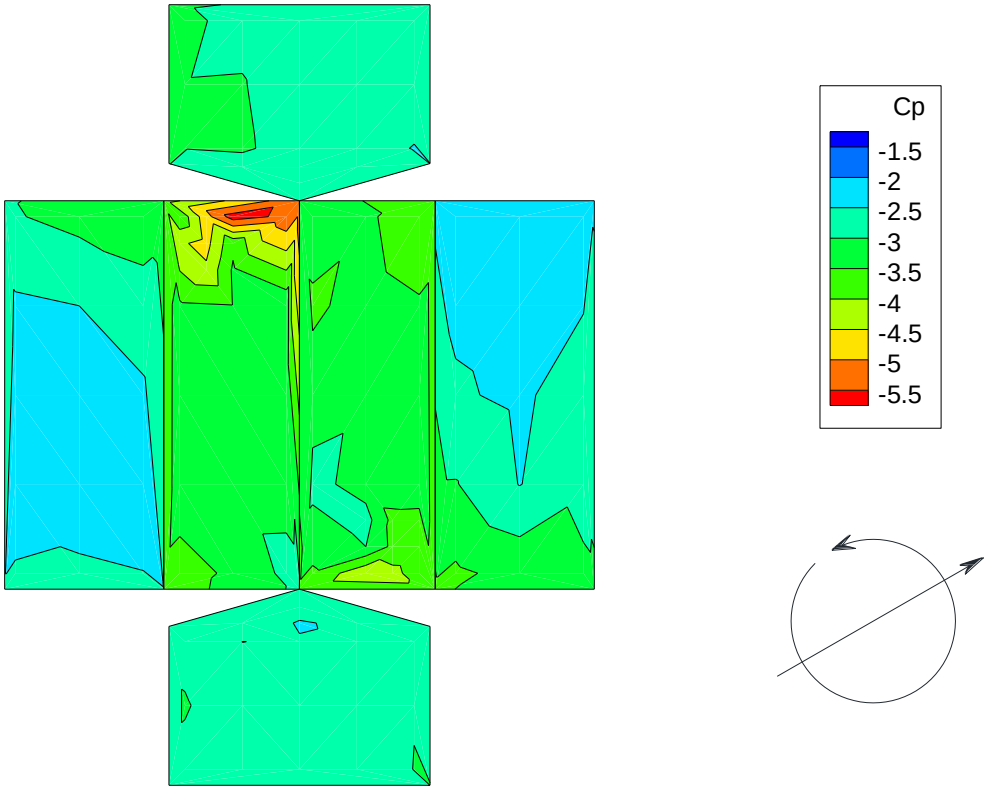

FIGURE 4- 87 PEAK PRESSURE CONTOURS MODEL 1 VT = 0.15 M/S BUILDING ORIENTATION = 60 DEG

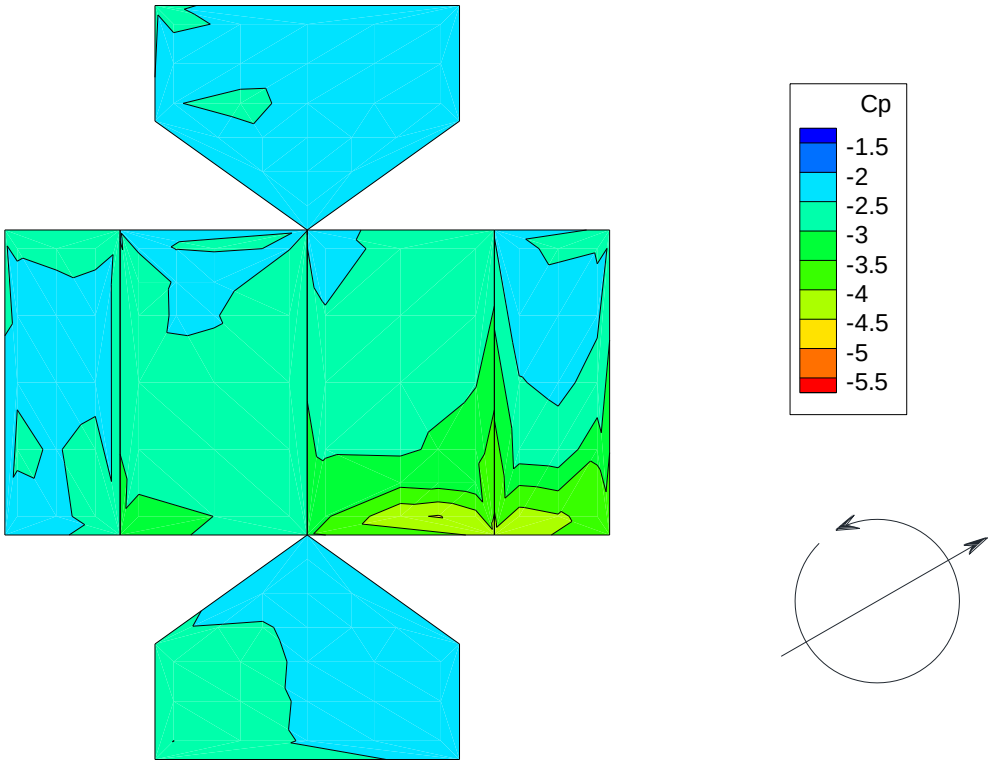

FIGURE 4- 86 PEAK PRESSURE CONTOURS MODEL 5 VT = 0.15 M/S BUILDING ORIENTATION = 60 DEG

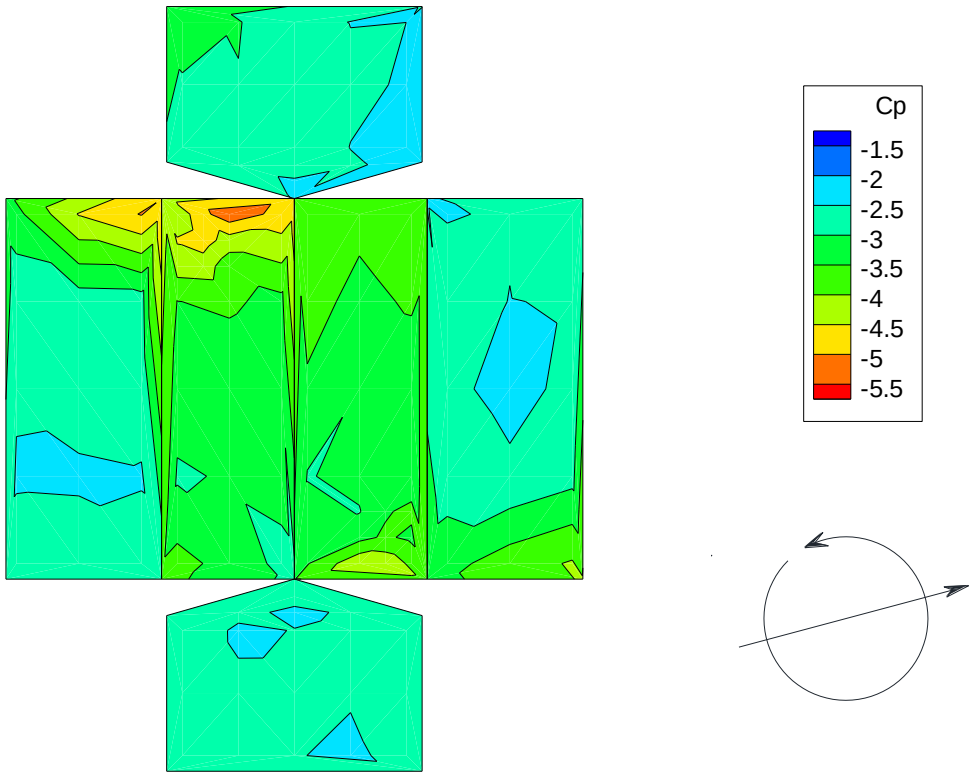

FIGURE 4- 88 PEAK PRESSURE CONTOURS MODEL 1 VT = 0.15 M/S BUILDING ORIENTATION = 75 DEG

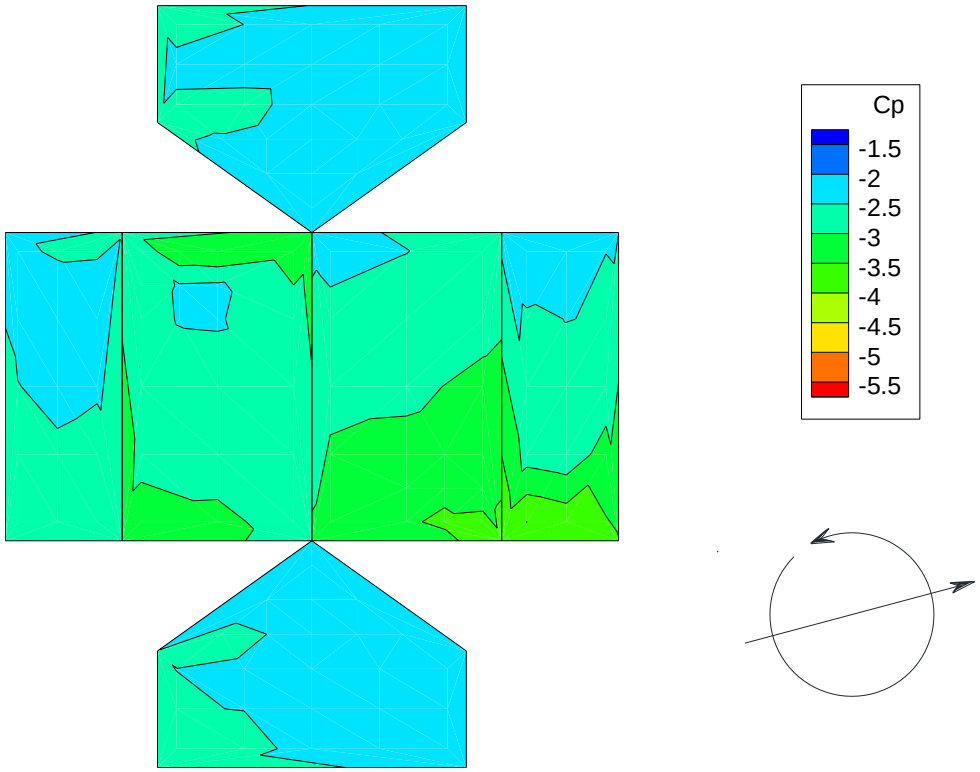

FIGURE 4- 89 PEAK PRESSURE CONTOURS MODEL 5 VT = 0.15 M/S BUILDING ORIENTATION = 75 DEG

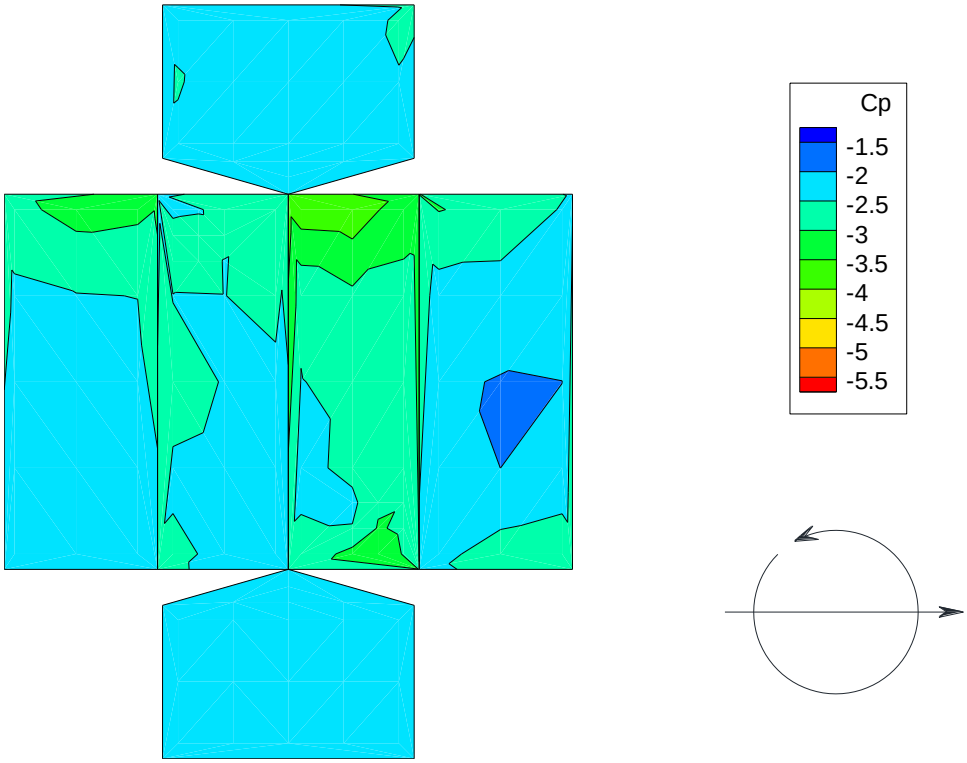

FIGURE 4- 90 PEAK PRESSURE CONTOURS MODEL 1 VT = 0.15 M/S BUILDING ORIENTATION = 90 DEG

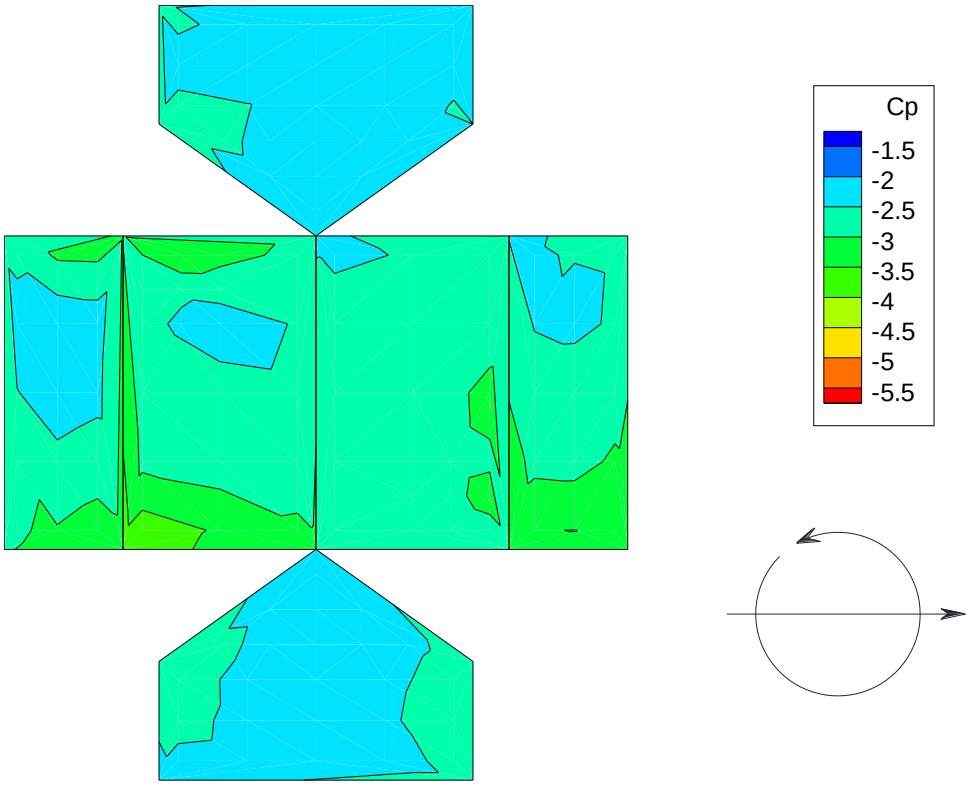

FIGURE 4- 91 PEAK PRESSURE CONTOURS MODEL 5 VT = 0.15 M/S BUILDING ORIENTATION = 90 DEG

In the field of aerodynamics terms such as “windward”, “leeward”, “leading”, and “trailing” are often used to describe certain parts of an object immersed in a straight line flow. These terms are not as easily defined for flow in a tornado, but because of a lack of alternatives they will be used in the following discussion. The terms are defined for the sides of the models for a BOA of 0° and counter-clockwise flow. The sides referred to by the terms do not change with the BOA. The definitions are as follows:

Windward	The side of the model that experiences the tangential velocity component first and is parallel to the direction of the translation of the tornado.
Leeward	The side of the model that is parallel to the windward side.
Leading	The side of the model that is perpendicular to the direction of translation and is closest to the tornado before the tornado reaches the model.
Trailing	The side of the model that is perpendicular to the direction of translation and is closest to the tornado after the tornado has passed the model

For the 0° building orientation angle the peak pressures for model 1 occur at the leading, leeward corner and roof edge. For building orientations 15° through 75°, the peak pressures occur on model 1 at the trailing leeward roof edge and at the windward leading roof edge while for model 5 the highest peak pressures occur mainly at the leading, windward roof edge and the leading, windward wall edge. For a building orientation of 90° the pressures are not as high as for other building orientations and the highest peaks for model 1 occur in the trailing, windward region of the roof and for model 5 occur in the leading, leeward region of the roof. The maximum peak pressure coefficient from all building orientation angles for model 1 is -6.1 and for model 5 is -4.9. The negative sign indicates that the pressure is acting away from the surface of the building model.

Peak pressure coefficient contours for the other models can be found in Appendix B.

Combining the capacities for sheathing uplift as found in the published literature and the pressure coefficients as determined by this study the required wind velocity to induce failure in the sheathing panels can be determined by using Eqn. 4-5.

TABLE 4- 36 REQUIRED WIND VELOCITIES FOR ROOF SHEATHING PANEL UPLIFT FAILURE

Capacity Number	Nail Type	Nailing Schedule	Capacity (kN/m²)	3 second wind velocity required for Cp=6.1	3 second wind velocity required for Cp=4.9
1	8d smooth shank	6”/12”	4.16	47.25 m/s (105.7 mph)	53.7 m/s (118 mph)
2	8d ring shank	6”/12”	8.04	65.7 m/s (147 mph)	73.3 m/s (164 mph)
3	8d smooth shank	6”/6”	7.3	62.6 m/s (140mph)	69.8 m/s (156 mph)
4	8d ring shank	6”/6”	12.5	81.9 m/s (183 mph)	91.4 m/s (204 mph)

The expected 3 second wind velocity to cause the degree of damage associated with uplift of roof decking according the proposal for the Enhanced Fujita Scale (Texas Tech University, 2004) is 97 mph. This value is significantly less than the calculated values in Table 4-15 except for the 8d smooth shank nail with a 6”/12” nailing schedule. For a given sheathing panel capacity, the wind speed required to induce failure varies between the two roof pitches by as much as 9.5 m/s (21 mph). The difference in roof pitch, therefore, is also a significant factor in inducing sheathing panel uplift failure and should be considered when using this particular degree of damage for wind speed estimates in tornadoes.

Roof sheathing panels using 8d ring shank nails with a 6”/6” nailing schedule on trusses or rafters spaced 0.61 m (24 inches) on-center should be capable of resisting uplift pressures induced by tornadoes with 91.4 m/s maximum horizontal wind speeds. These capacities are based on panel tests where the panels are under uniform pressure. The effect of spatially varying pressures on the capacities of roof panels has not been investigated, but according to the present state of knowledge, roof sheathing panels can be designed to resist tornado induced uplift pressures simply by using ring shank nails with heavier nailing schedules than are required by building codes in the tornado prone regions of the United States.

4.2.4 Peak Reactions

The peak roof truss reactions for model 1 are plotted in Figure 4-92. The reactions plotted are the peaks from all 7 building orientations.

The leeward side of model 1 experienced higher roof truss reactions than the windward side for each respective truss. The highest value is for reaction X2 which is on the trailing leeward side. The value of -10 kN is almost twice as high as the capacity of the hurricane tie. A possible method of increasing the RTWC capacity would be to incorporate toe nailed connections for construction purposes in addition to hurricane ties. This was found to increase the capacity of the RTWC to 8.47 kN for one hurricane tie per rafter and 14.35 kN when 2 hurricane ties of the same type as used in this analysis were used for each rafter (Reed et al., 1997).

Canfield et al. (1991) found that for the majority of tests conducted the failure mode of the hurricane tie connection was tearing of the metal hurricane tie. Therefore, another possible solution would be to increase the thickness of the metal used in the hurricane tie from 18 gauge to 14 or 16 gauge. Tests could be done to determine at which sheet metal gauge failure by tearing of the hurricane tie no longer occurs, but rather by splitting of the wood members. This gauge may not be the optimum gauge to use as failure of the metal hurricane ties is ductile while failure in the wood members would be much more brittle and would dissipate less energy.

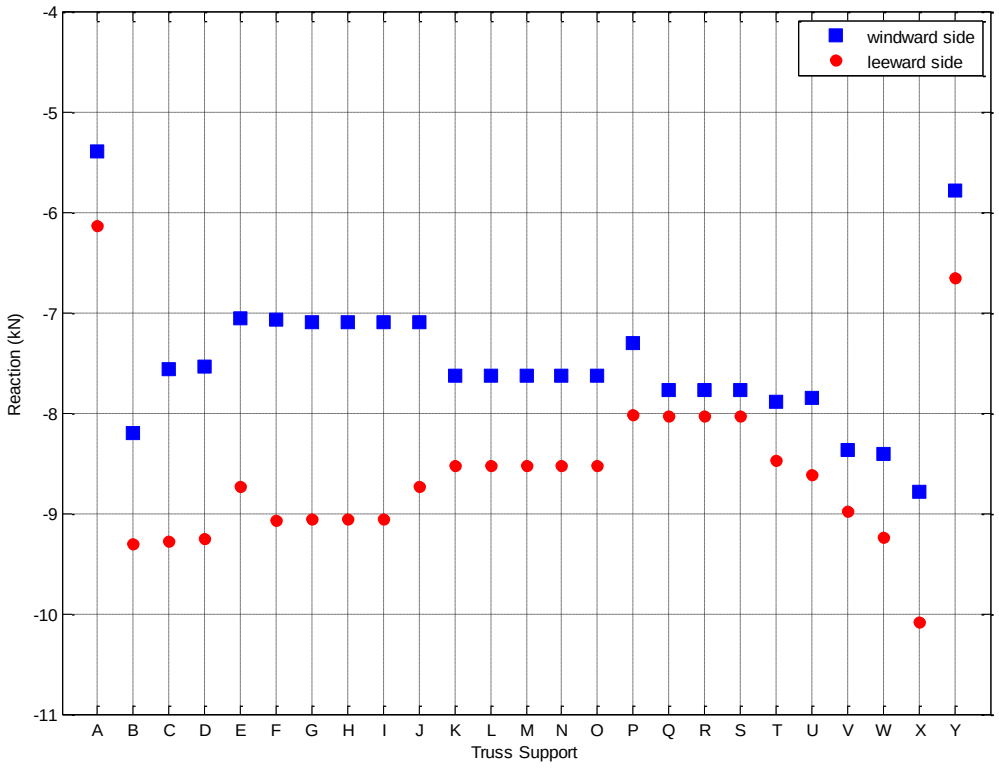

FIGURE 4- 92 PEAK TRUSS REACTIONS MODEL 1 VT = 0.15 M/S

The wood studs in the wall are usually toe nailed or end nailed to the top plate. In order to prevent the top plate from separating from the studs, the reaction force would have to be transferred directly to the studs rather than to the top plate and then to the studs for reactions of the magnitude determined in this analysis. Further investigation is necessary. These possibilities are presented here to show that tornado resistant, prescriptive design is, in fact, possible.

The peak truss reactions for model 5 are shown in Figure 4-93. The roof truss reactions for model 5 are smaller in magnitude than for model 1. They are also more similar for the windward and leeward sides of the building. The reactions for the windward side of truss B for the two models are similar in magnitude.

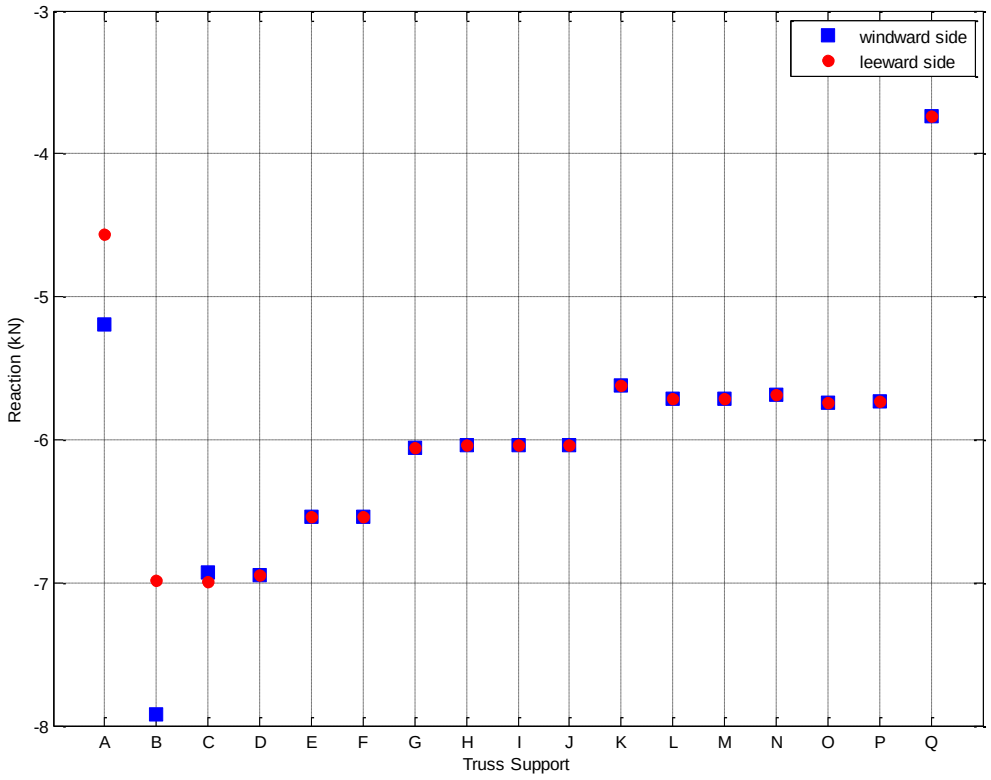

FIGURE 4- 93 PEAK TRUSS REACTIONS MODEL 5 VT = 0.15 M/S

Chapter 5 Summary, Conclusions and Recommendations

5.1 Summary

Nine low-rise building models were tested in a laboratory simulated, high swirl ratio tornado with building orientation angles (BOA) with respect to the tornado path varying from 0° to 90°. Two of those models were also tested for BOA's varying from 180° to 270° (i.e. the two garage models orientation B). Pressure measurements on the building models were taken for tornado translation speeds of 0.15 m/s and 0.46 m/s.

The intention of these tests was to better understand the effect of roof geometry on the pressures and loads on low-rise residential structures in tornadoes with high swirl ratios and to compare those loads and pressures with the capacities of the types of roof connections often used in tornado prone regions in the United States.

In order to meet these objectives the aerodynamic force coefficients, C_{Fx}, C_{Fy}, and C_{Fz}, were calculated along the horizontal direction parallel to the tornado's translation direction, the horizontal direction perpendicular to the tornado's translation direction, and the vertical direction, respectively. An xy force coefficient (C_{Fxy}) was also calculated as the square root of the sum of the squares of C_{Fx} and C_{Fy}. The peak pressures were plotted as pressure coefficients on 2 dimensional drawings of the models, the peak roof-to-wall connection (RTWC) reactions were plotted for two of the models, and the point in time at which initial failure of roof sheathing and RTWC failure occurred for the capacities of various types of fasteners as published in the literature were calculated using a simple analysis procedure.

5.2 Conclusions

The following conclusions were made:

1. The critical building orientation angles (BOA) for C_{Fx} were the least critical for C_{Fy} and the critical BOA's for C_{Fy} were the least critical for C_{Fx}.
2. The critical BOA is a function of the mean roof height to longest plan dimension (h/L) ratio, roof pitch, and roof geometry such as an overhang or "garage" addition.
3. The translation speed of the tornado affects the magnitudes of the force coefficients, but the trends with respect to change in roof pitch and h/L are similar for both translation speeds.

4. The addition of a roof overhang and enclosed soffit change the magnitudes of the external pressures and aerodynamic force coefficients on low-rise building models in high swirl ratio tornadoes.
5. The wind speed at which roof sheathing and roof-to-wall connections (RTWC) fail in tornadoes is a function of the type of connection and fastener, the building orientation angle, the roof pitch, and the eave height to longest plan dimension (h/L) ratio. These variables should be taken into consideration when estimating the peak horizontal wind speed in a tornado from roof damage indicators.
6. The capacity of residential structures in tornado prone areas of the United States to resist the pressures and loads induced by tornadoes could be greatly improved by relatively simple changes to the roof sheathing-to-truss/rafter and roof-to-wall connections.

5.3 Recommendations

5.3.1 Recommendations for Improving Performance of Roof Connections in Tornadoes

The connection of the roof sheathing panels to the roof truss/rafters and the roof truss-to-wall connections are critical in improving the performance of low-rise, wood-frame residential structures in extreme wind events such as tornadoes. In view of this fact, the following recommendations for improving these connections based upon the study done in this thesis and an understanding of the failure mechanisms of these connections based on the review of the literature are given.

1. It is recommended that toe nailed roof-to-wall connections (RTWC) without any additional means of resisting uplift should not be used.
2. It is recommended to use toe-nailed connections only as a construction joint for the RTWC while installing the roof truss/rafter and then to install hurricane ties of the type that connect the roof truss to the studs and not only to the top plate in order to increase the capacity of the RTWC.
3. It is recommended that for roof trusses/rafters spaced 0.6 m (24 inches) on-center that 8d ring shank nails with a 6”/6” nailing schedule be used as a means to improve the uplift capacity of roof sheathing panels.
4. It is recommended that the commonly used spacing between roof trusses/rafters be reduced from 0.6 m (24 inches) on-center. This recommendation is based on the idea that

the load that needs to be resisted by each connection decreases with the number of connections resisting the same load.

5. It is recommended that purlins of dimensional lumber similar to that of the roof truss/rafter be installed in residential construction to provide lateral stability for the roof structural system in the instance that the roof sheathing panels fail in uplift or are damaged due to debris impact.

5.3.2 Recommendations for Further Research

The field of wind engineering as it relates to improving the performance of structures in tornadoes is relatively unexplored. As such the following recommendations are made for further investigation:

1. This study found that the pressures and loads induced by a tornado are dependent on both roof pitch and h/L. It is therefore recommended that further research be done by testing more models of various roof pitches and h/L values to further fill in Table 3-3.
2. Based on the findings that soffits experience negative pressures, the possibility of creating internal pressures in the attic of residential, low-rise buildings through openings for ventilation in the soffit and thereby reducing the net pressures on the roof sheathing panels should be investigated as a possible strategy to mitigate damage to the roof in tornadoes.
3. The sequence of failure in tornadoes is complex and dependent upon where in the structure initial failure occurs. In order to understand how structures fail in tornadoes a more detailed and complete analysis of the sequence of failure than the one undertaken in this study is needed.
4. At present only testing of sheathing panels in uplift under spatially uniform pressure has been done. Actual pressures induced by tornadoes are neither spatially nor temporally uniform. An investigation into the capacities of sheathing panels under spatially varying, dynamic pressures should be done in order to obtain more realistic uplift capacities of roof sheathing panels.
5. This study has provided a first attempt at quantifying required strengths for roof connections in tornadoes. This attempt, although simplified, has shown that tornado resistant design is feasible for tornadoes of moderate intensity by making modest improvements to connection capacities. Further investigation into the capacities of other connections that have been found to fail in tornadoes (e.g. wall to foundation anchorage)

and comparing them with the forces obtained in laboratory simulated tornadoes should be done.

6. As was discussed in the literature review, acceptance of engineering recommendations for residential structures by building codes and the implementation of those recommendations by contractors is paramount to the success of tornado resistant design. It is, therefore, recommended that the sociological obstacles to the acceptance and implementation of these recommendations and how engineers can overcome them be investigated.

Appendix A. Building Model Pressure Tap Locations

MODEL 1

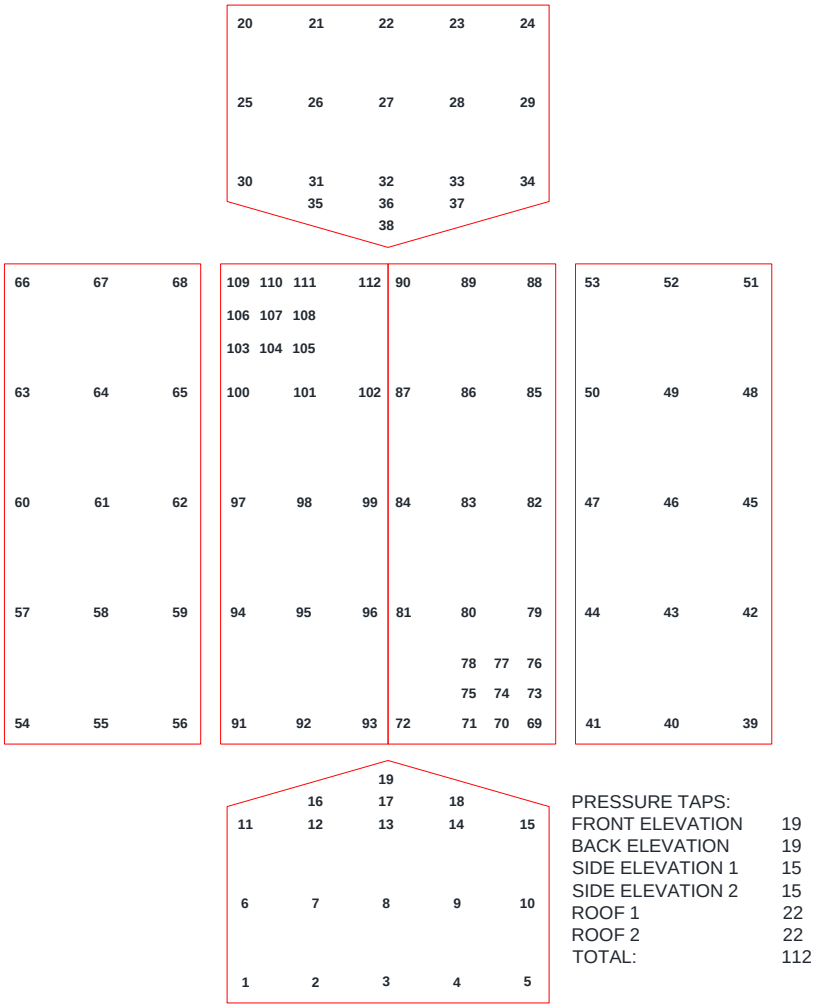

FIGURE A- 10 MODEL 1 PRESSURE TAP LOCATIONS/NUMBERS

MODEL 2

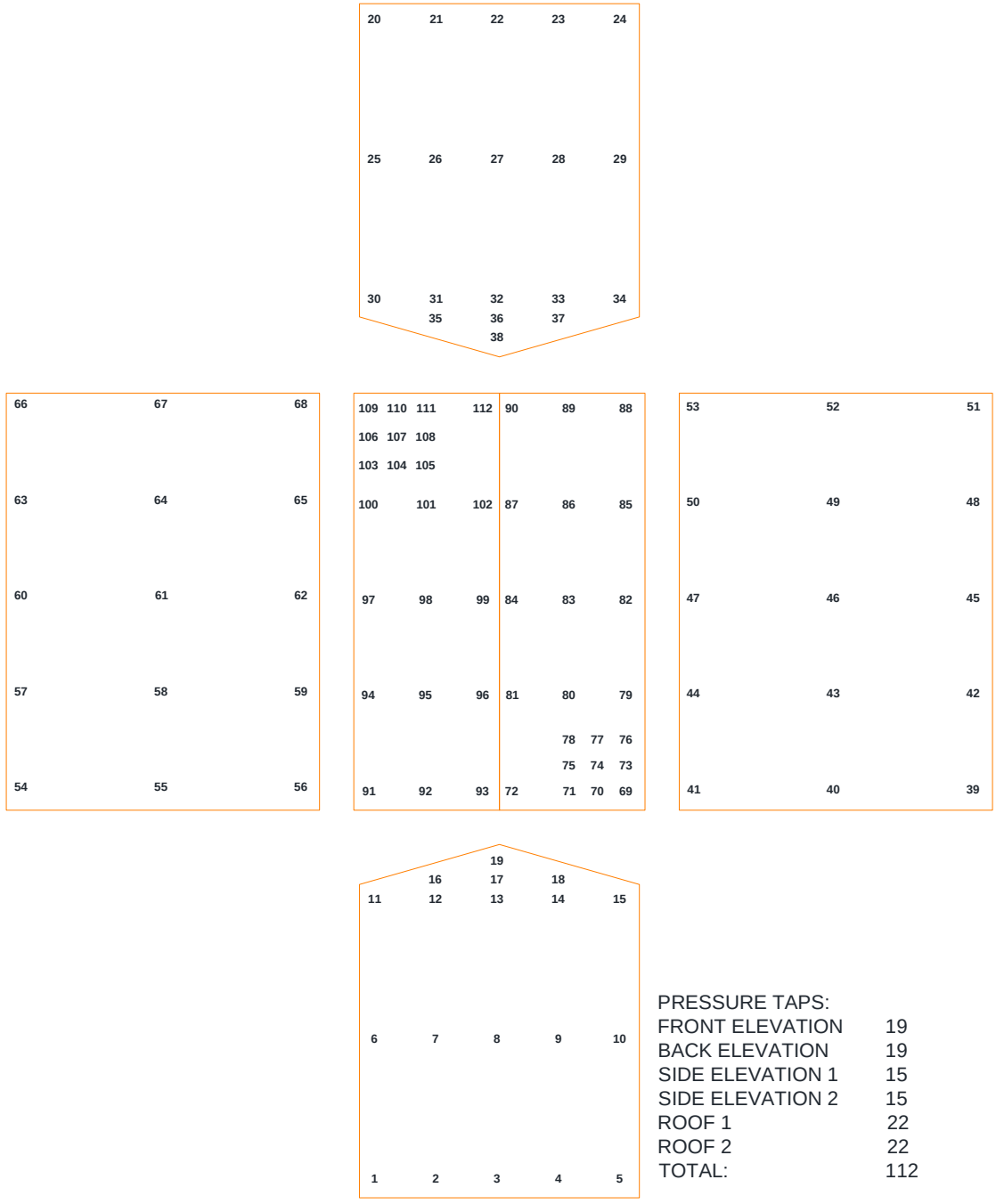

PRESSURE TAPS:	
FRONT ELEVATION	19
BACK ELEVATION	19
SIDE ELEVATION 1	15
SIDE ELEVATION 2	15
ROOF 1	22
ROOF 2	22
TOTAL:	112

FIGURE A- 11 MODEL 2 PRESSURE TAP LOCATIONS/NUMBERS

MODEL 3

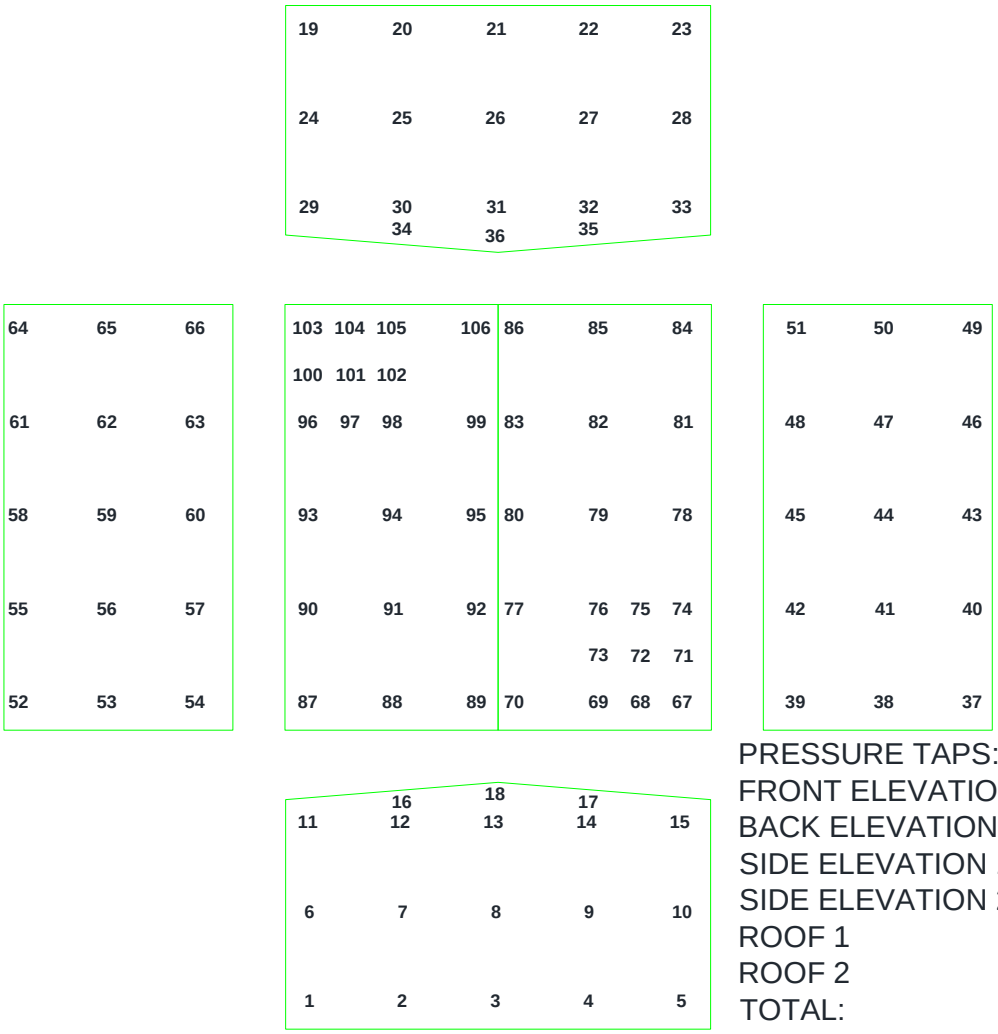

PRESSURE TAPS:

FRONT ELEVATION	18
BACK ELEVATION	18
SIDE ELEVATION 1	15
SIDE ELEVATION 2	15
ROOF 1	20
ROOF 2	20
TOTAL:	106

FIGURE A- 12 MODEL 3 PRESSURE TAP LOCATIONS/NUMBERS

MODEL 4

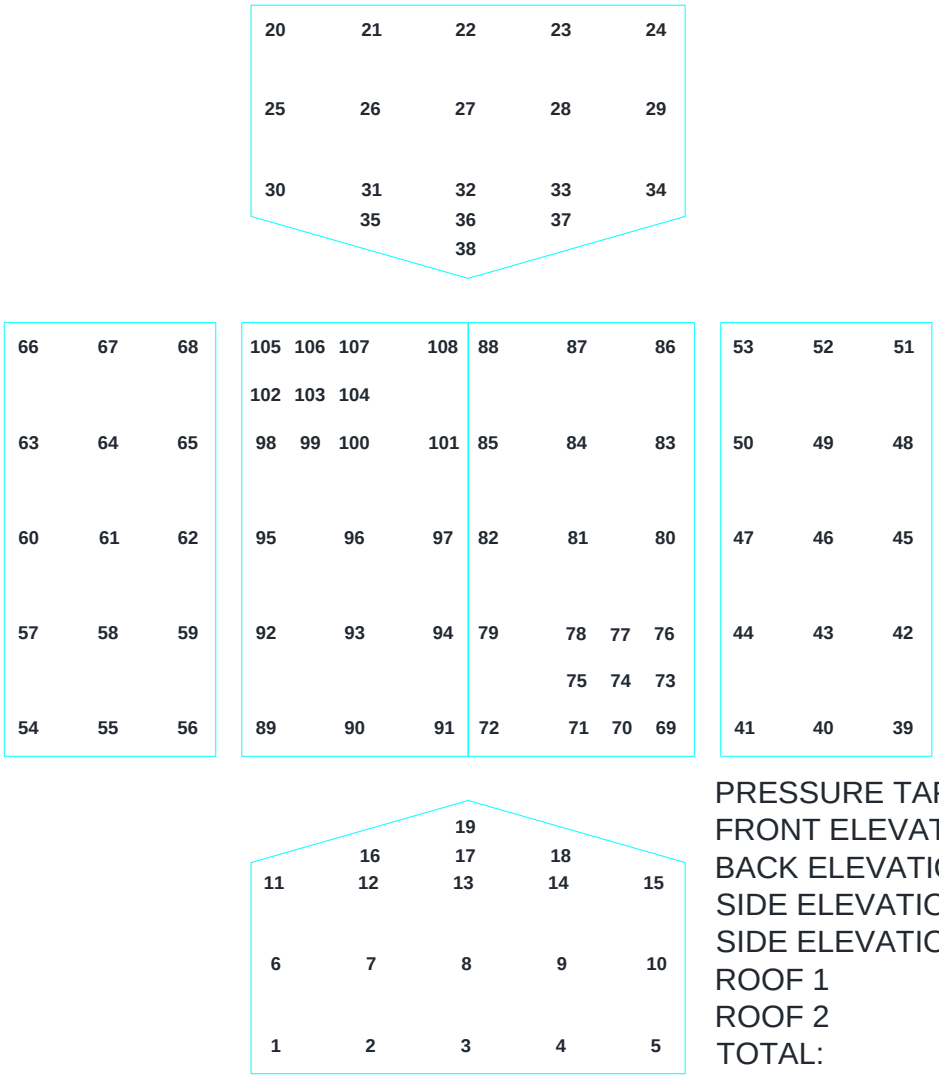

PRESSURE TAPS:	
FRONT ELEVATION	19
BACK ELEVATION	19
SIDE ELEVATION 1	15
SIDE ELEVATION 2	15
ROOF 1	20
ROOF 2	20
TOTAL:	108

FIGURE A- 13 MODEL 4 PRESSURE TAP LOCATIONS/NUMBERS

MODEL 5

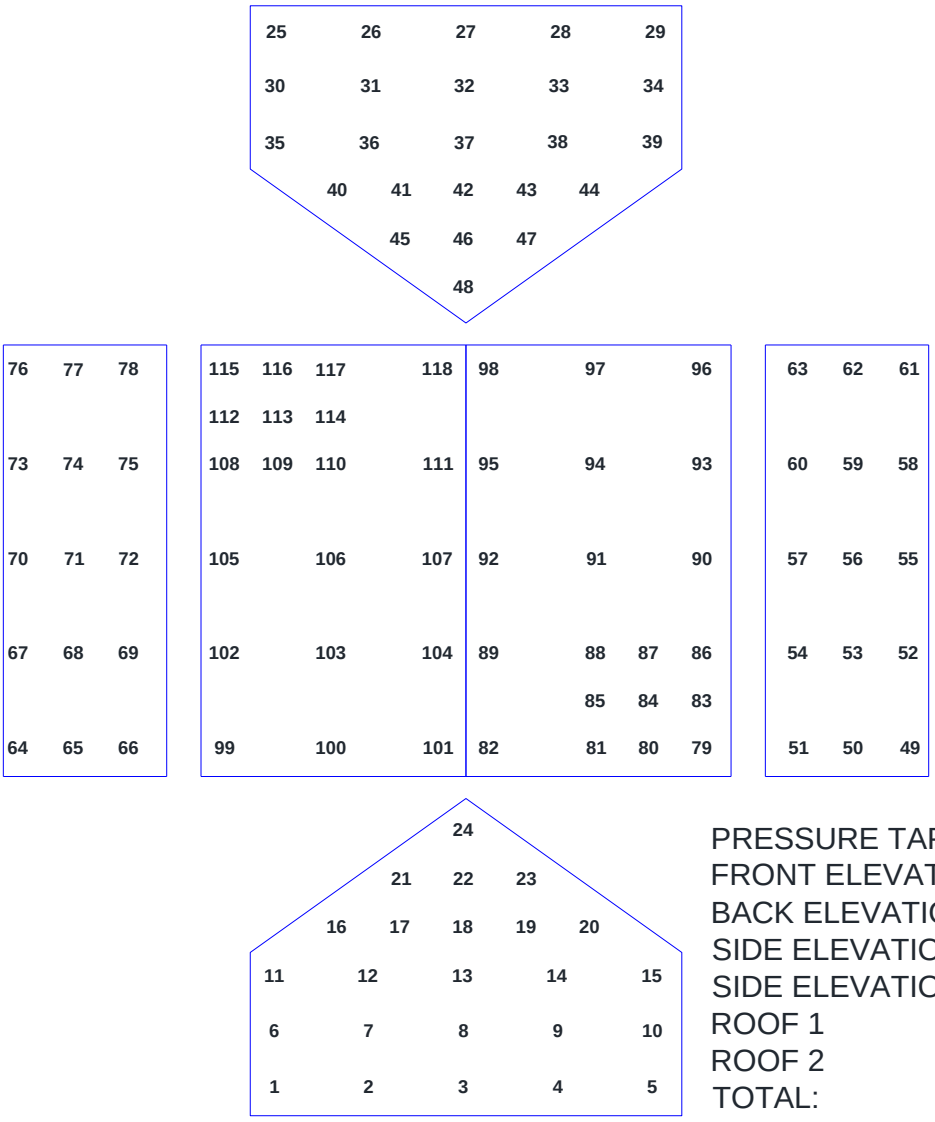

PRESSURE TAPS:	
FRONT ELEVATION	24
BACK ELEVATION	24
SIDE ELEVATION 1	15
SIDE ELEVATION 2	15
ROOF 1	20
ROOF 2	20
TOTAL:	118

FIGURE A- 14 MODEL 5 PRESSURE TAP LOCATIONS/NUMBERS

MODEL 6

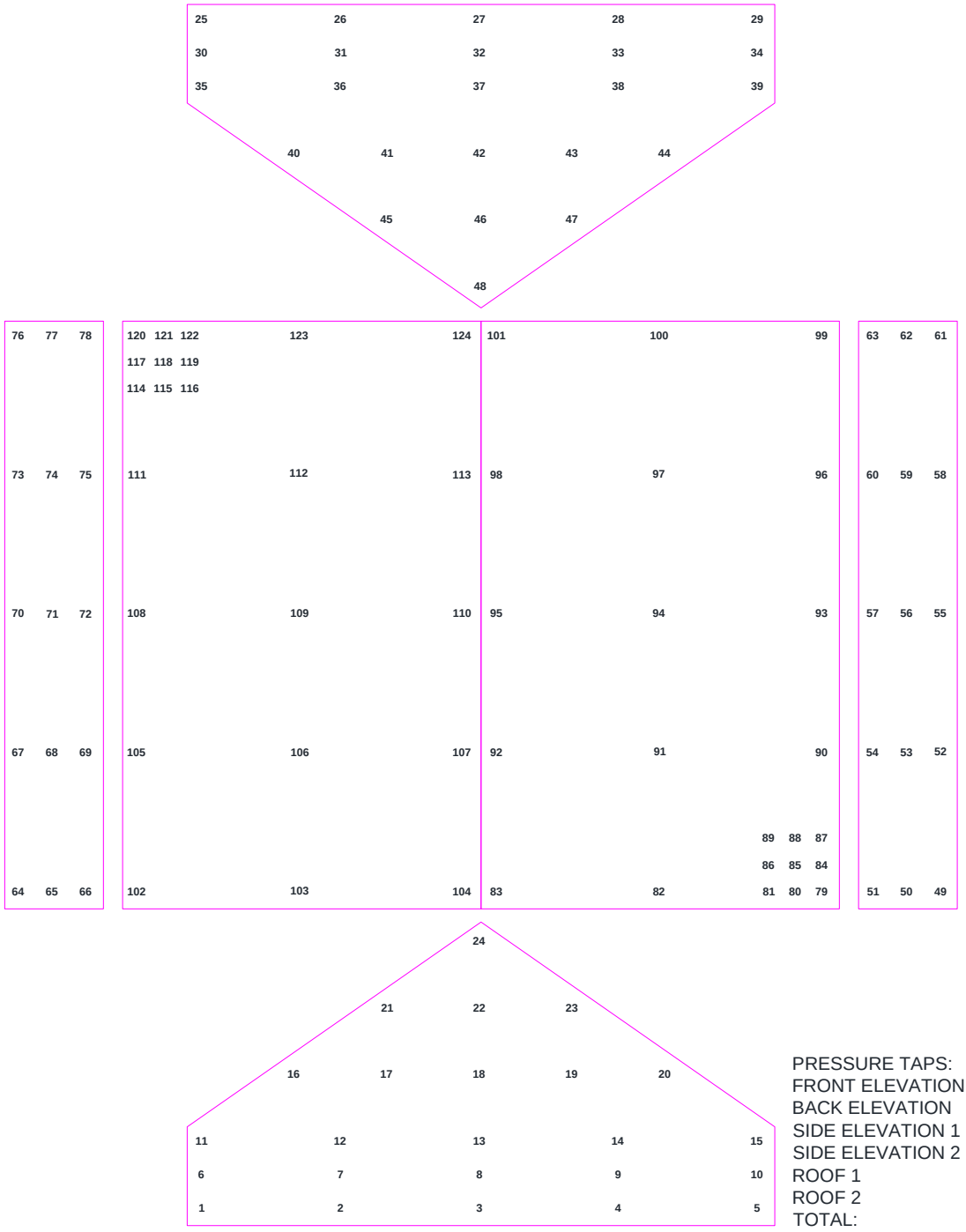

PRESSURE TAPS:	
FRONT ELEVATION	24
BACK ELEVATION	24
SIDE ELEVATION 1	15
SIDE ELEVATION 2	15
ROOF 1	23
ROOF 2	23
TOTAL:	124

FIGURE A- 15 MODEL 6 PRESSURE TAP LOCATIONS/NUMBERS

OVERHANG

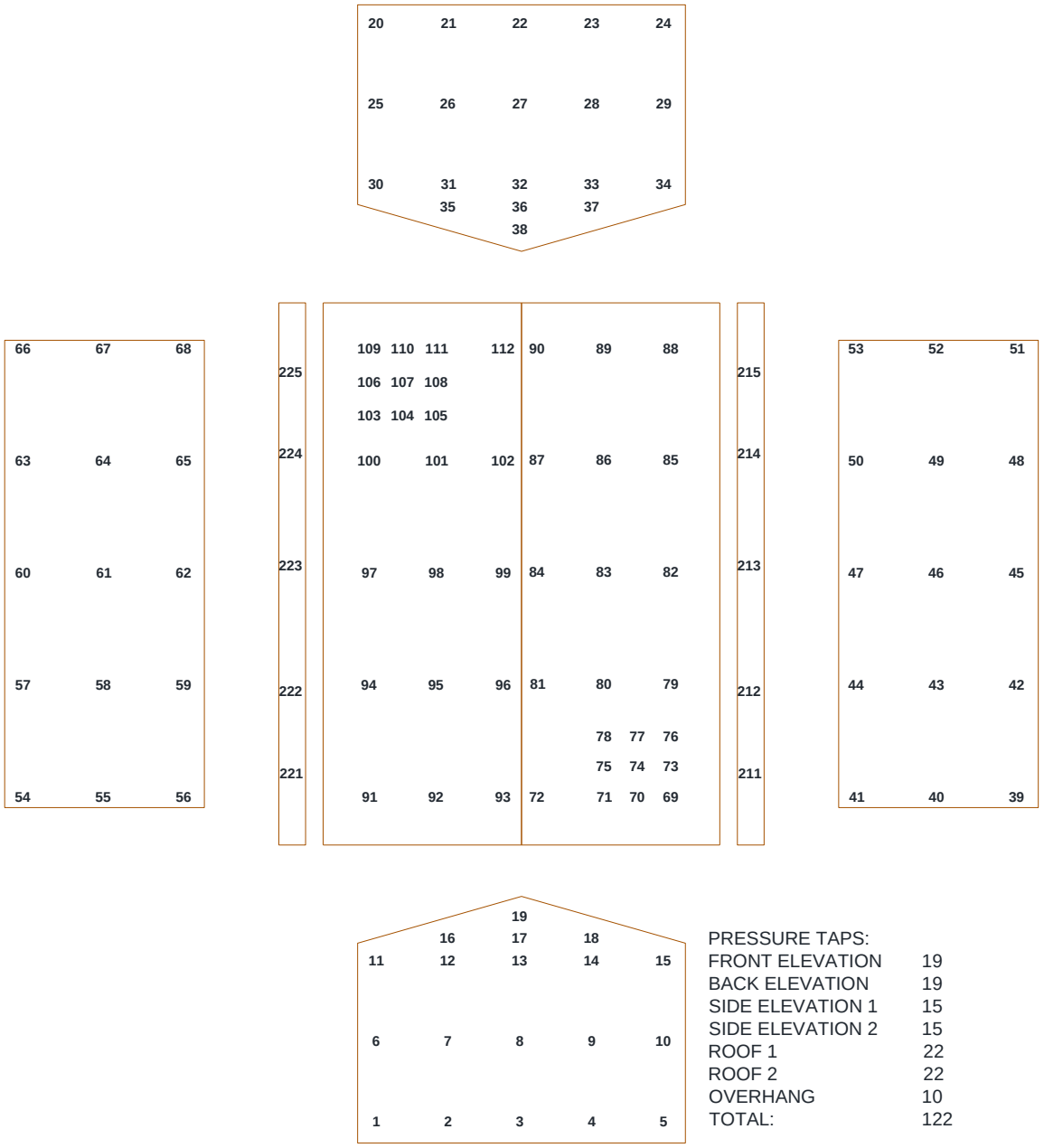

FIGURE A- 16 MODEL 7/OVERHANG PRESSURE TAP LOCATIONS/NUMBERS (3-DIGIT NUMBERS STARTING WITH 2 ARE LOCATED ON THE SOFFIT)

GARAGE 1

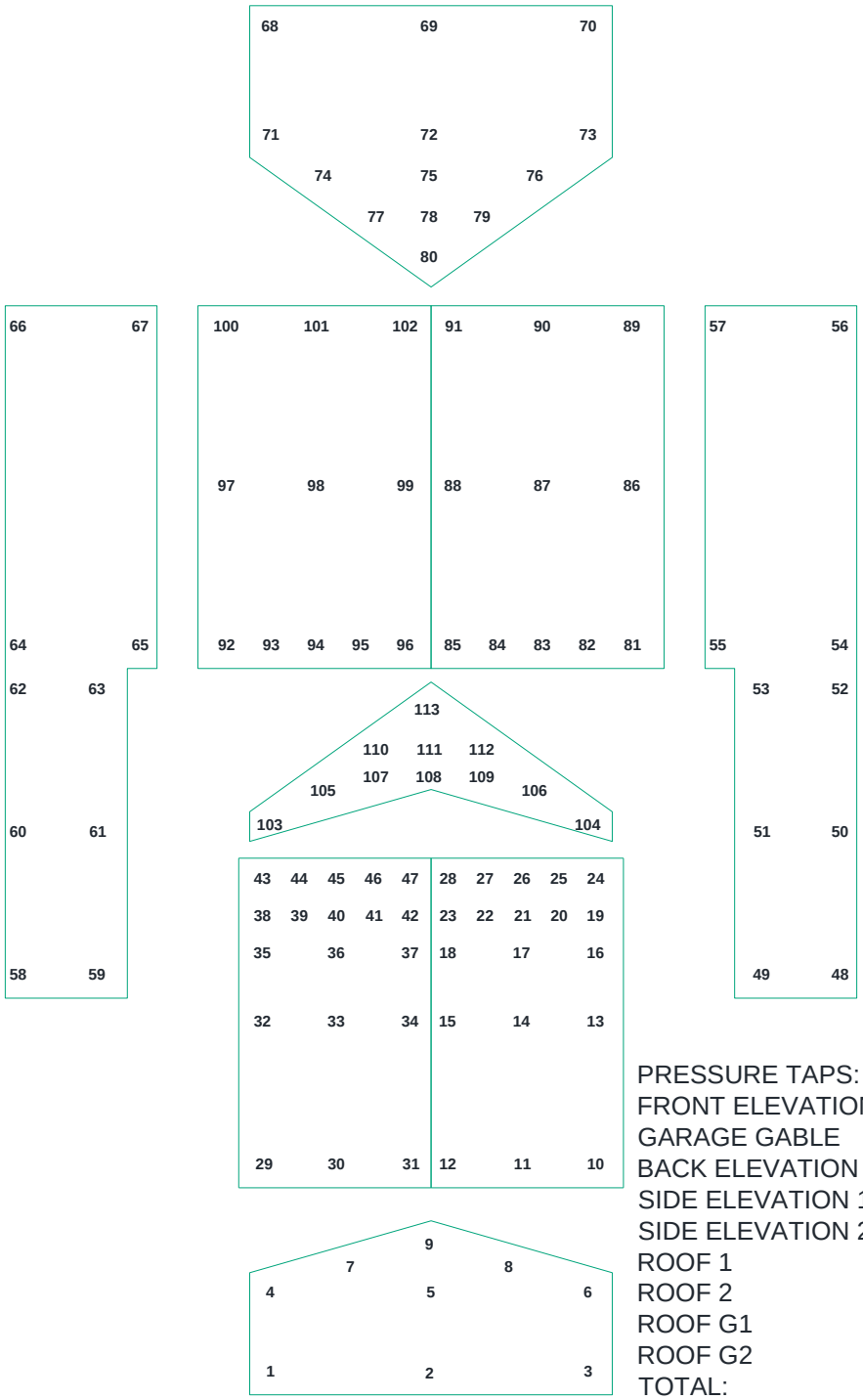

PRESSURE TAPS:	
FRONT ELEVATION	13
GARAGE GABLE	11
BACK ELEVATION	9
SIDE ELEVATION 1	10
SIDE ELEVATION 2	10
ROOF 1	11
ROOF 2	11
ROOF G1	19
ROOF G2	19
TOTAL:	113

FIGURE A- 17 MODEL 8/GARAGE 1 PRESSURE TAP LOCATIONS/NUMBERS

GARAGE 2

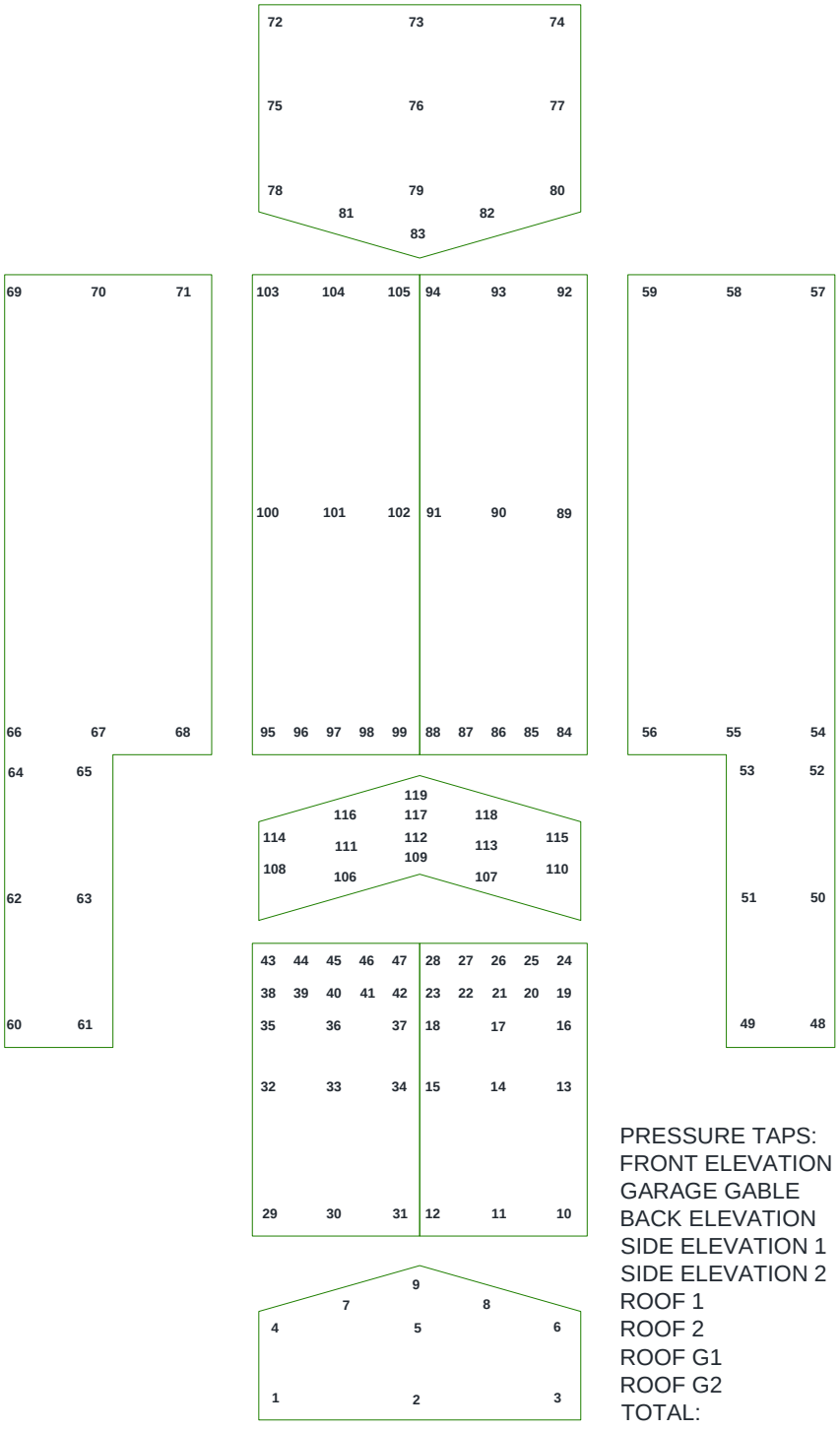

PRESSURE TAPS:	
FRONT ELEVATION	12
GARAGE GABLE	14
BACK ELEVATION	9
SIDE ELEVATION 1	12
SIDE ELEVATION 2	12
ROOF 1	11
ROOF 2	11
ROOF G1	19
ROOF G2	19
TOTAL:	119

FIGURE A- 18 MODEL 9/GARAGE 2 PRESSURE TAP LOCATIONS/NUMBERS

Appendix B. Peak Pressure Coefficient Contours

The peak pressure contours for the translation speed of 0.15 m/s are given below. Model1 and model 5 are given in Chapter 4, and so are not repeated here.

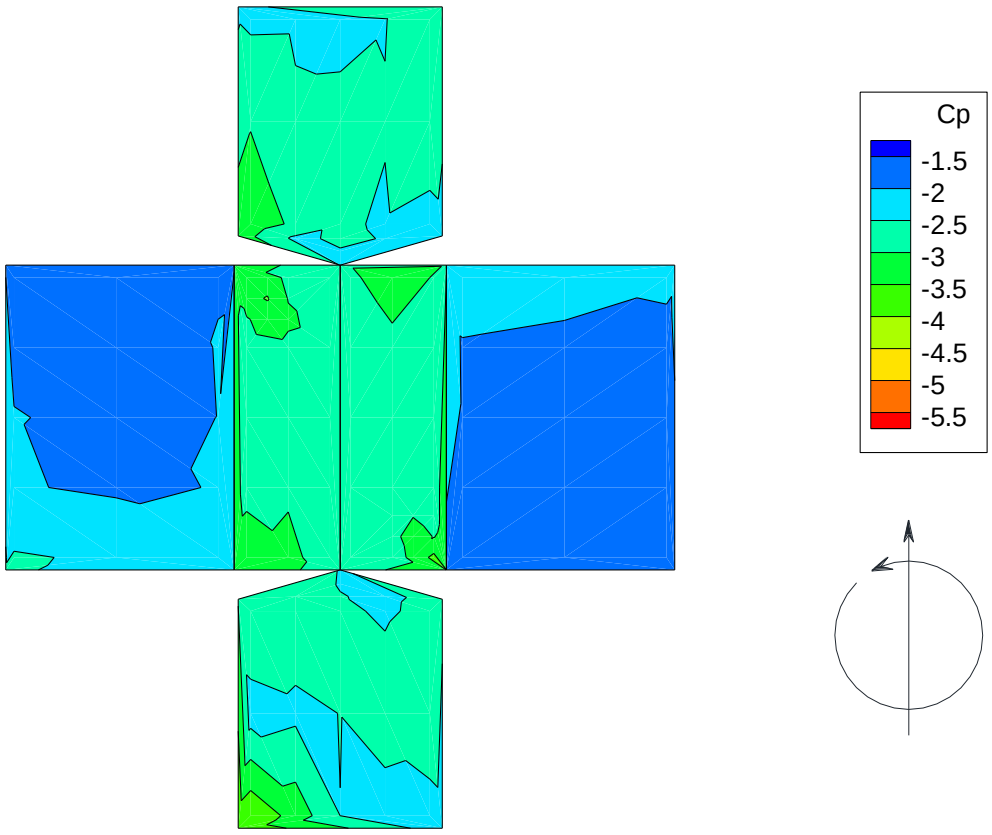

FIGURE B- 1 PEAK CP CONTOURS MODEL 2 BOA = 0°

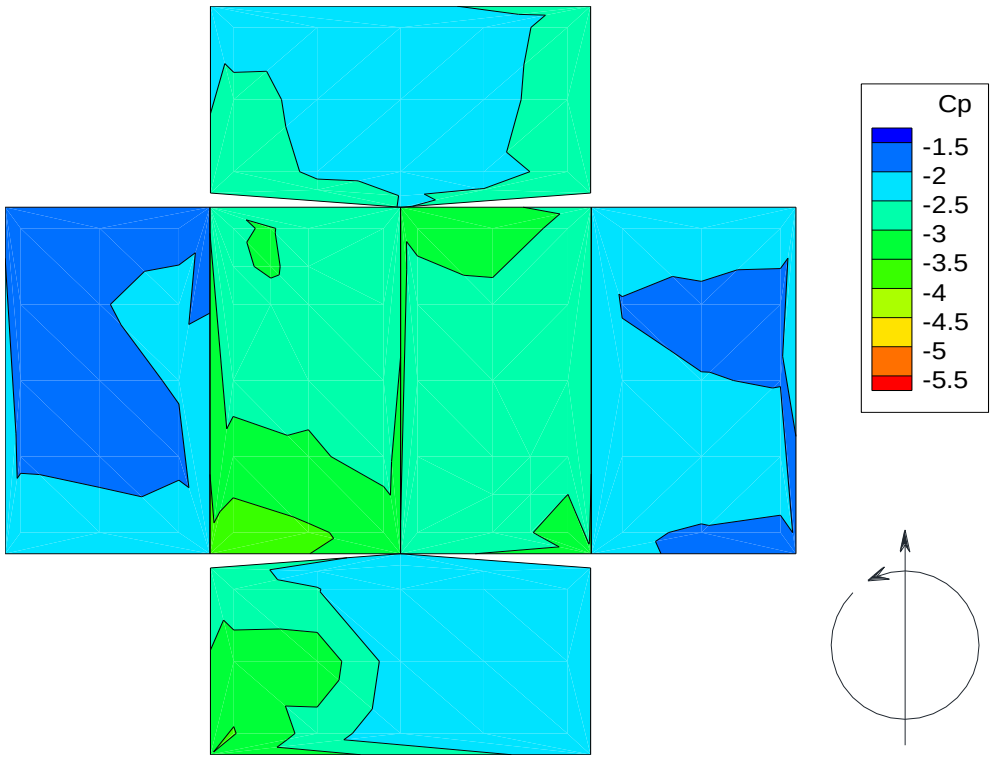

FIGURE B- 2 PEAK CP CONTOURS MODEL 3 BOA = 0°

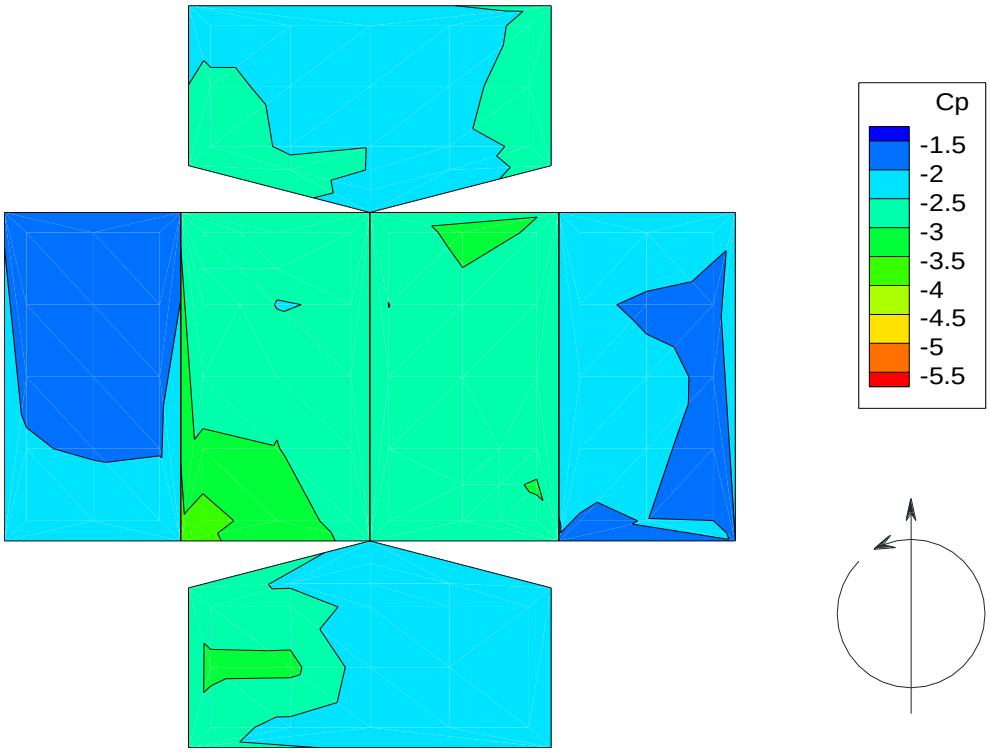

FIGURE B- 3 PEAK CP CONTOURS MODEL 4 BOA = 0°

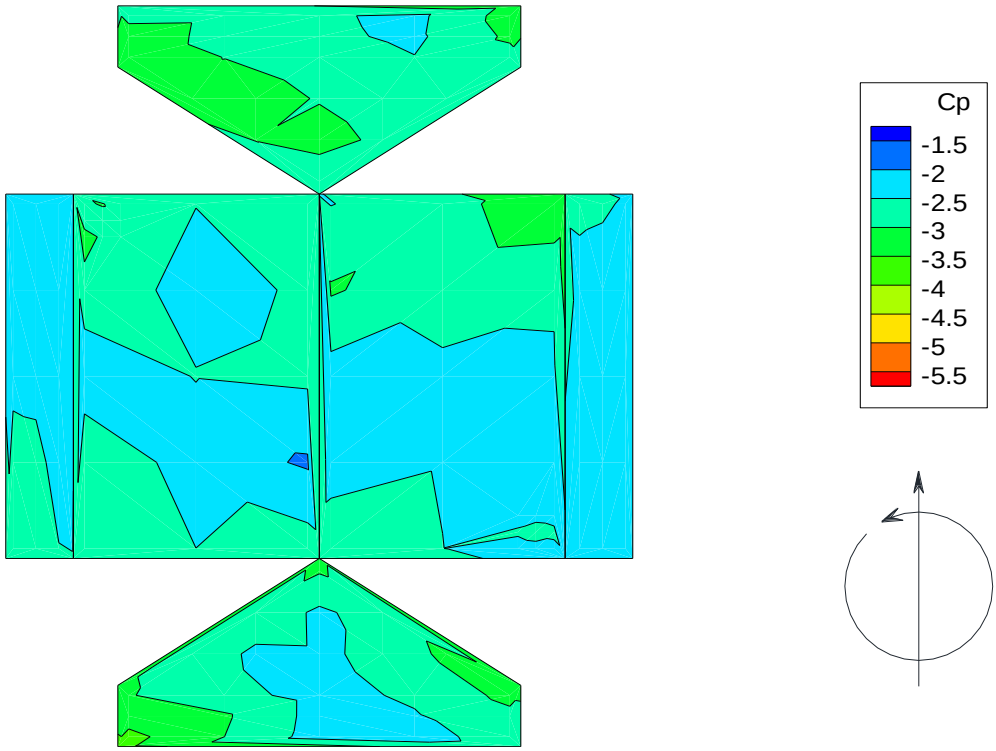

FIGURE B- 4 PEAK CP CONTOURS MODEL 6 BOA = 0°

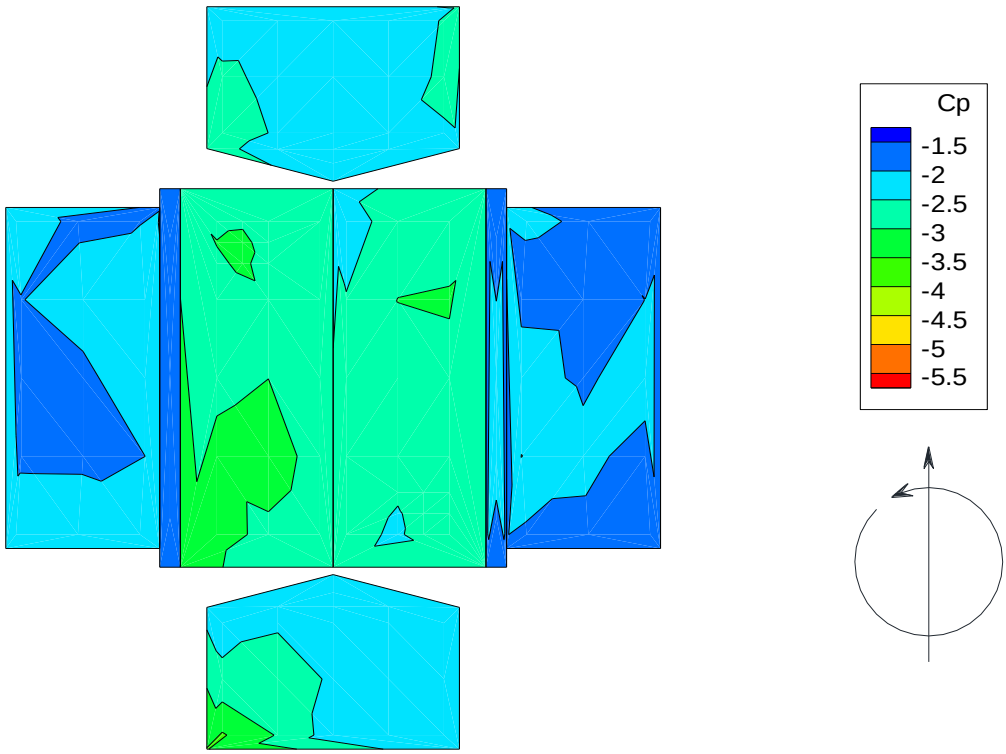

FIGURE B- 5 PEAK CP CONTOURS MODEL 7/OVERHANG BOA = 0°

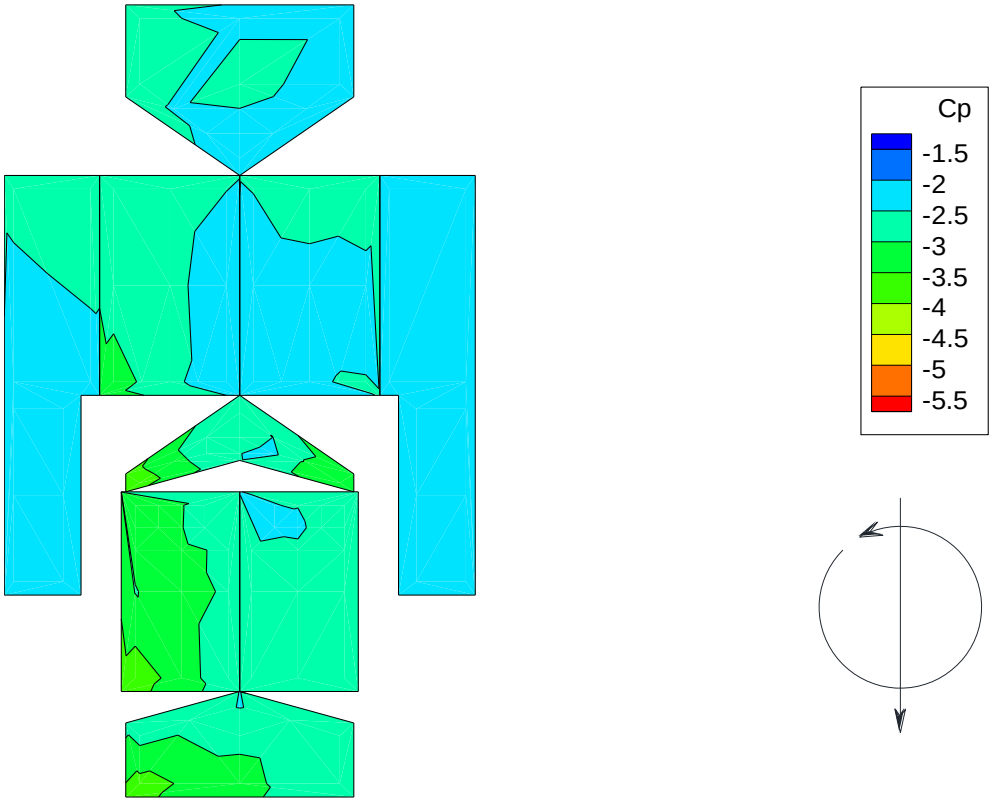

FIGURE B- 6 PEAK CP CONTOURS MODEL 8/GARAGE 1 ORIENTATION A BOA = 0°

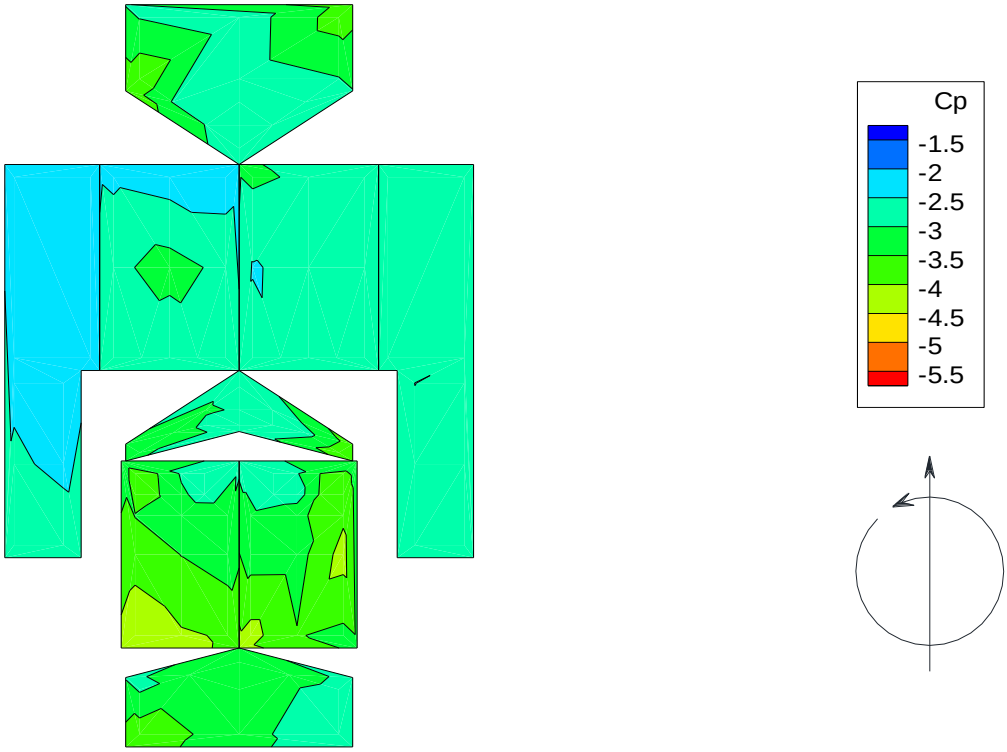

FIGURE B- 7 PEAK CP CONTOURS MODEL 8/GARAGE 1 ORIENTATION B BOA = 0°

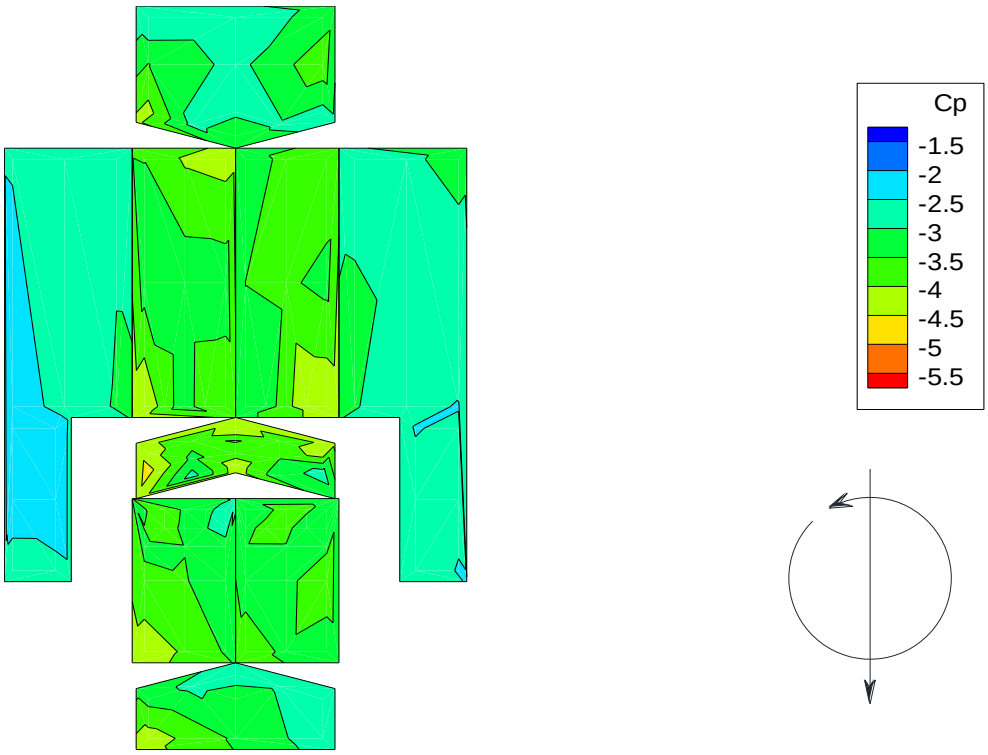

FIGURE B- 8 PEAK CP CONTOURS MODEL 9/GARAGE 2 ORIENTATION A BOA = 0°

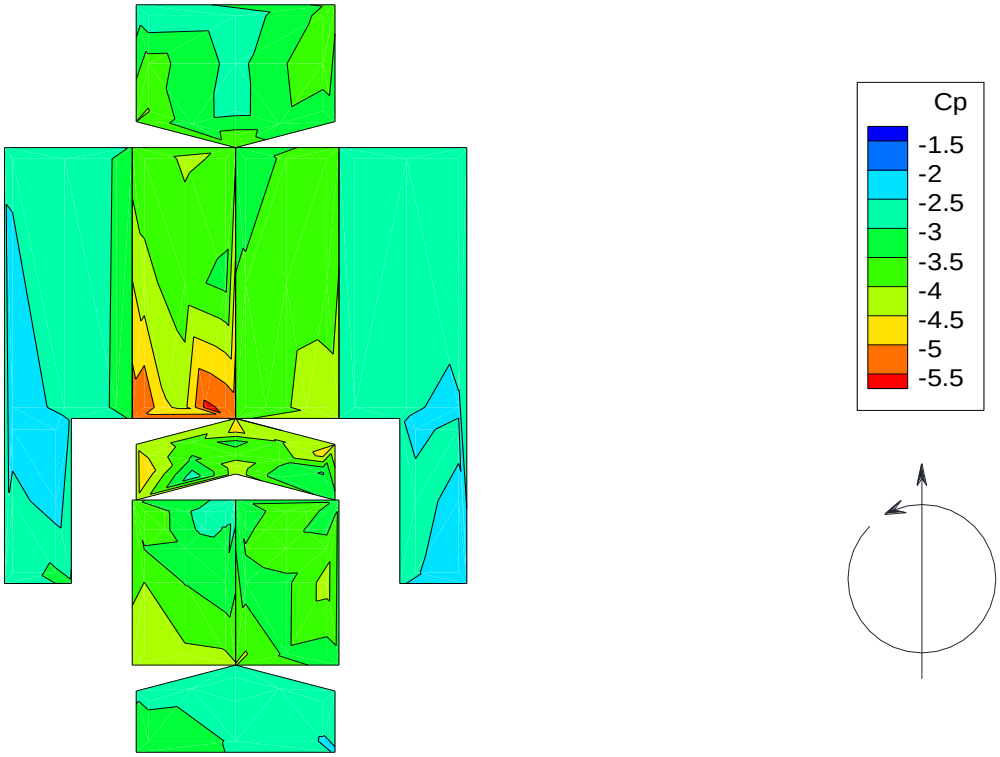

FIGURE B- 9 PEAK CP CONTOURS MODEL 9/GARAGE 2 ORIENTATION B BOA = 0°

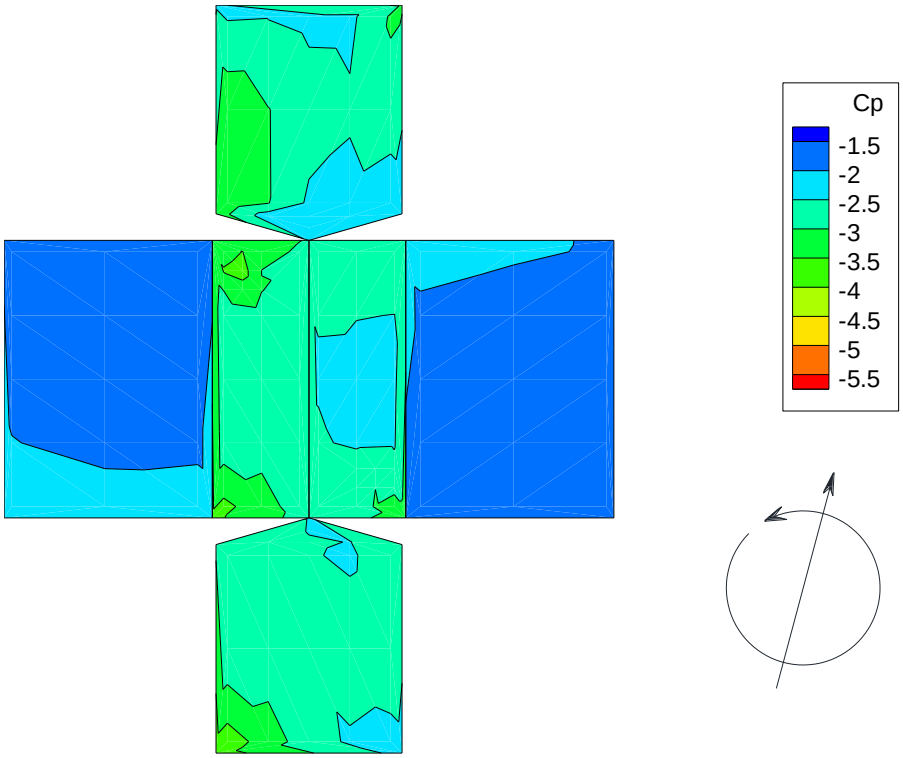

FIGURE B- 10 PEAK CP CONTOURS MODEL 2 BOA = 15°

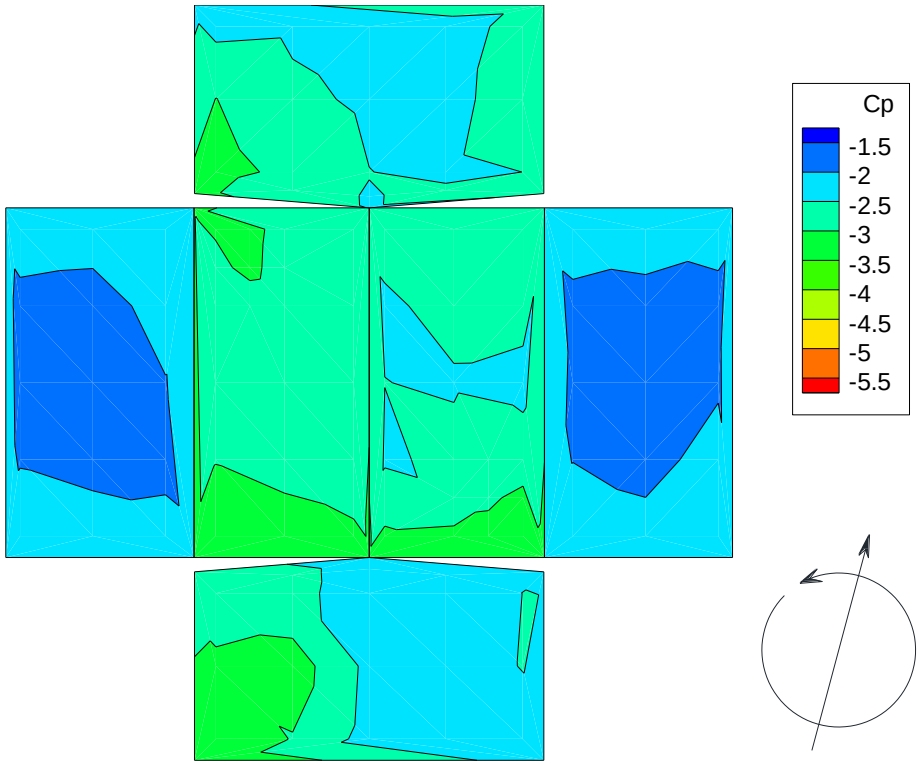

FIGURE B- 11 PEAK CP CONTOURS MODEL 3 BOA = 15°

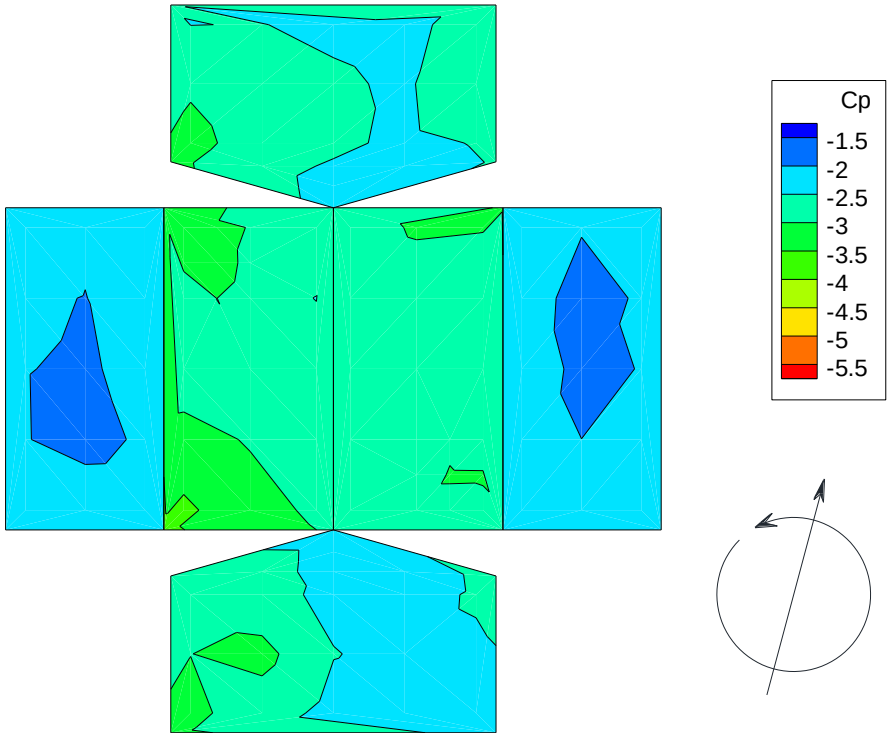

FIGURE B- 12 PEAK CP CONTOURS MODEL 4 BOA = 15°

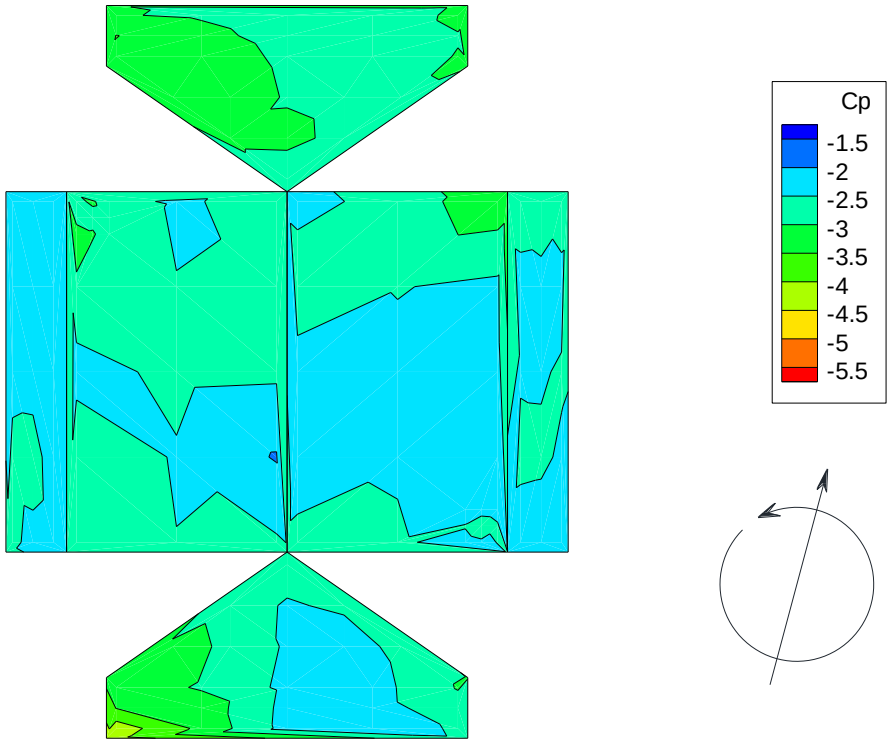

FIGURE B- 13 PEAK CP CONTOURS MODEL 6 BOA = 15°

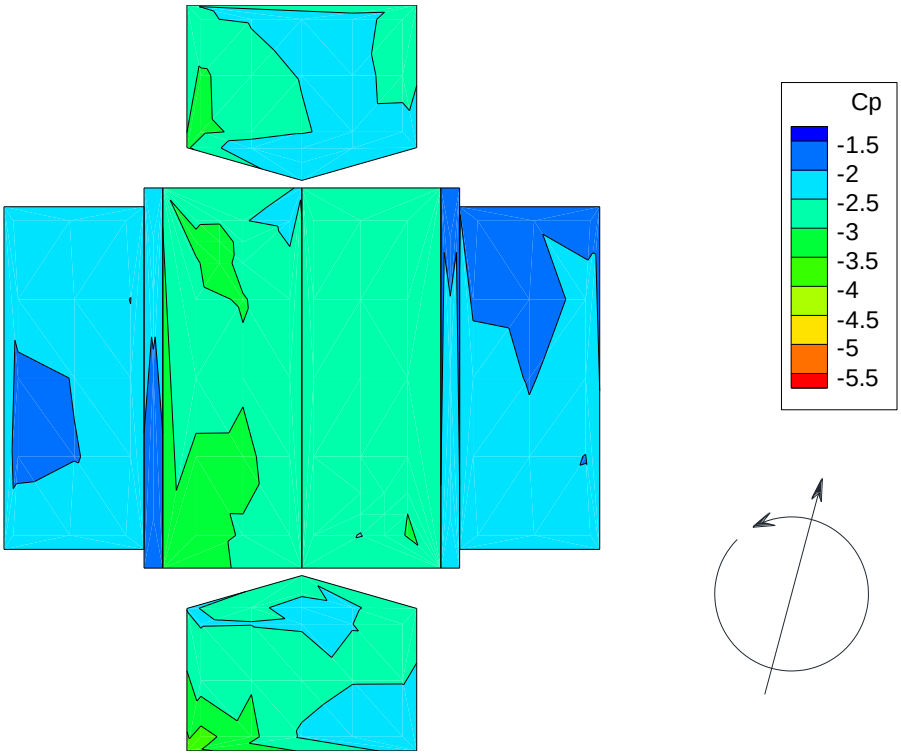

FIGURE B- 14 PEAK CP CONTOURS MODEL 7/OVERHANG BOA = 15°

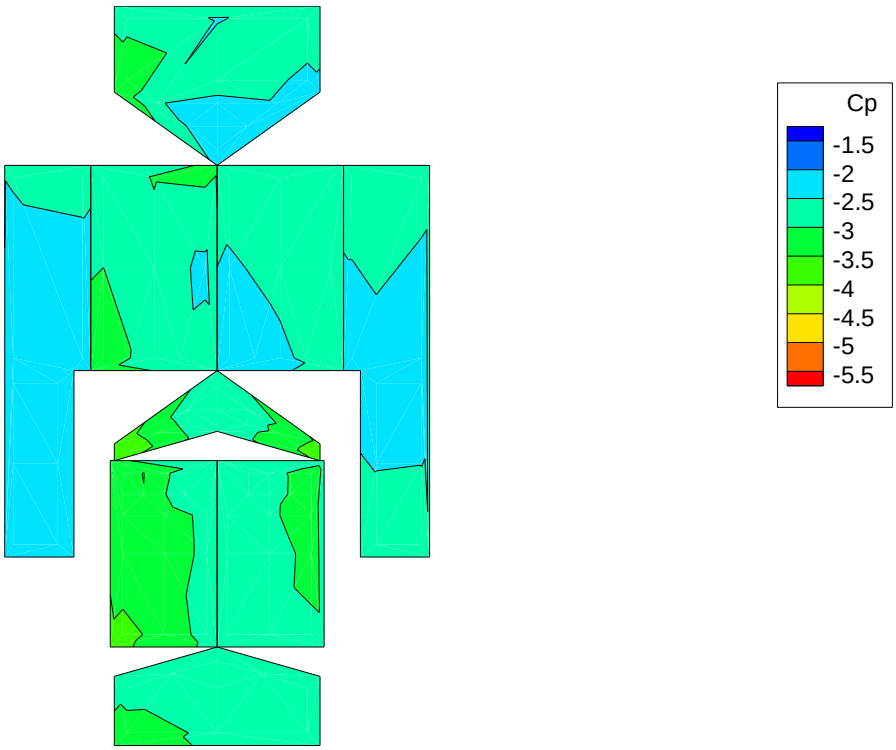

FIGURE B- 15 PEAK CP CONTOURS MODEL 8/GARAGE 1 ORIENTATION A BOA = 15°

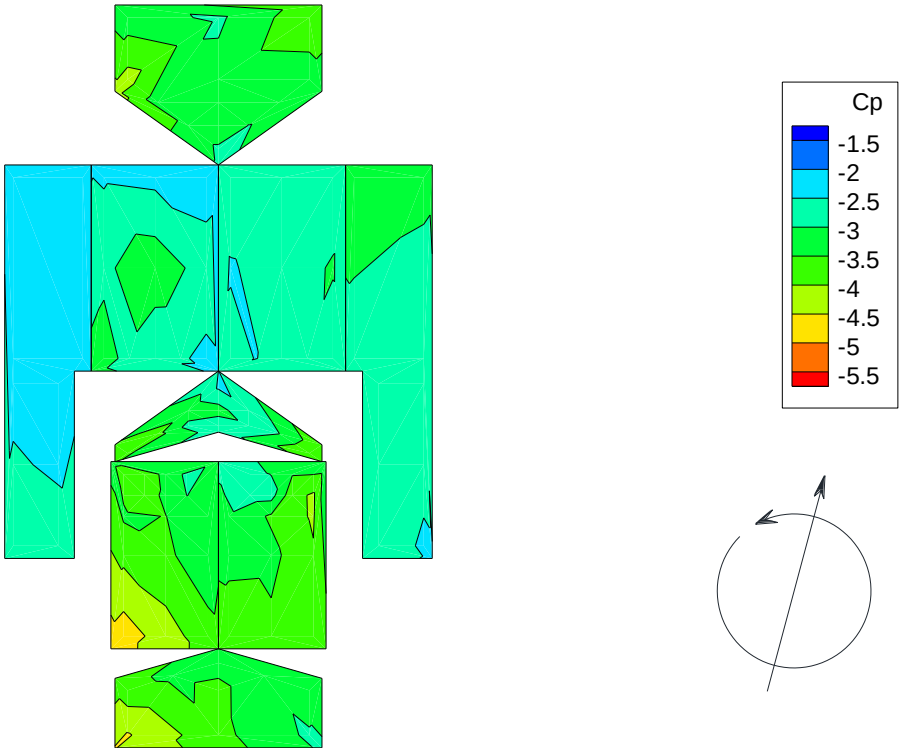

FIGURE B- 16 PEAK CP CONTOURS MODEL 8/GARAGE 1 ORIENTATION B BOA = 15°

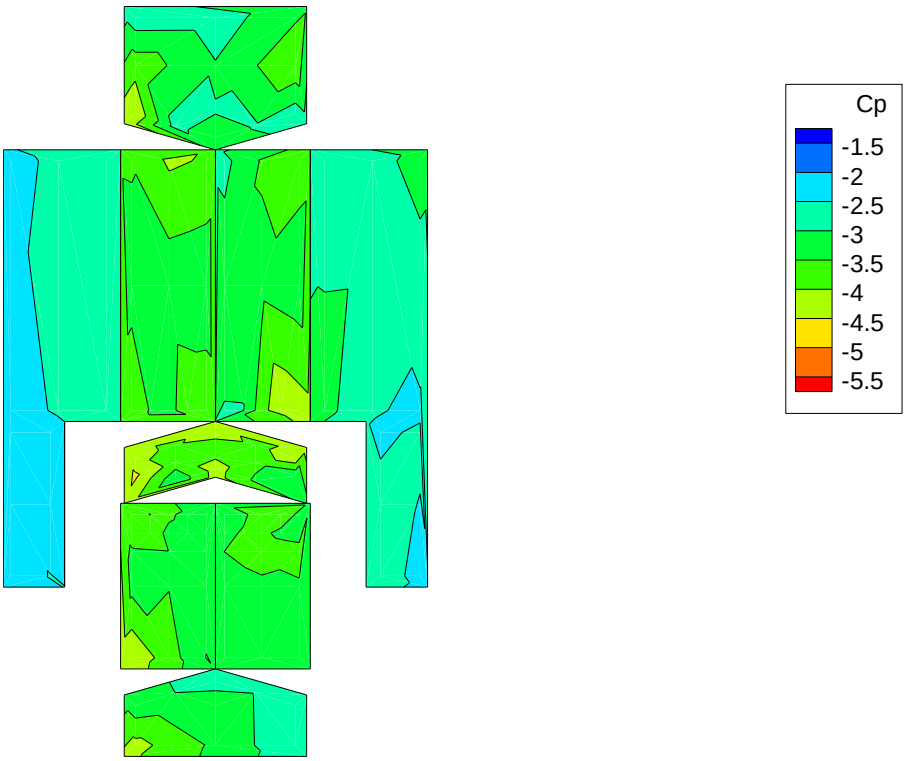

FIGURE B- 17 PEAK CP CONTOURS MODEL 9/GARAGE 2 ORIENTATION A BOA = 15°

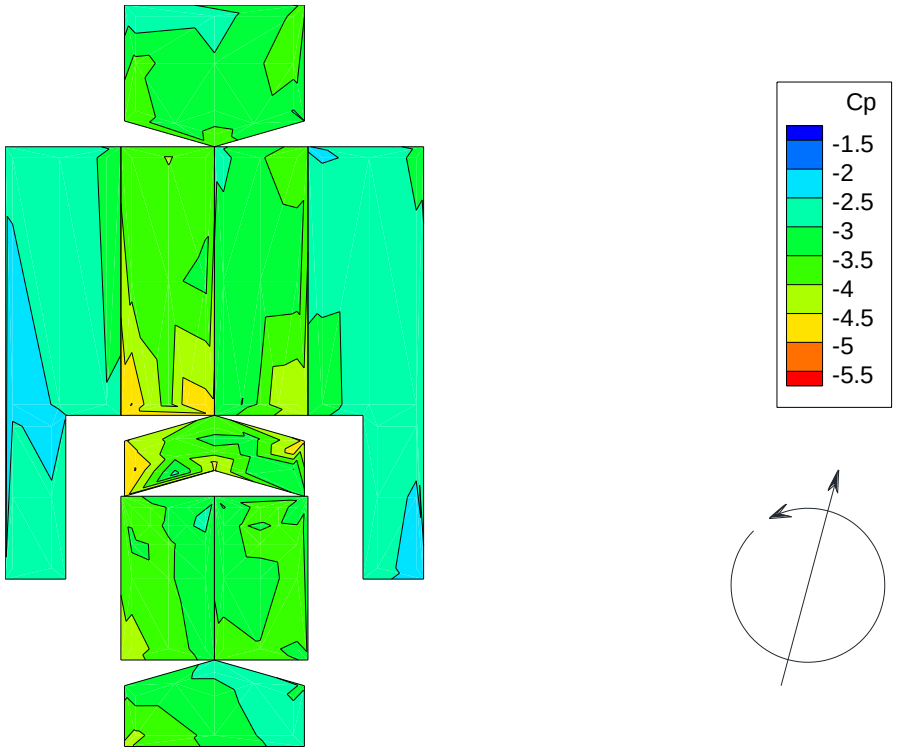

FIGURE B- 18 PEAK CP CONTOURS MODEL 9/GARAGE 2 ORIENTATION B BOA = 15°

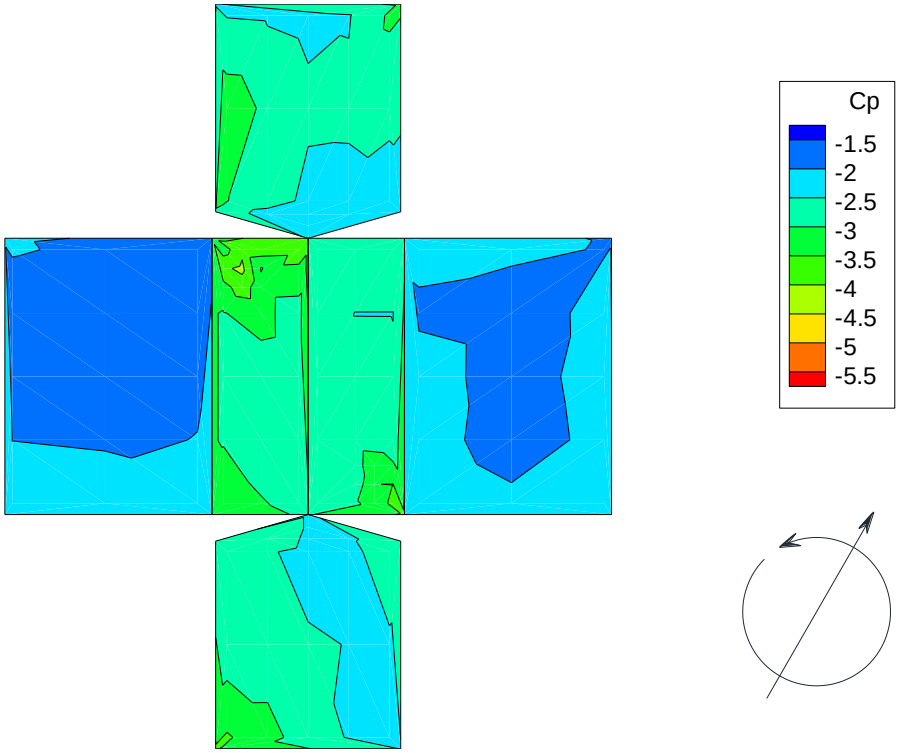

FIGURE B- 19 PEAK CP CONTOURS MODEL 2 BOA = 30°

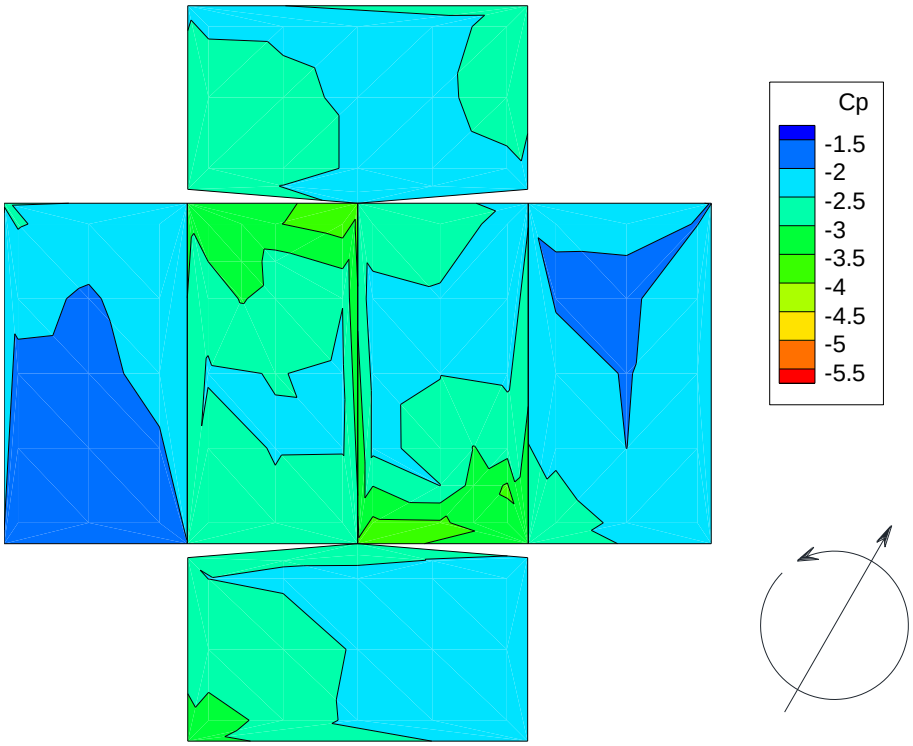

FIGURE B- 20 PEAK CP CONTOURS MODEL 3 BOA = 30°

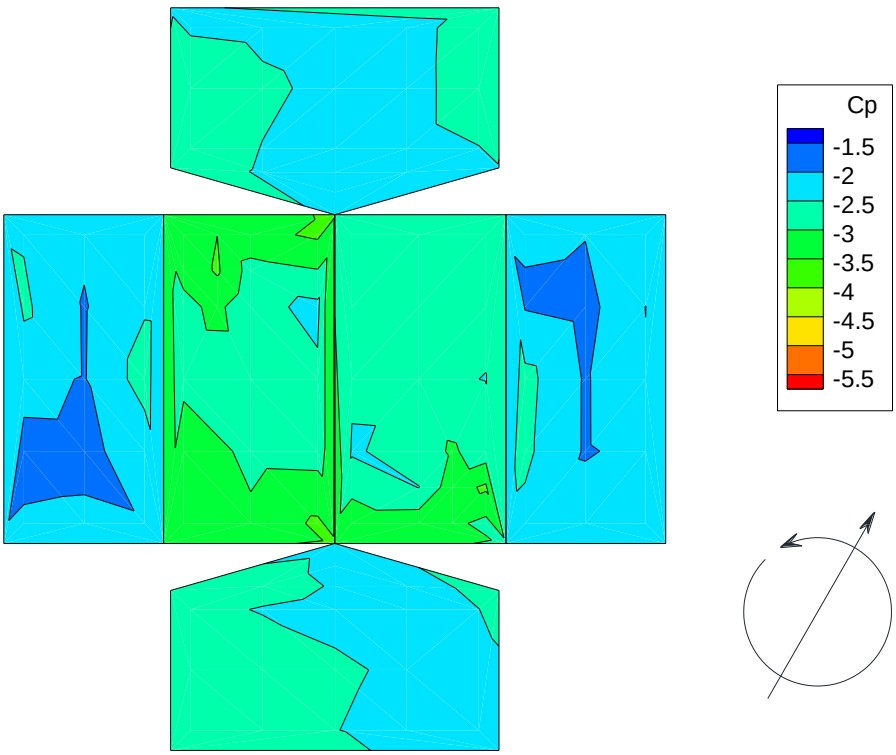

FIGURE B- 21 PEAK CP CONTOURS MODEL 4 BOA = 30°

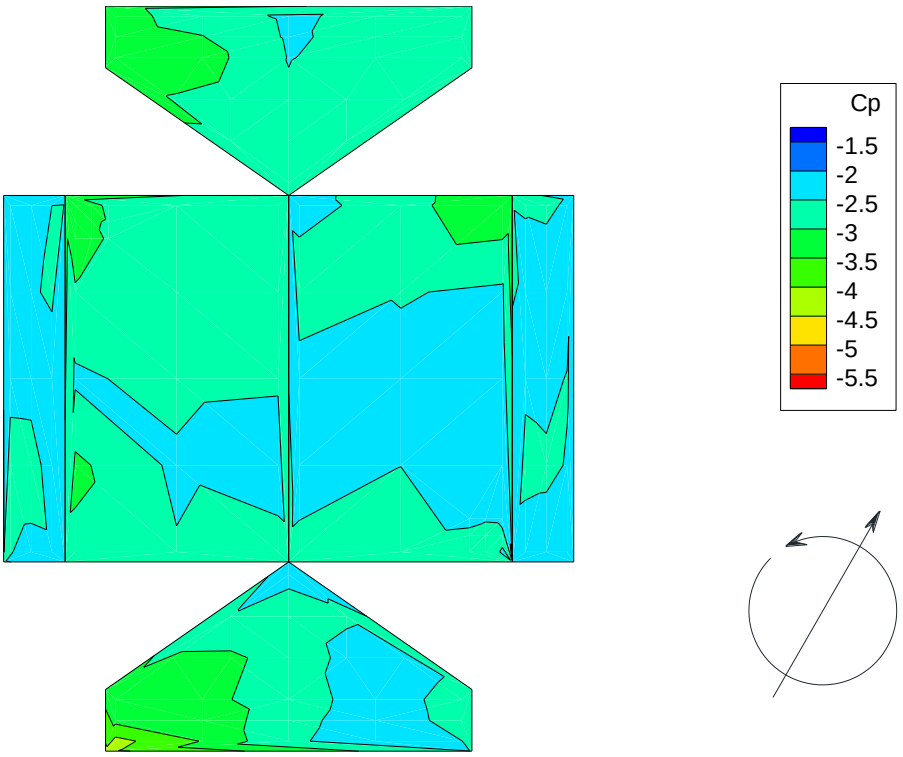

FIGURE B- 22 PEAK CP CONTOURS MODEL 6 BOA = 30°

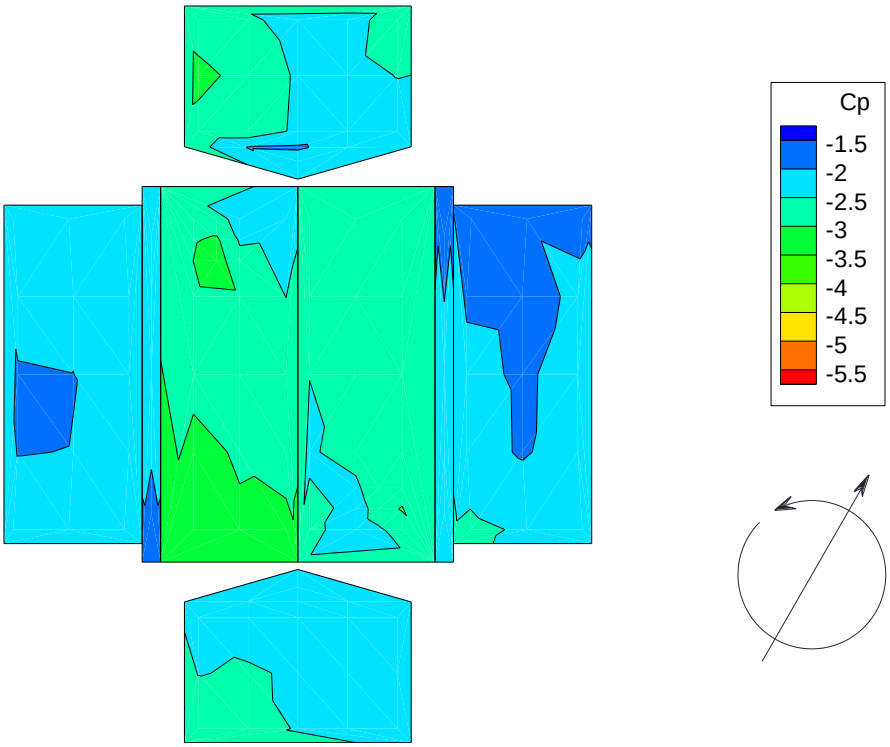

FIGURE B- 23 PEAK CP CONTOURS MODEL 7/OVERHANG BOA = 30°

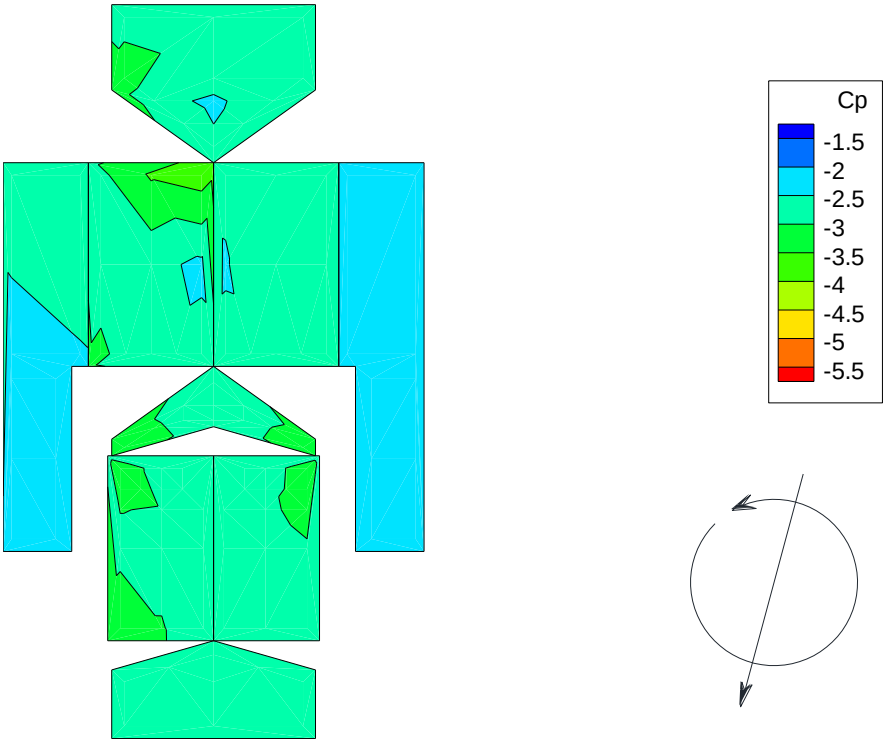

FIGURE B- 24 PEAK CP CONTOURS MODEL 8/GARAGE 1 ORIENTATION A BOA = 30°

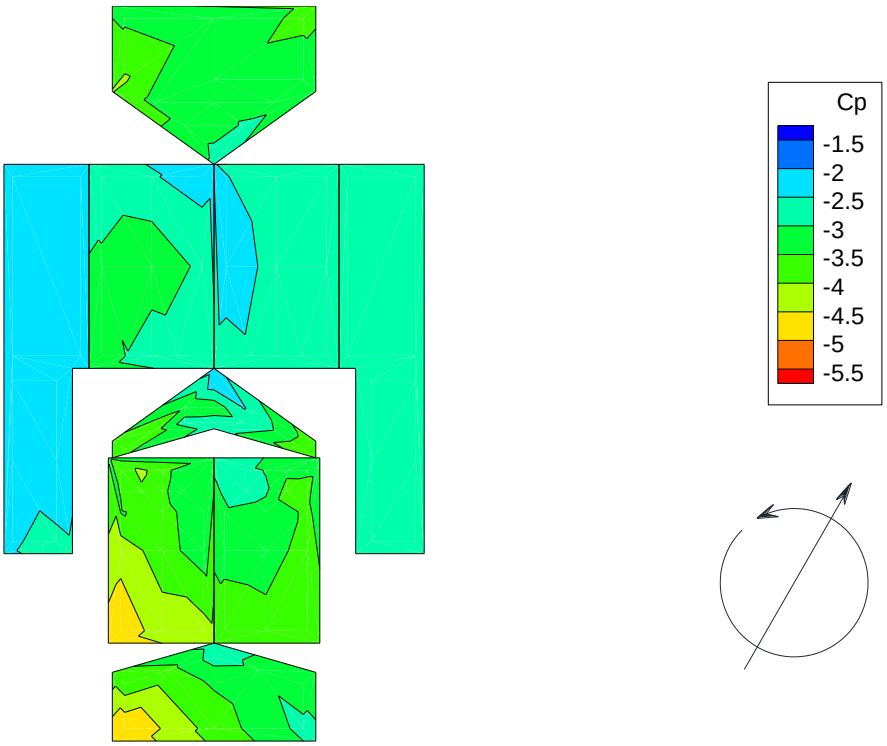

FIGURE B- 25 PEAK CP CONTOURS MODEL 8/GARAGE 1 ORIENTATION B BOA = 30°

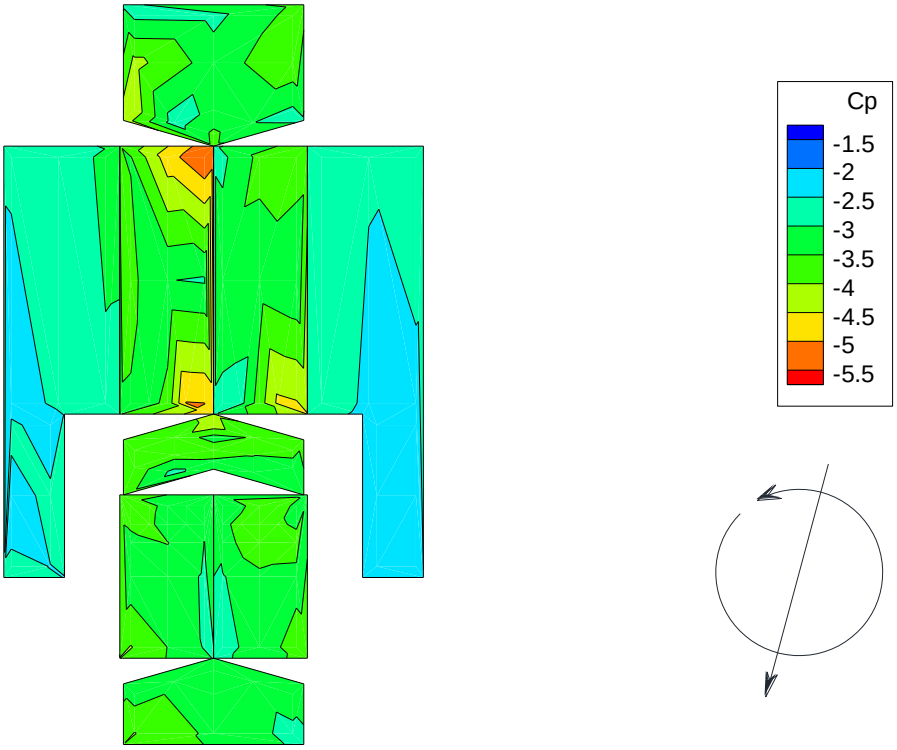

FIGURE B- 26 PEAK CP CONTOURS MODEL 9/GARAGE 2 ORIENTATION A BOA = 30°

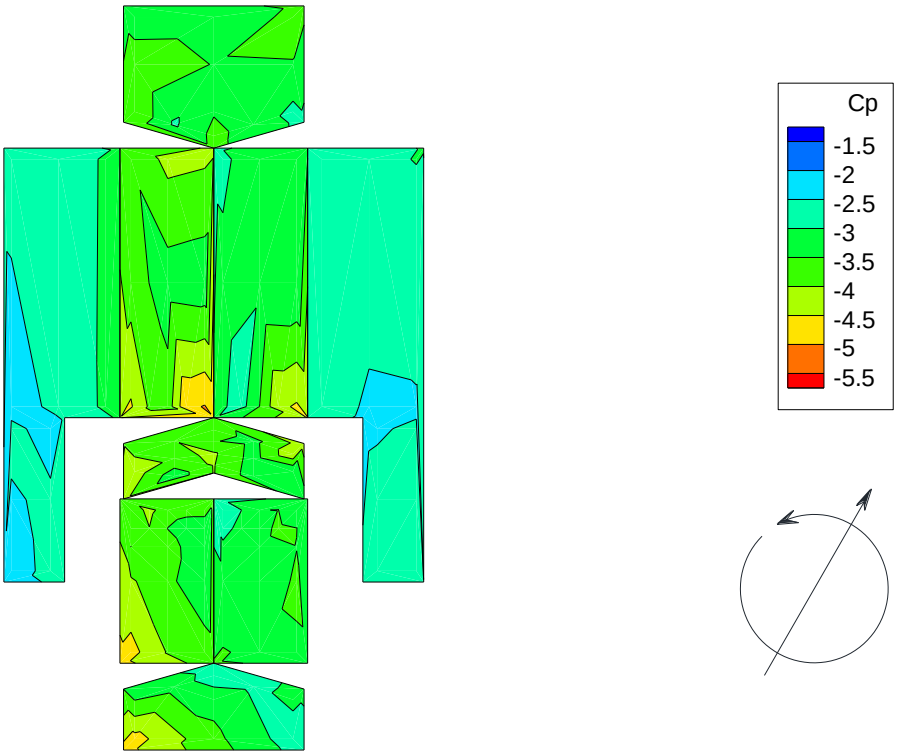

FIGURE B- 27 PEAK CP CONTOURS MODEL 9/GARAGE 2 ORIENTATION B BOA = 30°

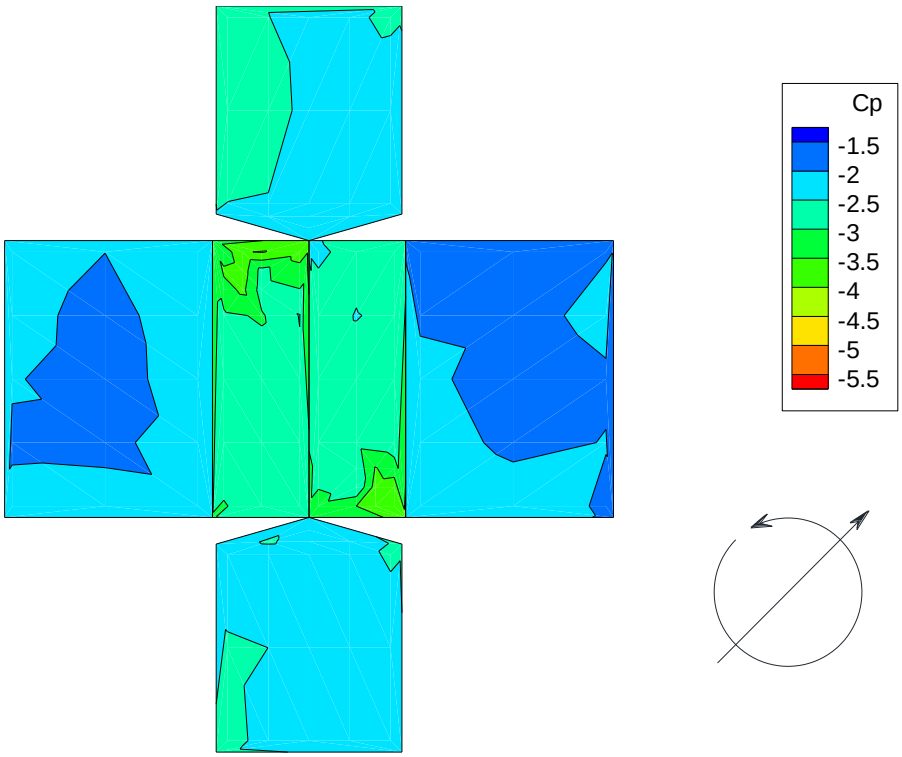

FIGURE B- 28 PEAK CP CONTOURS MODEL 2 BOA = 45°

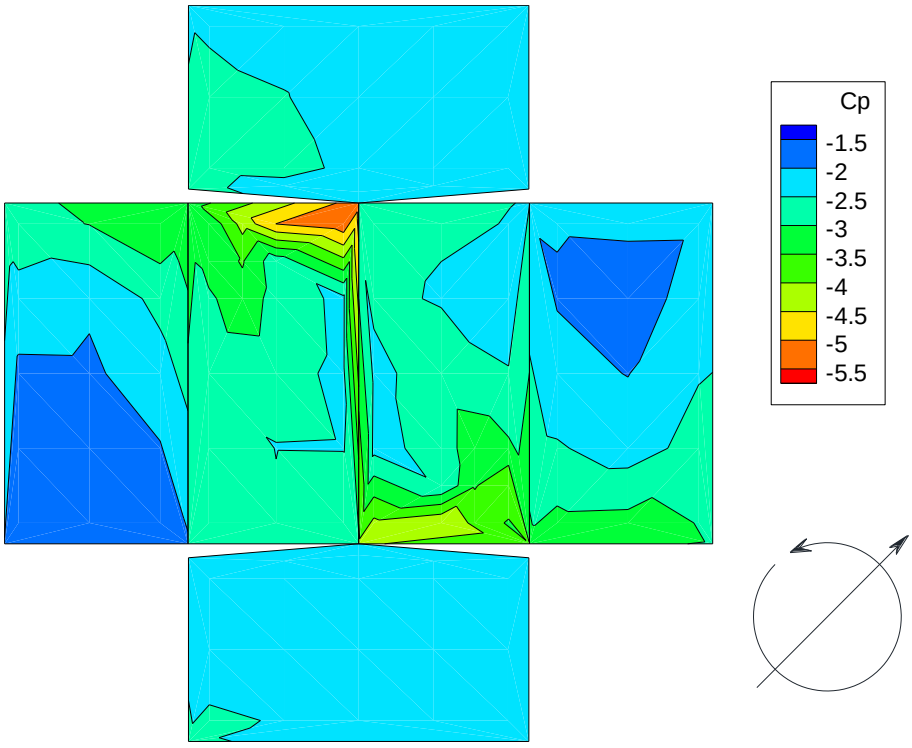

FIGURE B- 29 PEAK CP CONTOURS MODEL 3 BOA = 45°

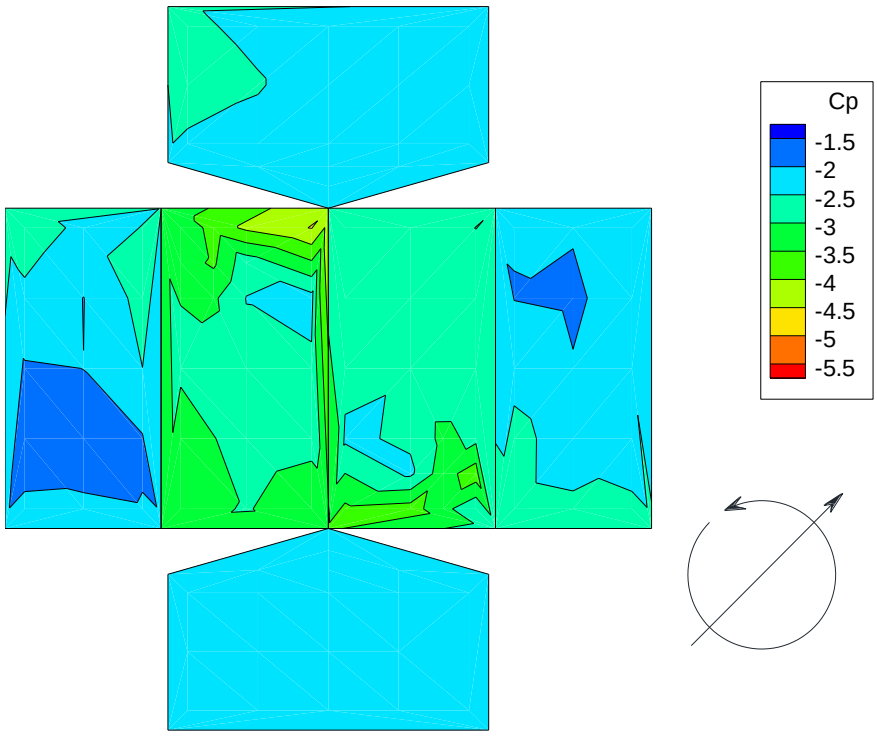

FIGURE B- 30 PEAK CP CONTOURS MODEL 4 BOA = 45°

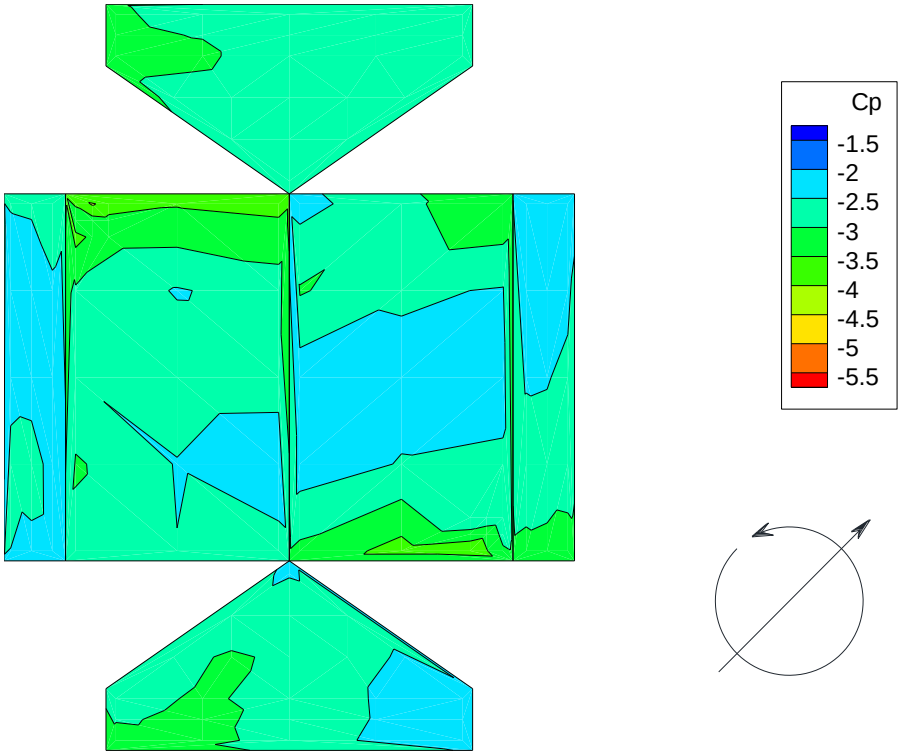

FIGURE B- 31 PEAK CP CONTOURS MODEL 6 BOA = 45°

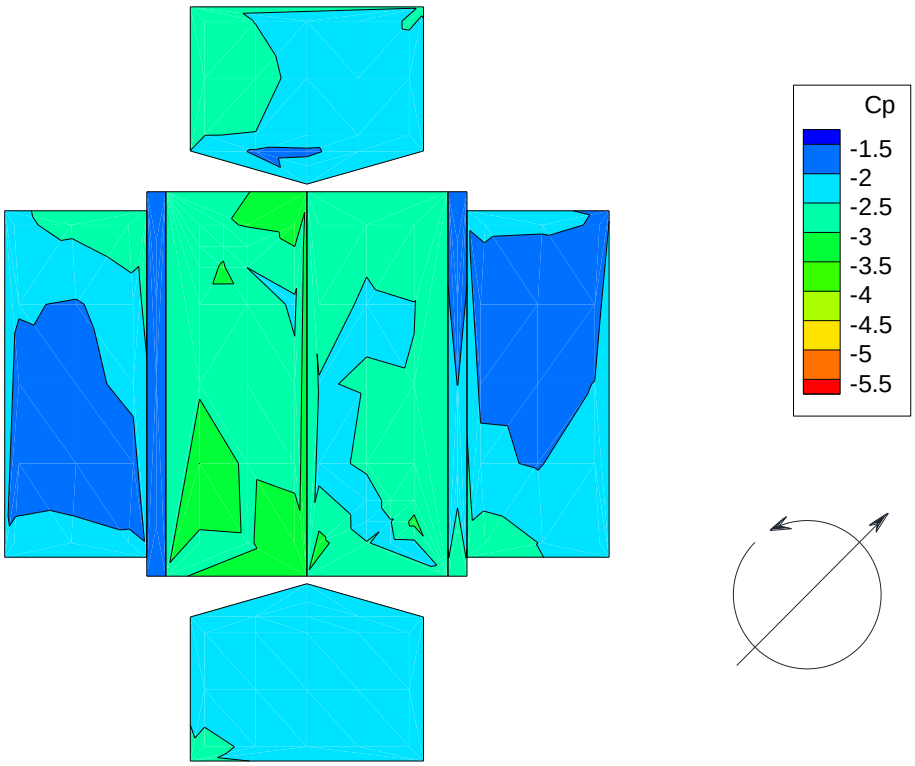

FIGURE B- 32 PEAK CP CONTOURS MODEL 7/OVERHANG BOA = 45°

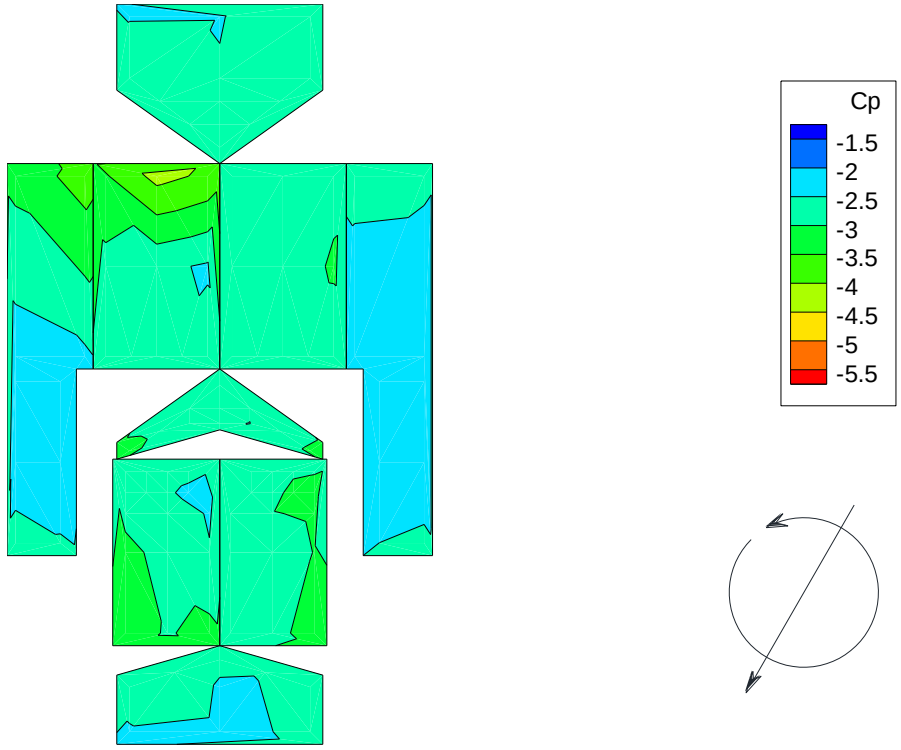

FIGURE B- 33 PEAK CP CONTOURS MODEL 8/GARAGE 1 ORIENTATION A BOA = 45°

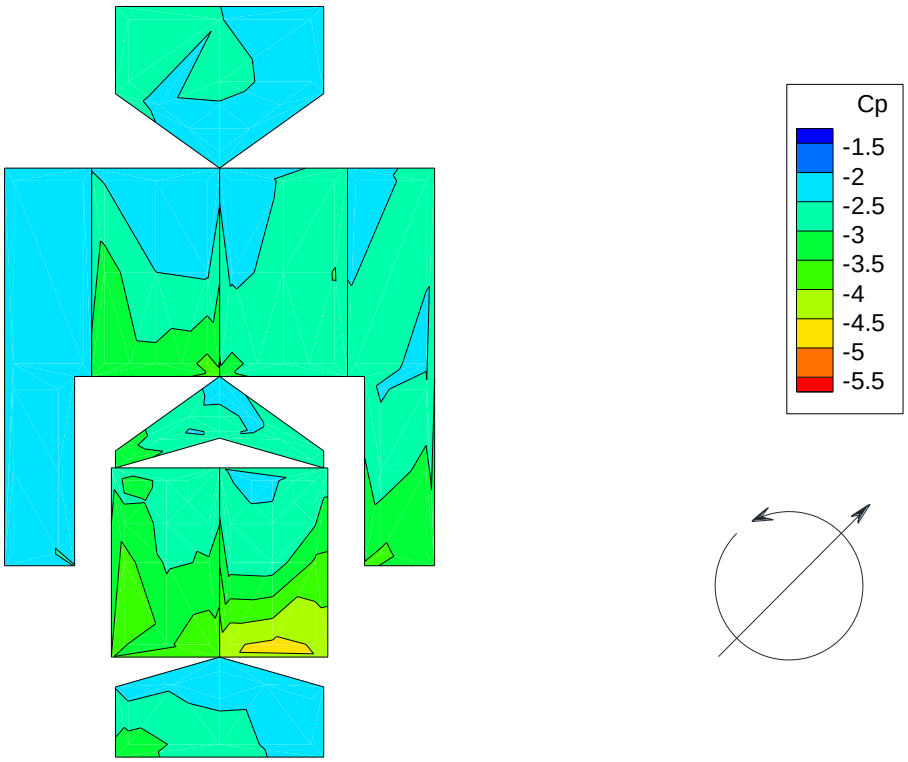

FIGURE B- 34 PEAK CP CONTOURS MODEL 8/GARAGE 1 ORIENTATION B BOA = 45°

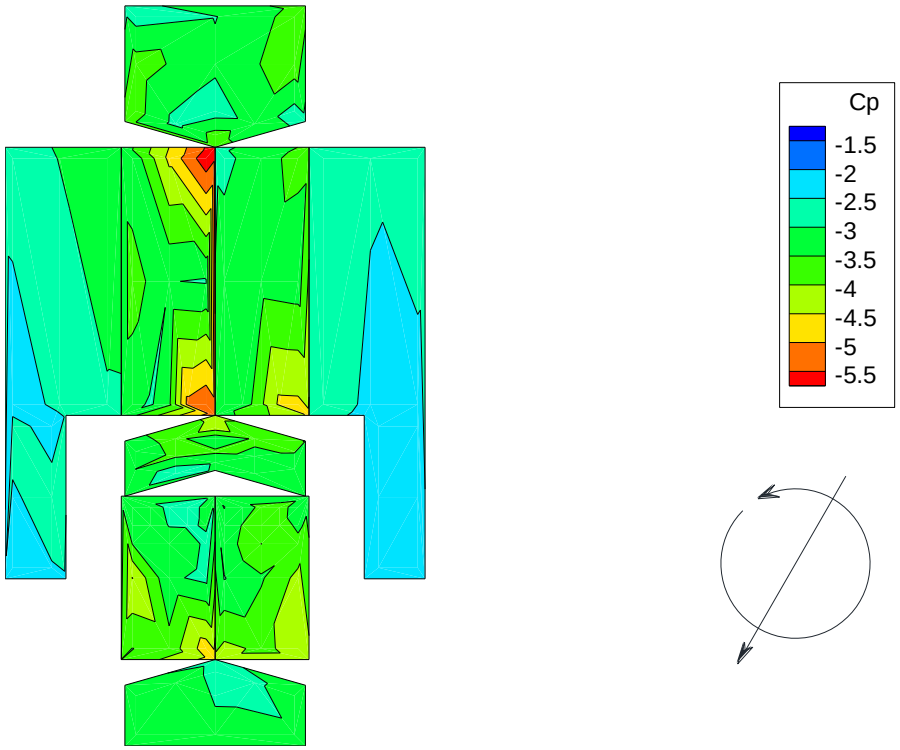

FIGURE B- 35 PEAK CP CONTOURS MODEL 9/GARAGE 2 ORIENTATION A BOA = 45°

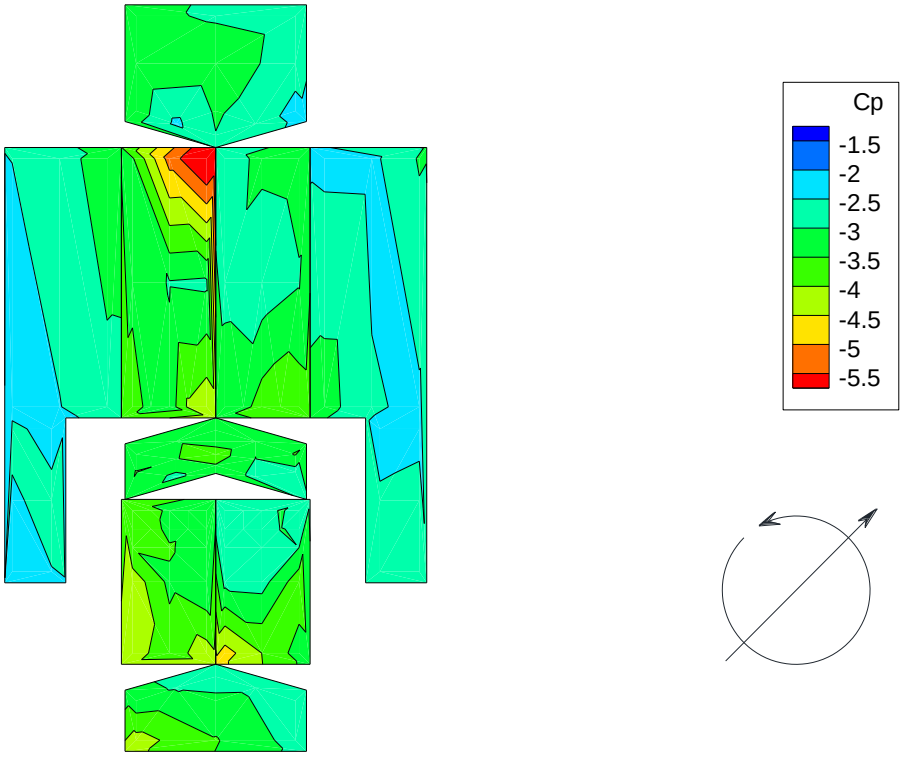

FIGURE B- 36 PEAK CP CONTOURS MODEL 9/GARAGE 2 ORIENTATION B BOA = 45°

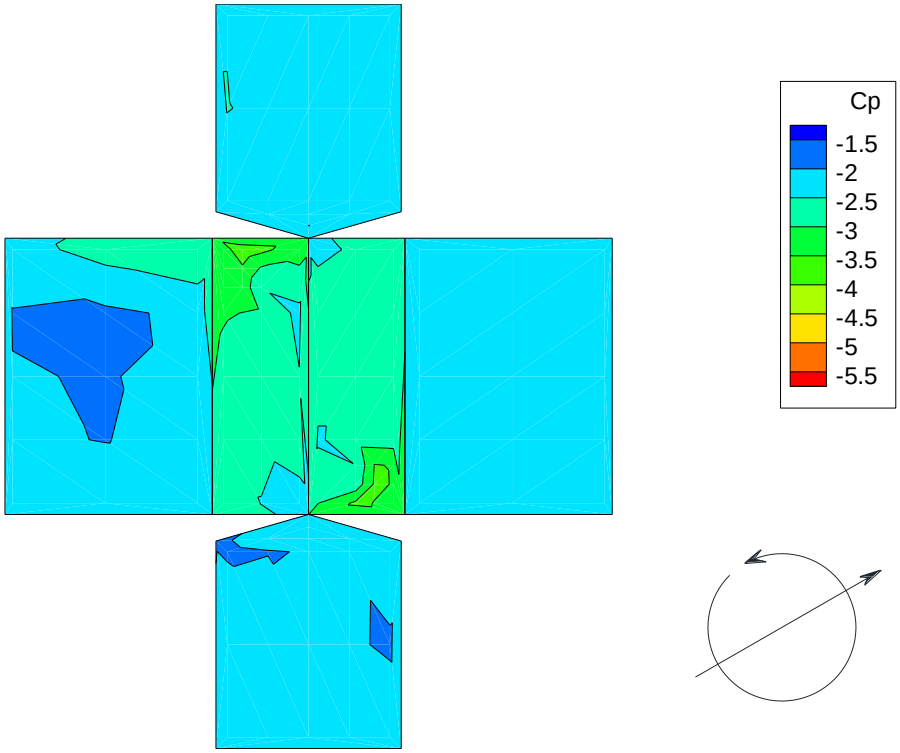

FIGURE B- 37 PEAK CP CONTOURS MODEL 2 BOA = 60°

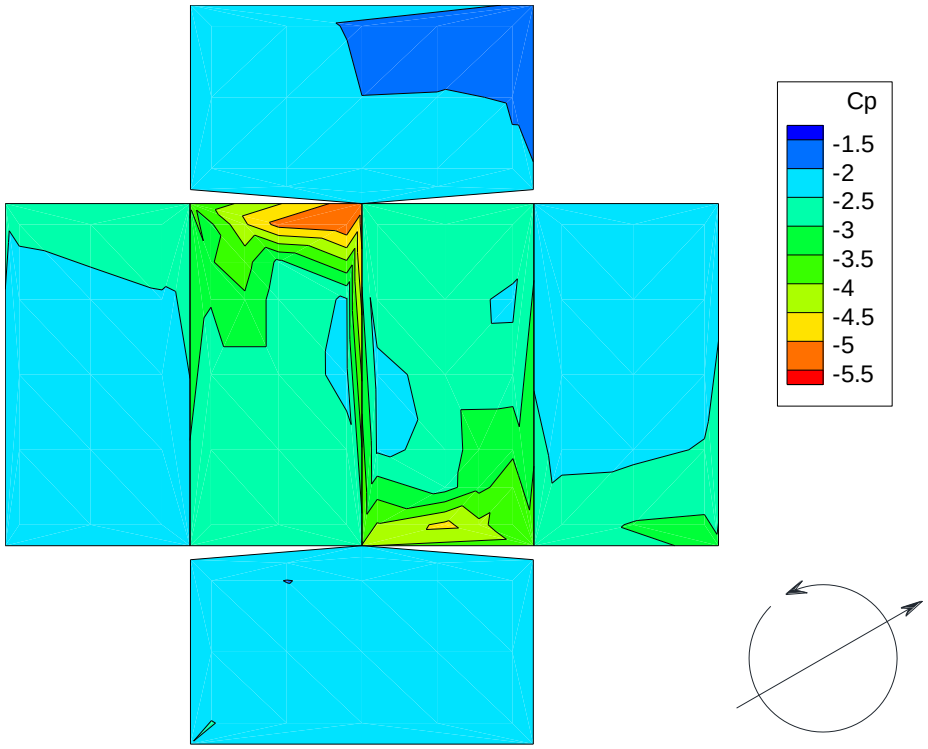

FIGURE B- 38 PEAK CP CONTOURS MODEL 3 BOA = 60°

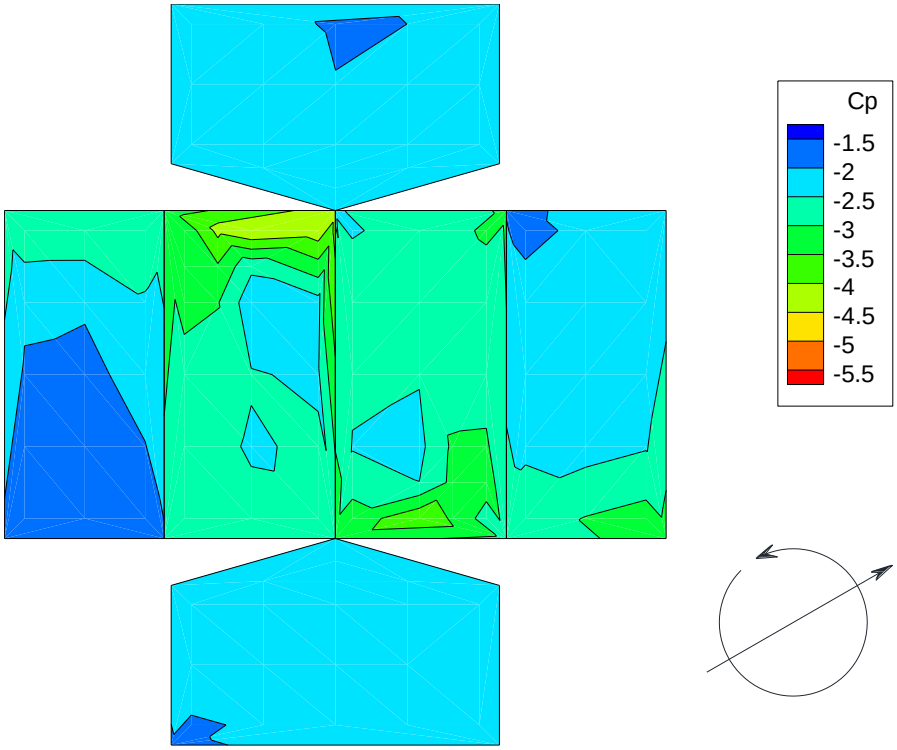

FIGURE B- 39 PEAK CP CONTOURS MODEL 4 BOA = 60°

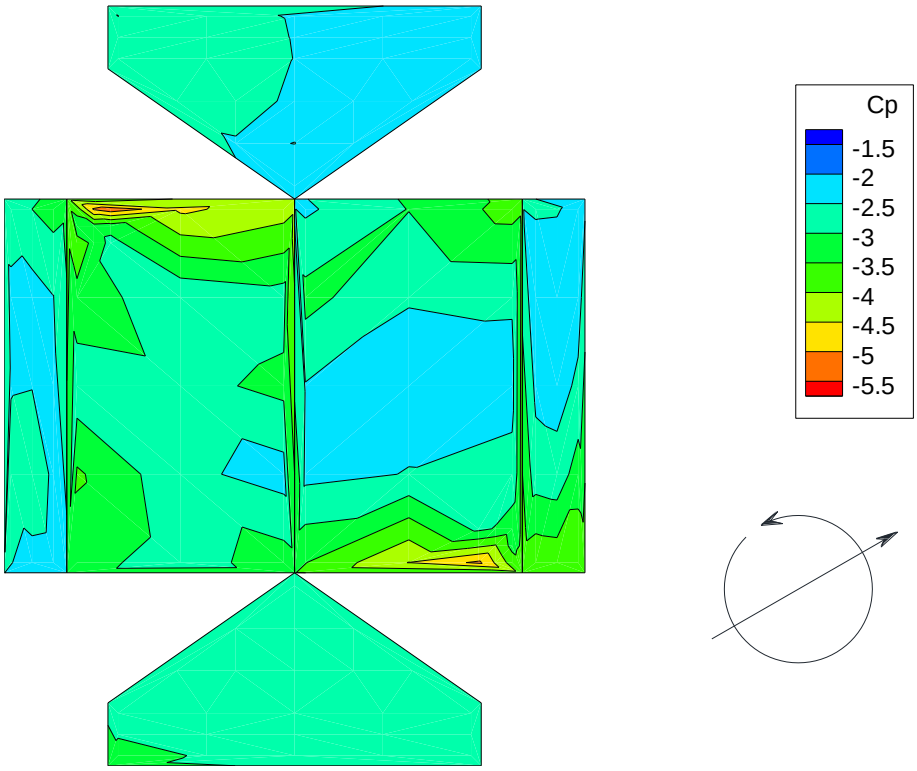

FIGURE B- 40 PEAK CP CONTOURS MODEL 6 BOA = 60°

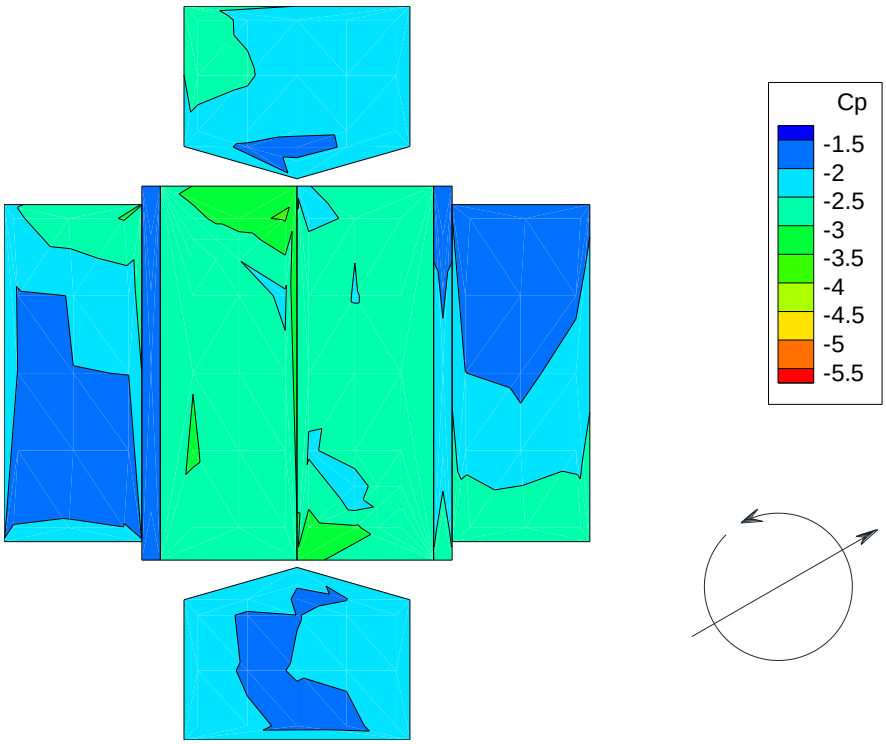

FIGURE B- 41 PEAK CP CONTOURS MODEL 7/OVERHANG BOA = 60°

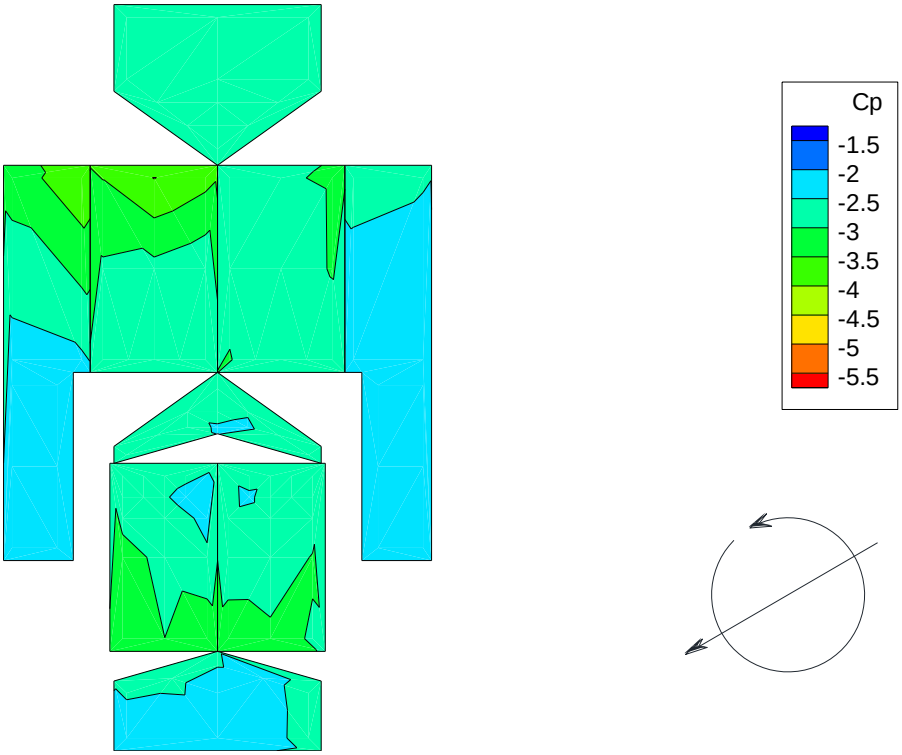

FIGURE B- 42 PEAK CP CONTOURS MODEL 8/GARAGE 1 ORIENTATION A BOA = 60°

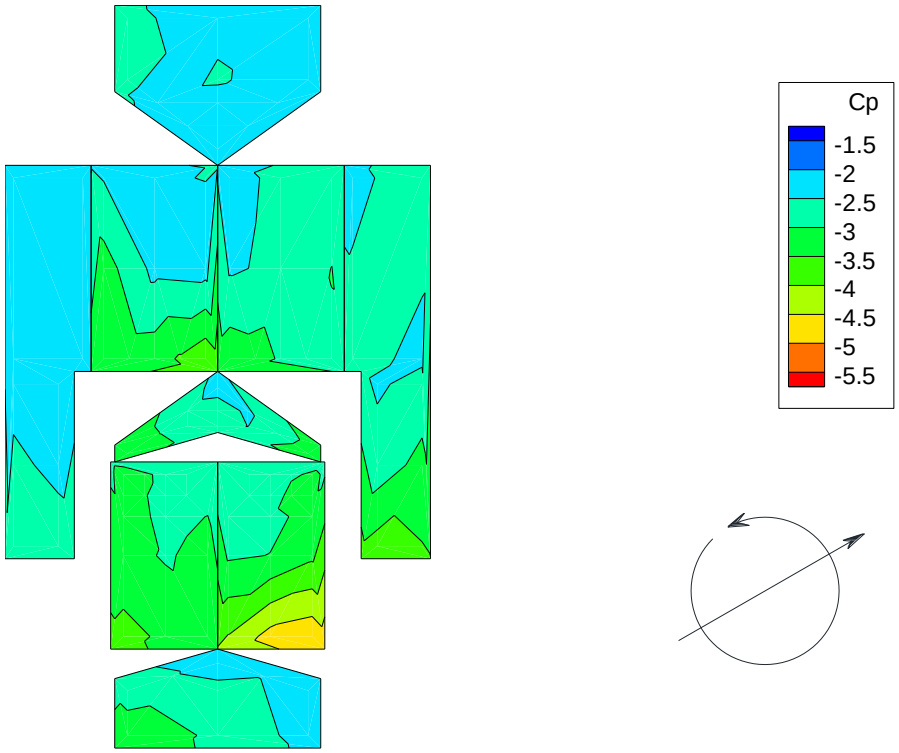

FIGURE B- 43 PEAK CP CONTOURS MODEL 8/GARAGE 1 ORIENTATION B BOA = 60°

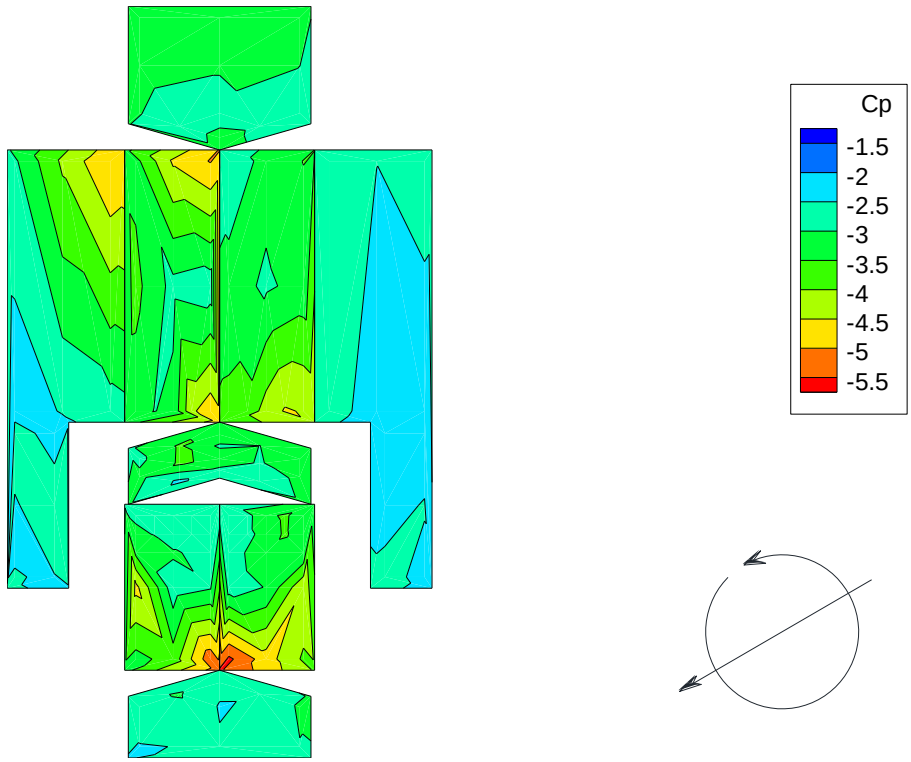

FIGURE B- 44 PEAK CP CONTOURS MODEL 9/GARAGE 2 ORIENTATION A BOA = 60°

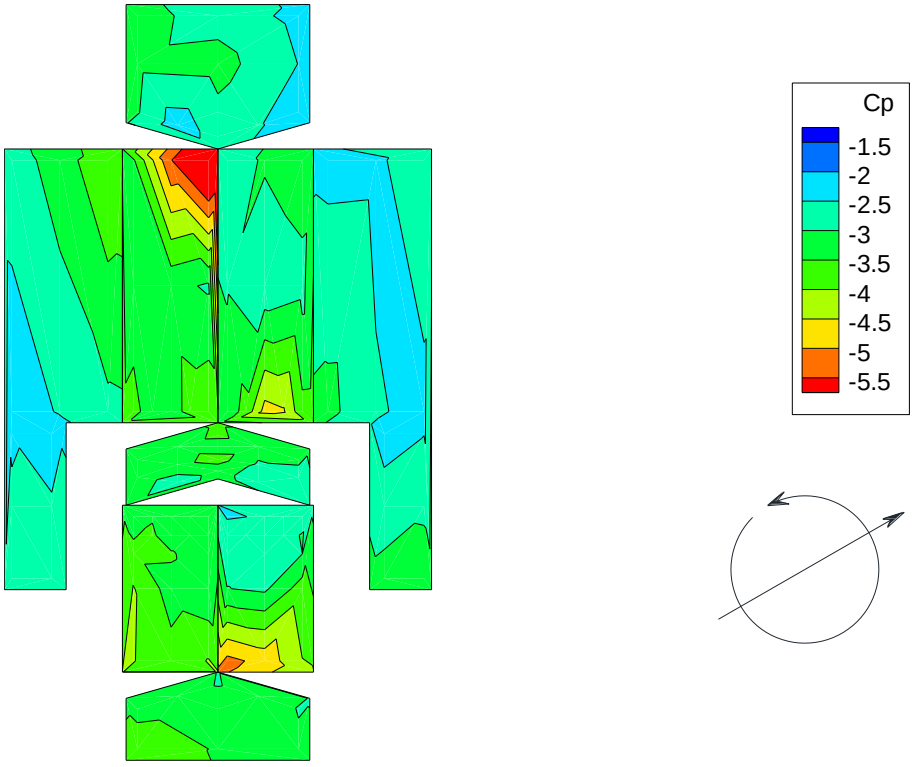

FIGURE B- 45 PEAK CP CONTOURS MODEL 9/GARAGE 2 ORIENTATION B BOA = 60°

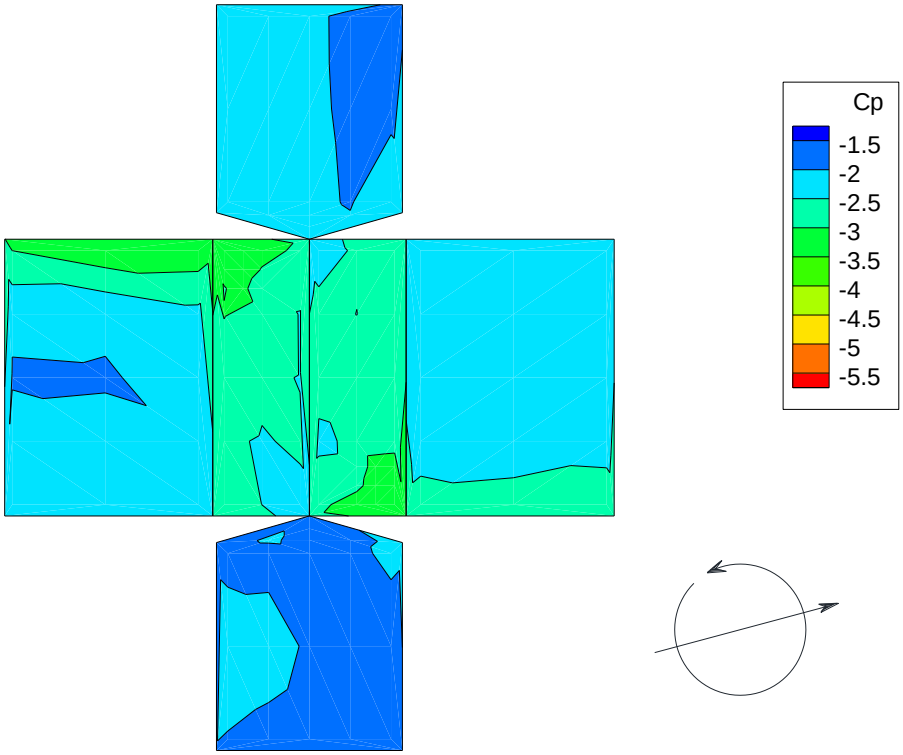

FIGURE B- 46 PEAK CP CONTOURS MODEL 2 BOA = 75°

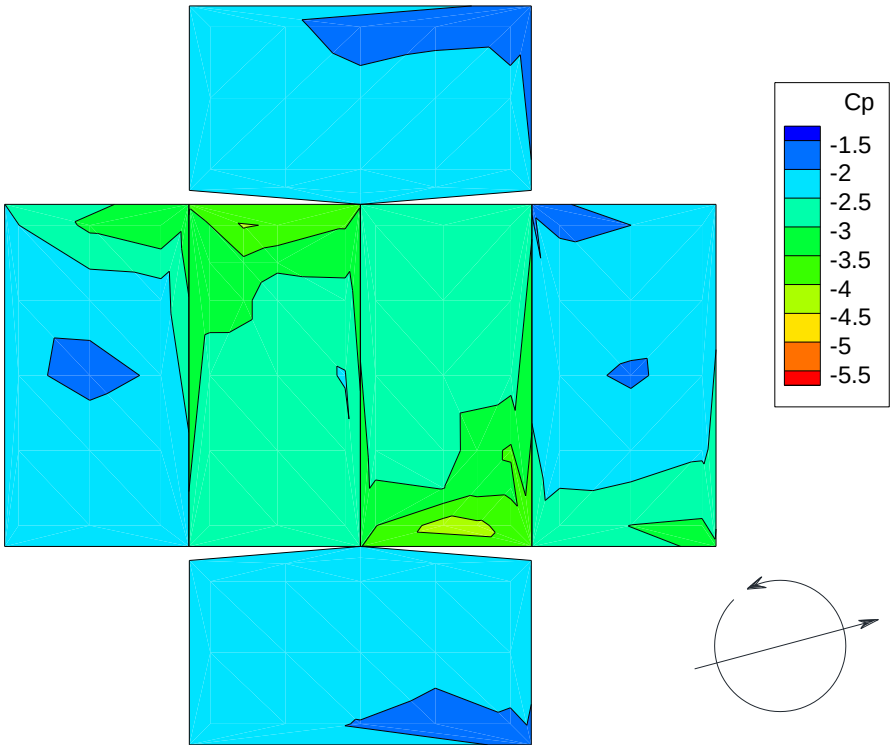

FIGURE B- 47 PEAK CP CONTOURS MODEL 3 BOA = 75°

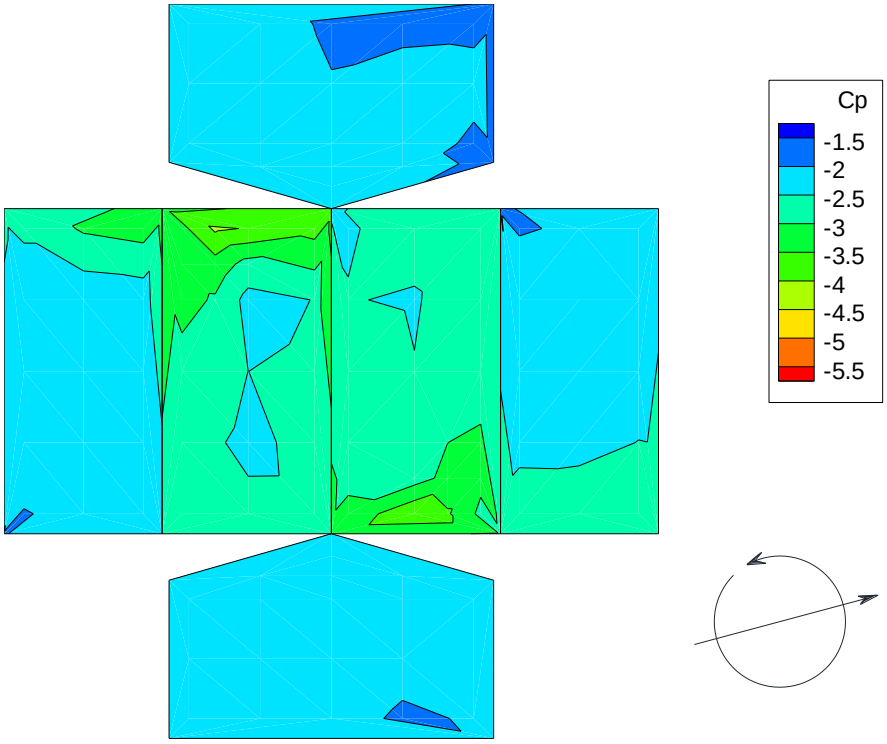

FIGURE B- 48 PEAK CP CONTOURS MODEL 4 BOA = 75°

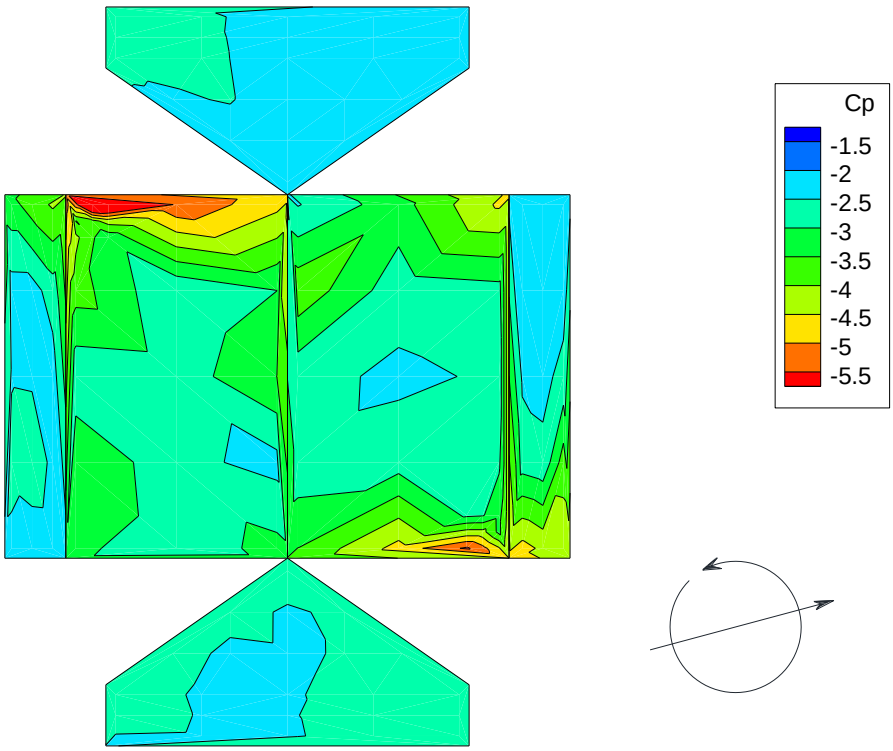

FIGURE B- 49 PEAK CP CONTOURS MODEL 6 BOA = 75°

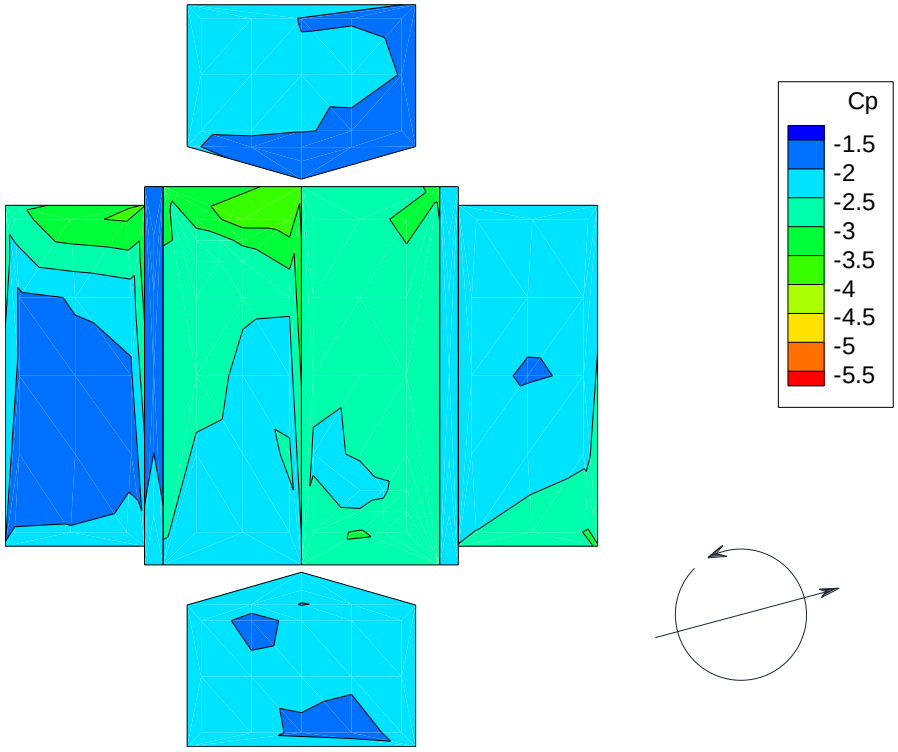

FIGURE B- 50 PEAK CP CONTOURS MODEL 7/OVERHANG BOA = 75°

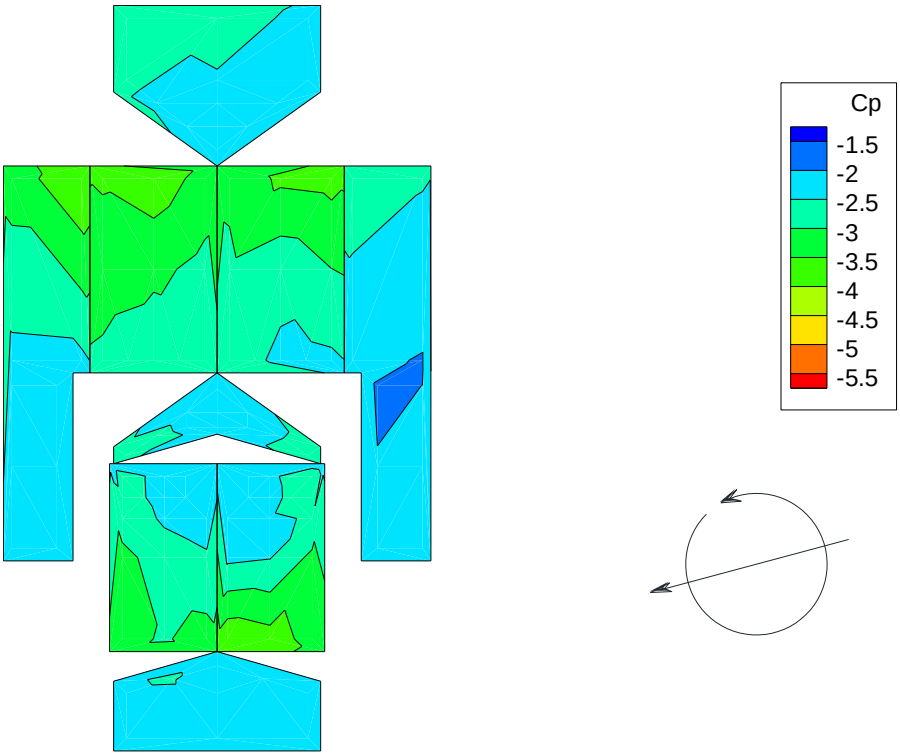

FIGURE B- 51 PEAK CP CONTOURS MODEL 8/GARAGE 1 ORIENTATION A BOA = 75°

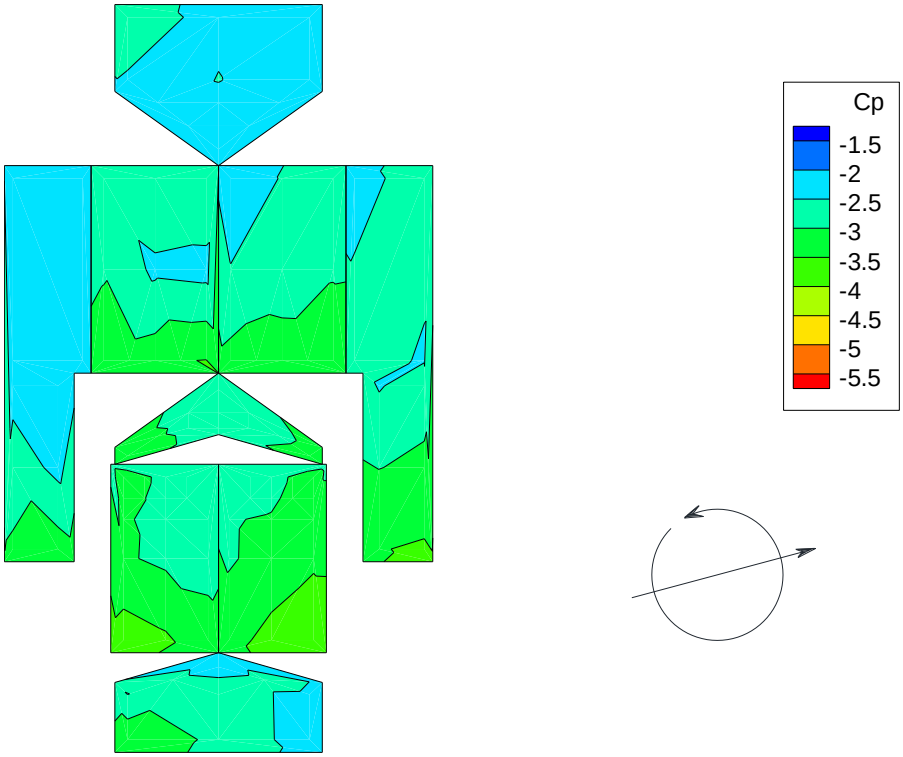

FIGURE B- 52 PEAK CP CONTOURS MODEL 8/GARAGE 1 ORIENTATION B BOA = 75°

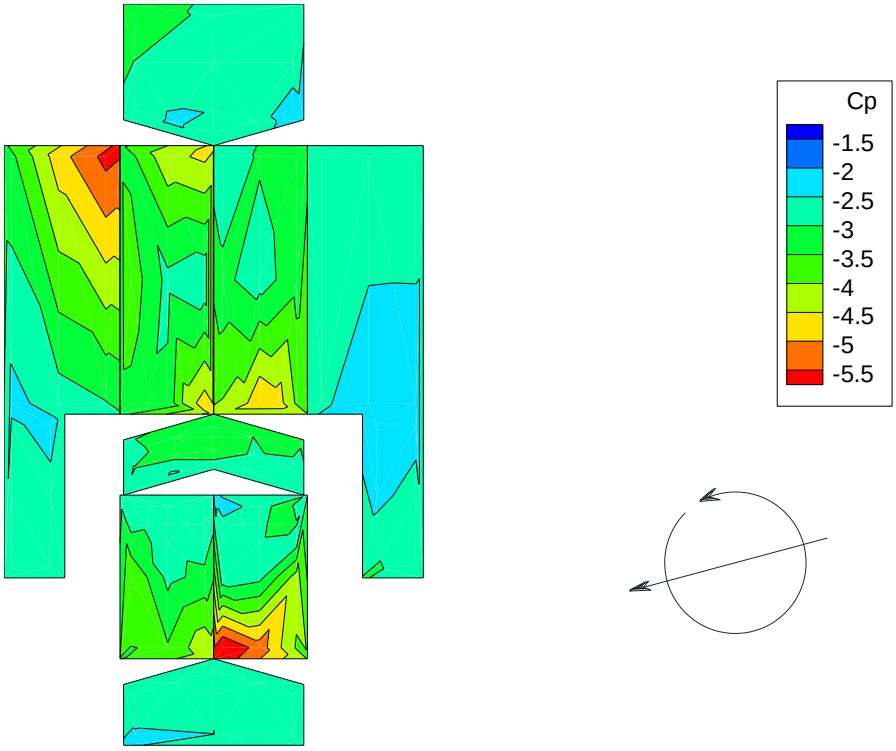

FIGURE B- 53 PEAK CP CONTOURS MODEL 9/GARAGE 2 ORIENTATION A BOA = 75°

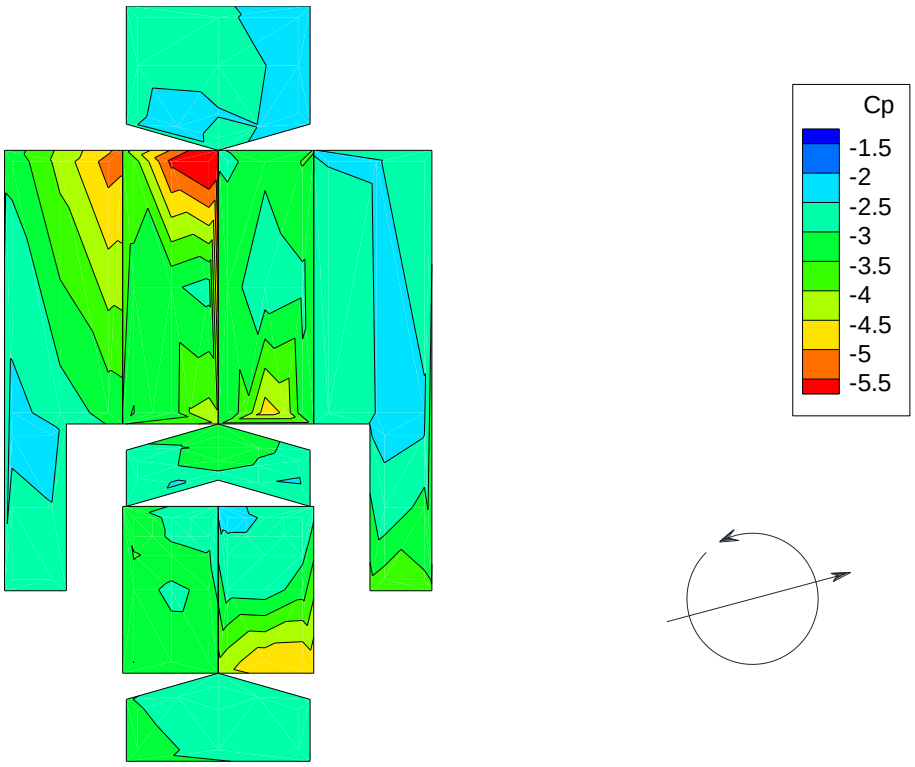

FIGURE B- 54 PEAK CP CONTOURS MODEL 9/GARAGE 2 ORIENTATION B BOA = 75°

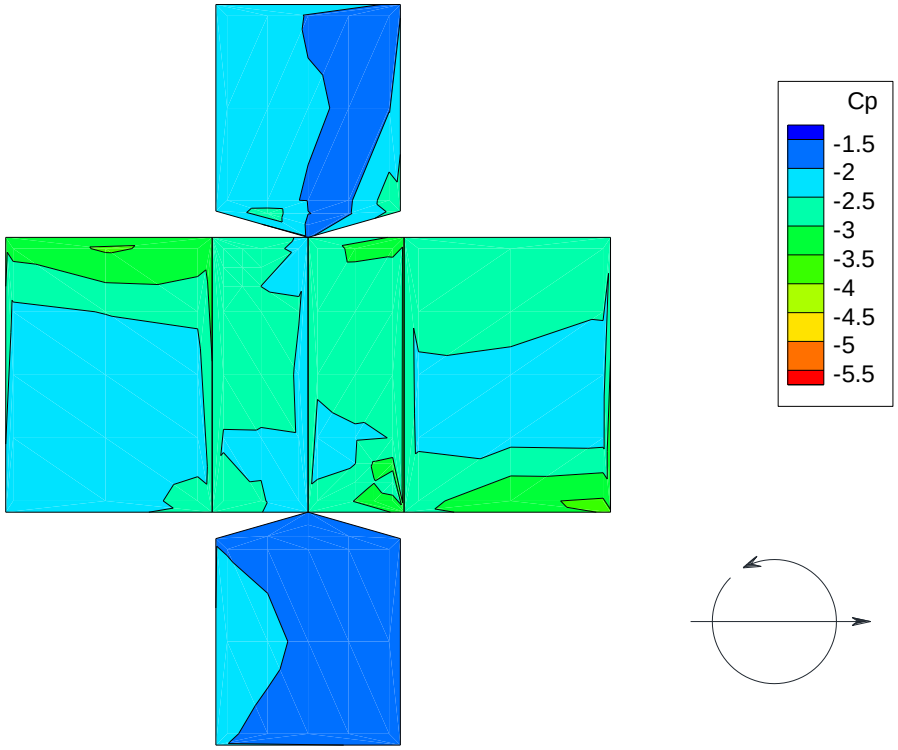

FIGURE B- 55 PEAK CP CONTOURS MODEL 2 BOA = 90°

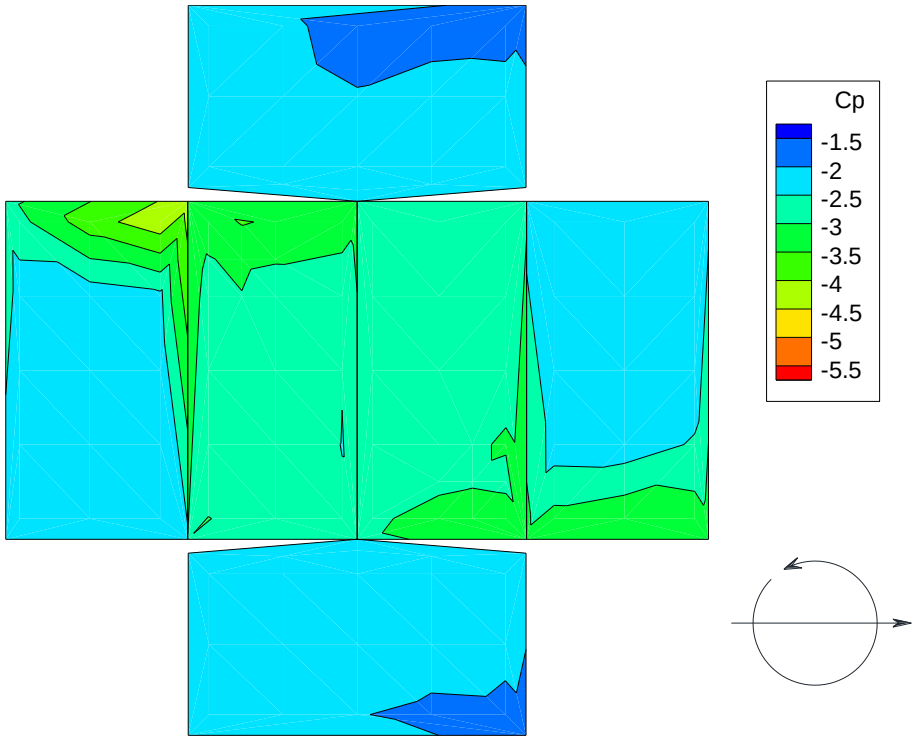

FIGURE B- 56 PEAK CP CONTOURS MODEL 3 BOA = 90°

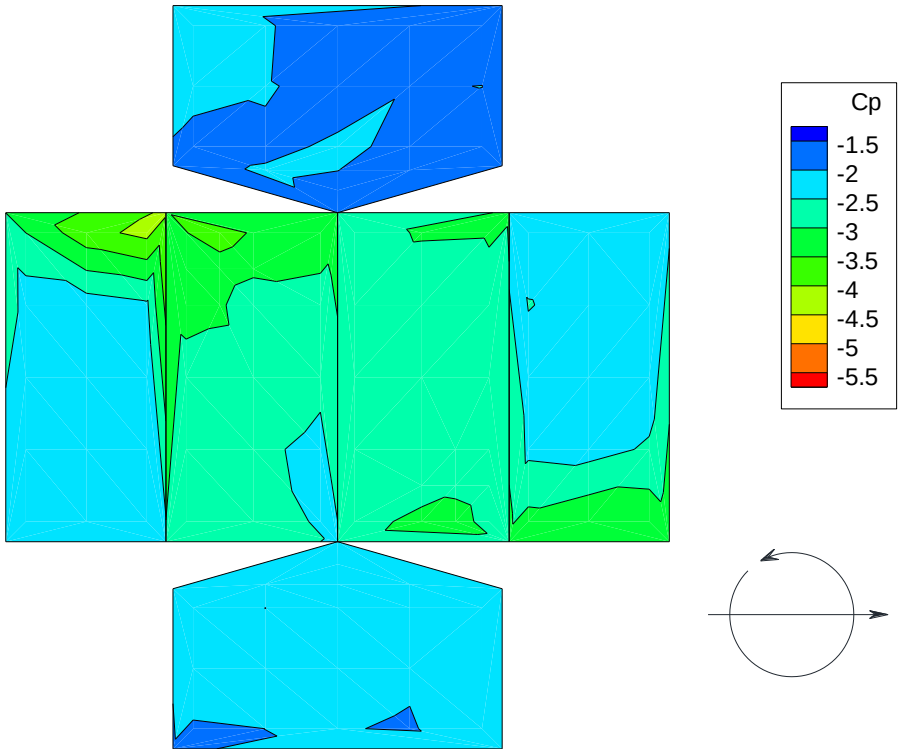

FIGURE B- 57 PEAK CP CONTOURS MODEL 4 BOA = 90°

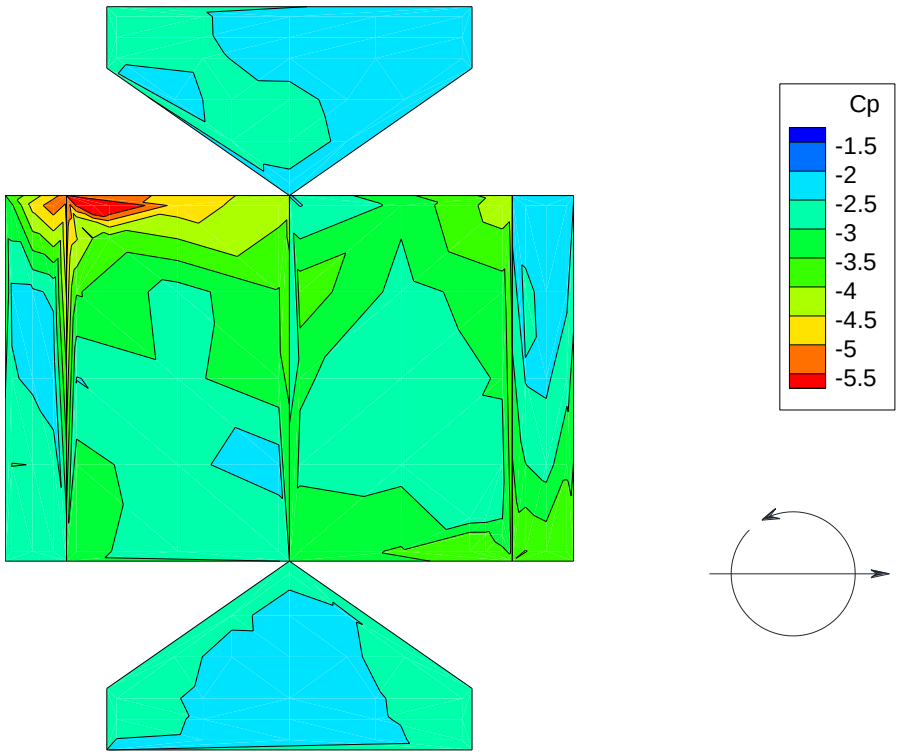

FIGURE B- 58 PEAK CP CONTOURS MODEL 6 BOA = 90°

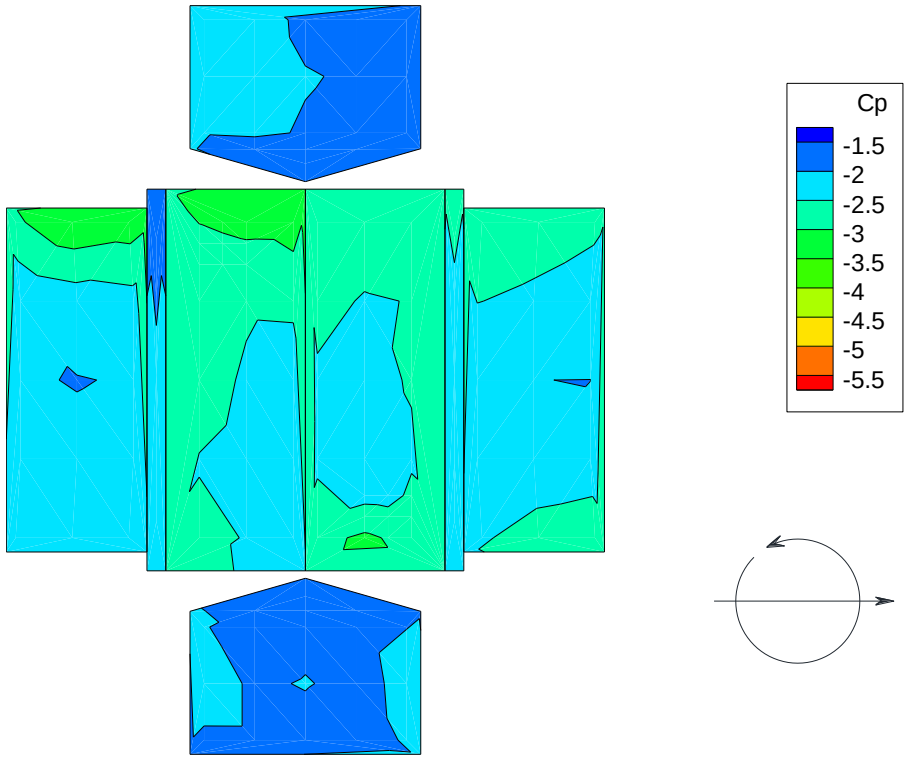

FIGURE B- 59 PEAK CP CONTOURS MODEL 7/OVERHANG BOA = 90°

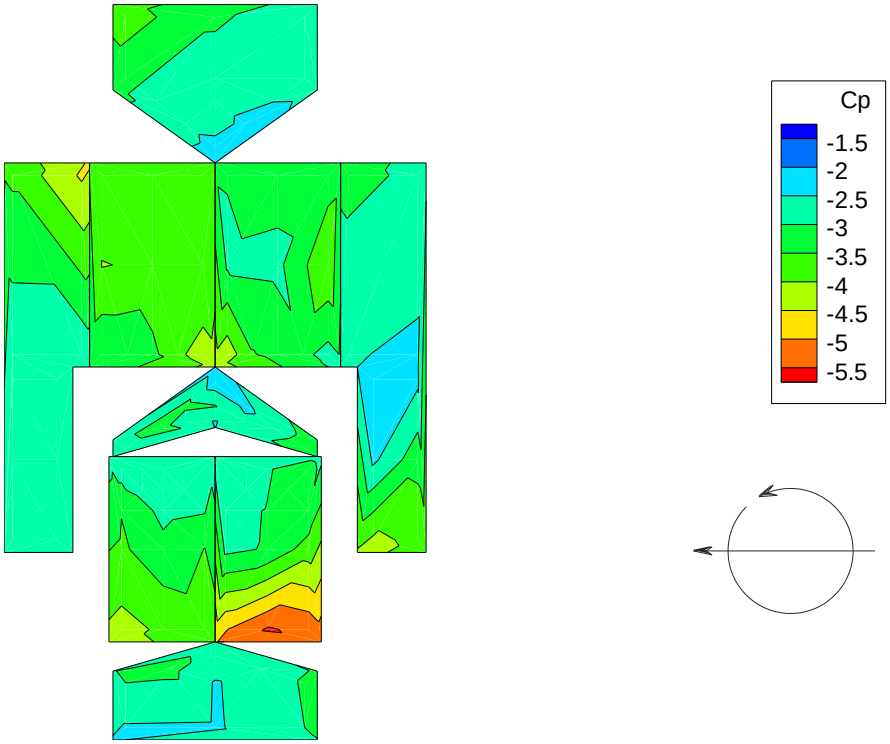

FIGURE B- 60 PEAK CP CONTOURS MODEL 8/GARAGE 1 ORIENTATION A BOA = 90°

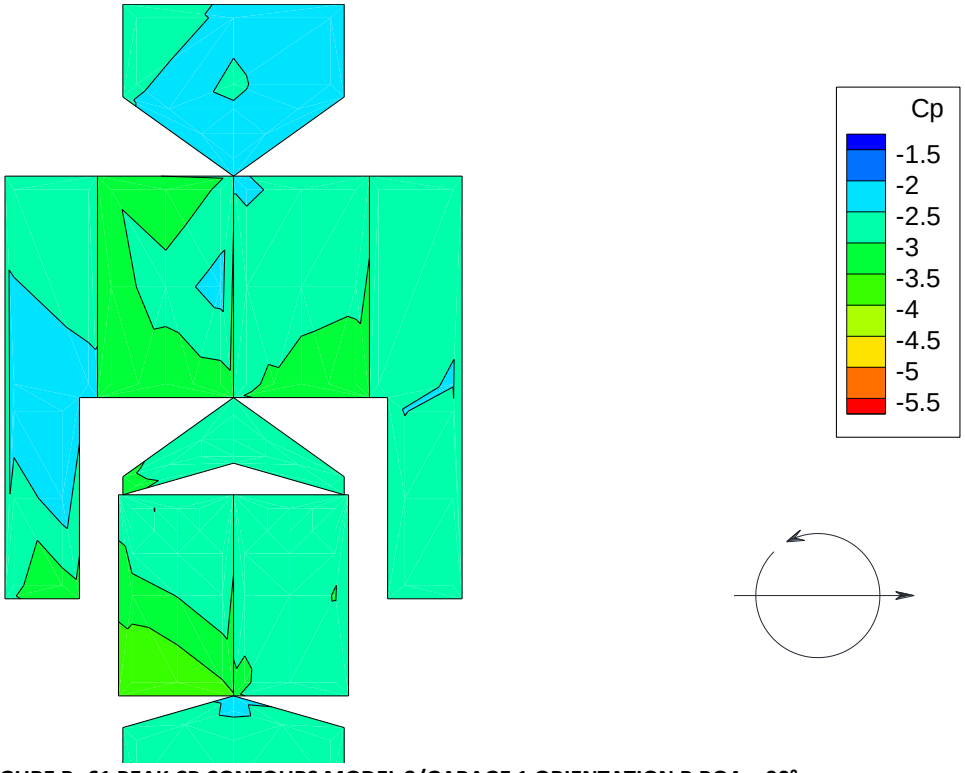

FIGURE B- 61 PEAK CP CONTOURS MODEL 8/GARAGE 1 ORIENTATION B BOA = 90°

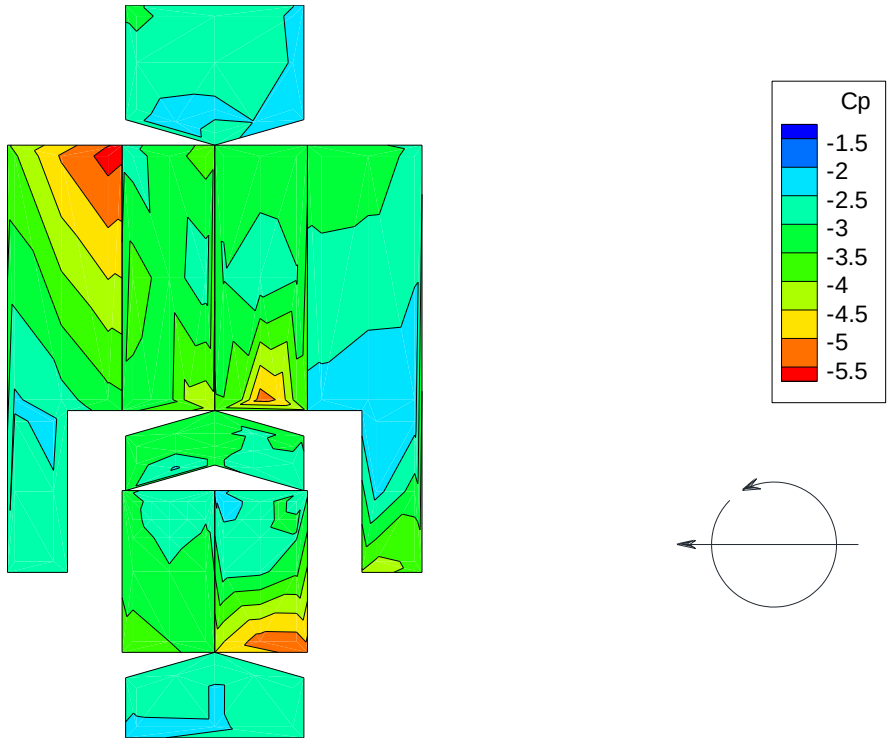

FIGURE B- 62 PEAK CP CONTOURS MODEL 9/GARAGE 2 ORIENTATION A BOA = 90°

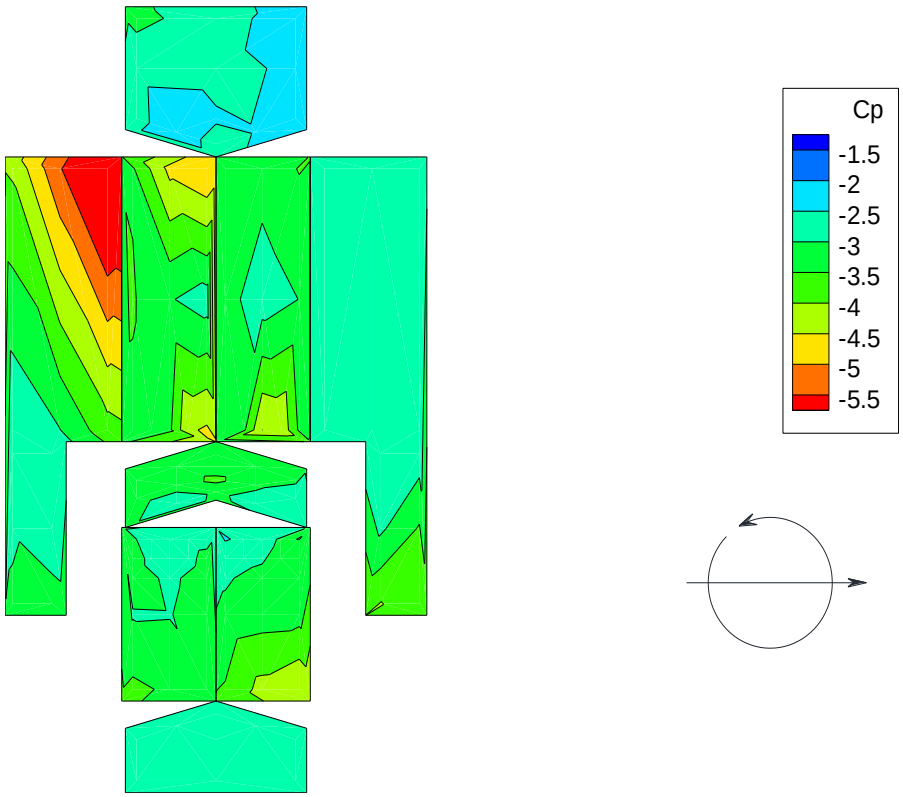

FIGURE B- 63 PEAK CP CONTOURS MODEL 9/GARAGE 2 ORIENTATION B BOA = 90°

Appendix C. Force Coefficients with Respect to the Building Axes

The force coefficients given in Chapter 4 were calculated with respect to the axis of translation of the simulated tornado (i.e., the orientation of the x direction force coefficient was along the path of the simulated tornado and the orientation of the y direction force coefficient was perpendicular to the path of the simulated tornado). Despite the usefulness of this convention for comparing the effect of the building geometry on the tornado induced pressures, its applicability to the design of lateral bracing for low-rise buildings is limited.

The lateral stiffness of the structures of most low-rise buildings comes from some sort of shear wall or system of shear walls. This is also the case for low-rise residential structures where the shear wall is composed of the external stud wall with either OSB/plywood sheathing attached to the studs or by dimensional lumber attached diagonally at the corners of the building. A diagram of the attachment of a sheathing panel for lateral bracing is shown in Figure C – 1.

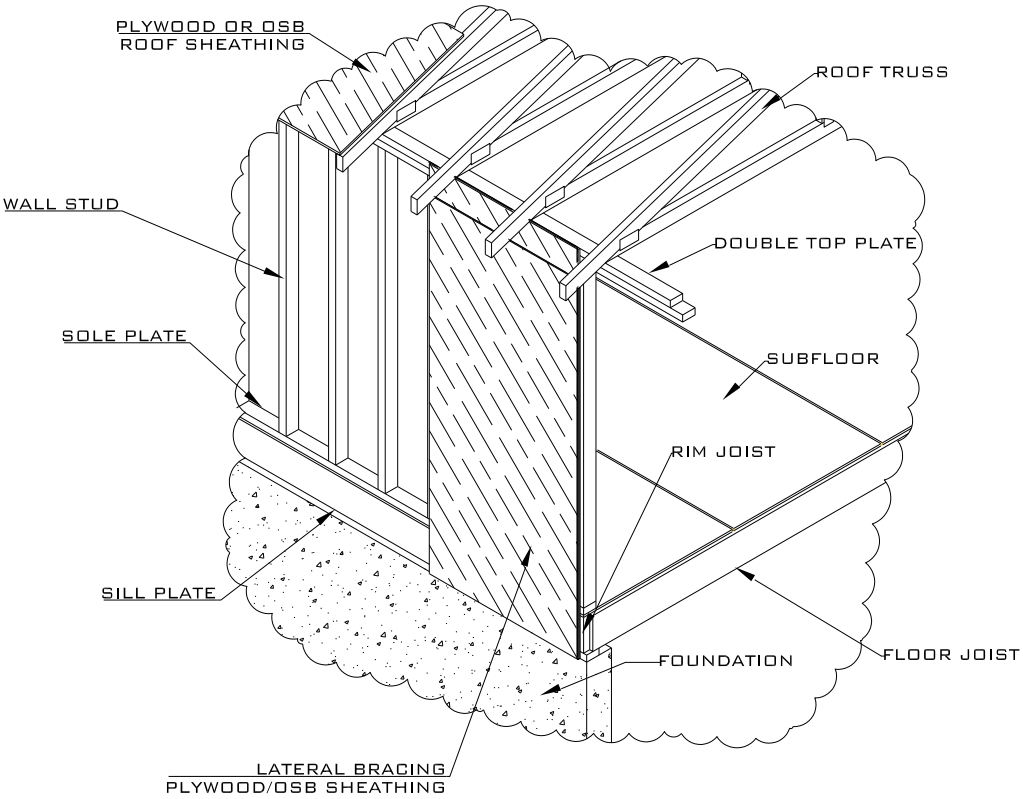

FIGURE C - 1 DIAGRAM OF RESIDENTIAL FRAMING SHOWING SHEATHING PANEL AS LATERAL BRACING

As with all shear walls, the lateral force resisting system of low-rise residential buildings is most effective when the lateral forces act in the plane of the wall or act parallel to the plane of the wall and can be transferred to the wall. In order to obtain the components of the tornado induced forces that act parallel to the walls of the residential low rise building a new orientation was used to recalculate the aerodynamic force coefficients. The orientation used to recalculate the force coefficients is defined in Figure C – 2 where the x direction is parallel to the ridge of the building model roof and the y direction is perpendicular to the building model roof. The orientation of the x and y directions stayed the same for all building orientation angles for the force coefficients presented in Chapter 4, but for the force coefficients presented in this appendix the x and y directions are defined with respect to the building and therefore, the orientation of the x and y directions with respect to the path of the simulated tornado changes with the building orientation angle (i.e., when the building orientation angle is β, the angle of the x axis with respect to the path of the simulated tornado is also β).

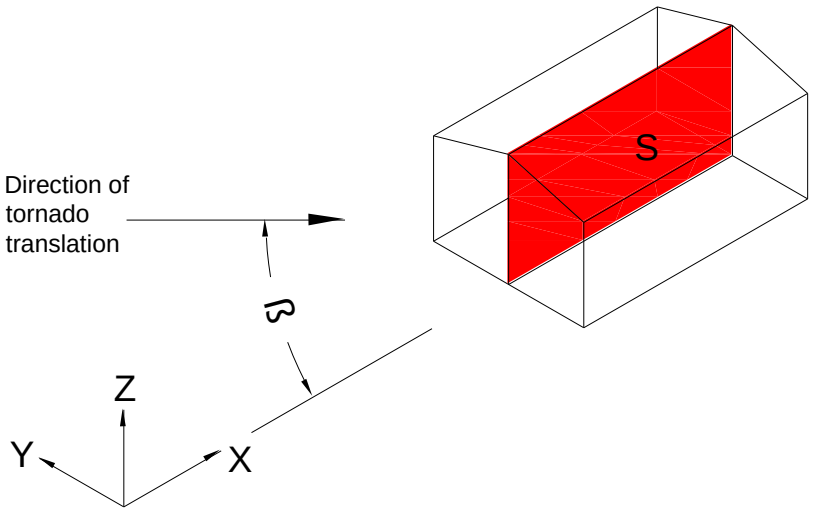

FIGURE C - 2 BUILDING AND AXES ORIENTATION WITH RESPECT TO DIRECTION OF TORNADO TRANSLATION

The same area, *S*, used to normalize the force coefficients in Chapter 4 was again used as shown in Figure C – 2. The same formulas used in Chapter 4 to calculate the force coefficients were used to calculate the force coefficients in this Appendix and are repeated below.

$$C_{F_x} = \frac{F_x}{\frac{1}{2}\rho V_H^2 S} \quad (4\text{-}1)$$

$$C_{F_y} = \frac{F_y}{\frac{1}{2}\rho V_H^2 S} \quad (4\text{-}2)$$

$$C_{F_{xy}} = \sqrt{C_{F_x}^2 + C_{F_y}^2} \quad (4\text{-}4)$$

It should be noted that for a given building orientation angle the z direction (vertical) force coefficient is independent of the orientation of the x and y axes with respect to the path of the tornado and were therefore not recalculated.

C.1. Force Coefficients Parallel to Ridge of Building Model Roof (C_{Fx})

The x direction (parallel to roof ridge) force coefficient time histories of each model for the 0°-90° building orientations and 0.15 m/s translation speed are given in Figures C-3 through C-9 and the time histories for the 0.46 translation speed are shown in Figures C-10 through C-16. The tabulated peak values are given in Table C-1 for the 0.15 m/s translation speed and Table C-2 for the 0.46 m/s translation speed. The peaks listed in the tables are absolute values.

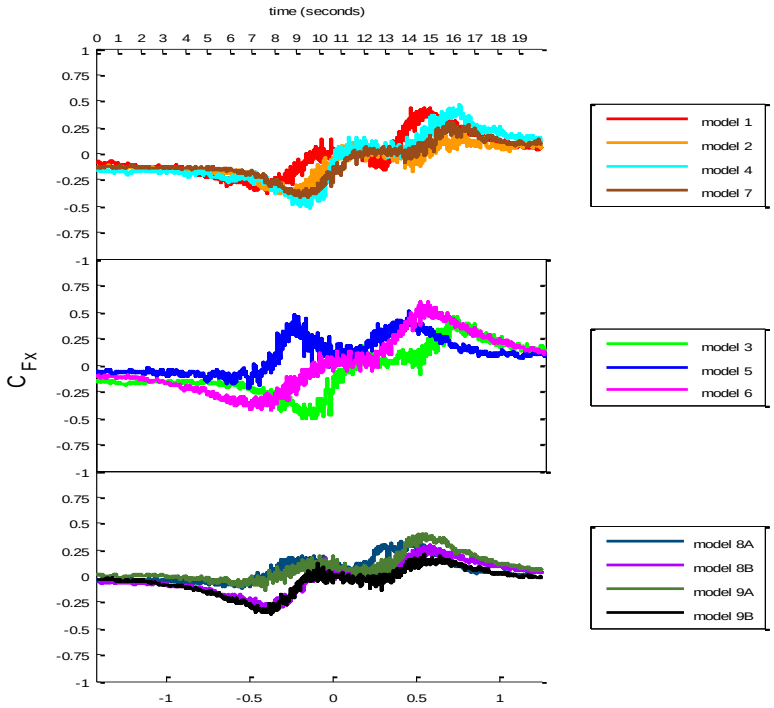

FIGURE C - 3 CFX TIME HISTORIES VT = 0.15 M/S BUILDING ORIENTATION = 0 DEGREES

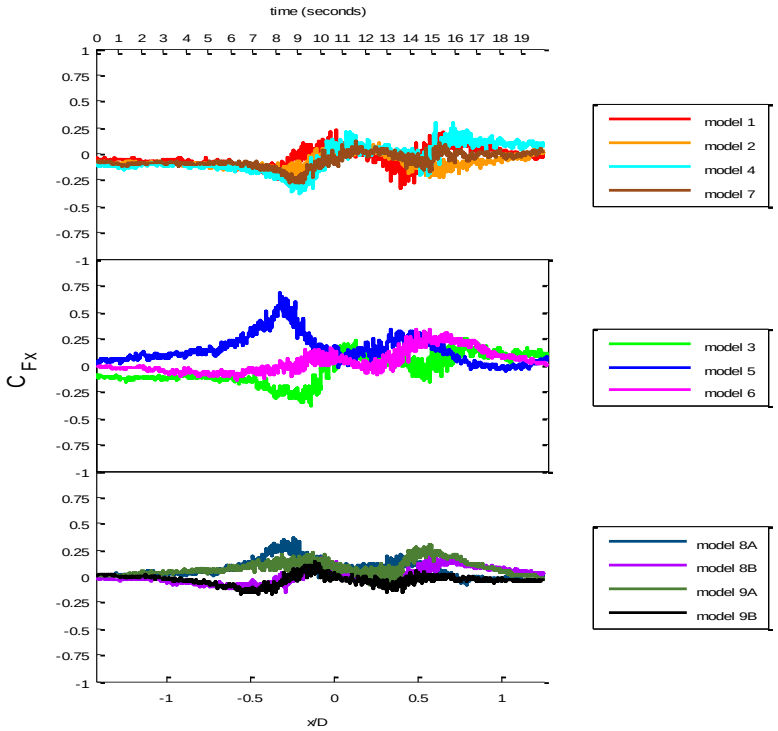

FIGURE C - 4 CFX TIME HISTORIES VT = 0.15 M/S BUILDING ORIENTATION = 15 DEGREES

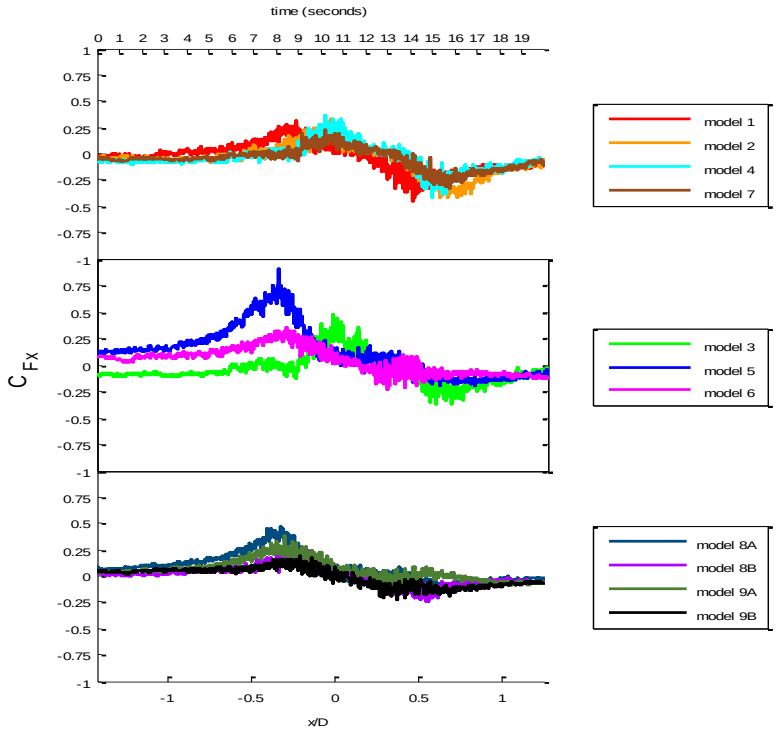

FIGURE C - 5 CFX TIME HISTORIES VT = 0.15 M/S BUILDING ORIENTATION = 30 DEGREES

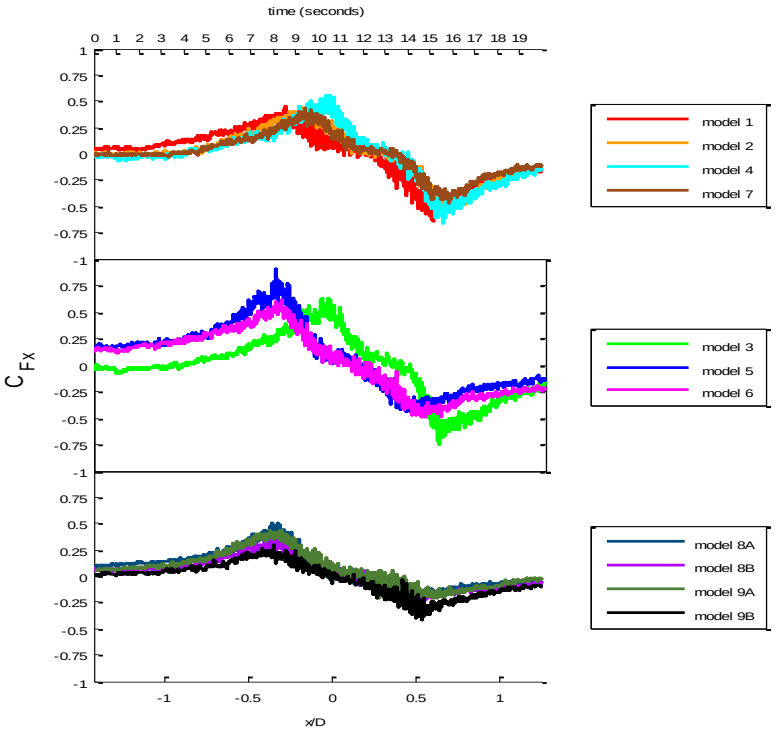

FIGURE C - 6 CFX TIME HISTORIES VT = 0.15 M/S BUILDING ORIENTATION = 45 DEGREES

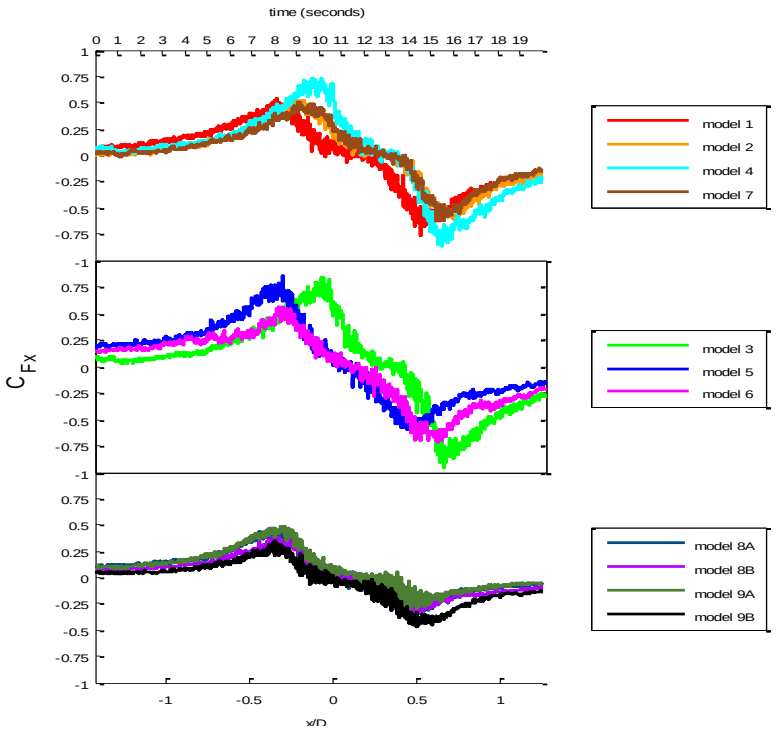

FIGURE C - 7 CFX TIME HISTORIES VT = 0.15 M/S BUILDING ORIENTATION = 60 DEGREES

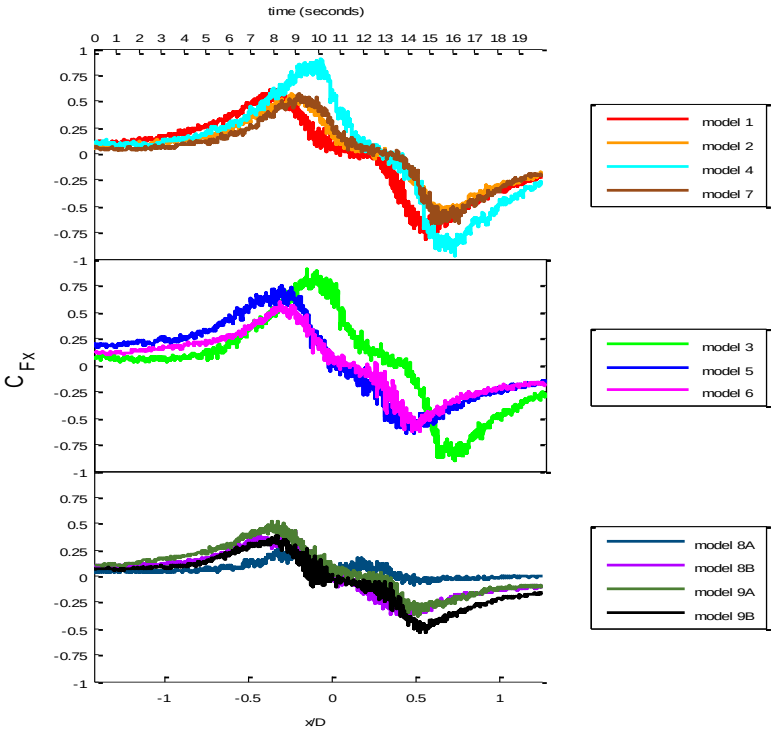

FIGURE C - 8 CFX TIME HISTORIES VT = 0.15 M/S BUILDING ORIENTATION = 75 DEGREES

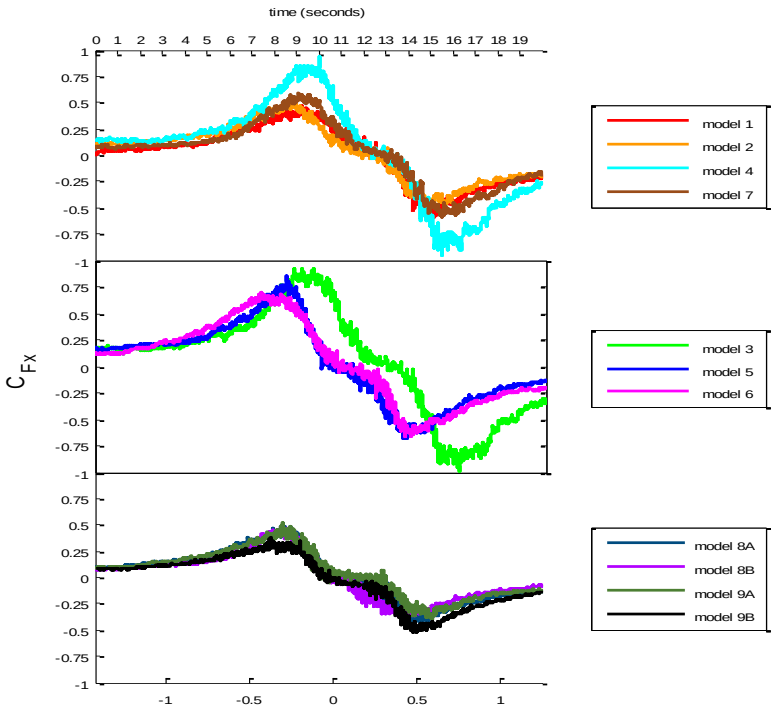

FIGURE C - 9 CFX TIME HISTORIES VT = 0.46 M/S BUILDING ORIENTATION = 90 DEGREES

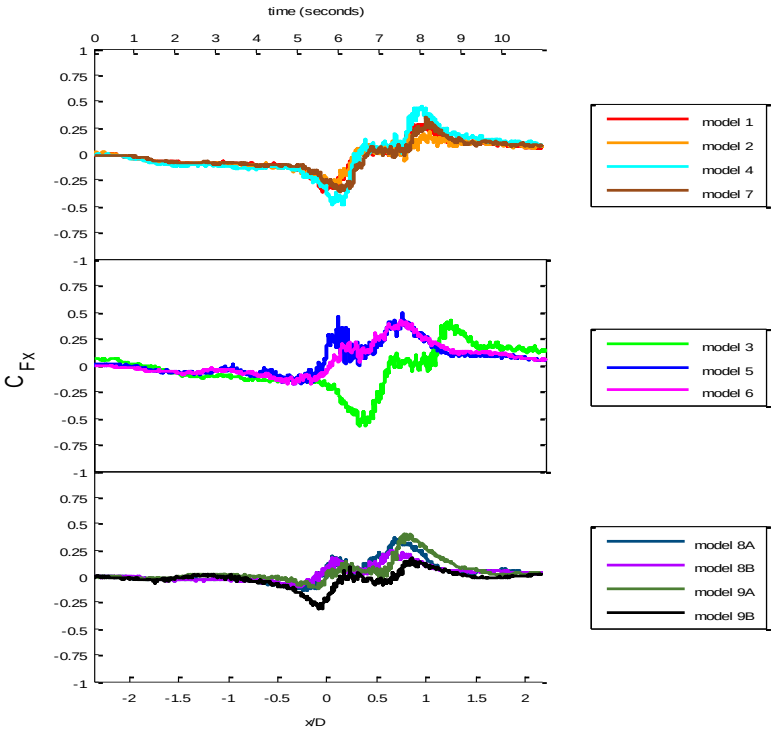

FIGURE C - 10 CFX TIME HISTORIES VT = 0.46 M/S BUILDING ORIENTATION = 0 DEGREES

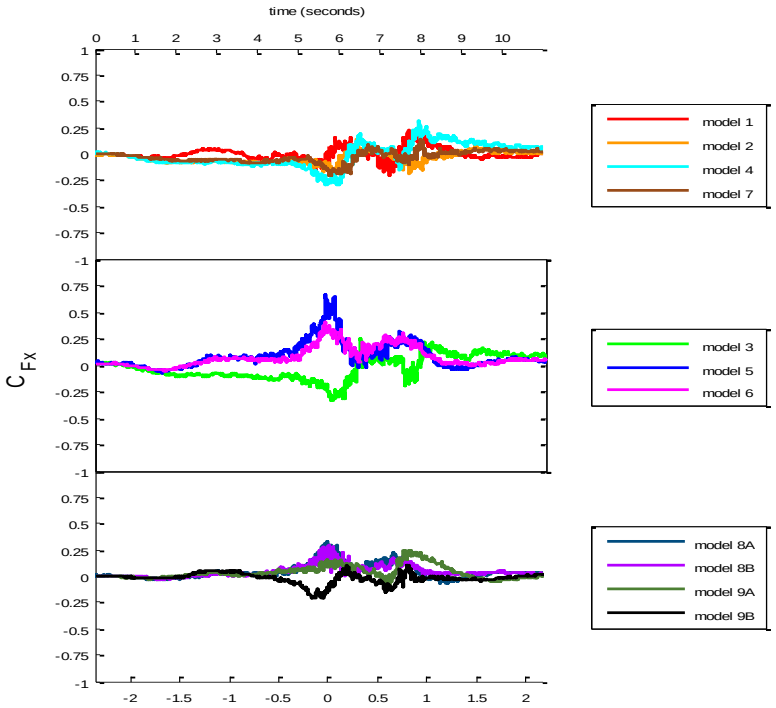

FIGURE C - 11 CFX TIME HISTORIES VT = 0.46 M/S BUILDING ORIENTATION = 15 DEGREES

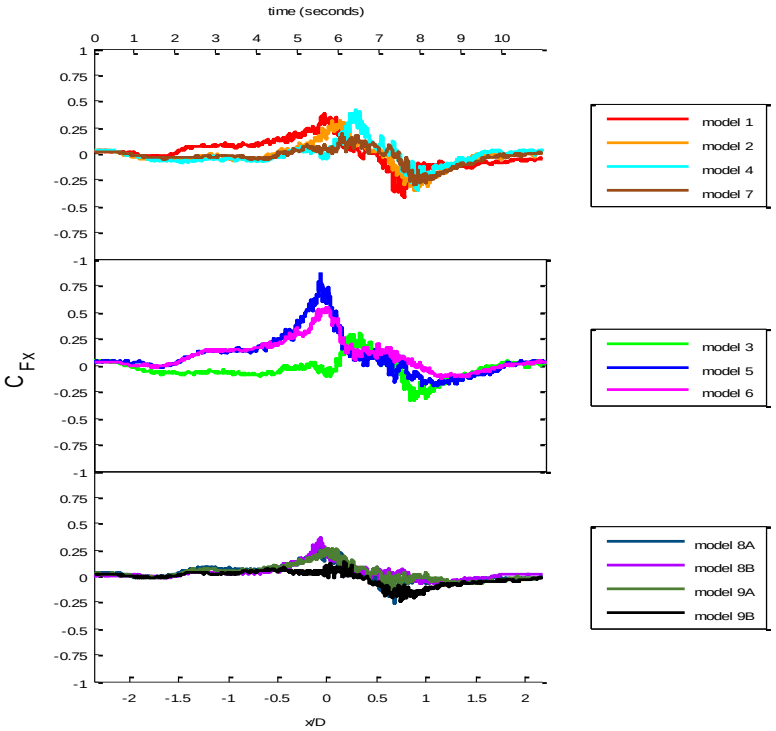

FIGURE C - 12 CFX TIME HISTORIES VT = 0.46 M/S BUILDING ORIENTATION = 30 DEGREES

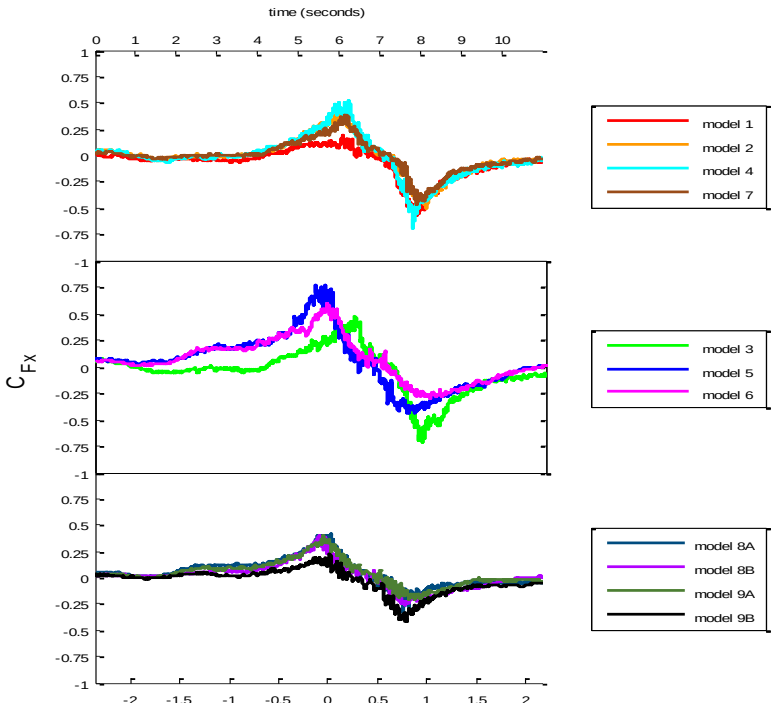

FIGURE C - 13 CFX TIME HISTORIES VT = 0.46 M/S BUILDING ORIENTATION = 45 DEGREES

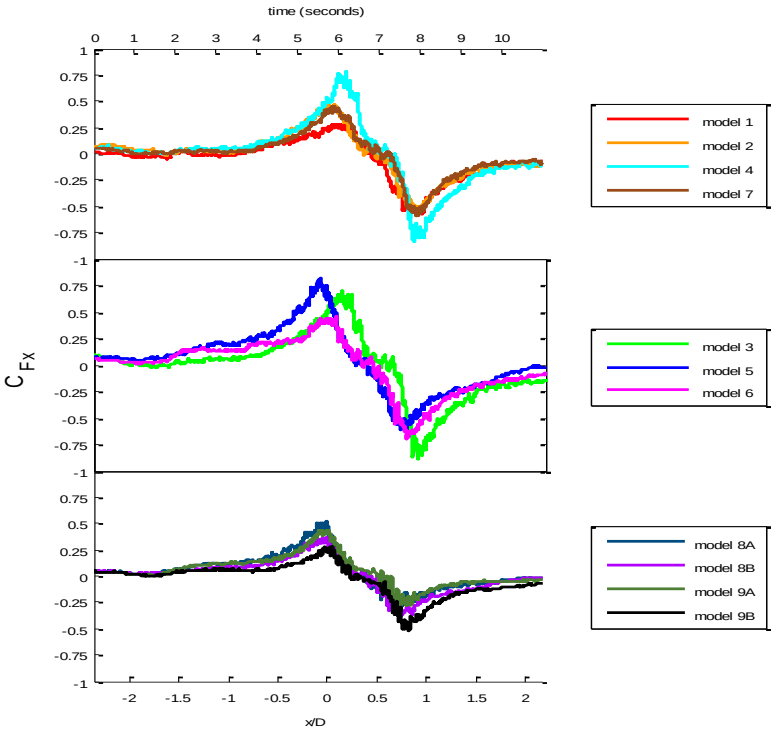

FIGURE C - 15 CFX TIME HISTORIES VT = 0.46 M/S BUILDING ORIENTATION = 60 DEGREES

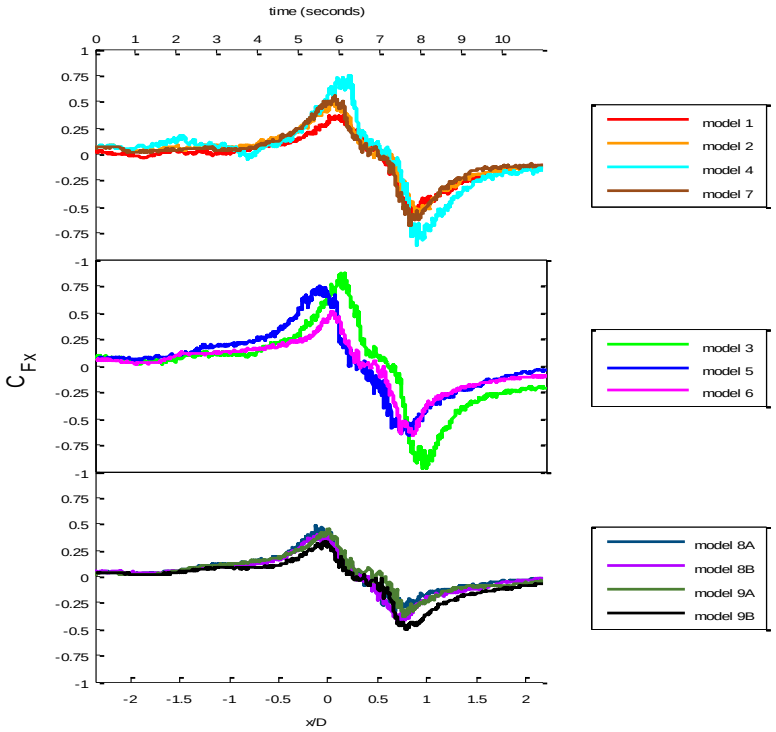

FIGURE C - 14 CFX TIME HISTORIES VT = 0.46 M/S BUILDING ORIENTATION = 75 DEGREES

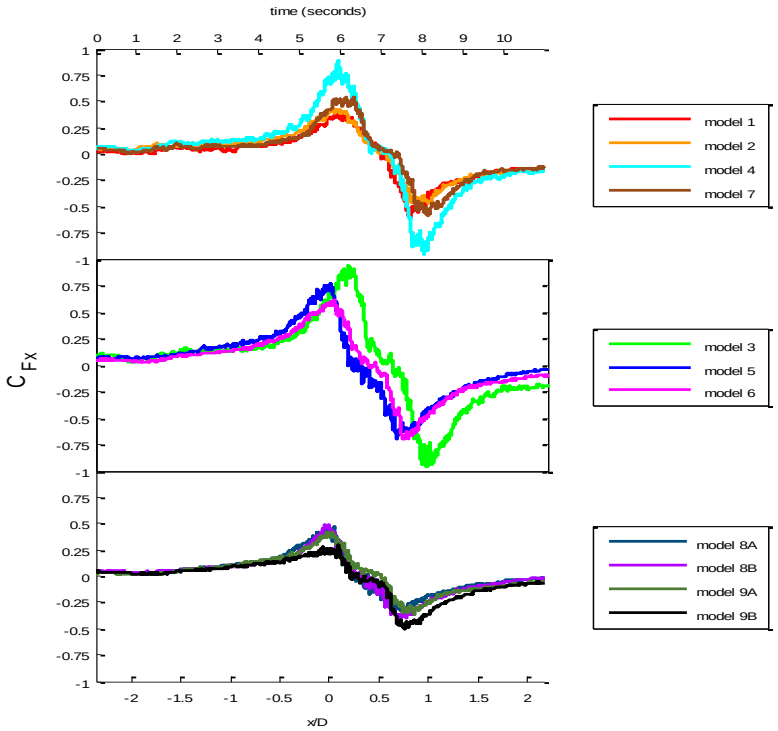

FIGURE C - 16 CFX TIME HISTORIES VT = 0.46 M/S BUILDING ORIENTATION = 90 DEGREES

From the time histories of the x direction force coefficient plotted above it is clear that for the building orientation angle 0° that C_{Fx} is dominated by the pressure drop in the center of the vortex and the radial component of velocity. As the building orientation angle increases to 90° the force coefficient becomes dominated by the tangential component of the wind velocity. This is also demonstrated in Table C -1 and Table C - 2.

TABLE C- 1 PEAK CFX VT = 0.15 M/S (X PARALLEL TO RIDGE OF ROOF)

MODEL / orientation	1	2	3	4	5	6	Overhang	G1A	G1B	G2A	G2B
0°	0.44	0.40	0.52	0.52	0.50	0.60	0.42	0.33	0.33	0.41	0.36
15°	0.33	0.24	0.38	0.39	0.69	0.34	0.28	0.36	0.22	0.32	0.17
30°	0.45	0.42	0.47	0.42	0.90	0.36	0.33	0.46	0.26	0.38	0.22
45°	0.65	0.61	0.75	0.66	**0.91**	0.62	0.47	**0.51**	0.39	0.43	0.42
60°	0.76	**0.63**	0.95	0.86	0.86	**0.71**	0.62	0.46	0.39	0.49	0.48
75°	**0.82**	0.59	0.90	**0.97**	0.74	0.63	**0.67**	0.31	0.44	0.52	**0.53**
90°	0.59	0.51	**0.99**	0.95	0.85	0.70	0.60	0.49	**0.47**	**0.52**	0.53

G = garage A and B = orientation

TABLE C- 2 PEAK CFX VT = 0.46 M/S (X PARALLEL TO RIDGE OF ROOF)

MODEL / orientation	1	2	3	4	5	6	Overhang	G1A	G1B	G2A	G2B
0°	0.36	0.30	0.58	0.49	0.49	0.42	0.36	0.36	0.25	0.41	0.32
15°	0.22	0.21	0.34	0.32	0.66	0.41	0.20	0.32	0.30	0.25	0.21
30°	0.41	0.36	0.34	0.42	**0.88**	0.55	0.30	0.26	0.36	0.26	0.23
45°	0.57	0.51	0.71	0.69	0.77	0.60	0.46	0.42	0.40	0.39	0.42
60°	0.57	0.54	0.89	0.84	0.82	0.69	0.60	**0.51**	0.39	0.44	**0.52**
75°	**0.61**	**0.57**	**0.98**	0.87	0.74	0.67	**0.68**	0.49	0.44	**0.46**	0.51
90°	0.61	0.49	0.95	**0.95**	0.76	**0.71**	0.60	0.46	**0.48**	0.42	0.50

G = garage A and B = orientation

C.2. Force Coefficients Perpendicular to Ridge of Building Model Roof (C_{Fy})

The y direction (perpendicular to the ridge of the building model roof) force coefficient time histories of each model for the 0°-90° building orientations and 0.15 m/s translation speed are given in Figures C-17 through C-23 and the time histories for the 0.46 translation speed are shown in Figures C-24 through C-30. The tabulated peak values are given in Table C-3 for the 0.15 m/s translation speed and Table C-4 for the 0.46 m/s translation speed. The peaks listed in the tables are absolute values.

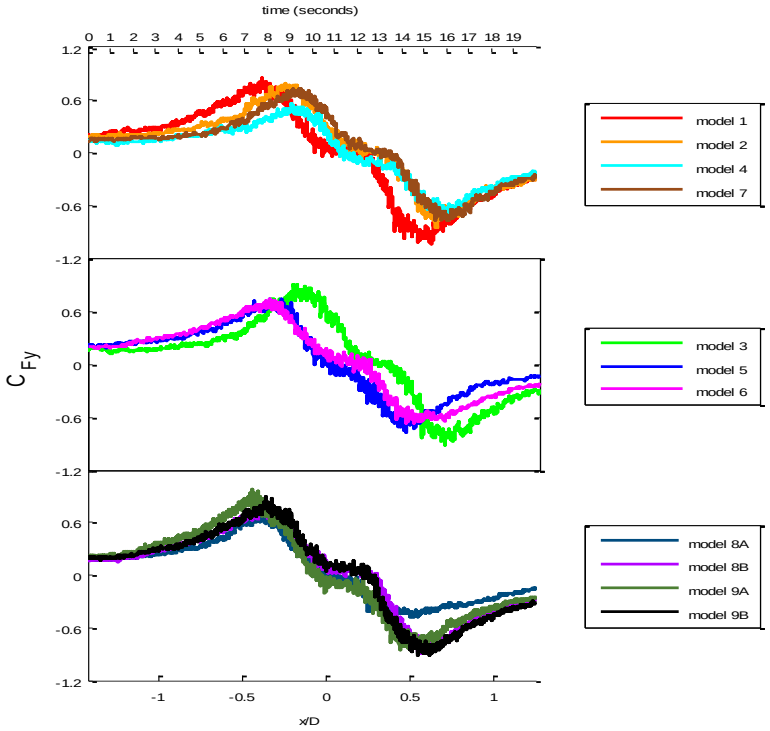

FIGURE C - 17 CFY TIME HISTORIES VT = 0.15 M/S BUILDING ORIENTATION = 0 DEGREES

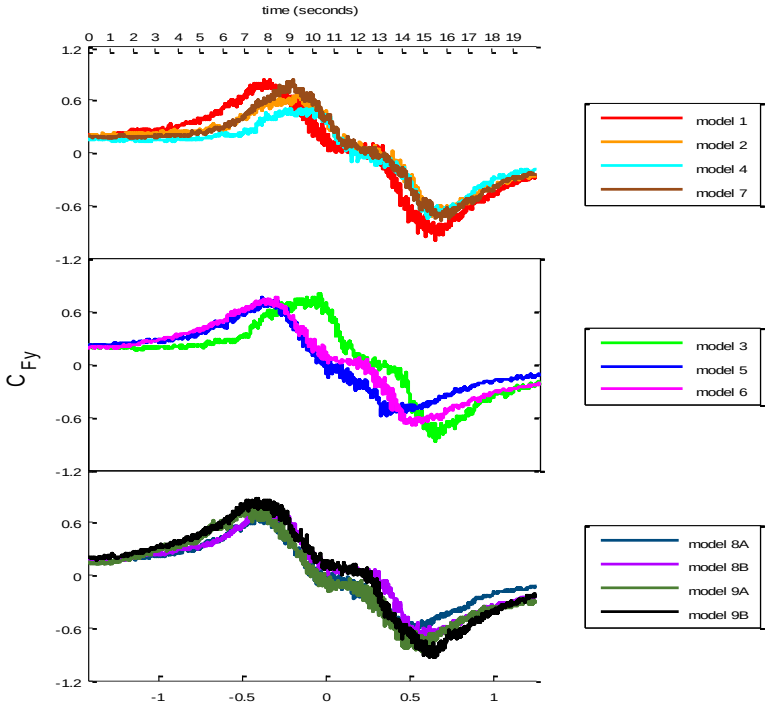

FIGURE C - 18 CFY TIME HISTORIES VT = 0.15 M/S BUILDING ORIENTATION = 15 DEGREES

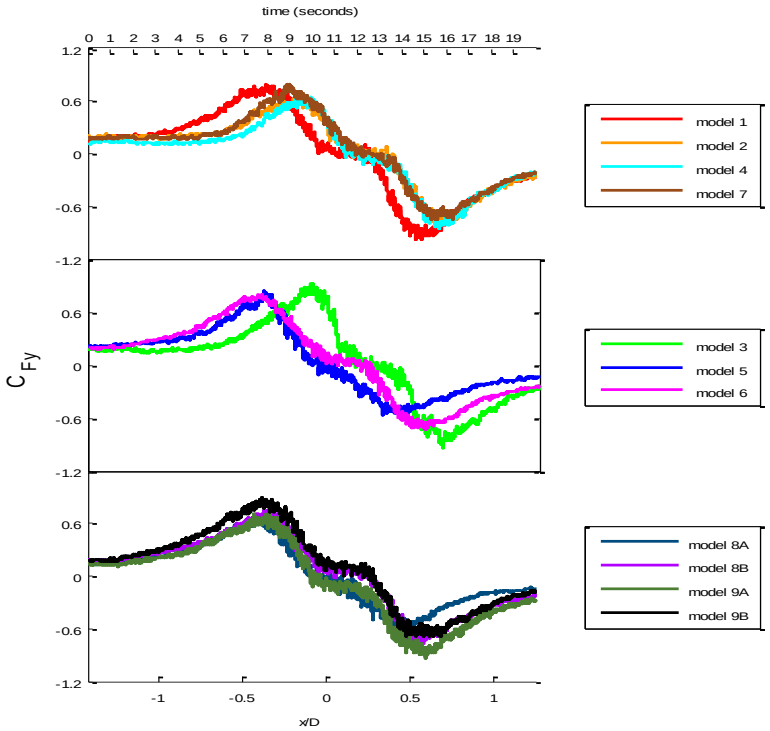

FIGURE C - 19 CFY TIME HISTORIES VT = 0.15 M/S BUILDING ORIENTATION = 30 DEGREES

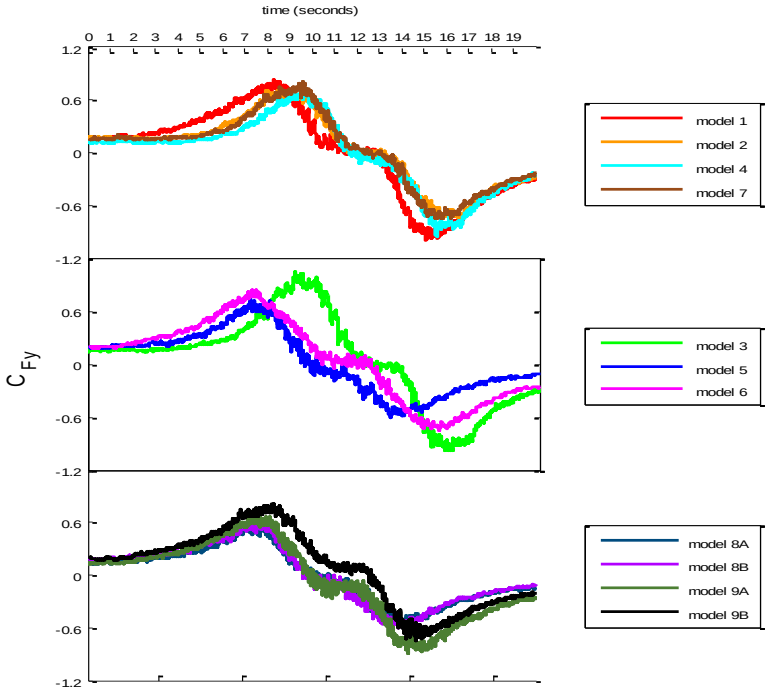

FIGURE C - 20 CFY TIME HISTORIES VT = 0.15 M/S BUILDING ORIENTATION = 45 DEGREES

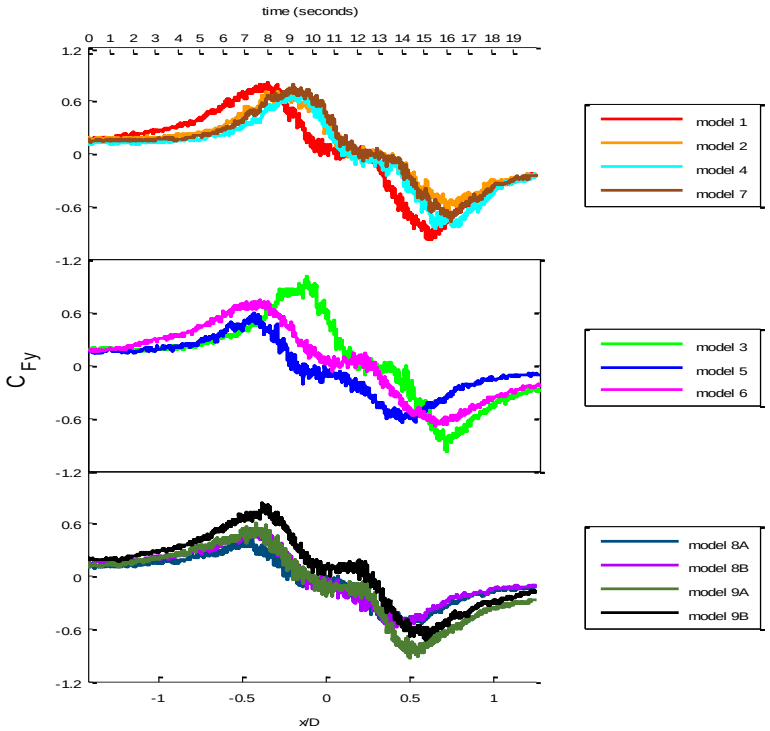

FIGURE C - 21 CFY TIME HISTORIES VT = 0.15 M/S BUILDING ORIENTATION = 60 DEGREES

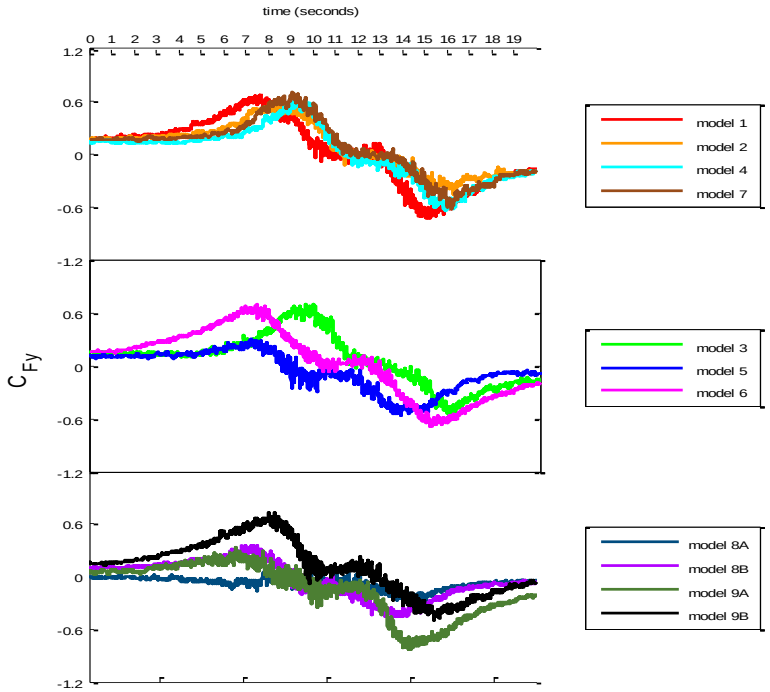

FIGURE C - 22 CFY TIME HISTORIES VT = 0.15 M/S BUILDING ORIENTATION = 75 DEGREES

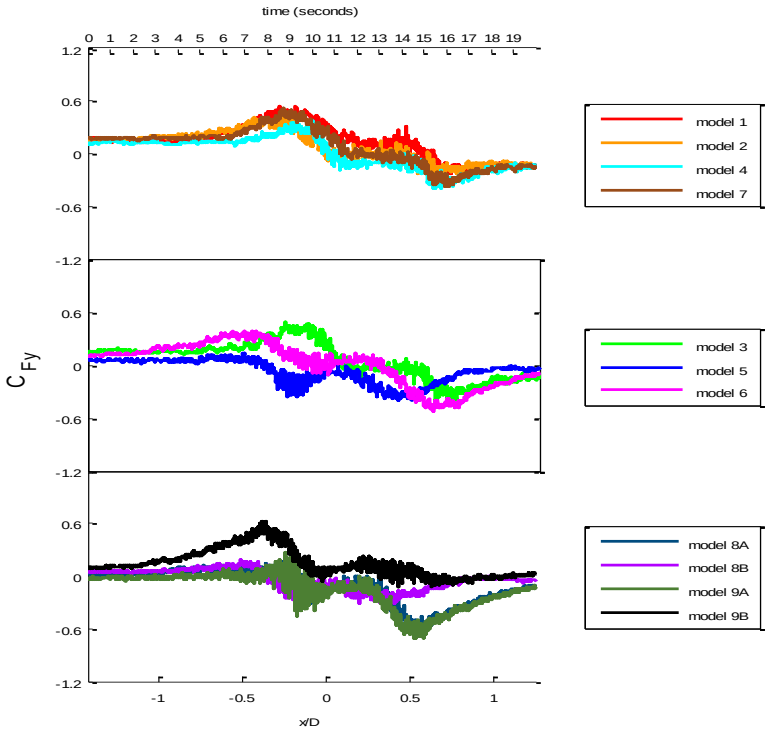

FIGURE C - 23 CFY TIME HISTORIES VT = 0.15 M/S BUILDING ORIENTATION = 90 DEGREES

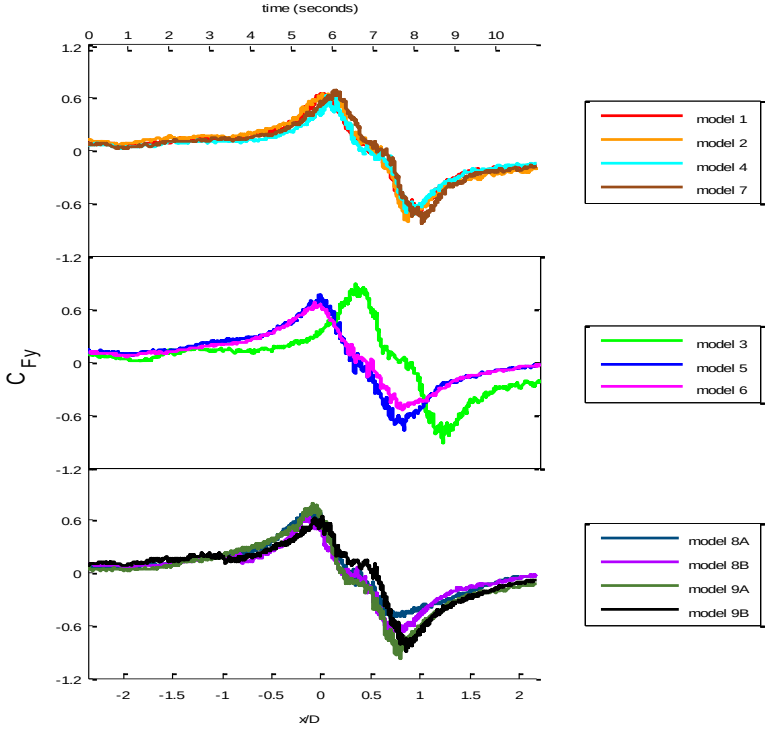

FIGURE C - 24 CFY TIME HISTORIES VT = 0.46 M/S BUILDING ORIENTATION = 0 DEGREES

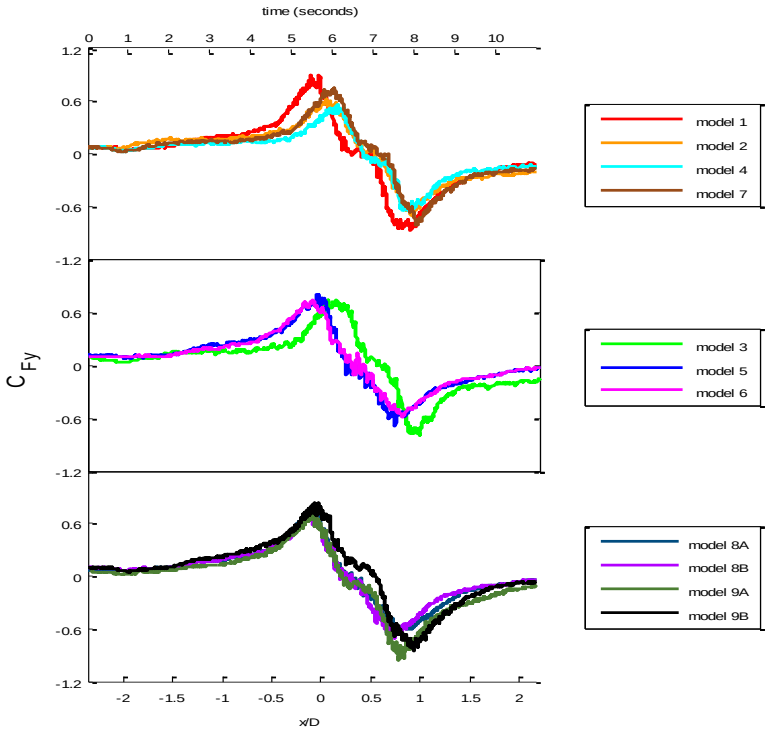

FIGURE C - 25 CFY TIME HISTORIES VT = 0.46 M/S BUILDING ORIENTATION = 15 DEGREES

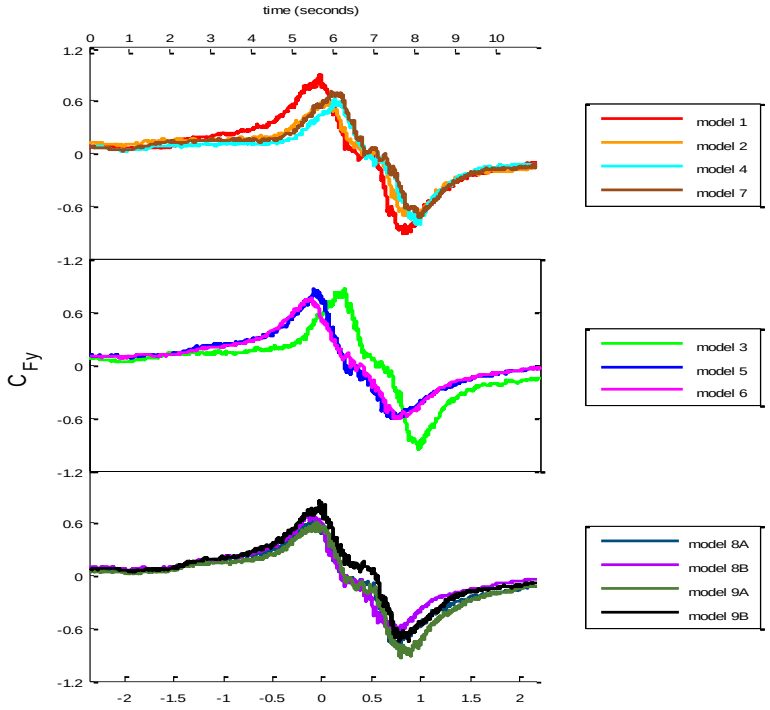

FIGURE C - 26 CFY TIME HISTORIES VT = 0.46 M/S BUILDING ORIENTATION = 30 DEGREES

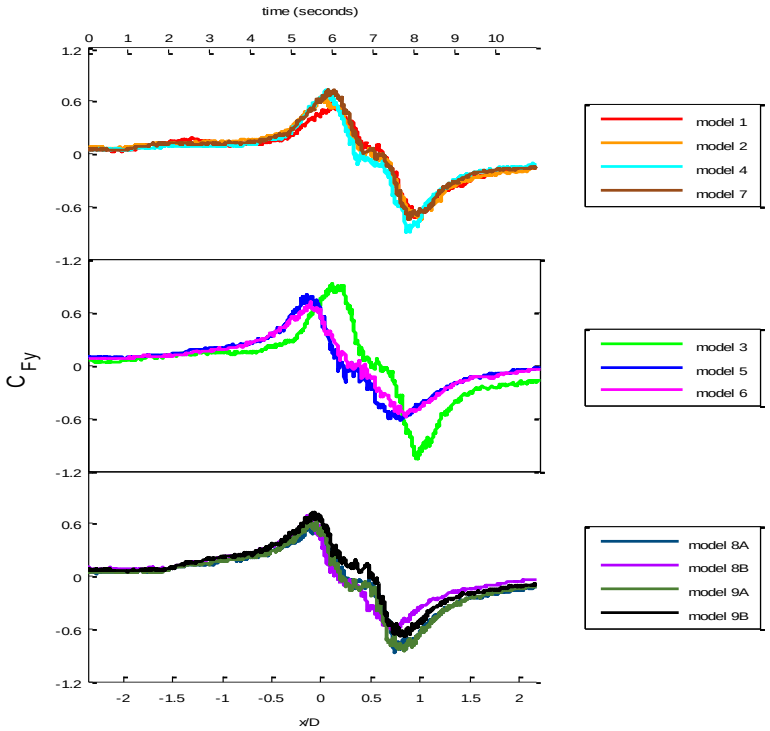

FIGURE C - 27 CFY TIME HISTORIES VT = 0.46 M/S BUILDING ORIENTATION = 45 DEGREES

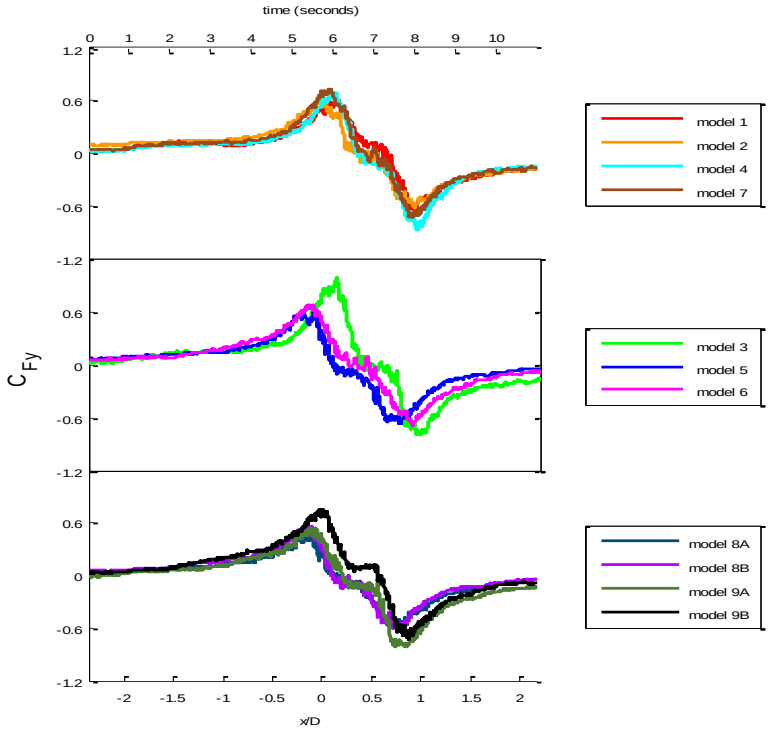

FIGURE C - 28 CFY TIME HISTORIES VT = 0.46 M/S BUILDING ORIENTATION = 60 DEGREES

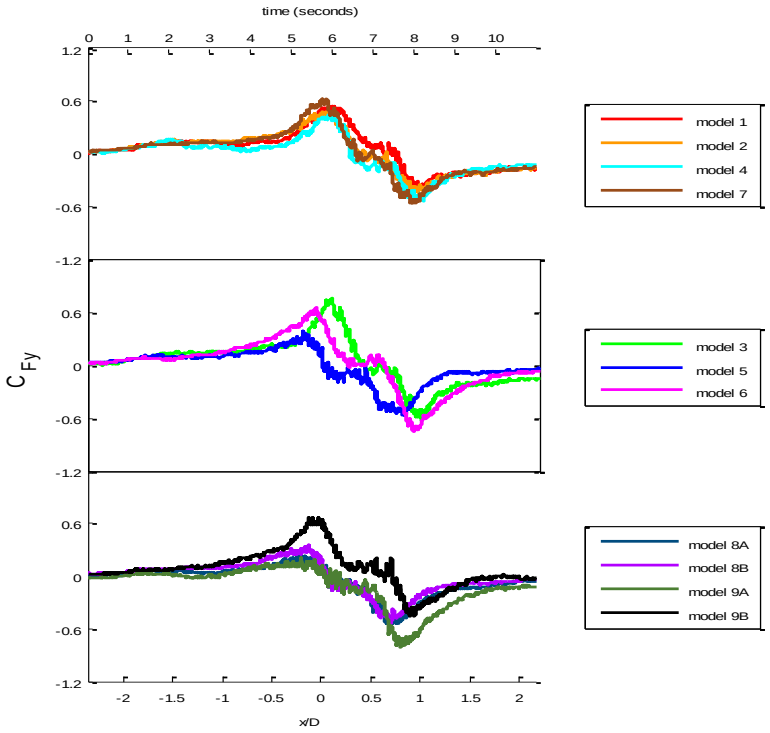

FIGURE C - 29 CFY TIME HISTORIES VT = 0.46 M/S BUILDING ORIENTATION = 75 DEGREES

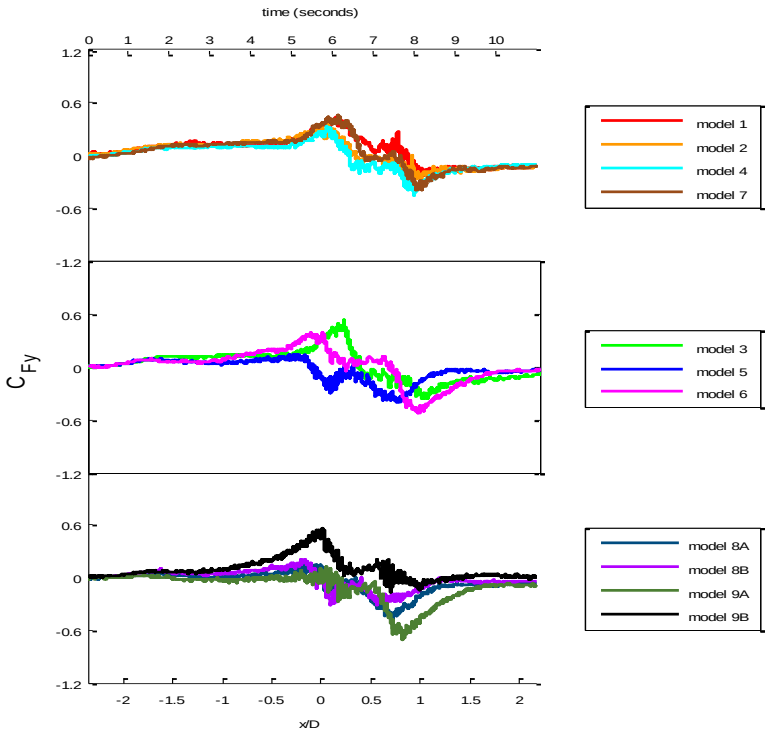

FIGURE C - 30 CFY TIME HISTORIES VT = 0.46 M/S BUILDING ORIENTATION = 90 DEGREES

The trend for the C_{Fy} force coefficient is the opposite from that of C_{Fx}; for the smaller building orientation angles, the force coefficient is dominated by the tangential velocity and as the building orientation angle increases to 90° the force coefficient becomes dominated by the pressure drop in the center of the vortex and the radial component of velocity. This results in the general trend that the majority of the peak y direction force coefficients occur at smaller building orientation angles. This trend is demonstrated in Table C -3 and Table C - 4. The fact that the general trend is toward lower peaks as the building orientation angle increases agrees with the well documented idea that the wind in a vortex is dominated by its tangential component.

TABLE C - 3 CFY VT = 0.15 M/S (Y PERPENDICULAR TO RIDGE OF ROOF)

MODEL / orientation	1	2	3	4	5	6	Overhang	G1A	G1B	G2A	G2B
0°	**1.03**	**0.86**	0.93	0.73	0.78	0.73	0.78	0.69	**0.89**	**0.98**	0.92
15°	1.00	0.74	0.88	0.75	0.75	0.75	**0.84**	**0.71**	0.76	0.87	**0.94**
30°	0.99	0.78	0.94	0.86	**0.84**	0.80	0.80	0.69	0.78	0.94	0.89
45°	1.00	0.76	**1.05**	**0.95**	0.73	**0.84**	0.80	0.58	0.65	0.89	0.82
60°	0.99	0.70	1.00	0.85	0.66	0.73	0.79	0.56	0.60	0.94	0.83
75°	0.73	0.59	0.69	0.64	0.56	0.70	0.71	0.29	0.47	0.84	0.73
90°	0.54	0.43	0.49	0.40	0.41	0.54	0.52	0.69	0.32	0.71	0.62

G = garage A and B = orientation

TABLE C - 4 CFY VT = 0.46 M/S (Y PERPENDICULAR TO RIDGE OF ROOF)

MODEL / orientation	1	2	3	4	5	6	Overhang	G1A	G1B	G2A	G2B
0°	0.75	**0.82**	0.92	0.73	0.77	0.66	**0.83**	0.72	0.67	**0.99**	**0.89**
15°	0.90	0.72	0.80	0.66	0.79	0.73	0.82	0.77	0.72	0.97	0.86
30°	**0.91**	0.74	0.95	0.82	**0.86**	**0.75**	0.72	0.78	**0.74**	0.95	0.87
45°	0.74	0.75	**1.07**	**0.90**	0.80	0.71	0.75	**0.88**	0.68	0.85	0.74
60°	0.66	0.63	0.98	0.88	0.66	0.69	0.74	0.59	0.61	0.82	0.75
75°	0.53	0.49	0.75	0.54	0.58	0.75	0.63	0.55	0.54	0.81	0.66
90°	0.43	0.34	0.52	0.45	0.41	0.53	0.45	0.47	0.32	0.71	0.56

G = garage A and B = orientation

C.1. Combined Force Coefficients (C_{Fxy})

The x y force coefficient time histories of each model for the 0°-90° building orientations and 0.15 m/s translation speed are given in Figures C-31 through C-37 and the time histories for the 0.46 translation speed are shown in Figures C-38 through C-44. The tabulated peak values are given in Table C-5 for the 0.15 m/s translation speed and Table C-6 for the 0.46 m/s translation speed.

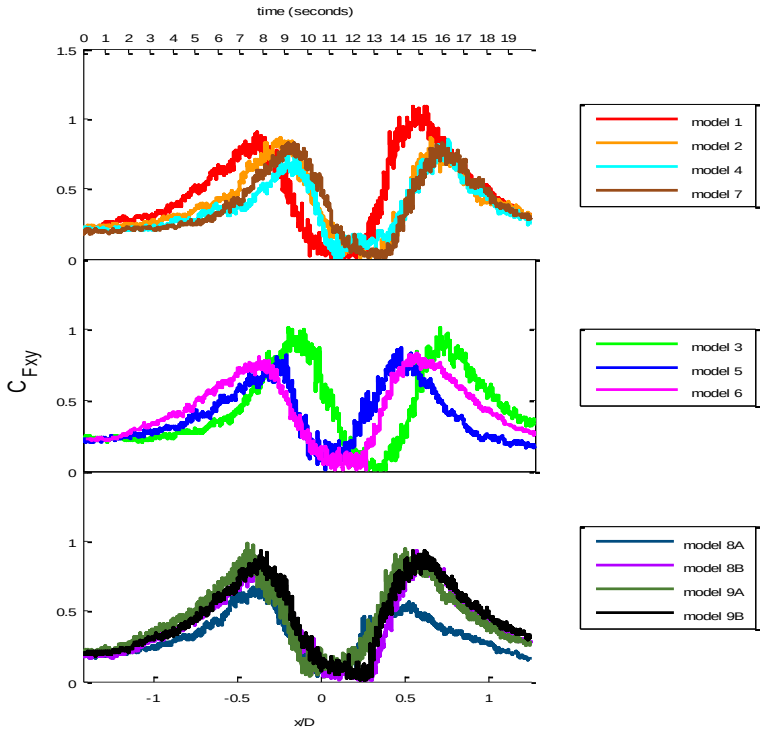

FIGURE C - 31 CFXY TIME HISTORIES VT = 0.15 M/S BUILDING ORIENTATION = 0 DEGREES

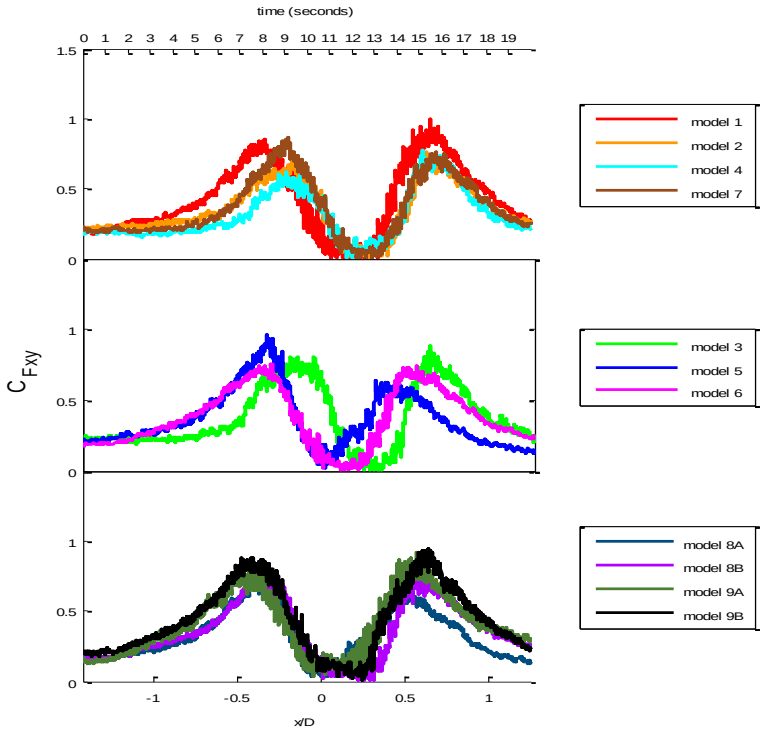

FIGURE C - 32 CFXY TIME HISTORIES VT = 0.15 M/S BUILDING ORIENTATION = 15 DEGREES

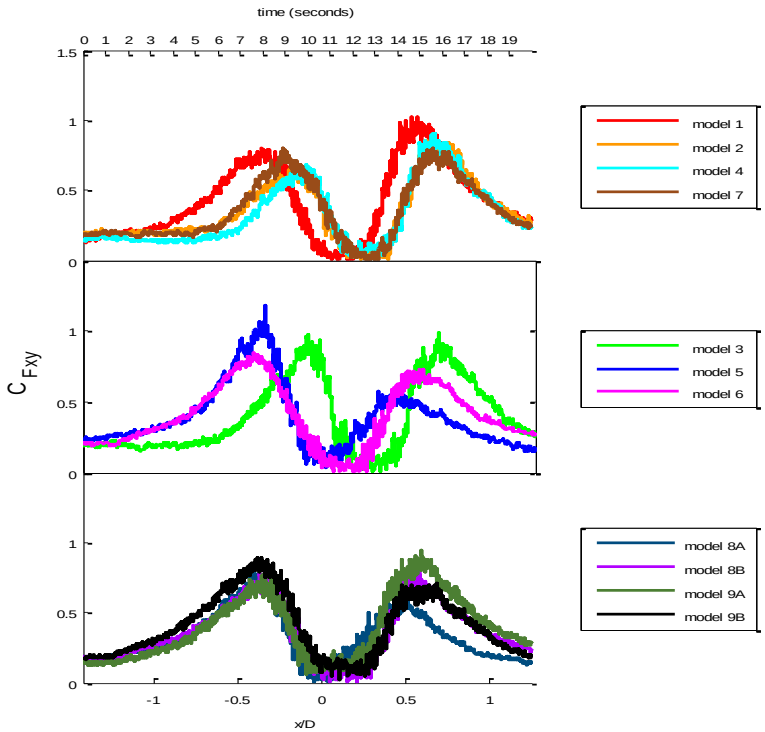

FIGURE C - 33 CFXY TIME HISTORIES VT = 0.15 M/S BUILDING ORIENTATION = 30 DEGREES

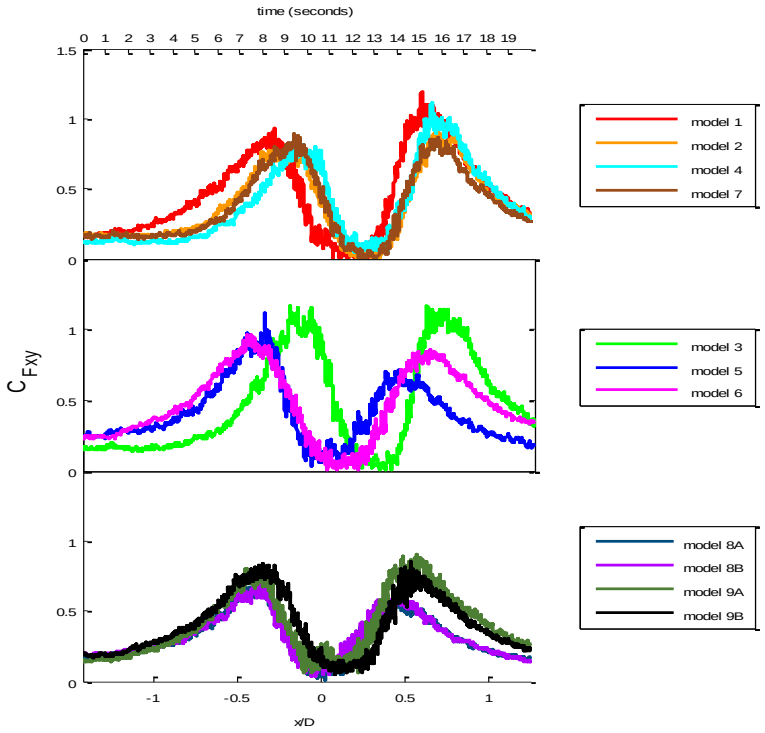

FIGURE C - 34 CFXY TIME HISTORIES VT = 0.15 M/S BUILDING ORIENTATION = 45 DEGREES

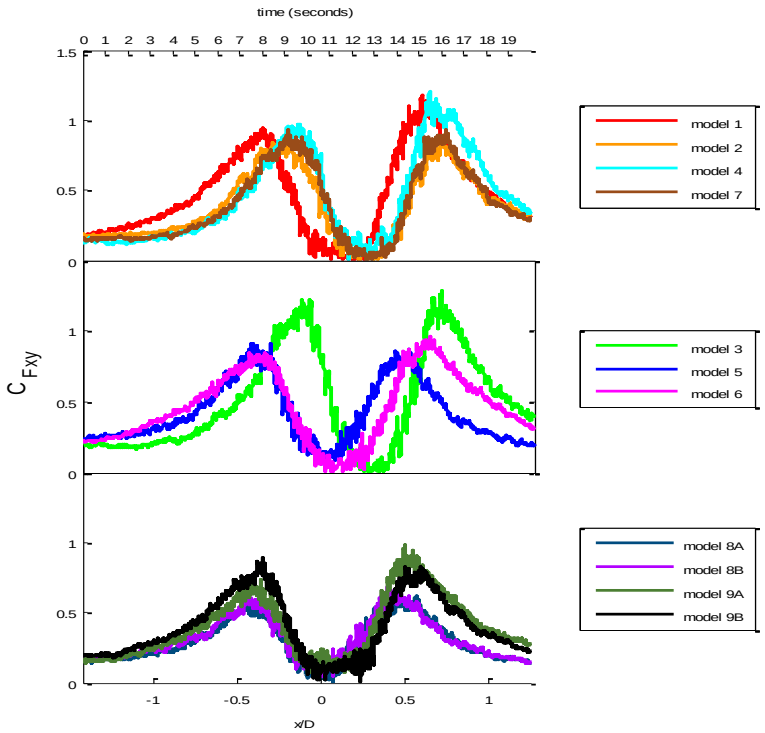

FIGURE C - 35 CFXY TIME HISTORIES VT = 0.15 M/S BUILDING ORIENTATION = 60 DEGREES

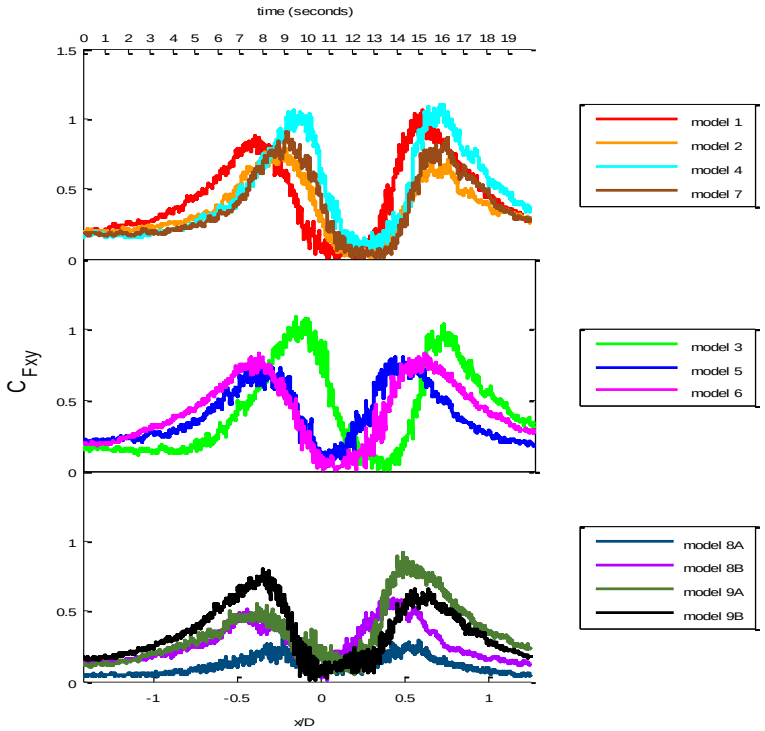

FIGURE C - 36 CFXY TIME HISTORIES VT = 0.15 M/S BUILDING ORIENTATION = 75 DEGREES

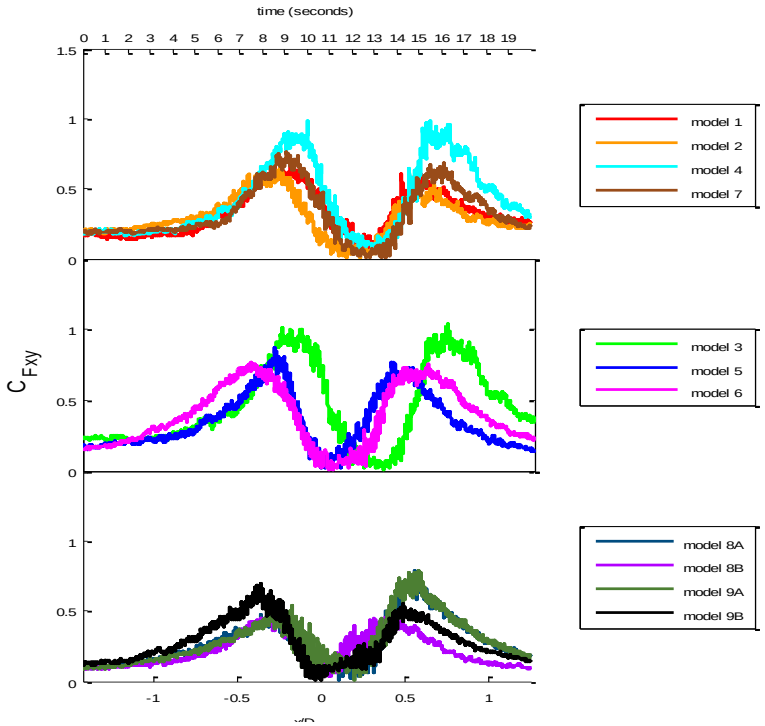

FIGURE C - 37 CFXY TIME HISTORIES VT = 0.15 M/S BUILDING ORIENTATION = 90 DEGREES

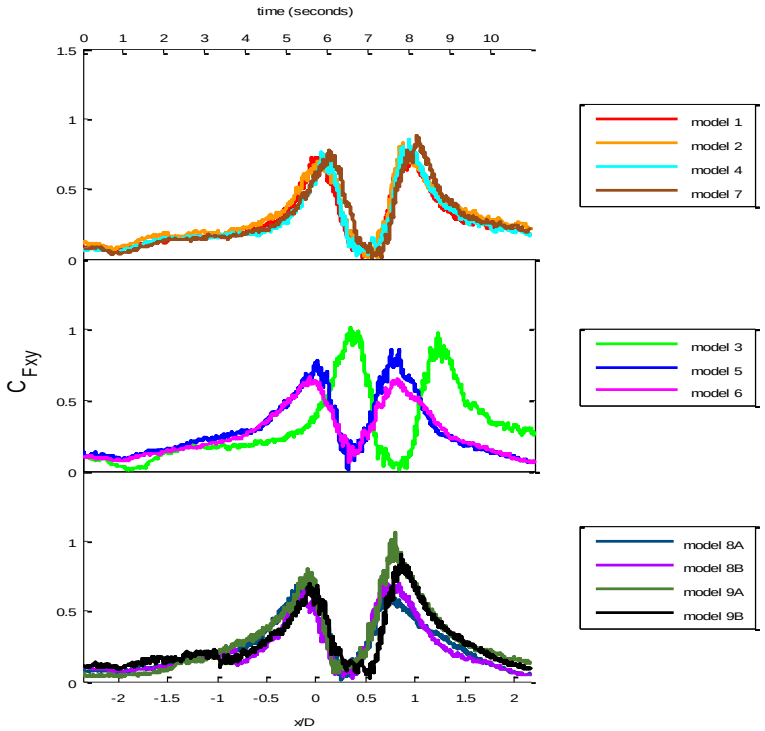

FIGURE C - 38 CFXY TIME HISTORIES VT = 0.46 M/S BUILDING ORIENTATION = 0 DEGREES

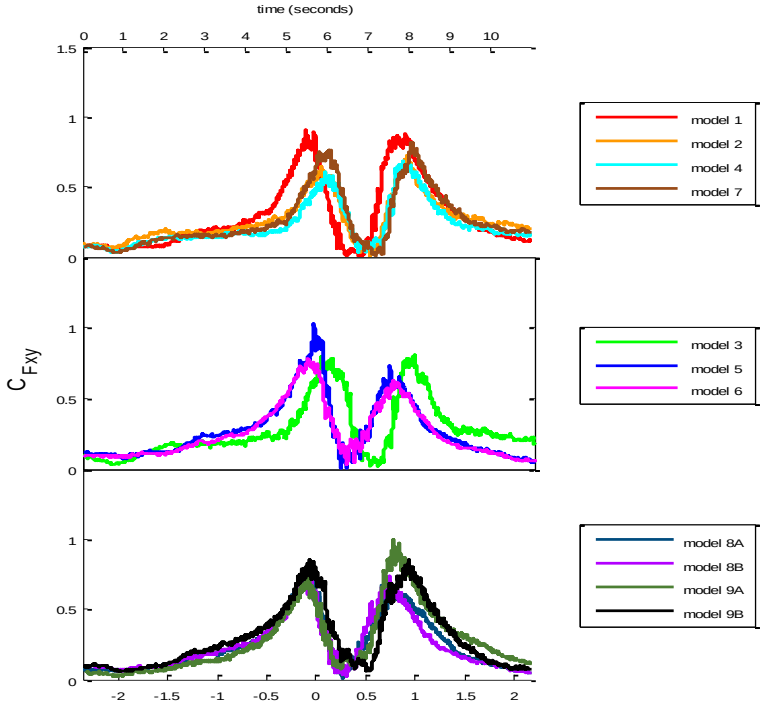

FIGURE C - 39 CFXY TIME HISTORIES VT = 0.46 M/S BUILDING ORIENTATION = 15 DEGREES

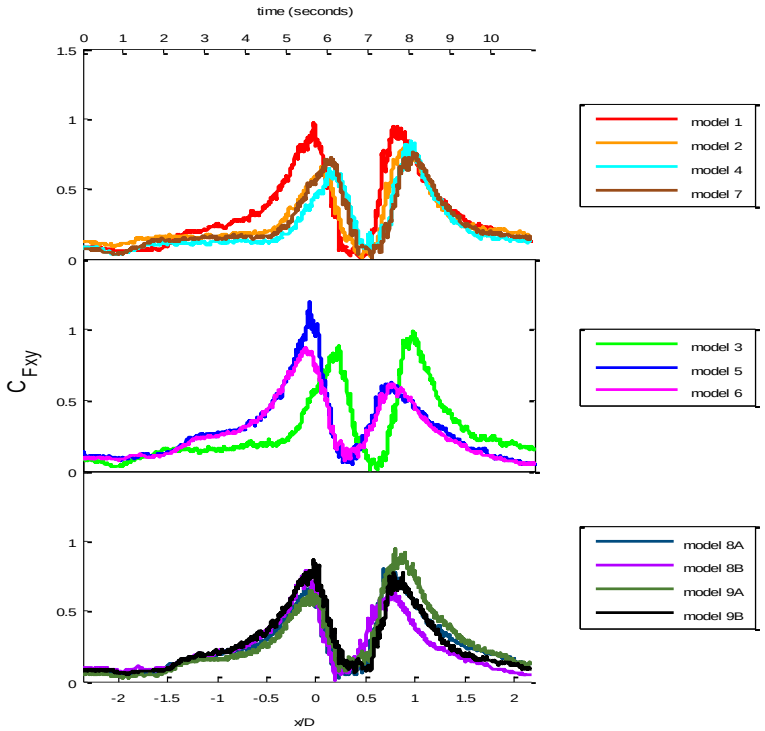

FIGURE C - 40 CFXY TIME HISTORIES VT = 0.46 M/S BUILDING ORIENTATION = 30 DEGREES

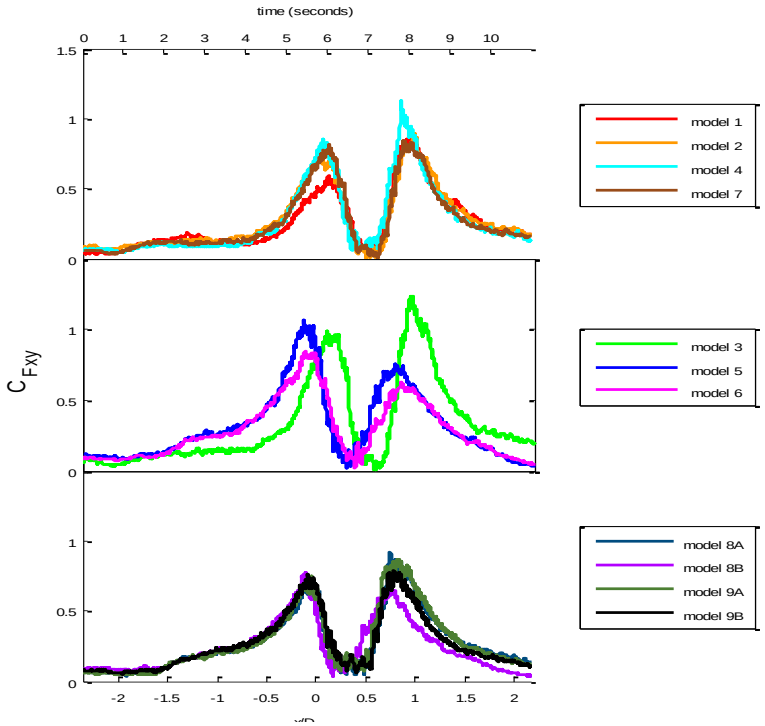

FIGURE C - 41 CFXY TIME HISTORIES VT = 0.46 M/S BUILDING ORIENTATION = 45 DEGREES

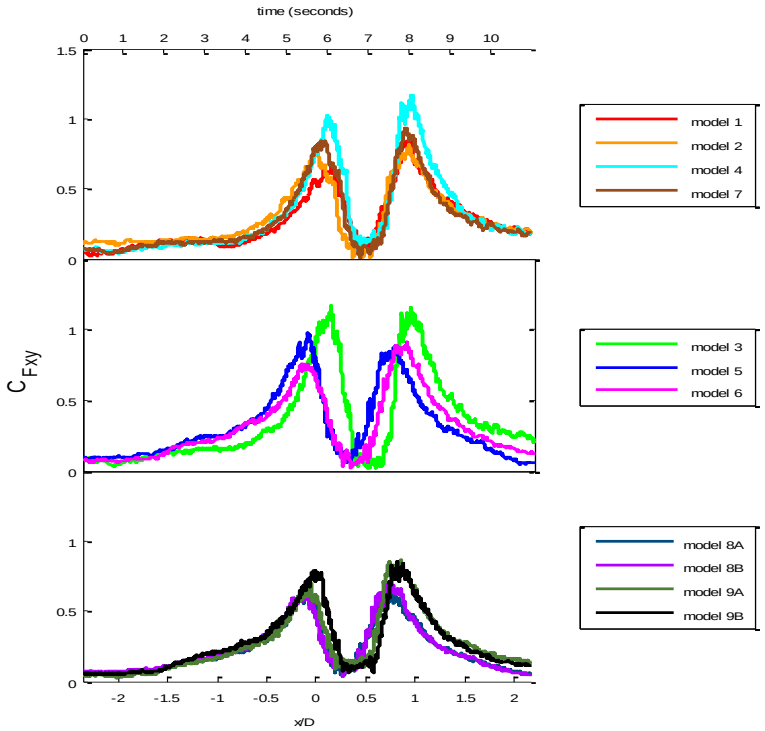

FIGURE C - 42 CFXY TIME HISTORIES VT = 0.46 M/S BUILDING ORIENTATION = 60 DEGREES

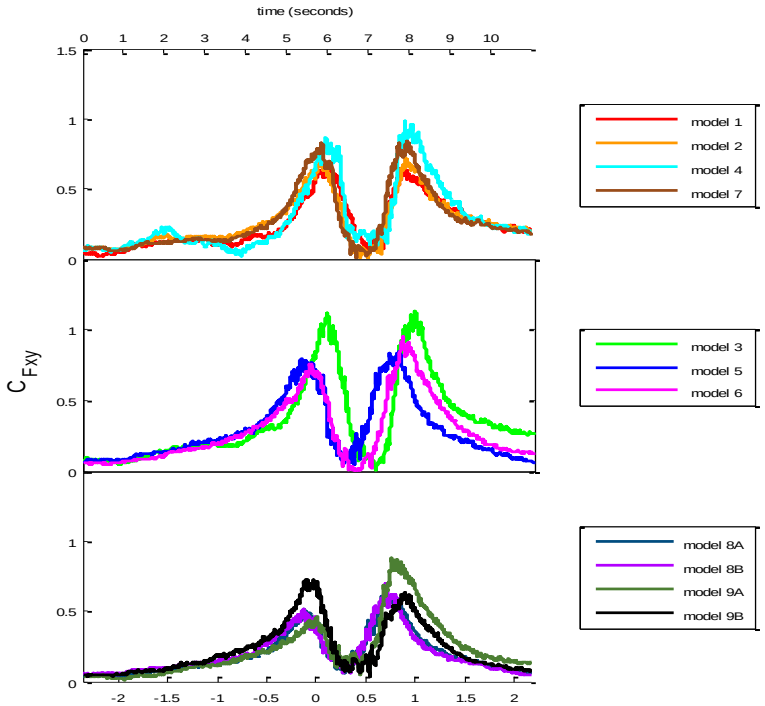

FIGURE C - 43 CFXY TIME HISTORIES VT = 0.46 M/S BUILDING ORIENTATION = 75 DEGREES

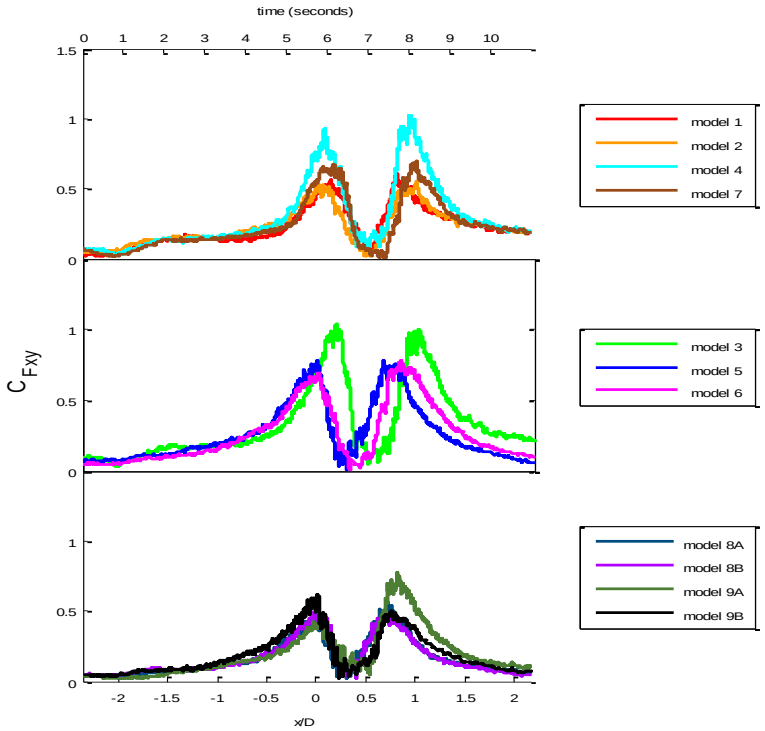

FIGURE C - 44 CFXY TIME HISTORIES VT = 0.46 M/S BUILDING ORIENTATION = 90 DEGREES

The shapes of the C_{Fxy} time histories for all of the models are similar to those in Chapter 4 where the x and y axis are oriented according to the path of the simulated tornado. From Table C – 5 and Table C – 6 the building orientation angle at which the peak C_{Fxy} occurs is influenced heavily by the building orientation angle at which the peak y direction force coefficient occurs, demonstrating again that the tangential component of the velocity is dominant in determining the forces acting on a low rise building in a tornado.

TABLE C - 5 PEAK CFXY VT = 0.15 M/S

MODEL / orientation	1	2	3	4	5	6	Overhang	G1A	G1B	G2A	G2B
0°	1.10	0.87	1.02	0.85	0.88	0.83	0.83	0.70	**0.93**	0.98	0.94
15°	1.00	0.76	0.88	0.77	0.97	0.75	0.87	0.75	0.77	0.92	**0.94**
30°	1.02	0.85	0.99	0.91	**1.18**	0.84	0.80	**0.82**	0.80	0.94	0.90
45°	**1.19**	**0.91**	1.18	1.12	1.12	**0.97**	0.90	0.73	0.72	0.91	0.85
60°	1.18	0.89	**1.29**	**1.21**	0.92	0.96	**0.93**	0.61	0.68	**0.98**	0.89
75°	1.06	0.79	1.09	1.11	0.81	0.84	0.90	0.31	0.59	0.91	0.81
90°	0.69	0.66	1.05	0.99	0.88	0.77	0.76	0.79	0.50	0.79	0.70

G = garage A and B = orientation

TABLE C - 6 PEAK CFXY VT = 0.46 M/S

MODEL / orientation	1	2	3	4	5	6	Overhang	G1A	G1B	G2A	G2B
0°	0.78	0.83	1.01	0.85	0.86	0.67	0.88	0.72	0.70	**1.07**	**0.91**
15°	0.91	0.73	0.81	0.69	1.02	0.79	0.82	0.81	0.73	1.00	0.86
30°	**0.97**	0.81	0.99	0.85	**1.19**	0.88	0.76	0.80	**0.79**	0.95	0.87
45°	0.89	**0.90**	**1.24**	1.13	1.07	0.84	0.84	**0.91**	0.77	0.87	0.79
60°	0.85	0.82	1.17	**1.17**	0.98	0.91	**0.94**	0.69	0.70	0.86	0.85
75°	0.65	0.72	1.13	0.98	0.84	**0.95**	0.84	0.61	0.69	0.88	0.73
90°	0.61	0.55	1.04	1.02	0.78	0.78	0.69	0.56	0.49	0.78	0.62

G = garage A and B = orientation

Tables C – 5 and C – 6 show that for the garage models (G1A, G1B, G2A, G2B) the smaller building orientation angles generally have larger peak C_{Fxy} values whereas for the other models the middle values (≈ 30° to 60°) of the building orientation angle have larger peak values. The reason for this can be explained by how dominant the y direction force coefficient is in the calculation of the total horizontal force coefficient. Table C – 7 gives the values of the maximum peak C_{Fy} divided by the maximum peak C_{Fx} for both translation speeds. The length-to-width ratio (L/B) of each of the models is also given in the same table. It is clear that the C_{Fy}/C_{Fx} ratio is a function of the L/B ratio. The values of the C_{Fy}/C_{Fx} ratios for the models with L/B ratios equal to 1.5 are all greater than those with L/B ratios of 1.0, and the garage models which have the largest L/B ratios have the largest C_{Fy}/C_{Fx} ratio values of all.

TABLE C - 7 CFY/CFX RATIOS COMPARED WITH L/B RATIOS

	1	2	3	4	5	6	Overhang	G1A	G1B	G2A	G2B
CFy/CFx (VT=0.15 m/s)	1.26	1.37	1.06	0.99	0.92	1.18	1.25	1.39	1.89	1.89	1.76
CFy/CFx (VT=0.46 m/s)	1.49	1.44	1.09	0.94	0.98	1.06	1.23	1.71	1.53	2.16	1.71
L/B	1.5	1.5	1.0	1.0	1.0	1.0	1.5	1.9	1.9	2.4	2.4

G = garage A and B = orientation

Bibliography

ASCE, 2006. Minimum Design Loads for Buildings and Other Structures. American Society of Civil Engineers.

Bluestein, H. B. & Golden, J., 1993. A review of tornado observations. In: Church et al., editors. *The tornado: Its structure, dynamics, prediction, and hazards.* Geophysical monograph, vol. 79. American Geophysical Union.

Brooks, H. E., 2004. On the Relationship of Tornado Path Length and Width to Intensity. *Weather and Forecasting,* April. pp. 310-319.

Brooks, H. E., Doswell III, C. A., 2001. Normalized Damage from Major Tornadoes in the United States: 1890-1999. *Weather and Forecasting,* February, Volume 16, pp. 168-176.

Canfield, L. R., Niu, S. H., Liu, H., 1991. Uplift resistance of various rafter-wall connections. *Forest Products Journal,* July/August, 41(7/8), pp. 27-34.

Cheng, J., 2004. Testing and Analysis of the Toe-Nailed Connection in the Residential Roof-to-Wall System. *Forest Products Journal,* April, 54(4), pp. 58-65.

Church, C. R., Snow, J. T., Baker, G. L., Agee, E. M., 1979. Characteristics of Tornado-Like Vortices as a Function of Swirl Ratio: A Laboratory Investigation. *Journal of the Atmospheric Sciences,* September, Volume 36, pp. 1755-1776.

Conner, H. W., Gromala, D. S., Burgess, D. W., 1987. Roof connections in Houses: Key to Wind Resistance. *Journal of Structural Engineering,* December, 113(2), pp. 2459-2474.

Cramer, S. M., Drozdek, J. M., Wolfe, R. W., 2000. Load sharing Effects in Light-Frame Wood-Truss Assemblies. *Journal of Structural Engineering,* December, 126(12), pp. 1388-1394.

Cunningham, T. P., 1993. *Roof Sheathing Fastening Schedules for Wind Uplift, APA Report T92-28,* Tacoma, Washington: APA-The Engineered Wood Association.

Dao, T. N., van de Lindt, J. W., 2008. New Nonlinear Roof Sheathing Fastener Model for Use in Finite-Element Wind Load Applications. *Journal of Structural Engineering,* October, 134(10), pp. 1668-1674.

Davies-Jones, R. P., 1973. The Dependence of the Core Radius on Swirl Ratio in a Tornado Simulator. *Journal of the Atmospheric Sciences,* October. pp. 1427-1430.

Davies-Jones, R. P., 1976. Laboratory Simulations of tornadoes. In: Proc. Symposium on Tornadoes Assessment of Knowledge and Implications for Man. Lubbock, Texas, Texas Tech University, pp. 151-174.

Haan Jr., F. L., Balaramudu, V. K., Sarkar, P. P., 2010. Tornado-Induced Wind Loads on a Low-Rise Building. *Journal of Structural Engineering,* January, 136(1), pp. 106-116.

Haan Jr., F. L., Sarkar, P. P., Gallus, W. A., 2008. Design, construction and performance of a large tornado simulator for wind engineering applications. *Engineering Structures,* pp. 1146-1159.

Hangan, H., Kim, J.-D., 2008. Swirl ratio effects on tornado vortices in relation to the Fujita scale. *Wind and Structures,* 11(4), pp. 291-302.

Hill, K. M., 2009. *Development of time-Warying Wind Uplift Test Protocols for Residential Wood Roof Sheathing Panels,* M.S. Thesis. Florida: University of Florida.

Jischke, M. C., Light, B. D., 1983. Laboratory Simulation of Tornadic Wind Loads on a Rectangular Model Structure. *Journal of Wind Engineering and Industrial Aerodynamics,* Volume 13, pp. 371-382.

Karstens, C. D., Samaras, T.M., Lee, B.D., Gallus Jr., W.A., Finley, C.A., 2010. Near Ground Pressure and Wind Measurements in Tornadoes. *Monthly Weather Review,* July, Volume 138, pp. 2570-2588.

Lee, W.C., Wurman, J., 2005. Diagnosed Three-Dimensional Axisymmetric Structure of the Mulhall Tornado on 3 May 1999. *Journal of the Atmospheric Sciences,* Volume 62, pp. 2373-2393.

Marshall, T. P., 2002. Tornado Damage Survey at Moore, Oklahoma. *Weather and Forecasting,* June, Volume 17, pp. 582-598.

McDonald, J. R., Selvam, P., 1990. The West Memphis, Arkansas Tornado of December 14, 1987. *Journal of Wind Engineering and Industrial Aerodynamics,* Volume 36, pp. 279-287.

Morrison, M. J., Kopp, G. A., 2011. Performance of toe-nail connections under realistic wind loading. *Engineering Structures,* Volume 33, pp. 69-76.

Murphy, S., Schiff, S., Rosowsky, D., Pye, S., 1996. *System Effects and Uplift Capacity of roof Sheathing Fasteners.* In: Proc. Fourteenth Structures Congress. Chicago, American Society of Civil Engineers, pp. 765-770.

NAHB, 2003. *Roof Sheathing Connection Tolerances,* Washington, DC: U.S. Department of Housing and Urban Development.

North Carolina Building Code Council, 1978. *The North Carolina State Building Code, with Amendments to 1984.* Raleigh, NC: North Carolina Building Code Council.

Pan, K., Montpellier, P., Zadeh, M., 2002. Engineering Observations of 3 May 1999 Oklahoma Tornado Damage. *Weather and Forecasting,* June, Volume 17, pp. 599-610.

Readling, B. T., 2003. *Midwest Tornadoes May 4, 2003,* Tacoma, Washington: APA The Engineered Wood Associations.

Reed, T. D., Rosowsky, D. V., Schiff, S. D., 1997. Uplift Capacity of Light-Frame Rafter to Top Plate Connections. *Journal of Architectural Engineering,* December, 3(4), pp. 156-163.

Riley, M. A., Sadek, F., 2003. *Experimental Testing of Roof to Wall Connections in Wood Frame Houses, NISTIR 6938,* Gaithersburg, MD: NIST.

Rosowsky, D. V., Reinhold, T. A., 1999. Rate-of-Load and duration-of-Load Effects for Wood Fasteners. *Journal of Structural Engineering,* July, 125(7), pp. 719-724.

Rosowsky, D. V., Schiff, S. D., 1996. *Probabilistic Modeling of Roof Sheathing Uplift Capacity.* In: Proc. Probabilistic Mechanics and Structural Specialty Conference. Worchester, MA, ASCE, pp. 334-337.

Sarkar, P. P.,Haan, F. L., Gallus, W. A., Le, K., Kardell, R., Wurman, J., 2005. *A Laboratory Tornado Simulator: Comparison of Laboratory, Numerical and Full-Scale Measurements.* In: Proc. Tenth American Conference on Wind Engieering. Baton Rouge, American Association for Wind Engineering.

Simiu, E., Scanlan, R. H. 1996. *Wind Effects on Structures: Fundamentals and Applications to Design* (3rd ed.). New York: John Wiley and Sons, Inc.

Sengupta, A., Haan, F. L., Sarkar, P. P., Balaramudu, V., 2008. Transient loads on buildings in microburst and tornado winds. *Journal of Wind Engineering and Industrial Aerodynamics,* Volume 96, pp. 2173-2187.

Shanmugam, B., Nielson, B. G., Prevatt, D. O., 2009. Statistical and Analytical Models for Roof Components in Existing Light-Framed Wood Structures. *Engineering Structures,* Volume 31, pp. 2607-2616.

Sparks, P. R., 1986. The Response of Low-rise Non-Engineered Structures to Extreme Wind conditions. *Journal of Wind Engineering and Industrial Aerodynamics,* Volume 23, pp. 181-192.

Sparks, P. R., Hessig, M. L., Murden, J. A., Sill, B. L., 1988. On the Failure of Single-Story Wood-Framed Houses in Severe Storms. *Journal of Wind Engineering and Industrial Aerodynamics,* Volume 29, pp. 245-252.

Sutt Jr., E. G., 2000. *The Effect of Combined Shear and Uplift Forces on Roof Sheathing Panels,* Ph.D. dissertation. Clemson, South Carolina: Clemson University.

Sutter, D., DeSilva, D., Kruse, J., 2009. An Economic Analysis of Wind Resistant Construction. *Journal of Wind Engineering and Industrial Aerodynamics,* Volume 97, pp. 113-119.

Texas Tech University, 2004. *A Recommendation for an Enhanced Fujita Scale,* Lubbock, Texas: Wind Science and Engineering Center, Texas Tech University.

Thampi, H., Dayal, V., Sarkar, P. P., 2011. Finite element analysis of interaction of tornados with a low-rise timber building. *Journal of Wind Engineering and Industrial Aerodynamics,* Volume 99, pp. 369-377.

van de Lindt, J. W., Graettinger, A., Gupta, R., Skaggs, T., Pryor, S., Fridley, K. J., 2007. Performance of Wood-Frame Structures during Hurricane Katrina. *Journal of Performance of Constructed Facilities,* March/April, 21(2), pp. 108-116.

Ward, N., 1972. The Exploration of Certain Features of Tornado Dynamics Using a Laboratory Model. *Journal of the Atmospheric Sciences,* Volume 29, pp. 1194-1204.

Wurman, J., 2002. The Multiple-Vortex Structure of a Tornado. *Weather and Forecasting,* June, Volume 17, pp. 473-505.

Yang, Z., Sarkar, P., Hu, H., 2010. Visualization of flow structures around a bagle-roofed building model in tornado-like winds. *Journal of Visualization,* pp. 285-288.

Biographical Sketch

Jeremy Michael Case was born in Merriam, Kansas in 1982. In 2003 he moved to Baguio City, Philippines where he began his undergraduate degree in engineering at St. Louis University. In 2006 he transferred to Institut Teknologi Bandung in Bandung, Indonesia where he completed his undergraduate degree in civil engineering in 2009 and was awarded the title of "Sarjana Teknik". In 2010 he began his Master of Science in Civil Engineering at Iowa State University. After completing his graduate degree, he began working for the Infrastructure business unit of Stanley Consultants in Muscatine, Iowa as a Structural Engineer Intern.